The Dissertation Committee for Timothy James Povich
certifies that this is the approved version of the following dissertation:

Discontinuous Galerkin (DG) Methods for Variable Density Groundwater Flow and Solute Transport

Committee:

Clint N. Dawson, Supervisor

Irene M. Gamba

Todd Arbogast

Omar Ghattas

Marc Hesse

Discontinuous Galerkin (DG) Methods for Variable Density Groundwater Flow and Solute Transport

by

Timothy James Povich, B.S.M.E.; M.A.

DISSERTATION

Presented to the Faculty of the Graduate School of

The University of Texas at Austin

in Partial Fulfillment

of the Requirements

for the Degree of

DOCTOR OF PHILOSOPHY

THE UNIVERSITY OF TEXAS AT AUSTIN

December 2012

To my parents, my wife Jessica and my children James and Caroline, with love.

Acknowledgments

In my 19 years of service in the Army, I have learned that no major accomplishment can ever be attributed solely to one person. It is the interaction among people with differing backgrounds and experiences that allows seemingly impossible goals to become reality. I must acknowledge and thank those people without whom this work would not have been possible.

I first thank my advisor, Dr. Clint Dawson, for his infinite patience and guidance during this journey. Through my Master's work, my efforts to come back to the University of Texas and throughout the Ph.D. process, he has been a valued source of advice and support. In particular, he understood the time constraints imposed by the Army and helped me to navigate the obstacles imposed by my shortened time frame.

I also thank my primary collaborators from the Corps of Engineers' Coastal and Hydraulics Lab in Vicksburg, Mississippi, Dr.'s Chris Kees and Matthew Farthing. Their patience and sage advice on both the Proteus software and general computational issues were instrumental throughout my research. Their knowledge of and passion for this work was an inspiration to me.

I am grateful to my fellow students and the Computational Hydraulics Group who shared my struggles and kept me motivated and moving in the right direction. I especially thank Steve Mattis whose knowledge of Proteus was an invaluable resource.

I am extremely grateful to the Institute for Computational Engineering and Sciences for giving me the opportunity to do this research and for providing great examples of academic professionalism. A special thanks to my committee members Professors Irene Gamba, Todd Arbogast, Omar Ghattas and Marc Hesse for their guidance and support throughout the process.

Lastly and most of all, I would like to thank my family for their love and support over the past three years. Their encouragement allowed me to maintain my perspective when times were rough. This accomplishment is for all of you.

Timothy James Povich

The University of Texas at Austin

December 2012

Discontinuous Galerkin (DG) Methods for Variable Density Groundwater Flow and Solute Transport

Timothy James Povich
The University of Texas at Austin, 2012

Supervisor: Clint N. Dawson

ABSTRACT

Coastal regions are the most densely populated regions of the world. The populations of these regions continue to grow which has created a high demand for water that stresses existing water resources. Coastal aquifers provide a source of water for coastal populations and are generally part of a larger system where freshwater aquifers are hydraulically connected with a saline surface-water body. They are characterized by salinity variations in space and time, sharp freshwater/saltwater interfaces which can lead to dramatic density differences, and complex groundwater chemistry. Mismanagement of coastal aquifers can lead to saltwater intrusion, the displacement of fresh water by saline water in the freshwater regions of the aquifers, making them unusable as a freshwater source. Saltwater intrusion is of significant interest to water resource managers and efficient simulators are needed to assist them.

Numerical simulation of saltwater intrusion requires solving a system of flow

and transport equations coupled through a density equation of state. The scale of the problem domain, irregular geometry and heterogeneity can require significant computational resources. Also, modeling sharp transition zones and accurate flow velocities pose numerical challenges. Discontinuous Galerkin (DG) finite element methods (FEM) have been shown to be well suited for modeling flow and transport in porous media but a fully coupled DG formulation has not been applied to the variable density flow and transport model. DG methods have many desirable characteristics in the areas of numerical stability, mesh and polynomial approximation adaptivity and the use of non-conforming meshes. These properties are especially desirable when working with complex geometries over large scales and when coupling multi-physics models (e.g. surface water and groundwater flow models).

In this dissertation, we investigate a new combined local discontinuous Galerkin (LDG) and non-symmetric, interior penalty Galerkin (NIPG) formulation for the non-linear coupled flow and solute transport equations that model saltwater intrusion. Our main goal is the formulation and numerical implementation of a robust, efficient, tightly-coupled combined LDG/NIPG formulation within the Department of Defense (DoD) Proteus Computational Mechanics Toolkit modeling framework. We conduct an extensive and systematic code and model verification (using established benchmark problems and proven convergence rates) and model validation (using experimental data) to verify accomplishment of this goal. Lastly, we analyze the accuracy and conservation properties of the numerical model. More specifically, we derive an *a priori* error estimate for the coupled system and conduct a flow/transport model compatibility analysis to prove conservation properties.

Table of Contents

List of Tables

List of Figures

Chapter 1

Introduction

1.1 Background, Motivation and Challenges

Coastal regions are the most densely populated regions of the world and the populations of these regions continue to grow. About one in every three people on the planet now live within 100 kilometers of the sea and about 44 percent of the world's population live within 150 kilometers of the ocean [9]. The population increase has created a high demand for water that stresses existing water resources [106]. Coastal aquifers provide one source of water for large coastal populations. These aquifers are generally part of a larger system where freshwater aquifers are hydraulically connected to a saline surface-water body. Saltwater occupies the void space underlying the freshwater because of the proximity to the sea and this saltwater wedge can extend some distance landward. Typically, in a coastal aquifer, a hydraulic gradient exists towards the sea and the sea receives the excess of freshwater from the aquifer. This excess is the difference between natural or manmade replenishment and any freshwater pumping that may occur. A natural, stable transition zone (or zone of dispersion) appears between the freshwater and saltwater where the salinity varies between that of lighter freshwater and that of heavier saltwater (see Figure 1.1). The lighter freshwater tends to flow to the sea. The shape of this transition zone can depend on whether the saltwater wedge is moving landward or

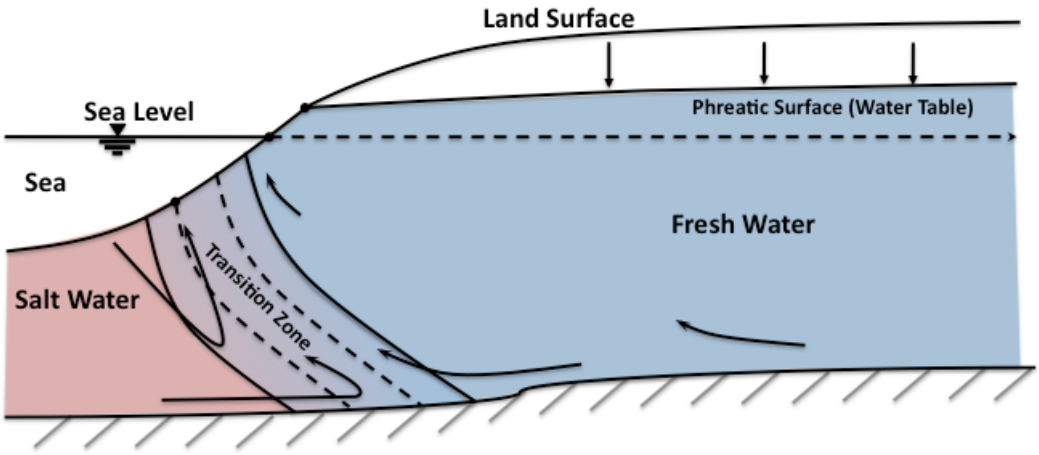

Figure 1.1: Idealized Unconfined Coastal Aquifer.

seaward and the type of aquifers (confined, unconfined). The natural equilibrium that controls this wedge can be affected in several ways. When pumping occurs, excess freshwater flow to the sea is decreased, water levels or piezometric heads decrease, and the saltwater wedge advances inward until another stable equilibrium is reached. Existing freshwater wells may be impacted if they exist within this transition zone. Also, saltwater upconing can occur in parts of the aquifer further inland which can contaminate freshwater wells. Rising sea levels, reclamation of coastal areas, irrigation and drainage and many other natural and manmade phenomena can lead to changes in the hydrogeology regime that can cause an inward movement of the saltwater wedge [59]. Because of these effects, pollution of freshwater aquifers by saltwater is a significant environmental problem and freshwater usage from coastal aquifers must be closely managed. A relatively small proportion of seawater (1%) will render freshwater unfit for drinking [52]. Different methods have

been used to help alleviate the stress on coastal aquifers. Application of freshwater injection barriers, extraction of saline groundwater, land reclamation, creation of physical barriers and aquifer storage and recovery (ASR) are some of the methods used [58]. Effective and reliable numerical simulation is needed to help determine the long term effect of these methods. Saltwater intrusion (SWI) into littoral zones and eventually into coastal aquifers is of significant interest to water resource managers and efficient simulators are needed to assist in the management. Mismanagement of coastal aquifers can lead to saltwater intrusion into freshwater regions of the aquifers, making them unusable as a freshwater source.

Modeling flow and transport in coastal aquifers has many challenges. It is an active area of research as demonstrated by a recent issue of the Hydrogeology Journal [104] which was devoted to the topic of saltwater and freshwater interaction in coastal aquifers, focusing on the state of modeling the phenomena and the extent of saltwater intrusion problems around the world. Coastal aquifers are characterized by salinity variations in space and time, sharp freshwater/saltwater interfaces which can lead to dramatic density differences, and complex groundwater chemistry [104]. Also, the large spatial domains can have irregular geometry and heterogeneity and physical processes may have long temporal scales which make modeling a challenge. Although simpler sharp interface models have been used with success in some situations, a variable transition zone must be modeled to truly capture the physics of the phenomena in many situations [52]. Thus, effectively modeling these processes requires using a variable density flow and transport model. In this model, the bulk fluid mass and momentum balance equations and the solute mass balance equation

are coupled through density and viscosity equations of state. Since the transport equation is often advection-dominated, it presents numerical difficulties when trying to resolve the sharp moving fronts or freshwater/saltwater transition zones that characterize coastal aquifers. For the flow equation, a high numerical accuracy of the Darcy velocity is essential to capturing the correct physics of the problem. A poor approximation of the flow velocity can produce spurious numerical velocities that lead to increased advective and dispersive transport of solute. Also, large physical and temporal scale computations with irregular domain and large scale porous medium heterogeneity creates numerical and computational challenges.

Discontinuous Galerkin (DG) finite element methods are a natural choice for modeling the coupled system because of their ability to use complicated computational meshes, capture sharp gradients and ease in implementing *hp*-adaptivity. Numerous numerical methods have been used previously to model variable density flow and transport. Primarily, continuous Galerkin (CG) finite element, finite difference and finite volume methods have been applied to the VDFT model, but in the past 15 years, several combined methods that utilize DG methods with mixed and mixed hybrid finite element methods have been used with success. A full DG formulation, though, has not been posed for this model to our knowledge. However, fully DG formulations have been shown to be well suited for modeling coupled flow and transport problems. Fully DG models have been formulated and analyzed for the coupled flow and reactive transport model [119] and the miscible displacement problem [111]. DG methods have been shown to effectively model these problems with many desirable characteristics over CG models in the areas of numerical stabil-

ity, mesh and polynomial approximation adaptivity and the use of non-conforming meshes. In this dissertation, we focus on modeling the physical phenomena of saltwater intrusion using the variable density and solute transport model with a fully DG approximation of the coupled system. In our formulation, we discretize the flow equation using a local discontinuous Galerkin (LDG) method as presented by Dawson [46] which provides a locally conservative, consistent approximation of the Darcy velocity. For the solute transport equation, we utilize a a non-symmetric, interior penalty Galerkin (NIPG) method with classical upwinding for the advection terms as formulated by Sun and Wheeler [120]. We use an implicit time discretization with an iterative coupling strategy and we formulate and solve the numerical model utilizing the DoD Proteus Computational Mechanics Toolkit software [78]. In the rest of this section, we will give a brief historical review and background of variable density flow and transport modeling, the history of its application in coastal aquifers through saltwater intrusion modeling and the use of DG methods in flow and transport modeling.

1.2 A Literary and Historical Review

In this section, we give a brief background on the more general topic of variable density flow and transport in a porous medium with a focus on the broad applications in the field of hydrological studies. We narrow our focus to primarily concentration dependent density flows and its applications to the saltwater intrusion problem.

1.2.1 Variable Density Flow and Transport

In continuum fluid mechanics, a fluid is considered an effectively continuous medium with several fundamental bulk properties that describe its behavior [54]. The density, ρ, is the bulk property of a fluid that describes its mass per unit volume. The fluid density is often non-uniform and can vary in different situations with pressure, temperature, and the partial densities of the chemical species which make up the fluid. Fluid flow that is influenced by changes in density is termed *variable density flow*. The phenomena of variable density flow and transport appears in many different areas of engineering and physics. Specifically in our area of focus, groundwater hydrology, field and laboratory experiments have shown that fluid density gradients due to temperature and/or concentration variations can have a strong influence on solute transport in groundwater systems. If an invading fluid's density is significantly greater than the density of the existing groundwater, density driven flow can manifest itself in the form of instabilities or free convection. These instabilities usually arise when heavier fluids overlie lighter fluids. The classic example of free convection is the Hele-Shaw cell experiment and numerical simulation results from Elder [56, 57] where finger-like instabilities develop as a result of an unstable density layering caused by heating.

Density driven convection is important in groundwater transport because it enhances hydrodynamic mixing which, in the constant density case, is the result of forced convective, dispersive and diffusive affects. In the variable density case, however, we can have the following effects [117]: (1) convective transport is typically far greater than diffusive transport of the solute; (2) mixing process time scales are

significantly reduced; (3) mixing zone dimensions are typically larger which enable solutes to be transported over greater distances. These effects influence many different hydrogeological phenomena such as seawater intrusion and saltwater upconing in coastal aquifers and migration of contaminant plumes around landfills and radioactive storage sites.

Although initial developments in this field date back over a century, over the past three decades, there has been significant work in the field because of worldwide concerns about the future of energy and water resources and environmental pollution [116]. Simmons [117] describes the evolution of this field from its beginning in fluid dynamics as having evolved in four stages. In the early 1900s, the field initially evolved from traditional fluid mechanics with focuses on applications to flow in heated fluids. In 1916, Lord Rayleigh analyzed an idealized model and determined the characteristics of the instabilities that resulted from density effects induced by thermal differences. The dimensionless Rayleigh number, named after Lord Rayleigh, which gives the ratio of buoyancy to dispersive forces, is used in fluid dynamics to describe and predict the onset of instabilities. In the 1940s, studies began to combine heat and porous media and in the 1950s and 1960s the focus moved to solute and porous medium studies. Finally in the 1960s, the combined thermal and solute concentration impacts on variable density were explored in thermohaline studies. However, earnest application of these concepts in groundwater hydrology did not begin until post 1950s and there are still many unresolved issues in this area. Numerous reviews have accessed the state of variable density flow theory and current practices. Most recently, Diersch and Kolditz [54] conducted an exhaustive

development of the history and current state of variable density flow and transport theory. We refer the readers to their work for additional information. In this work, we will present some background of the general development of the mathematical model and numerical methods and challenges associated with solution of the model. In the following section, we will go into more detail of the history of the use of the VDFT model in saltwater intrusion.

Modeling general variable density flow and transport has many challenges. The mathematical model can have nonunique solutions and issues of physical instability and oscillations arise because of the non-linearity of the coupled flow and transport model [54]. The nonlinearity of the system also creates many challenges in solving the system and verifying numerical methods is difficult since few analytic solutions exist. Fingering and convective cell development brought on by free convection are sensitive to spatial discretization and as a result, grid convergence cannot be achieved for many variable density problems [116]. The first numerical computations of variable density flow processes were conducted by Wooding [128] and Elder [56] and over the succeeding years, with the interest in environmental processes influenced by variable density flow increasing, many numerical methods were developed to simulate the phenomena. Numerical techniques such as standard continuous, mixed and mixed hybrid Galerkin finite element, finite volume, finite difference, spectral and boundary element methods were applied to explore the distinct variable density flow phenomena such as convection rolls, oscillatory convection, high Rayleigh number cellular convection, and thermohaline convection [54].

Different formulations of the VDFT mathematical model have been investigated extensively. The general model that is commonly used assumes a continuum approach for multiphase, multispecies flow in porous media and is presented in several works [21, 54, 65, 68, 74]. Mazzia and Putti [93] investigated different combinations of state variables (e.g. pressure head/concentration, pressure/mass fraction). Post and coauthors [105] examined the proper use of the hydraulic head formulation for variable density groundwater flow analyses and the pitfalls associated with it. Oltean and Buès [98] compared non-conservative and conservative formulations of the model. Various assumptions have been employed to simplify the system. The Oberbeck-Boussinesq approximation neglected density variations in the fluid mass balance equation to reduce the amount of coupling. The density variation in the fluid flow direction was also neglected [20]. The validity of these assumptions was explored in numerous papers [3, 5, 54, 129]. Several authors conducted investigations into the appropriate forms of the constitutive relations for the diffusive mass flux and Darcy velocity [65, 66, 93, 114].

Another area of investigation has been the treatment of the fluxes (Darcy and solute mass flux). The numerical accuracy of these fluxes, especially the Darcy flux, is essential for capturing the physics of VDFT. Modeling these fluxes as primary variables in the formulation is costly, so the fluxes are often evaluated in a decoupled manner where the Darcy flux is constructed from the solution of the pressure field using direct differentiation and Darcy's equation. This leads to a lower order of approximation (compared to the pressure) and discontinuous velocities across element boundaries. Local and global projection methods have been used to improve

accuracy and give a continuous representation of the fluxes over the entire domain [54]. Others have applied mixed FEM to the flow equations which yielded higher accuracy and a continuous normal flux approximation across element boundaries [2, 93]. Previously, we have used a conservative velocity post-processing algorithm developed by Larson and Niklasson [86] to construct a mass conservative velocity for a CG formulation of the VDFT model. This construction, however, increases the computational expense of the method.

Another issue with approximating the velocity arises when using CG FEM. When using FEM approximations of equal order for the pressure and the concentration, spurious velocities can arise which can lead to a method's inability to model hydrostatic conditions. Voss and Souza [124] identified the need for a consistent formulation of the velocity and presented a modified scheme that approximated the buoyancy term in Darcy's equation with the same order as the pressure gradient. Frolković and Knabner [62, 80] presented a general consistent velocity algorithm that has been applied in a number of CG FEM simulators.

Solving the coupled nonlinear system of equations has also posed a numerical challenge and different solution methods have been explored. Due to the nonlinearity of the coupled system, it must be solved in an iterative manner. The most common methods involved Picard, modified Newton and Newton iterative schemes. In the Picard method, after discretization of the continuous equations, the resulting matrix equations are linearized by evaluating coefficient matrices and right hand side vectors at previous values. In the modified Newton method, the discrete equations are solved in a fully coupled way but only utilize the block diagonal components of the

system Jacobian matrix giving two uncoupled equations that are solved iteratively. In the Newton method, the system is fully coupled and the full Jacobian is utilized in the solution. Putti and Paniconi [107] investigate and compare convergence of these different methods for VDFT. Relaxation methods [74] and adaptive predictor/corrector schemes [54] were also used to improve the convergence of the Picard and Modified Newton methods. Recently, there has been research to determine new, more efficient coupling methods that have shown promise [2, 3, 131, 132].

With the increase in numerical techniques and methods for simulating VDFT, the availability of analytic solutions and benchmark problems to verify numerical models has been a major issue. As a result, significant research has been conducted to determine suitable numerical benchmark problems as well as laboratory experiments to assist in model verification. Simmons [116] discusses the current state of this process and compares different models. Due to the non-linear nature of the model, few analytical solutions exist to the problem. As a result, verification of numerical models has been a challenge and has been accomplished through comparison to existing numerical codes. Analysis and comparison of numerical codes and benchmark problems is done often in the literature [54, 81]. Recently, Voss and coauthors [123] reviewed existing benchmarks and the role they play in the verification of 2D and 3D numerical models. In the paper, they classified different benchmark problems in terms of being *necessary* and *sufficient* benchmarks. A benchmark problem is necessary if good performance on it indicates the method is functioning properly but does not prove that the method correctly "represents the variable-density problem class" [123]. A benchmark problem is sufficient if good performance on the

benchmark indicates that the method represents the tested variable-density problem class. We focus on benchmarks for 2D and 3D stable variable-density problems and used this methodology in selecting our specific benchmark problems for verification and validation.

Of the existing benchmarks, some are designed to test specific aspects of the code which are easily verifiable and are necessary, but not sufficient, conditions for the model to properly capture the physics of variable density flow. We will use one problem from this class to verify our code: the Henry steady-state seawater intrusion problem. The Henry problem has been modeled and developed by numerous authors to capture wide transition zone physics. We will utilize a version of Henry's problem proposed by Arbarca and coauthors [1] which uses a full dispersion tensor with more physical inflow/outflow sea-side boundary conditions than posed in Henry's original work.

Many problems, however, have differing numerical solutions and there is often disagreement in the literature upon the correct solution. This class of models is used for comparison only against other codes but are not a necessary nor sufficient test for model verification. Two of the most widely utilized examples from this class of benchmark problems are the 2-D Salt Dome problem (strong coupling, hydrodynamic dispersion), and the saline Elder problem (strong coupling, pure convection). The 2D Salt Dome problem is Case 5, Level 1 of the International Hydrologic Code Intercomparison (HYDROCOIN) groundwater flow modeling project and has been simulated in a number of works [54, 81, 82, 97, 130] This problem verifies the physics under strong coupling and hydrodynamic dispersion. The saline

Elder problem was adapted from the classic thermal convection problem of Elder [56, 57] by Voss and Souza in [124] and has been simulated in a number of works [2, 4, 54, 63, 81, 97, 98, 124]. This benchmark problem has strong density coupling and free convection. Each of these problems contains difficulties in numerical implementation and are not necessarily characteristic of the saltwater intrusion dynamics. We chose not to implement them for this work but will look at them in future work.

There are several verification problems which have been developed that arise from laboratory experiments and that have data with which numerical results can be compared. One of these is a recent experimental problem from MacMinn and coauthors [92] which looks at the development of a gravity current from an initial vertical interface. Sharp interface approximation analytical solutions have also been developed for the evolution of a gravity current in a vertically confined aquifer which we use in conjunction with the experimental results to assess the numerical method. The second problem is the 2D Saltwater Intrusion problem by Goswami and Clement [64]. This is a laboratory version of the Henry problem which tests the dyamics of saltwater intrusion. The third experimental problem is the 3D Salt Pool problem developed by Oswald and Kinzelbach [99, 100], which is a theoretical upconing problem with experimental results that has been simulated by a number of authors [54, 75]. The 3D Salt pool problem is identified in [123] as being a necessary and sufficient benchmark for 3D stable variable density physics.

The VDFT has been studied extensively and applied to many different hydrogeological phenomena but we are particularly interested in its application to modeling in coastal aquifers.

1.2.2 Saltwater Intrusion

Saltwater intrusion and the interaction of freshwater and saltwater in coastal aquifers has been studied and modeled for over one hundred years, but the variable density flow theory was not applied until a little over forty years ago. Traditionally, SWI models have been divided into two classes: sharp interface models and transition zone models. The sharp interface approach grew out of the works of Badon-Ghijben (1888) and Herzberg (1901) and earlier work by Du Commun (1828) [31]. The so-called Badon-Ghijben Herzberg principle described the position of the fresh/salt groundwater interface by relating the salt and freshwater groundwater pressures. Assuming a hydrostatic equilibrium exists between freshwater and saltwater and that the interface, sea level, and the water table meet at one point, they obtained a relationship that along any vertical line, the depth of the interface below sea level was proportional to the elevation of the water table above sea level [24]. The constant of proportionality is the ratio of the freshwater density to the difference of the saltwater and freshwater densities. This relationship gives a good approximation to the interface location in some situations.

The general sharp interface approach assumes that the saltwater and freshwater are immiscible fluids of different densities that are separated by a sharp interface. Sharp interface methods are effective in understanding the location of the saltwater interface but are only applicable in limited situations where the transition zone is abrupt and not affected by hydrodynamic dispersion. The methods do not take into account the dominant factors in the saltwater intrusion phenomena: the flow regime in the region above the saltwater wedge, the variable density effects

and hydrodynamic dispersion [21]. However, sharp interface models utilizing the Badon-Ghijben approximation and other simplifying assumptions can yield analytic solutions and in the 1950s and 60s were used extensively to provide a fundamental understanding of saltwater intrusion dynamics [74].

Transition zone models treat saltwater and freshwater as miscible fluids (or a single fluid with a variable salt concentration) and take into account a variable density and the dominant factors mentioned above. In 1964, Henry [67] applied the steady state variable density flow model to simulate saltwater intrusion. He developed an analytic solution for predicting the steady state salt distribution in a two dimensional slice of a coastal aquifer. The Henry problem still remains one of the few saltwater intrusion benchmark problems and the physical viability of his solution has been tested and debated vigorously [118]. Using a transient version of Henry's model, Pinder and Cooper [103] developed the first numerical solution for salt water intrusion with the method of characteristics. The first finite element model was introduced by Lee and Cheng [87] in 1974 which utilized the VDFT model formulated in terms of flow stream functions and concentration. In the next twenty years, numerous models were developed and applied to the 2D Henry problem [43, 115, 124]. These models were restricted to two dimensions because of the computational limitations of the day. The first 3D finite element model was developed by Huyakorn and coauthors [74] for the hydraulic head/concentration model formulation. Since then, numerous variable density flow and transport simulators were developed utilizing different numerical methods. The majority of the methods in the literature were formulated for the fully saturated model. When the fully

saturated model is applied to an unconfined aquifer, the phreatic boundary (water table) is treated using a suitable boundary condition (which we will discuss in Section 2). However, some methods have been formulated to model variable density flow within both the saturated and unsaturated zones. Some of the most commonly used saltwater intrusion simulators are: Saturated-Unsaturated, Variable-Density Groundwater Flow with Transport (SUTRA), a 2D/3D hybrid finite element and integrated finite difference based simulator developed by C. Voss [122]; Finite Element Subsurface Flow System (FEFLOW) [53] is a CG finite element-based model for simulating 2D/3D density dependent subsurface flow, mass transport and heat transport in unsaturated-saturated zones; SEAWAT [85], a finite volume based 3D variable density ground-water flow and transport model that modifies the standard MODFLOW (the US Geological Services Modular 3D ground-water flow model) and MT3DMS (a modular 3D model for multi-species transport) models. Bear [21] conducts a detailed review of other VDFT simulators.

Researchers have conducted numerous field scale investigations of saltwater intrusion using these simulators. They conducted these investigations using both 2D vertical cross section of the aquifer and 3D simulations. They conducted studies of coastal and island aquifers using 3D models in Florida [84], Israel [23], Japan [101] and Greece [83] and using 2D models in Hawaii [124] and Germany[61]. Bear and coauthors in [133] studied salt water upconing processes. Misut and Voss [94] explored the regional impact of aquifer storage and recovery on saltwater intrusion in New York City aquifers. Recently, Walther and coauthors explored saltwater intrusion in an agricultural coastal arid region in Oman [125].

Diersch and Kolditz [54] identify several factors that make large field scale modeling a challenge. One is the inherent numerical expense due to the level of mesh refinement needed to capture the natural spatial heterogeneity and density driven effects. This has been prohibitive in the past but with new advances in supercomputing, larger scale simulations are becoming more viable. Another challenge is how to properly characterize the subsurface and to deal with the spatial heterogeneity which creates particular problems for variable density modeling. In variable-density flow systems, heterogeneity in the subsurface hydraulic properties can perturb flow over many different length scales to generate instabilities in density stratified systems [117]. Numerous authors have studied the impacts of spatial heterogeneity on variable density flow. Arbarca and coauthors [1] investigated the influence of anisotropy and heterogeneity on saltwater intrusion using the dispersive Henry problem. Simmons and coauthors [116] determined that heterogeneity served to trigger the onset of instabilities as well as control whether instabilities, once generated, will grow or decay. Kerrou and Renard [79] also studied the dispersive Henry problem and determined that heterogeneity plays a key role in modeling the SWI process and that the affects can be different in 2D and 3D simulations.

Although effectively modeling saltwater intrusion poses many challenges, we hope that the implementation of a fully DG method will provide flexibility in dealing with some of these challenges. In the next section, we give a brief history of the DG methods and their desirable properties we wish to leverage when applying it to the SWI model.

1.2.3 Discontinuous Galerkin Methods

In this section, we give a brief history of the development of DG methods from original ideas to give a general background and then present more recent work in coupled flow and transport. DG methods are characterized by the use of fully discontinuous approximation spaces, weak enforcement of the partial differential equations on each element by means of a Galerkin formulation and solution values characterized by suitable "numerical fluxes" on inter-element boundaries. DG methods were not originally developed for the treatment of convection-diffusion phenomena and elliptic/parabolic partial differential equations but recently have been used in these areas. The two methods which we explore in this dissertation grew out of different lines of development in the history of DG methods. Recently, Arnold and coauthors [8] presented a unified analysis of these methods and provided a common framework for studying these methods for elliptic problems. We refer the readers to this paper for a more detailed development. We give a brief summary of the history while maintaining the focus on the two methods that we propose for our formulation: the LDG and NIPG methods.

The local DG method found its roots in the classical DG line of development. The classical DG methods were originally designed to treat hyperbolic problems. The first use of these methods was proposed by Reed and Hill [108] in 1973 to solve the neutron transport problem. The first detailed analysis of the DG method was done by Lesaint and Raviart [88] in which they coined the name "discontinuous Galerkin" method. The method was further developed over the next 20 years and used extensively for modeling hyperbolic problems and non-linear hyperbolic

systems. The most notable of these methods is the Runge-Kutta Discontinuous Galerkin (RKDG) method developed by Cockburn and Shu [36, 37, 38, 39, 41] for nonlinear hyperbolic systems. In the 1990's, much work was done to extend the traditional DG methods to equations involving diffusion. In 1992, Richter [109] applied the DG methods for hyperbolic equations to convection dominated equations with diffusion. Dawson used an operator splitting approach by combining high resolution methods for convective terms and utilizing mixed finite element methods for the second order diffusion operators in the Godunov-mixed [50, 44] and upwind-mixed methods [45]. A fully discontinuous approximation for the second order diffusion operators was presented by Bassi and Rebay [17] where they utilized a mixed formulation in dealing with the second order derivatives in the compressible Navier-Stokes equations and the RKDG method to treat the first order terms. In 1998, Cockburn and Shu [40] extended this work and introduced the so-called local discontinuous Galerkin method as the first fully discontinuous classical DG method for transient, nonlinear convection-diffusion equations. The method is a generalization of the methods of Bassi and Rebay, in which they pose the PDE in mixed form and apply RKDG methods to the first order equations. The LDG method has since been investigated extensively and applied to numerous problems. It has been applied and analyzed for advection-diffusion problems in several works [34, 35, 40, 48]. For application to elliptic and parabolic PDEs, there has also been significant investigation. Convergence and stability properties for purely parabolic problems were investigated by Cockburn and Shu [40] in their original work. Castillo and coauthors [33] conducted an *a priori* error analysis of the method for elliptic

problems for arbitrary meshes. Castillo [32] investigated the numerical performance of the method for elliptic problems in comparison with other primal DG methods. The *hp* version of the LDG method was analyzed by Perugia and Schötzau [102] for pure diffusion problems. It has been applied to modeling groundwater flow [47] and convective-diffusive transport [6, 48].

The LDG method has many desirable properties. The method gives symmetric matrices and is stable for any positive penalty parameter. It gives a direct approximation for the two primary variables, which is important in variable-density flow. It also gives excellent approximations to elliptic equations that arise in subsurface flow. Finally, it provides locally conservative, flux-continuous solutions [46].

The so-called primal DG methods, which include the NIPG methods, grew out of the early interior penalty methods that have their origins in classical works of Lions, Nitsche, and Babuška. The initial motivation for Lions' work [91] was solving second order elliptic boundary value problems with very rough boundary data which resulted in the idea of weak enforcement of Dirichlet boundary conditions through the use of a penalty parameter. Babuška [10] first applied this idea in the finite element context but the method was inconsistent and did not converge to optimal order. Nitsche [95], during the same time period, used a different approach which still used a penalty term but applied an adjoint boundary term to maintain the consistency of the method which converges to optimal order. Interior penalty methods grew out of these same ideas but used interior penalties to enforce inter-element continuity weakly instead of through the finite element space. This idea was first presented by Babuška and Zlámal [12] in 1973 where they utilized previous ideas to

impose C^1 continuity weakly for fourth-order problems.

In the following years, numerous authors utilized penalty methods for linear parabolic/elliptic equations and nonlinear hyperbolic equations. In 1978, Wheeler [126] generalized Nitsche's method in a discontinuous collocation-finite element method with interior penalties for linear elliptic equations. In 1982, Arnold [7] extended Wheeler's work to the solution of second order nonlinear parabolic boundary value problems by using the same bilinear form with discontinuous approximation spaces. Wheeler and Arnold's work would later become known as the symmetric interior penalty Galerkin methods (SIPG). Investigation into interior penalty methods continued throughout the 1970's but went out of favor in the early 1980's because they were no more efficient than the finite element method, a major drawback given the current computational capabilities and the difficulty in finding optimal values for the penalty parameters [8]. However, in the late 1990's, there was an increased interest in these methods, possibly as a result of the increasing computational power. In 1998, Baumann [18] and Oden, Baumann and Babuška [11, 96] introduced a new DG method for diffusion problems and then extended it to convection-diffusion equations [19], which we refer to as the OBB-DG method. The OBB-DG method utilizes a formulation for the second order operator that did not require the introduction of auxiliary variables and utilized a non-symmetric modification of the bilinear form previously used by Wheeler, Arnold and several other IPG methods [7, 55, 126, 127] but did not use a penalty term. Rivière, Wheeler and Girault [112] utilized the same anti-symmetric bilinear form for elliptic problems but introduced a penalty parameter. The nonsymmetry of the form reduced the stability requirements on the

penalty parameter that were required for the SIPG method. This method became known as the non-symmetric interior penalty Galerkin method. The final member of this group of primal methods, the incomplete interior penalty Galerkin method (IIPG), uses the same bilinear form without the adjoint stabilization and was presented by Dawson, Sun, and Wheeler [49] in 2004. For the NIPG method, Rivière and Wheeler [113] proved *hp* estimates for several versions of the method for elliptic problems. The different primal methods have different convergence and stability properties as a result of the bilinear form and penalties utilized. The NIPG and OBB-DG methods have nonsymmetric system matrices even if the underlying operators are symmetric but are stable for any nonzero penalty parameter. This leads to a lack of adjoint-consistency for the methods which can lead to less than optimal convergence rates. The SIPG methods give symmetric matrices but are only stable for a sufficiently large penalty parameter.

Recently, primal DG methods have been applied to the parabolic and convective-diffusive PDEs that govern flow and transport models in porous media. This has happened for a number of reasons. The properties of local mass conservation, less numerical diffusion and the ability to treat rough and discontinuous coefficients make DG methods uniquely suited for this problem [119]. Since DG methods use discontinuous approximation spaces, flexibility is allowed for general non-conforming meshes with varying degrees of approximation for easier *hp*-adaptivity. The localized nature of the discontinuous approximation spaces leads to simple connectivity between elements which makes DG highly parallelizable. This is crucial for large field-scale simulations that have excessive memory and computation time require-

ments. In addition, the non-conforming nature of DG allows for an easy and effective mesh modification dynamically with time [121]. This dynamic adaptivity is well suited for large transient problems like the saltwater intrusion problem, where strong physics occur only in a small portion of the domain which may change over time.

Sun and Wheeler [120] presented and analyzed DG methods for reactive-transport in porous media. Primal DG methods (NIPG, SIPG and OBB-DG) were formulated and applied to the convection-diffusion reactive transport problem. They established $L^2(H^1)$ error estimates for the NIPG method which are optimal in h and nearly optimal in p. They then extended their investigation to coupled flow and reactive transport problems in porous media [119]. They utilized cut-off operators in the analysis to treat the coupling of flow/transport and transport/reaction and proved error estimates for concentration, pressure and velocity as well as concentration and pressure jumps. Rivière and Wheeler [111] presented a fully DG coupled model for the miscible displacement problem. They conducted numerical comparisons with the MFEM and higher-order Godunov methods showing comparable results.

In the area of variable density flow and transport in porous media, DG methods have been used primarily to treat the convective part of the transport equation while utilizing a continuous approximation for the flow. Buès and Oltean [29] and Ackerer, Younes and Mose [4] both utilized a discontinuous method for the advective transport coupled with the MHFEM method for the dispersive transport which was similar to Dawson's upwind-mixed method. They utilized the MHFEM to approximate the flow equations. Ackerer and Younes [2] presented a method that

uses a combination of DGFEM for advection and a Multipoint Flux Approximation method for dispersion. They couple this with a lumped formulation of the MFEM for the flow equations. However, to our knowledge, a full DG model has not been implemented.

In advection-diffusion equations formulated using standard conforming or discontinuous Galerkin methods, it is well known that the solution can become oscillatory in the presence of steep gradients. This can be the case in salt water intrusion modeling when sharp fronts exist. The behavior of numerical solutions of advection-diffusion equations is characterized by the element Péclet number defined (for the linear constant coefficient case) as

$$P_e = \frac{\|\mathbf{u}\| \, \Delta_e}{2D},$$

where Δ_e is the element diameter, $\|\mathbf{u}\|$ is the vector norm of the velocity, and D is the diffusion coefficient. This quantity relates the convection effects to diffusion/dispersion effects in fluid flows. At high element Péclet numbers ($P_e > 1$), the equation becomes convection-dominated and it is possible to get overshoots and undershoots in the solution around sharp gradients. These non-physical oscillations can also lead to instability in the solutions. The effect of non-physical oscillations can be alleviated by sufficient mesh refinement or using mesh adaptive methods. In the variable density model when molecular diffusion is small compared to mechanical dispersion, the element Péclet number can be approximated [124] as

$$P_e \approx \frac{\Delta_e}{2\alpha_L}$$

leading to a restriction on the mesh given by $\Delta_e \leq 2\alpha_L$, where α_L is the longitudinal dispersivity. For small longitudinal dispersivities, this requirement can be computationally prohibitive, especially with DG methods, so additional stability is needed in the solution to reduce these oscillations. In the past, several methods have been used to improve stability in the face of high element Péclet numbers and reduce non-physical oscillations. Within DG methods, the most common approach has been slope limiting, most often used with explicit time integration schemes. In the context of implicit schemes, Rivière [110] presents and analyzes the use of slope limiting with the NIPG formulation for convection-diffusion equations where convection was dominant. However, slope limiting can reduce the solution to first order accuracy. Another stabilization mechanism is the so called *Hughes-Franca* type stabilization. These methods involve adding residual-dependent stabilization terms to the weak formulation. These terms are consistent in that they vanish for the true solution. The different stability mechanisms in DG methods are throughly discussed by Brezzi and coauthors [27]. The streamline- upwind/Petrov-Galerkin (SUPG) type stabilization originally presented in [28] is one example of this type of stabilization. SUPG-type stabilization was first used in primal DG methods for linear advection equations in [69] and for advection-diffusion equations in [70, 30]. This is the method that we will adopt. Although this type of stabilization will provide stabilized solutions, overshoots and undershoots may still appear in the vicinity of sharp fronts [76]. One method to deal with the remaining oscillations is the addition of a non-linear shock capturing term, this term attempts to damp out non-physical oscillations by introducing solution dependent damping in the vicinity

of steep gradients. This was introduced by Hughes and Mallet [71] and was used in context with the SUPG method. In our method, we will restrict our focus to the use of residual based stabilization and shock-capturing because they are less computationally expensive than slope limiters within our solution framework.

Finally, with the application of DG methods to coupled flow and transport problems, the question of compatibility between DG formulations arose. Dawson, Sun and Wheeler [49] investigated the compatibility of several different DG methods (NIPG, OBB-DG, IIPG, SIPG, LDG) when using them in coupled flow and transport. Since mass conservation in numerical methods is important for coupled flow and transport, preserving this property is essential. In modeling transport, local conservation in the flow equations can be important and can directly affect the accuracy and conservation properties of the transport method [49]. They showed that the approximate numerical satisfaction of the flow equation is crucial to preserving the accuracy, stability and global conservation properties of the transport methods and our methods must be chosen to satisfy this compatibility.

1.3 Summary of Contributions

In this dissertation, a coupled DG formulation for the saltwater intrusion model has been formulated, analyzed, and implemented within the DoD Proteus Toolkit modeling framework. The code is designed for two or three dimensional structured and unstructured triangular meshes and it is parallelized for implementation on high performance computers. Several numerical benchmark and experimental problems were simulated for verification and validation. Specifically, we have

achieved the following:

- We have presented the governing equations for variable density flow and transport and formulated the coupled DG method for the specific boundary conditions. The numerical implementation and solution methods are also presented. (see Section 2)

- We have conducted a basic consistency and compatibility analysis for the continuous in time coupled DG model. These show that the method is consistent and that the flow and transport models are compatible in a sense that global mass conservation is achieved. We have also conducted an *a priori* error analysis showing convergence rates for the coupled formulation. (see Section 3)

- A verification and validation of the method was conducted. This consisted of a convergence analysis of the uncoupled DG methods as well as the coupled system. The method was then applied to four benchmark problems and its performance was assessed. (see Section 4)

1.4 Outline of Dissertation

The remainder of the dissertation is as follows. In Chapter 2, we present a detailed development of the model and solution methodology. We develop the mathematical model for variable density flow and solute transport in a saturated, isotropic porous medium and discuss the relevant boundary conditions and initial conditions that will be utilized in the method analysis, validation problems and salt water intrusion modeling. The formulation of the coupled system DG Model is

presented for each part of the system: the LDG method for the flow model and the NIPG method for the transport model. We present the semi-discrete coupled model, the time discretization, and the solution method for the coupled model. We finish this section with some details about the code utilized to implement the model. In Chapter 3, we conduct a basic analysis of the coupled system, showing consistency, flow and transport formulation compatibility, and an *a priori* error analysis of the coupled system. In Chapter 4, we present the numerical results for the saturated model starting with the convergence analysis and then look at 2D and 3D benchmark problems. Finally, we conclude in Chapter 5 with some general observations and future areas of research.

Chapter 2

Solution Methodology

2.1 Model Development and Problem Statement

A continuum model is used to describe the flow and transport in porous media which is restricted to assumptions appropriate for the specific case of saltwater intrusion in coastal aquifers. A full development of the general model for multi-species, multiphase variable density flow in porous media can be found in several works [21, 54, 65, 68]. We note that the macroscopic continuum equations describing flow and transport that we use here are derived from averaging the microscopic description of the phenomena over a representative elementary volume that we assume exists for all of our domain. A detailed description of volume averaging and homogenization techniques can be found in Bear [21] and other works and will not be discussed here.

The general model we adopt is based on the works of Bear [20, 21, 22]. We formulate the model in terms of the equivalent freshwater head and normalized mass fraction. Although the numerical method can be extended to modeling the variably saturated flow and transport case, we restrict our development in this work to modeling saltwater intrusion in only the saturated (phreatic) zone. Any affects from the unsaturated zone will enter the model through a boundary condition. To this end, we make several assumptions that affect the formulation of the model.

(A1) The porous media is fully saturated so we only model the flow of the liquid phase. This amounts to modeling the flow and transport in the phreatic zone.

(A2) The aquifer is under isothermal conditions.

(A3) There is a single liquid phase (water) with a variable concentration of dissolved matter. We will not assume a sharp interface so there will be a transition zone where the density transitions from salt water to freshwater.

(A4) The flow of liquid in the porous media is described by the generalized Darcy's Law and the solute mass dispersive flux is described by a Fickian-type law which is reasonable based on the ranges of concentration considered in the saltwater intrusion case.

(A5) For the range of pressures considered, the pressure dependence of the water density is negligible in comparison with the concentration dependence. The effect of pressure on the density is neglected in the model except in its contribution to the specific storativity so the water density only depends explicitly on the concentration of dissolved matter.

(A6) Viscosity may vary with concentration at higher concentrations, but does not depend on the pressure.

(A7) Dissolved matter does not adsorb in the solid or undergo any chemical reaction or decay.

(A8) The density and solute concentration of infiltrating water is specified.

(A9) The porous media is isotropic but can be heterogeneous (the porosity, ϕ, and permeability tensor, $\mathbf{k}$, can depend on the location in the porous medium but do not vary with respect to coordinate directions).

(A10) The dispersive flux of the total fluid mass is much smaller than the advective flux of mass so it will not be considered in the bulk fluid mass flux.

(A11) The solid matrix considered is rigid except for the effect of its compressibility on the specific storativity [22].

We make two notes about the assumptions. First, we note that with assumptions (A5) and (A11), the effects of fluid compressibility and solid matrix deformation enter the model through the scalar, storage coefficient [21]. Second, we note here that we will relax the isotropy assumption (A9) when we utilize an anisotropic hydraulic conductivity tensor for the Henry problem in Section 4. Under these assumptions, we can present the balance equations that govern the flow and transport in porous media and the equations of state that couple the flow and transport. The general model is nonlinear and coupled through the state equations for density and viscosity and we will first present these equations of state.

2.1.1 Density and Viscosity Equations of State

Numerous equations of state exist for the density and dynamic viscosity. We utilize the equations of state for density and viscosity presented for the SWI model presented by Bear [21] and follow his development. At increased solute concentration and pressures and given isothermal conditions, the density of a fluid is given by the

general constitutive equation

$$\rho = \rho(p, \omega) = \rho_0 \exp\left(\beta_p(p - p_0) + \beta_\omega(\omega - \omega_0)\right), \tag{2.1}$$

where ω is the solute mass fraction in the fluid and $\rho_0 = \rho(p_0, \omega_0)$, is the density at the reference pressure and mass fraction. The coefficients describe the change in density with each quantity and are defined by:

$$\beta_p = \frac{1}{\rho}\frac{\partial \rho}{\partial p},$$
$$\beta_\omega = \frac{1}{\rho}\frac{\partial \rho}{\partial \omega},$$

where β_p is the coefficient of water compressibility at constant mass fraction and β_ω is the coefficient that describes the effect of solute mass fraction on density. The linearized version is given by

$$\rho = \rho_0(1 + \beta_p''(p - p_0) + \beta_\omega''(\omega - \omega_0)),$$

where

$$\beta_p'' = \frac{1}{\rho_0}\frac{\partial \rho}{\partial p},$$
$$\beta_\omega'' = \frac{1}{\rho_0}\frac{\partial \rho}{\partial \omega}.$$

For the case of salt water intrusion, we can assume $\beta_\omega'' |\Delta\omega| > \beta_p'' |\Delta p|$ which allows us to neglect the pressure effects on density [21] and we have a linear relationship for density given by

$$\rho = \rho_0(1 + \beta_\omega''(\omega - \omega_0)). \tag{2.2}$$

We introduce the normalized solute mass fraction, c, given by

$$c = \frac{\omega - \omega_0}{\omega_1 - \omega_0}, \tag{2.3}$$

where $\omega, \omega_0, \omega_1$ are the solute mass fractions of saltwater, freshwater and seawater (fluid with maximum solute mass fraction), respectively. Using our assumption of linearity, we define

$$\frac{\partial \rho}{\partial c} \equiv \frac{\rho(\omega_1) - \rho(\omega_0)}{\omega_1 - \omega_0}$$

and applying (2.3), we have

$$\begin{aligned}
\rho &= \rho_0(1 + \beta_\omega''(\omega - \omega_0)) \\
&= \rho_0(1 + \frac{1}{\rho_0}\frac{(\rho(\omega_1) - \rho_0)}{(\omega_1 - \omega_0)}(\omega - \omega_0)) \\
&= \rho_0(1 + \frac{\rho(\omega_1) - \rho_0}{\rho_0}c).
\end{aligned}$$

Our constitutive relation for density, in terms of normalized salt mass fraction, is then given by

$$\rho = \rho_0(1 + \epsilon c), \tag{2.4}$$

where

$$\epsilon = \frac{\rho_1 - \rho_0}{\rho_0}$$

is the density contrast, $\rho_1 = \rho(\omega_1)$, the density of seawater (or of fluid saturation).

The dynamic viscosity of a fluid is to a first approximation, independent of pressure and temperature but demonstrates a dependence on concentration for higher values of concentration. We will use an experimentally derived polynomial fit for the viscosity [89]:

$$\mu = \mu_0(1 + 1.85\omega - 4.1\omega^2 + 44.50\omega^3), \tag{2.5}$$

where μ_0 is the reference fluid viscosity (usually taken to be the viscosity of fresh water at standard pressure and temperature).

2.1.2 Fluid Flow Model.

The mass balance of fluid (which we will refer to as the *flow* equation) takes the form

$$\frac{\partial(\phi\rho)}{\partial t} = -\nabla \cdot (\rho \mathbf{u}) + \rho_s Q_s, \tag{2.6}$$

where ϕ is the effective porosity of the porous medium, ρ is the fluid density $[ML^{-3}]$, $\mathbf{u}$ is the specific discharge (or Darcy velocity) $[LT^{-1}]$, Q_s is a general fluid source/sink term $[T^{-1}]$ with a density ρ_s (where we define general units $M =$ Mass, $T =$ Time, $L =$ Length). This source or sink term usually is represented as a point source to replicate pumping or injecting fluid into the domain. The density is either prescribed for inflow $\rho_s = \rho(c_s)$ or based on the concentration of outflowing fluid $\rho_s = \rho(c)$.

The momentum balance of fluid is given by the generalized Darcy's equation for variable density flow

$$\mathbf{u} \equiv \phi \mathbf{v} = -\frac{\mathbf{k}}{\mu}\big(\nabla p + \rho g \nabla z\big), \tag{2.7}$$

where $\mathbf{v}$ is the averaged fluid velocity (or seepage velocity), $\mathbf{u}$ is the Darcy velocity (or specific discharge) p is the pressure $[ML^{-1}T^{-2}]$, $\mathbf{k}$ is the permeability tensor for the porous medium $[L^2]$, μ is the dynamic viscosity $[ML^{-1}T^{-1}]$, g is the gravitational constant $[LT^{-2}]$ and z is the vertical distance from an established datum $[L]$ and ∇z is the unit vector in the vertical (z) direction.

Using (A2), (A5) and (A11) and assuming the porosity can be written only

as a function of pressure, we have

$$\begin{aligned}\frac{\partial(\phi\rho)}{\partial t} &= \rho\frac{\partial\phi}{\partial t} + \phi\frac{\partial\rho}{\partial t} \\ &= \rho S_p\frac{\partial p}{\partial t} + \phi\frac{\partial\rho}{\partial c}\frac{\partial c}{\partial t},\end{aligned}$$

where

$$S_p = \xi(1-\phi) + \beta_p\phi$$

is the specific mass storativity related to pressure changes $[M^{-1}LT^2]$ with ξ the compressibility of the bulk porous material and β_p is the coefficient of compressibility of the fluid. This relation gives the new fluid flow equation:

$$\rho S_p\frac{\partial p}{\partial t} + \phi\frac{\partial\rho}{\partial c}\frac{\partial c}{\partial t} + \nabla\cdot(\rho\mathbf{u}) = \rho_s Q_s.$$

Finally, we introduce the relation $h = p/\rho_0 g + z$ defining the equivalent freshwater head to write the flow equations as

$$\rho S\frac{\partial h}{\partial t} + \phi\frac{\partial\rho}{\partial c}\frac{\partial c}{\partial t} + \nabla\cdot(\rho\mathbf{u}) = \rho_s Q_s,$$

$$\mathbf{u} = -\mathbf{K}\big(\nabla h + \frac{\rho-\rho_0}{\rho_0}\nabla z\big).$$

The hydraulic conductivity tensor of freshwater, $\mathbf{K}$ $[MT^{-1}]$, is given by

$$\mathbf{K} = \frac{\mathbf{k}\rho_0 g}{\mu} \tag{2.8}$$

and

$$S = \rho_0 g S_p \tag{2.9}$$

is the specific mass storativity related to head changes $[L^{-1}]$. Using this, we arrive at our equations for the flow model:

$$\rho S\frac{\partial h}{\partial t} + \phi\frac{\partial\rho}{\partial c}\frac{\partial c}{\partial t} + \nabla\cdot(\rho\mathbf{u}) = \rho_s Q_s, \tag{2.10}$$

$$\mathbf{u} = -\mathbf{K}\big(\nabla h + \frac{\rho - \rho_0}{\rho_0}\nabla z\big). \tag{2.11}$$

2.1.3 Solute Transport Model.

With the assumption that the transport of solute is governed by advection, molecular diffusion and mechanical dispersion, the solute mass balance (which we will refer to as the *transport* equation) is given by

$$\frac{\partial(\phi\rho\omega)}{\partial t} = -\nabla\cdot(\rho\omega\mathbf{u} - \rho\mathbf{D}\nabla\omega) + \omega_s\rho_s Q_s, \tag{2.12}$$

where ω is the solute mass fraction [M.salt/M.fluid], $\mathbf{D}$ is the dispersivity tensor. We use the Bear-Scheidegger dispersion relation for the isotropic dispersion tensor [21, 54]

$$\mathbf{D} = \phi D_m\mathbf{I} + (\alpha_L - \alpha_T)\frac{\mathbf{u}\otimes\mathbf{u}}{|\mathbf{u}|} + \alpha_T|\mathbf{u}|\mathbf{I}, \tag{2.13}$$

where $|\mathbf{u}|$ is the magnitude of the Darcy velocity vector, D_m is the pore water diffusion coefficient [L^2T^{-1}], $\mathbf{I}$ is the identity matrix and α_T, α_L are the longitudinal and transverse dispersivities [L]. Again, we note that in the mass source term, $\rho_s\omega_s Q_s$, the mass fraction, ω_s and density, ρ_s is specified for a source term but is taken as the unknown solution mass fraction and density of the fluid leaving the domain for a sink term. If we define our reference mass fraction, $\omega_0 = 0$, then we can rewrite the equation in terms of a normalized mass fraction, $c = \omega/\omega_1$ [21]

$$\frac{\partial(\phi\rho c)}{\partial t} = -\nabla\cdot(\rho c\mathbf{u} - \rho\mathbf{D}\nabla c) + c_s\rho_s Q_s, \tag{2.14}$$

with $c_s = \omega_s/\omega_1$ the normalized mass fraction of the source/sink term.

2.1.4 Governing System of Equations.

The final system of equations in terms of our state variables $[h, \mathbf{u}, c]$ which we will use in our method development is given by

$$\rho S \frac{\partial h}{\partial t} = -\nabla \cdot (\rho \mathbf{u}) - \phi \frac{\partial \rho}{\partial c} \frac{\partial c}{\partial t} + \rho_s Q_s, \tag{2.15}$$

$$\mathbf{u} = -\mathbf{K}\big(\nabla h + \frac{\rho - \rho_0}{\rho_0} \nabla z\big), \tag{2.16}$$

$$\frac{\partial (\rho \phi c)}{\partial t} = -\nabla \cdot (\rho c \mathbf{u} - \rho \mathbf{D} \nabla c) + c_s \rho_s Q_s. \tag{2.17}$$

These equations combined with the relations (2.8,2.9,2.13) and the state equations, (2.4,2.5) make up the variable density flow and transport models that we will implement in the DG formulation.

2.1.5 Initial and Boundary Conditions

Along with these equations, appropriate initial mass fraction and hydraulic head conditions are specified for the domain. Also, appropriate boundary conditions for the flow and transport are specified. For analysis, we will utilize the following boundary conditions and initial conditions. The open, fixed domain $\Omega \in \mathbb{R}^d$ is given a Lipschitz boundary $\partial\Omega = \overline{\Gamma_N} \cup \overline{\Gamma_D} = \overline{\Gamma}_- \cup \overline{\Gamma}_+$ with corresponding outward unit normal vector, $\mathbf{n}$, where we define inflow and outflow boundaries as

$$\Gamma_- = \{\mathbf{x} \in \partial\Omega : \mathbf{u} \cdot \mathbf{n} < 0\},$$

$$\Gamma_+ = \{\mathbf{x} \in \partial\Omega : \mathbf{u} \cdot \mathbf{n} \geq 0\}.$$

On our boundaries, we define the following boundary conditions for the flow equations:

$$h = h^b \quad \forall (\mathbf{x}, t) \in \Gamma_D \times (0, T],$$

$$\mathbf{u} \cdot \mathbf{n} = \mathbf{u}_b \cdot \mathbf{n} \quad \forall (\mathbf{x}, t) \in \Gamma_N \times (0, T],$$

and for the transport equation:

$$(\rho c \mathbf{u} - \rho \mathbf{D} \nabla c) \cdot \mathbf{n} = c_I \rho_I \mathbf{u}_I \cdot \mathbf{n} \quad \forall (\mathbf{x}, t) \in \Gamma_- \times (0, T],$$

$$\rho \mathbf{D} \nabla c \cdot \mathbf{n} = 0 \quad \forall (\mathbf{x}, t) \in \Gamma_+ \times (0, T],$$

where h^b,$\mathbf{u}_b$ are specified freshwater head and inflow Darcy velocity, respectively, and c_I, ρ_I and $\mathbf{u}_I$ are the specified inflow mass fraction, density and Darcy velocity. We impose the following initial conditions:

$$h(\mathbf{x}, 0) = h^0(\mathbf{x}),$$

$$c(\mathbf{x}, 0) = c^0(\mathbf{x}).$$

In practical applications of modeling salt water intrusion in an unconfined aquifer, we follow [21] and use the idealized aquifer in Figure 2.2 to identify appropriate boundary conditions when applying the fully saturated VDFT model.

1. Lateral Sea Side Boundary (AF). On the lateral seaside boundary, for the flow equation, we assume that seawater is always present and specify an equivalent freshwater head corresponding to the seawater hydraulic head,

$$h = \frac{\rho_s}{\rho_0} h_s - \epsilon z,$$

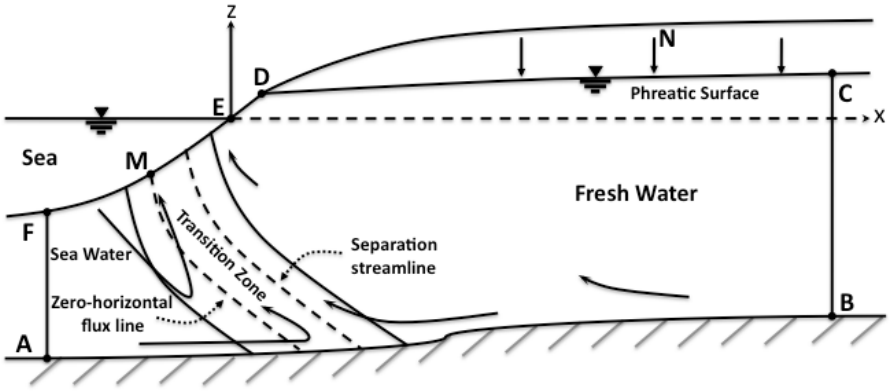

Figure 2.2: Unconfined Coastal Aquifer (adapted from [22]).

where h_s is the seawater hydraulic head at a point on the line AF and z is the elevation of the point from a given datum. For the transport equation, a normalized mass fraction of seawater is set to $c = 1.0$.

2. Lateral Land Side (CB). At the lateral landside boundary, assuming that freshwater is always present, we prescribe the freshwater head as a Dirichlet-type boundary, $h = h_b$, or we can prescribe a Neumann-type flux boundary, $\mathbf{u} \cdot \mathbf{n} = \mathbf{u}_b \cdot \mathbf{n}$. We specify a constant normalized mass fraction for freshwater, $c = 0$.

3. Impervious Bottom (AB). To represent the lower confining aquifer, we impose a no fluid flux normal to the boundary, $\mathbf{u} \cdot \mathbf{n} = 0$ and a zero normal dispersive mass flux, $\rho \mathbf{D} \nabla c \cdot \mathbf{n} = 0$.

4. Sea/Land Interface (DF)

a. Seepage Face (DE). On segment DE in Figure 2.2, we have the aquifer in contact with the atmosphere so freshwater discharges from the aquifer. On this boundary, for the flow, we specify the condition $h = \zeta_{DE}$ where ζ_{DE} is the elevation at a point on the seepage face above a given datum. For the transport equation, we treat this as an outflow boundary with a zero dispersive mass flux Neumann condition, $\mathbf{D}\nabla c \cdot \mathbf{n} = 0$.

b. Sea Bottom (EF). For the sea bottom segment EF, we specify the reference head based on a seawater hydraulic head on the sea bottom

$$h = \frac{\rho_s}{\rho_0} h_s - \epsilon \zeta_{EF},$$

where h_s is the seawater hydraulic head and ζ_{EF} is the elevation at a point on the sea bottom from a given datum. For the transport equation, there can be either inflow or outflow so there are two possible cases. In the first case, there is only flow seaward and so a zero diffusive flux outflow condition is imposed. For inflow, the total flux into the domain is specified $(\rho c \mathbf{u} - \rho \mathbf{D} \cdot \nabla c) \cdot \mathbf{n} = c_I \rho_I \mathbf{u}_b \cdot \mathbf{n}$. For the combination of inflow/outflow boundaries on EF, the point of zero-normal diffusive flux, M, is not known and can change over time.

5. Phreatic Surface (CD). The phreatic surface boundary condition is difficult to implement in the case of the saturated flow model. The shape of the surface is not *a priori* known. One way of implementing this boundary condition is presented in [21]. Assuming an atmospheric pressure at the surface ($p_{atm} = 0$), the phreatic surface can be described by a function $F = F(x, y, z, t) \equiv h - z = 0$

with an outward pointing unit normal given by $\mathbf{n}_F = \frac{\nabla F}{|\nabla F|} = [n_x, n_y, n_z]^T$. Assuming a continuous total fluid and solute flux on this surface, the following boundary conditions for the flow and transport equations can be derived:

$$\rho \mathbf{u} \cdot \mathbf{n}_F = -\rho_N N n_z - \frac{(\phi\rho - \theta_{w0}\rho_N)}{|\nabla F|}\frac{\partial h}{\partial t},$$
$$\mathbf{D}\nabla c \cdot \mathbf{n}_F = -\big(\frac{\rho_N c}{\rho} - c_N\big)\big(N n_z + \frac{\theta_{w0}}{|\nabla F|}\frac{\partial h}{\partial t}\big),$$

where N is the replenishment of the aquifer with density ρ_N, θ_{w0} is the (assumed) irreducible water content in the unsaturated zone. We note that this boundary condition is difficult in that the solution h is needed to define the phreatic surface F.

Different combinations of boundary conditions 1-4 are utilized in the benchmark problems in Chapter 4 but boundary conditions 4a and 5 are not implemented in this work.

2.2 Discontinuous Galerkin Formulation

We will utilize the Local Discontinuous Galerkin (LDG) method as presented by Dawson [46] to discretize the flow equation and an NIPG method for the transport equation as presented in Sun and Wheeler [120] with standard upwinding for the the advective flux.

2.2.1 Notation and Function Spaces

We introduce the following notation and function spaces to facilitate the development. Let $\mathcal{T}_\Delta$ be a general triangulation of a domain $\Omega \in \mathbb{R}^d$, $d = 1, 2, 3$,

into elements Ω_e of diameter Δ_e and with maximum diameter $\Delta > 0$. We denote $(\cdot,\cdot)_R$ the L^2-inner product over a d-dimensional domain, R; $\langle\cdot,\cdot\rangle_{\partial R}$ is integration over a $(d-1)$-dimensional surface. Let $\mathcal{E}_i$ denote the set of all interior element faces of $\mathcal{T}_\Delta$. A *face*, $\gamma \in \mathcal{E}_i$, is taken to be a face in 3D and an edge in 2D. We assume that no element face intersects both Γ_- and Γ_+ or both Γ_N and Γ_D. The notation $\langle\cdot,\cdot\rangle_{\mathcal{E}_i}$ denotes integration over all interior element faces. Define $W_{\Omega_e} = H^s(\Omega_e)$, $s \geq 1$ and $\mathbf{V}_{\Omega_e} = (W_{\Omega_e})^d$ and then we can define the standard DG function spaces

$$W = \{w \in L^2(\Omega) : \text{ on each } \Omega_e \in \mathcal{T}_\Delta, w \in W_{\Omega_e}\},$$
$$\mathbf{V} = \{\mathbf{v} \in (L^2(\Omega))^d : \text{ on each } \Omega_e \in \mathcal{T}_\Delta, \mathbf{v} \in \mathbf{V}_{\Omega_e}\}.$$

Let γ be an interior face in a finite element mesh, then γ has two elements, Ω_e^+, Ω_e^-, adjacent to it. Suppose, $(\mathbf{v}, w)$ are smooth functions defined on these elements and let $(\mathbf{v}^\pm, w^\pm)$ denote the traces of $(\mathbf{v}, w)$ on γ from the interiors of Ω_e^+, Ω_e^-. We define the following unit normal vectors for the elements:

$$\mathbf{n}^- = \text{ the unit vector normal to } \gamma \text{ pointing from } \Omega_e^- \to \Omega_e^+,$$
$$\mathbf{n}^+ = -\mathbf{n}^- = \text{ the unit vector normal to } \gamma \text{ pointing from } \Omega_e^+ \to \Omega_e^-.$$

Here we note that in the implementation of the method, a consistent normal is needed for all interior faces. Using these definitions, we define the *upwind* value of w as

$$w^u(\mathbf{x})\big|_\gamma = \begin{cases} w^-(\mathbf{x}), & \mathbf{q}\cdot\mathbf{n}^- \geq 0, \\ w^+(\mathbf{x}), & \mathbf{q}\cdot\mathbf{n}^- < 0. \end{cases}$$

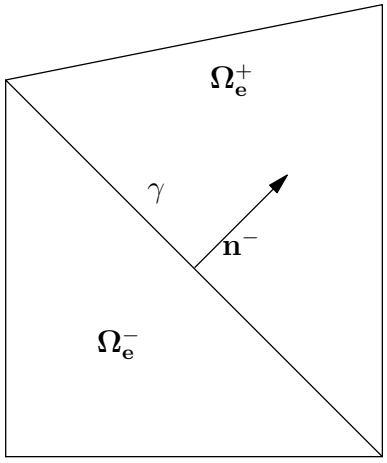

Figure 2.3: Element Neighbor Diagram.

We also define the following trace operators, the *average* $\{\!\{\cdot\}\!\}$ and the *jump* $[\![\cdot]\!]$ in the standard way

$$\{\!\{\mathbf{v}\}\!\} = \frac{\mathbf{v}^- + \mathbf{v}^+}{2}, \qquad \{\!\{w\}\!\} = \frac{w^- + w^+}{2},$$
$$[\![\mathbf{v}]\!] = \mathbf{v}^+ \cdot \mathbf{n}^+ + \mathbf{v}^- \cdot \mathbf{n}^-, \qquad [\![w]\!] = w^+\mathbf{n}^+ + w^-\mathbf{n}^-.$$

where we note $\{\!\{\mathbf{v}\}\!\}$ and $[\![w]\!]$ are vector quantities and $[\![\mathbf{v}]\!]$ and $\{\!\{w\}\!\}$ are scalar quantities. We will make use of the following two identities when working with the trace operators. For vector $\mathbf{v}$ and scalar w:

$$[\![\mathbf{v}w]\!] = [\![\mathbf{v}]\!]\,\{\!\{w\}\!\} + \{\!\{\mathbf{v}\}\!\} \cdot [\![w]\!]\,, \tag{2.18}$$
$$\frac{1}{2}\left[\left[w^2\right]\right] = [\![w]\!]\,\{\!\{w\}\!\}\,. \tag{2.19}$$

2.2.2 Flow Model Weak Formulation

We develop the mixed weak form of the LDG formulation in a standard way. To simplify the development, we define $f(c) = \rho_s Q_s - \frac{\partial \rho}{\partial c}\frac{\partial c}{\partial t}$ and $\hat{\rho}\mathbf{e}_z = \frac{\rho - \rho_0}{\rho_0}\nabla z$ and

assume that viscosity is independent of mass fraction. Let $(\mathbf{u}, h)$ be the solution to the flow equations (2.15,2.16) and $(w, \mathbf{v}) \in W \times \mathbf{V}$ be test functions. From (2.15), on a given element, Ω_e, we have

$$(\rho S h_t, w)_{\Omega_e} + (\nabla \cdot (\rho \mathbf{u}), w)_{\Omega_e} = (f, w)_{\Omega_e}.$$

An integration by parts on the divergence term gives

$$(\rho S h_t, w)_{\Omega_e} - (\rho \mathbf{u}, \nabla w)_{\Omega_e} + \langle \rho \mathbf{u} \cdot \mathbf{n}, w \rangle_{\partial \Omega_e} = (f, w)_{\Omega_e}.$$

Summing over all elements gives

$$(\rho S h_t, w)_{\Omega} - (\rho \mathbf{u}, \nabla w)_{\Omega} + \langle \hat{\mathbf{q}}, [\![w]\!] \rangle_{\mathcal{E}_i} + \langle \hat{\mathbf{q}}, w \rangle_{\partial \Omega} = (f, w)_{\Omega},$$

where $\hat{\mathbf{q}}$ is the numerical flux which we define as

$$\hat{\mathbf{q}}(c, \mathbf{u}, h) = \begin{cases} \{\!\{ \rho(c)\mathbf{u} \}\!\} + \sigma_h [\![h]\!], & \gamma \in \mathcal{E}_i, \\ \rho(c) u^b, & \gamma \in \Gamma_N, \\ \rho(c)\mathbf{u} \cdot \mathbf{n} + \sigma_h (h - h^b), & \gamma \in \Gamma_D, \end{cases} \tag{2.20}$$

where $\sigma_h > 0$ is a penalty parameter. We note for the true solution $(\mathbf{u}, h, c)$, we recover the original weak formulation.

From (2.16), assuming $\mathbf{K}$ is positive definite, we have

$$(\mathbf{K}^{-1}\mathbf{u}, \mathbf{v})_{\Omega_e} + (\nabla h, \mathbf{v})_{\Omega_e} = -(\hat{\rho}\mathbf{e}_z, \mathbf{v})_{\Omega_e},$$

and integrating by parts on the head gradient term gives

$$(\mathbf{K}^{-1}\mathbf{u}, \mathbf{v})_{\Omega_e} - (h, \nabla \cdot \mathbf{v})_{\Omega_e} + \langle \hat{h}, \mathbf{v} \cdot \mathbf{n} \rangle_{\partial \Omega_e} = -(\hat{\rho}\mathbf{e}_z, \mathbf{v})_{\Omega_e}.$$

Summing over all elements gives

$$(\mathbf{K}^{-1}\mathbf{u}, \mathbf{v})_{\Omega} - (h, \nabla \cdot \mathbf{v})_{\Omega} + \langle \hat{h}, [\![\mathbf{v}]\!] \rangle_{\mathcal{E}_i} + \langle \hat{h}, \mathbf{v} \cdot n \rangle_{\partial \Omega} = -(\hat{\rho}\mathbf{e}_z, \mathbf{v})_{\Omega},$$

where we define the numerical trace, $\hat{h}$, as

$$\hat{h} = \begin{cases} \{\{h\}\}, & \gamma \in \mathcal{E}_i, \\ h, & \gamma \in \Gamma_N, \\ h^b, & \gamma \in \Gamma_D. \end{cases}$$

If we introduce our definitions for the numerical fluxes and define the following forms:

$$\begin{aligned} \mathcal{A}_1(h, \mathbf{u}, w; c) \equiv & -(\rho\mathbf{u}, \nabla w)_\Omega + \langle \{\{\rho\mathbf{u}\}\}, [\![w]\!] \rangle_{\mathcal{E}_i} + \langle (\rho\mathbf{u}) \cdot \mathbf{n}, w \rangle_{\Gamma_D} \\ & + \langle \sigma_h [\![h]\!], [\![w]\!] \rangle_{\mathcal{E}_i} + \langle \sigma_h h, w \rangle_{\Gamma_D}, \\ \mathcal{A}_2(h, \mathbf{u}, \mathbf{v}) \equiv & (\mathbf{K}^{-1}\mathbf{u}, \mathbf{v})_\Omega - (h, \nabla \cdot \mathbf{v})_\Omega + \langle \{\{h\}\}, [\![\mathbf{v}]\!] \rangle_{\mathcal{E}_i} + \langle h, \mathbf{v} \cdot \mathbf{n} \rangle_{\Gamma_N}, \end{aligned}$$

and

$$\begin{aligned} \mathcal{L}_1(w; c) &\equiv (f, w)_\Omega - \langle \rho u^b, w \rangle_{\Gamma_N} + \langle \sigma_h h^b, w \rangle_{\Gamma_D}, \\ \mathcal{L}_2(\mathbf{v}; c) &\equiv -(\hat{\rho}\mathbf{e}_z, \mathbf{v})_\Omega - \langle h^b, \mathbf{v} \cdot \mathbf{n} \rangle_{\Gamma_D}, \end{aligned}$$

then we can write our mixed weak form for the flow equations as

$$\begin{aligned} (\rho S h_t, w)_\Omega + \mathcal{A}_1(h, \mathbf{u}, w; c) &= \mathcal{L}_1(w; c), \\ \mathcal{A}_2(h, \mathbf{u}, \mathbf{v}) &= \mathcal{L}_2(\mathbf{v}; c). \end{aligned} \tag{2.21}$$

2.2.3 The Transport Model Weak Formulation

We develop the weak form for the transport formulation. The development is in terms of numerical fluxes instead of the standard primal form development to be consistent with the previous flow formulation development. Assuming the solution is sufficiently smooth, we multiply the (2.17) by a test function, $w \in W$,

and on each element Ω_e have

$$((\rho\phi c)_t, w)_{\Omega_e} + (\nabla \cdot (c\rho\mathbf{u} - \rho\mathbf{D}\nabla c), w)_{\Omega_e} = (c_s\rho_s Q_s, w)_{\Omega_e}. \tag{2.22}$$

An integration by parts on the divergence term in (2.22) gives

$$((\rho\phi c)_t, w)_{\Omega_e} - (c\rho\mathbf{u} - \phi\rho\mathbf{D}\nabla c, \nabla w)_{\Omega_e} + \langle (\rho c\mathbf{u} - \phi\rho\mathbf{D}\nabla c)\cdot\mathbf{n}, w\rangle_{\partial\Omega_e} = (c_s\rho_s Q_s w)_{\Omega_e}.$$

Summing over all elements gives

$$((\rho\phi c)_t, w)_{\Omega} - (c\rho\mathbf{u} - \rho\mathbf{D}\nabla c, \nabla w)_{\Omega} + \langle \hat{\mathbf{F}}, [\![w]\!]\rangle_{\mathcal{E}_i} + \langle \hat{\mathbf{F}}, w\rangle_{\partial\Omega} = (c_s\rho_s Q_s w)_{\Omega}.$$

where we define the numerical flux, $\hat{\mathbf{F}}$ as

$$\hat{\mathbf{F}} = \begin{cases} c^u\hat{\mathbf{q}} - \{\!\{\rho\mathbf{D}\nabla c\}\!\} + \sigma_c [\![c]\!], & \gamma \in \mathcal{E}_i, \\ c\hat{\mathbf{q}}, & \gamma \in \Gamma_+, \\ c_I\hat{\mathbf{q}}, & \gamma \in \Gamma_-, \end{cases}$$

where $\hat{\mathbf{q}}$ is the numerical flux from the LDG method (2.20) and

$$\{\!\{\rho\mathbf{D}\nabla c\}\!\} = \frac{1}{2}(\rho^-\mathbf{D}^-\nabla c^- + \rho^+\mathbf{D}^+\nabla c^+).$$

with $\mathbf{D}^\pm = \mathbf{D}(\mathbf{u}^\pm)$ when $\mathbf{u}$ is multivalued. We note that the "upwind" value here is based on $\hat{\mathbf{q}}$. The penalty term $\sigma_c > 0$ is given on each edge γ by $\sigma_c = \frac{\sigma_\gamma}{|\gamma|^\beta}$ with $|\gamma|$ the measure of the edge/face, σ_γ a positive penalty parameter and β a positive number that depends on the dimension, d.

Following the NIPG method, we add the adjoint stabilization term $\langle \{\!\{\rho\mathbf{D}\nabla w\}\!\}, [\![c]\!]\rangle_{\mathcal{E}_i}$ to get the final weak form:

$$\begin{aligned}((\rho\phi c)_t, w)_{\Omega} - (c\rho\mathbf{u} - \rho\mathbf{D}\nabla c, \nabla w)_{\Omega} + \langle \hat{\mathbf{F}}, [\![w]\!]\rangle_{\mathcal{E}_i} + \langle \hat{\mathbf{F}}, w\rangle_{\partial\Omega} + \langle \{\!\{\rho\mathbf{D}\nabla w\}\!\}, [\![c]\!]\rangle_{\mathcal{E}_i} \\ = (c_s\rho_s Q_s w)_{\Omega}.\end{aligned}$$

We substitute in our numerical flux representation and we define the following forms:

$$\mathcal{B}(c,w;\mathbf{u},h) \equiv -(c\rho\mathbf{u},\nabla w)_\Omega + (\rho\mathbf{D}\nabla c,\nabla w)_\Omega + \langle C^u\hat{\mathbf{q}},[\![w]\!]\rangle_{\mathcal{E}_i} - \langle\{\!\{\rho\mathbf{D}\nabla c\}\!\},[\![w]\!]\rangle_{\mathcal{E}_i}$$
$$+ \langle\sigma_c[\![c]\!],[\![w]\!]\rangle_{\mathcal{E}_i} + \langle c\hat{\mathbf{q}},w\rangle_{\Gamma_+} + \langle\{\!\{\rho\mathbf{D}\nabla w\}\!\},[\![c]\!]\rangle_{\mathcal{E}_i},$$
$$\mathcal{L}(w) \equiv (c_s\rho_s Q_s,w)_\Omega - \langle c_I\hat{\mathbf{q}},w\rangle_{\Gamma_-},$$

so that we can write our transport weak form as

$$((\rho\phi c)_t,w)_\Omega + \mathcal{B}(c,w;\mathbf{u},h) = \mathcal{L}(w). \tag{2.23}$$

2.2.3.1 Transport Stabilization

An SUPG-type stabilization has been applied to NIPG DG formulations similar to the method in [30, 69] where the authors applied it to linear advection-diffusion equations. In residual based stabilization, an element-residual term is added to the original formulation of the transport equation in the form of

$$r(u_h,\tilde{w}) = \sum_{\Omega_e\in\mathcal{T}_\Delta}\int_{\Omega_e}\mathcal{L}_e(\tilde{w})\tau_e\mathcal{R}(u_h)d\Omega,$$

where $\mathcal{L}_e$ is a special operator applied to the test function, τ_e is a stabilization parameter and $\mathcal{R}(u_h)$ is the element strong residual of the approximate solution. In the case of SUPG stabilized methods, $\mathcal{L}_e \equiv \boldsymbol{\beta}\cdot\nabla u_h$, the non-conservative form of the advection operator where $\boldsymbol{\beta}$ is typically the divergence-free velocity. In the case of our problem, we define

$$\mathcal{R}_\Delta(C) = (\rho(C)\phi C)_t + \nabla\cdot(C\rho(C)\mathbf{U} - \rho(C)\mathbf{D}(\mathbf{U})\nabla C) - c_s\rho_s Q_s, \tag{2.24}$$
$$\mathcal{L}_e \equiv \rho(C)\mathbf{U}\cdot\nabla\tilde{w}, \tag{2.25}$$

where $\mathcal{L}_e$ is a linearized, non-conservative approximation of the conservative non-linear advection operator.

Defining the stability parameter, τ_e, is the biggest challenge. There are numerous ways to define it, many of which are motivated by the analysis of the 1D linear, constant coefficients case where it can be defined as a function of the element Péclet number, P_e,

$$\tau_e = \frac{\Delta_e}{2\,|\mathbf{u}|}\left[\coth\big(P_e\big) - \frac{1}{P_e}\right], \tag{2.26}$$

where P_e is as previously defined. For the linear case presented in [30], it is defined as

$$\tau_e = \tau \min\{\frac{\Delta_e}{u_T}, \frac{\Delta_e^2}{\kappa_T}\}, \tag{2.27}$$

where $u_T = |\mathbf{u}|$ is the magnitude of the velocity on an element and κ_T is the diffusion coefficient on an element and τ is a specified positive constant. We will use a multi-dimensional approximation of τ_e motivated by variational multiscale stabilization techniques used in [42, 77]

$$\tau_e = \left[\left(2\frac{\|\rho(C)\mathbf{U} - \varepsilon\rho_0\mathbf{D}(\mathbf{U})\nabla C\|_2}{\Delta_e}\right)^2 + 9\left(4\frac{\|\rho(C)\mathbf{D}(\mathbf{U})\|_\infty}{\Delta_e^2}\right)^2 + \left(\frac{\rho(C)\phi + \epsilon\rho_0\phi C}{\Delta t}\right)^2\right]^{-1/2}. \tag{2.28}$$

Finally, in some cases, non-physical oscillations can still exist in the presence of steep fronts even with the SUPG stabilization so nonlinear residual-based shock capturing may be needed. We have implemented an isotropic shock capturing term [72] by adding on each element the term $(\nu\nabla c, \nabla w)_{\Omega_e}$ where $\nu = \nu_c\frac{\Delta_e}{2}\frac{|\mathcal{R}_\Delta|}{\|\nabla C\|_2}$. This is a residual based numerical diffusion method where $\mathcal{R}_\Delta$ is the strong residual approximation as defined above and ν_c is a problem-dependent parameter which we

set to $\nu_c = .25$ unless otherwise noted.

Using the above definitions, we can define the stabilized transportation weak form as

$$((\rho\phi c)_t, w)_\Omega + \mathcal{B}_S(c, w; \mathbf{u}, h) = \mathcal{L}_S(w), \tag{2.29}$$

where we define

$$\begin{aligned}
\mathcal{B}_S(c, w; \mathbf{u}, h) \equiv \mathcal{B}(c, w; \mathbf{u}, h) &+ \sum_{\Omega_e \in \mathcal{T}_\Delta} (\nu \nabla c, \nabla w)_{\Omega_e} \\
&+ \sum_{\Omega_e \in \mathcal{T}_\Delta} \left(\mathcal{L}_e(w), \tau_e \left[(\rho(c)\phi c)_t + \nabla \cdot (c\rho(c)\mathbf{u} - \rho(c)\mathbf{D}(\mathbf{u})\nabla c)\right]\right)_{\Omega_e}, \\
\mathcal{L}_S(w) \equiv \mathcal{L}(w) &+ \sum_{\Omega_e \in \mathcal{T}_\Delta} \left(\mathcal{L}_e(w), \tau_e c_s \rho_s Q_s\right)_{\Omega_e}.
\end{aligned}$$

2.3 Implementation Overview

2.3.1 Continuous in Time DG Formulation

We seek approximations $(H, \mathbf{U}, C)$ to our solutions $(h, \mathbf{u}, c)$ in the finite element space $\tilde{W} \times \tilde{\mathbf{V}} \times \tilde{W}$ given by

$$\begin{aligned}
\tilde{\mathbf{V}} \subset \mathbf{V} &= \{\tilde{\mathbf{v}} \in L^2(\Omega)^d : \tilde{\mathbf{v}}|_{\Omega_e} \in (\mathcal{P}^{k_e}(\Omega_e))^d, \forall \Omega_e \in \Omega\}, \\
\tilde{W} \subset W &= \{\tilde{w} \in L^2(\Omega) : \tilde{w}|_{\Omega_e} \in \mathcal{P}^{k_e}(\Omega_e), \forall \Omega_e \in \Omega\},
\end{aligned}$$

where $k_e \geq 1$. $\mathcal{P}^{k_e}(\Omega_e)$ consists of complete polynomials and k_e can vary from element to element. Using the weak formulation, the combined, semi-discrete DG formulation is stated as follows:

We seek approximations $C(\cdot,t), H(\cdot,t) \in \tilde{W}$, $\mathbf{U}(\cdot,t) \in \tilde{\mathbf{V}}$ which satisfy for $t > 0$

$$\begin{aligned}
(\rho S H_t, \tilde{w})_\Omega + \mathcal{A}_1(H, \mathbf{U}, \tilde{w}; C) &= \mathcal{L}_1(\tilde{w}; C), \quad \forall \tilde{w} \in \tilde{W}(\Omega), \\
\mathcal{A}_2(H, \mathbf{U}, \tilde{\mathbf{v}}; C) &= \mathcal{L}_2(\tilde{\mathbf{v}}; C), \quad \forall \tilde{\mathbf{v}} \in \tilde{\mathbf{V}}(\Omega), \\
((\rho\phi C)_t, w)_\Omega + \mathcal{B}(C, w; \mathbf{U}, H) &= \mathcal{L}(w), \quad \forall w \in \tilde{W}(\Omega).
\end{aligned} \tag{2.30}$$

Furthermore, $H(\mathbf{x}, 0)$ and $C(\mathbf{x}, 0)$ are defined to be the L^2 projections of $c^0(\mathbf{x})$ and $h^0(\mathbf{x})$, respectively and are defined by

$$\begin{aligned}
(H(\mathbf{x}, 0) - h^0(\mathbf{x}), \tilde{w})_\Omega &= 0, \quad \forall \tilde{w} \in \tilde{W}, \\
(C(\mathbf{x}, 0) - c^0(\mathbf{x}), w)_\Omega &= 0, \quad \forall w \in \tilde{W}.
\end{aligned}$$

2.3.2 Time Discretization

Numerous time-integration routines have been used in the variable density flow and transport literature. Explicit predictor-corrector and implicit θ-schemes are the most widely implemented. We will utilize an implicit $\theta-$scheme with $\theta = 1$, the backward Euler method. At time step, t^{n+1}, we approximate the time derivatives as

$$\frac{\partial m}{\partial t} \approx \frac{m^{n+1} - m^n}{t^{n+1} - t^n}$$

and all other terms in the spatial discretization are evaluated at t^{n+1}. This method is only first order in time and in future works we will explore higher order time integration techniques to improve method convergence and numerical efficiency.

2.3.3 Numerical Implementation

Using our semi-discrete equations and our time integration routine, we wish to define global discrete equations on a triangular or tetrahedral mesh. For development, we decompose our domain, Ω into N_e conforming, non-overlapping elements, Ω_e such that $\Omega \approx \mathcal{T}_\Delta = \cup_{e=1}^{n_e} \Omega_e$. Suppose $\tilde{W}(\Omega_e)$ consists of polynomials of degree k. Let $n_h = n_c$ denote the dimension of the space. Also, suppose $\tilde{V}(\Omega_e)$ consists of vector functions that are polynomials of degree k in each component. Denote n_u the dimension of the space. We denote $\psi_{e,l}$ a basis for $\tilde{W}$ and $\boldsymbol{\psi}_{e,l}$ a basis for $\tilde{V}$ where e denotes the element Ω_e and $l = 1, ..., n_i$ where $i = u, c, h$. Then our global approximation, $(H, \mathbf{U}, C)$ can be written as

$$\begin{aligned} H &= \sum_{e=1}^{N_e} \sum_{l=1}^{n_h} H_{e,l} \psi_{e,l}(\mathbf{x}), \\ \mathbf{U} &= \sum_{e=1}^{N_e} \sum_{l=1}^{n_u} U_{e,l} \boldsymbol{\psi}_{e,l}(\mathbf{x}), \\ C &= \sum_{e=1}^{N_e} \sum_{l=1}^{n_c} C_{e,l} \psi_{e,l}(\mathbf{x}), \end{aligned} \tag{2.31}$$

where $H_{e,l}, U_{e,l}, C_{e,l}$ are the degrees of freedom for the approximation. Locally, on each element, we will have $n_h + n_u + n_c$ degrees of freedom and we will have $N_e[n_h + n_u + n_c]$ degrees of freedom for the global system. Let $\mathbf{U}, \mathbf{H}$, and $\mathbf{C}$ denote the vectors of unknowns associated with the above approximations (2.31). Then, after introducing our time discretization, the flow equations can be written in the matrix form:

$$\mathbf{M}_{h,1}(\mathbf{C}^{n+1}) \frac{\mathbf{H}^{n+1} - \mathbf{H}^n}{\Delta t} + \mathbf{M}_{h,2} \mathbf{H}^{n+1} + \mathbf{A}_1(\mathbf{C}^{n+1}) \mathbf{U}^{n+1} = \mathbf{G}_1(\mathbf{C}^{n+1}), \tag{2.32}$$

$$\mathbf{A}_2 \mathbf{H}^{n+1} + \mathbf{M}_u \mathbf{U}^{n+1} = \mathbf{G}_2(\mathbf{C}^{n+1}), \tag{2.33}$$

where $\mathbf{M}_{h,1}(\mathbf{C})$ is a $(n_e*n_h)\times(n_e*n_h)$ block diagonal matrix. $\mathbf{M}_{h,2}$, $\mathbf{A}_1(\mathbf{C})$, $\mathbf{A}_2$ and $\mathbf{M}_u$ are sparse block matrices of dimension $(n_e*n_c)\times(n_e*n_c)$, $(n_e*n_u)\times(n_e*n_c)$, $(n_e*n_c)\times(n_e*n_u)$, and $(n_e*n_u)\times(n_e*n_c)$, respectively, with a maximum of $d+2$ non-zero block matrices in each row. $\mathbf{H}, \mathbf{G}_1(\mathbf{C})$ and $\mathbf{U}, \mathbf{G}_2(\mathbf{C})$ are vectors of dimension $(n_e*n_h)\times 1$ and $(n_e*n_u)\times 1$, respectively. Each matrix is defined as:

$$
\begin{aligned}
(\rho(C)SH_t, w)_\Omega &\Rightarrow \mathbf{M}_{h.1}\mathbf{H},\\
-(\rho(C)\mathbf{U}, \nabla w)_\Omega + \langle \{\!\{\rho(C)\mathbf{U}\}\!\}, [\![w]\!]\rangle_{\mathcal{E}_i} + \langle(\rho(C)\mathbf{U})\cdot\mathbf{n}, w\rangle_{\Gamma_D} &\Rightarrow \mathbf{A}_1\mathbf{U},\\
\langle\sigma_h [\![H]\!], [\![w]\!]\rangle_{\mathcal{E}_i} + \langle\sigma_h H, w\rangle_{\Gamma_D} &\Rightarrow \mathbf{M}_{h,2}\mathbf{H},\\
(f(C), w)_\Omega - \langle\rho(C)u^b, w\rangle_{\Gamma_N} + \langle\sigma_h h^b, w\rangle_{\Gamma_D} &\Rightarrow \mathbf{G}_1,\\
(\mathbf{K}^{-1}\mathbf{U}, \mathbf{v})_\Omega &\Rightarrow \mathbf{M}_u\mathbf{U},\\
-(H, \nabla\cdot\mathbf{v})_\Omega + \langle\{\!\{H\}\!\}, [\![\mathbf{v}]\!]\rangle_{\mathcal{E}_i} + \langle H, \mathbf{v}\cdot\mathbf{n}\rangle_{\Gamma_N} &\Rightarrow \mathbf{A}_2\mathbf{H},\\
-(\hat{\rho}\mathbf{e}_z, \mathbf{v})_\Omega - \langle h^b, \mathbf{v}\cdot\mathbf{n}\rangle_{\Gamma_D} &\Rightarrow \mathbf{G}_2.
\end{aligned}
$$

We note that with the introduction of the auxiliary variable, $\bar{\mathbf{u}} = \rho\mathbf{u}$, we have $\mathbf{A}_2 = -\mathbf{A}_1^T$ and we can write Equation 2.33 as $\mathbf{U} = \mathbf{M}_u^{-1}\mathbf{A}_1^T\mathbf{H} + \mathbf{M}_u^{-1}\mathbf{F}_2$ and substitute into Equation 2.32 to get a single matrix system involving $\mathbf{H}$:

$$
\begin{aligned}
\mathbf{M}_{h,1}(\mathbf{C}^{n+1})\frac{\mathbf{H}^{n+1}-\mathbf{H}^n}{\Delta t} &+ (\mathbf{M}_{h,2} + \mathbf{A}_1(\mathbf{C}^{n+1})\mathbf{M}_u^{-1}\mathbf{A}_1^T(\mathbf{C}^{n+1}))\mathbf{H}^{n+1}\\
&= \mathbf{G}_1(\mathbf{C}^{n+1}) - \mathbf{A}_1(\mathbf{C}^{n+1})\mathbf{M}_u^{-1}\mathbf{G}_2, \qquad (2.34)
\end{aligned}
$$

where $\mathbf{M}_{h,1} + \mathbf{A}_1\mathbf{M}_u^{-1}\mathbf{A}_1^T$ is a symmetric, positive definite matrix. Because of the localized nature of the DG approximation, this process can be done locally. In the next section, we will discuss specifically how this is done within the solution procedure.

For the transport equation, following a similar development, we obtain the nonlinear system

$$\frac{\Theta(\mathbf{C}^{n+1}) - \Theta(\mathbf{C}^n)}{\Delta t} + \mathbf{A}_3(\mathbf{C}^{n+1}, \mathbf{U}^{n+1})\mathbf{C}^{n+1} = \mathbf{G}_3, \tag{2.35}$$

where

$$\begin{aligned}
(\rho(C)\phi C, w)_\Omega \Rightarrow & \Theta(\mathbf{C}), \\
-(C\rho(C)\mathbf{u}, w)_\Omega + (\rho(C)\mathbf{D}\nabla C, w)_\Omega & \\
+\langle C^u \hat{\mathbf{q}}, [\![w]\!]\rangle_{\mathcal{E}_i} - \langle \{\!\{\rho(C)\mathbf{D}\nabla C\}\!\}, [\![w]\!]\rangle_{\mathcal{E}_i} & \\
+\langle \sigma_c [\![C]\!], [\![w]\!]\rangle_{\mathcal{E}_i} + \langle C\hat{\mathbf{q}}, w\rangle_{\Gamma_+} + \langle \{\!\{\rho(C)\mathbf{D}\nabla w\}\!\}, [\![C]\!]\rangle_{\mathcal{E}_i} \Rightarrow & \mathbf{A}_3\mathbf{C}, \\
(c_s\rho_s Q_s, w)_\Omega - \langle c_I\hat{\mathbf{q}}, w\rangle_{\Gamma_-} \Rightarrow & \mathbf{G}_3.
\end{aligned}$$

We note $\Theta(\mathbf{C})$ is a $(n_e * n_c) \times (n_e * n_c)$ block diagonal matrix consisting of $n_c \times n_c$ block matrices, $\mathbf{A}_3(\mathbf{U}, \mathbf{C}, \mathbf{H})$ is a sparse block matrix and both the solution vector $\mathbf{C}$ and right hand side vector $\mathbf{G}_3$ are $(n_e * n_c) \times 1$ vectors. Here we have emphasized the non-linear dependence of the coefficients.

2.3.4 Solution Procedure

Simultaneously solving the fully coupled, nonlinear system for the state variables is generally not applicable to large, 3D problems because of the computational costs. As discussed in Section 1, several methods have been utilized in the literature to solve the coupled system. Our solution method will implement a modified Newton iterative scheme in which the flow equations are reduced to a single system only involving the freshwater head degrees of freedom and this reduced system is solved

with the transport system. We will discuss the solution method in detail but first need to discuss how to locally reduce the flow system to a single equation involving **H**.

2.3.4.1 Flow System Reduction

The goal is to locally solve for the velocity degrees of freedom in terms of the freshwater head degrees of freedom and reduce the flow system to a single equation in terms of the head variable. Because of the discontinuous approximation spaces, this operation can be done locally. In this section, we present the method used in the solution algorithm. We start with the flow equations (Equations 2.15 and 2.16) which are in mixed form and then focus only on the steady state case with no source terms for this development:

$$\nabla \cdot \rho \mathbf{u} = 0,$$
$$\mathbf{u} = -\mathbf{K}\big(\nabla h + \frac{\rho - \rho_0}{\rho_0}\nabla z\big).$$

For simplification, we will assume **K**, the hydraulic conductivity tensor, is a diagonal matrix and we will consider two situations in which we either define the Darcy mass velocity, $\mathbf{q} = \rho\mathbf{u}$ or the Darcy velocity from the original formulation. We can write either situation in the general form:

$$\nabla \cdot \tilde{\mathbf{a}}\bar{\mathbf{u}} = 0,$$
$$\hat{\mathbf{a}}^{-1}\bar{\mathbf{u}} = -\nabla h - \frac{\rho - \rho_0}{\rho_0}\nabla z = -\nabla h - \hat{\rho}\nabla z,$$

where $\bar{\mathbf{u}} = \mathbf{q}$, $\tilde{\mathbf{a}} = \mathbf{I}$, and $\hat{\mathbf{a}} = \rho\mathbf{K}$ in the case of using the Darcy mass velocity variable or $\bar{\mathbf{u}} = \mathbf{u}$, $\tilde{\mathbf{a}} = \rho\mathbf{I}$, and $\hat{\mathbf{a}} = \mathbf{K}$.

Let $\Omega_e \in \mathcal{T}_h$ be an element in the partition of our domain $\Omega \in \mathbb{R}^3$ with boundary $\partial\Omega_e$. We multiply by test functions $w_h \in W_h(\Omega_e)$ and $\mathbf{w}_u \in (W_h(\Omega_e))^3$ to get

$$\begin{aligned}
&\int_{\Omega_e} \nabla \cdot \tilde{\mathbf{a}}\bar{\mathbf{u}} w_h dV = 0, \\
&\int_{\Omega_e} \hat{\mathbf{a}}^{-1}\bar{\mathbf{u}} \cdot \mathbf{w}_u dV = -\int_{\Omega_e} \left(\nabla h + \hat{\rho}\nabla z\right) \cdot \mathbf{w}_u dV \\
&\qquad\qquad = -\int_{\Omega_e} \nabla h \cdot \mathbf{w}_u dV - \int_{\Omega_e} \hat{\rho}\nabla z \cdot \mathbf{w}_u dV,
\end{aligned}$$

and integrating by parts gives the mixed weak form

$$-\int_{\Omega_e} \tilde{\mathbf{a}}\bar{\mathbf{u}} \cdot \nabla w_h dV + \int_{\partial\Omega_e} \widehat{\mathbf{q}} \cdot \mathbf{n} w_h dS = 0, \tag{2.36}$$

$$\int_{\Omega_e} \hat{\mathbf{a}}^{-1}\bar{\mathbf{u}} \cdot \mathbf{w}_u dV = \int_{\Omega_e} h\nabla \cdot \mathbf{w}_u dV - \int_{\partial\Omega_e} \hat{h}\mathbf{w}_u \cdot \mathbf{n} dS - \int_{\Omega_e} \hat{\rho}\nabla z \cdot \mathbf{w}_u dV, \tag{2.37}$$

where $\hat{\mathbf{q}}$ and $\hat{h}$ are the numerical flux and numerical trace, respectively, which we restate are

$$\hat{\mathbf{q}} = \begin{cases} \{\!\{\tilde{\mathbf{a}}\bar{\mathbf{u}}\}\!\} + \sigma_h [\![h]\!], & \gamma \in \partial\Omega_e \cap \mathcal{E}_i, \\ \rho(c) u_b, & \gamma \in \partial\Omega_e \cap \Gamma_N, \\ \tilde{\mathbf{a}}\bar{\mathbf{u}} \cdot \mathbf{n} + \sigma_h (h - h^b) & \gamma \in \partial\Omega_e \cap \Gamma_D, \end{cases}$$

and

$$\hat{h} = \begin{cases} \{\!\{h\}\!\}, & \gamma \in \partial\Omega_e \cap \mathcal{E}_i, \\ h, & \gamma \in \partial\Omega_e \cap \Gamma_N, \\ h^b, & \gamma \in \partial\Omega_e \cap \Gamma_D. \end{cases}$$

Using these definitions, we will locally solve for $\bar{\mathbf{u}}$ in terms of h. The idea is to reduce the mixed system to a scalar equation by solving for $\mathbf{u}$ as a function of h on each element before assembling and solving the global system. So, we write the elements of the basis for $(W_h)^3$ as

$$\mathbf{w}_{i,I} = w_i(x)\mathbf{e}_I, \quad \text{where} \quad i = 1, \ldots, n_h, \quad I = 1, 2, 3,$$

and $n_h = \dim(W_h)$. Substituting we have

$$\int_{\Omega_e} (\hat{\mathbf{a}}^{-1}\bar{\mathbf{u}})_I w_i dV = \int_{\Omega_e} h\frac{\partial w_i}{\partial x_I} dV - \int_{\partial\Omega_e} \hat{h} n^{x_I} w_i dS - \int_{\Omega_e} \hat{\rho}\delta_{I3} w_i dV, \tag{2.38}$$

with

$$\delta_{ij} = \begin{cases} 1, & i = j, \\ 0, & i \neq j. \end{cases}$$

We expand $\hat{\mathbf{u}}$ in our basis as

$$\bar{\mathbf{u}} = \sum_j \bar{\mathbf{U}}_j w_j(x)$$

and substitute into Equation 2.38 to get

$$\int_{\Omega_e} (\hat{\mathbf{a}}^{-1} \sum_j \bar{\mathbf{U}}_j w_j)_I w_i dV = \int_{\Omega_e} h\frac{\partial w_i}{\partial x_I} dV - \int_{\partial\Omega_e} \hat{h}\mathbf{n}_I w_i dS - \int_{\Omega_e} \hat{\rho}\delta_{I3} w_i dV.$$

Looking at the left hand side, we use linearity and expand the matrix product

$$\begin{aligned} \int_{\Omega_e} (\hat{\mathbf{a}}^{-1} \sum_j \bar{\mathbf{U}}_j w_j)_I w_i dV &= \sum_j \int_{\Omega_e} (\hat{\mathbf{a}}^{-1}\bar{\mathbf{U}}_j)_I w_j w_i dV \\ &= \sum_j \int_{\Omega_e} \sum_J (\hat{\mathbf{a}}^{-1})_{I,J} \bar{U}_{j,J} w_j w_i dV \\ &= \sum_j \sum_J \bar{U}_{j,J} \int_{\Omega_e} (\hat{\mathbf{a}}^{-1})_{I,J} w_j w_i dV, \end{aligned}$$

and so we have the final system of equations for the degrees of freedom of $\mathbf{u}$:

$$\sum_j \sum_J \bar{U}_{j,J} \int_{\Omega_e} (\hat{\mathbf{a}}^{-1})_{I,J} w_j w_i dV = \int_{\Omega_e} h\frac{\partial w_i}{\partial x_I} dV - \int_{\partial\Omega_e} \hat{h}\mathbf{n}_I w_i dS - \int_{\Omega_e} \hat{\rho}\delta_{I3} w_i dV,$$

or

$$\mathbf{A}\bar{\mathbf{U}} = \mathbf{B}\mathbf{H} + \mathbf{C} \equiv \mathbf{b}(\mathbf{H}),$$

where $\mathbf{H}$ is a $(\dim(W_h)*(d+1))\times 1$ vector consisting of the potential freshwater head degrees of freedom for the element and all neighboring elements, $\bar{\mathbf{U}}$ is a $(\dim(W_h)*d)\times 1$ vector consisting of the velocity degrees of freedom on the element and $\mathbf{b}(\mathbf{H})$ is a $(\dim(W_h)*d)\times 1$ vector which is computed in the numerical algorithm (here d is the spatial dimension).

We make the following remarks about the matrix $\mathbf{A}$ and the vector $\mathbf{b}(\mathbf{H})$. First, the integrals defining the matrix $\mathbf{A}$, which is of dimension $(d\cdot\dim(W_h))\times(d\times\dim(W_h))$, are independent of $\mathbf{H}$ but can depend on $\mathbf{C}$ depending on the type of splitting used. Second, the structure of $\mathbf{A}$ depends on the structure of $\mathbf{K}$ as well as the basis functions. In the variable density case with a diagonal hydraulic conductivity matrix, $\mathbf{A}$ is a block diagonal matrix. Also, since $\mathbf{K}$ does not depend on h, the system is linear in h. Lastly, the vector, $\mathbf{b}(\mathbf{H})$, because of the definition of the numerical trace $\hat{h}$, depends not only the values of $\mathbf{H}$ on Ω_e, but also the values of each element neighbor $\Omega_{e,i}$, where $i=d+1$ for triangular and tetrahedral conforming meshes. Based on these properties, our system simplifies to

$$\begin{aligned}\sum_j \bar{U}_{j,I}\int_{\Omega_e}(\hat{\mathbf{a}}^{-1})_{I,I}w_j w_i dV &= \int_{\Omega_e} h\frac{\partial w_i}{\partial x_I}dV - \int_{\partial\Omega_e}\hat{h}\mathbf{n}_I w_i dS - \int_{\Omega_e}\hat{\rho}\delta_{I3}w_i dV \\ &= \mathbf{b}_I(\mathbf{H}),\end{aligned} \tag{2.39}$$

or simply

$$\bar{U}_{j,I} = [\mathbf{A}_I^{-1}\mathbf{b}_I(\mathbf{H})]_j, \qquad I=1,2,3. \tag{2.40}$$

Jacobian Terms

Since we are using a Newton solution method, we must introduce the quadrature in order to develop the expressions for building the Jacobian matrix. The fully discrete boundary integral term is given by

$$\int_{\partial\Omega_e} \hat{h} n^{x_I} w_i dS = \sum_{k'} \hat{h}\big(\sum_j h_{e,j} w_{e,f,k',j}, \sum_j h_{e',f} w_{e',f,k',j}\big) w_{e,f,k',i} n^{x_I}_{e,f,k'} \Delta S_{e,f,k'} \tag{2.41}$$

for $I = 1, 2, 3$, where the indices e, e' correspond to interior and exterior elements, f the element face, k' the boundary quadrature point and j the degree of freedom. $\Delta S_{e,f,k'}$ are the quadrature weights. We differentiate with respect to the element degrees of freedom, $h_{e,j}$ to get

$$\frac{\partial(\int_{\partial\Omega_e} \hat{h} n^{x_I} w_i dS)}{\partial h_{e,j}} = \sum_{k'} \frac{\partial \hat{h}}{\partial h_{e,f,k'}} w_{e,f,k',j} w_{e,f,k',i} n^{x_I}_{e,f,k'} \Delta S_{e,f,k'} \tag{2.42}$$

$$= \frac{1}{2} w_{e,f,k',j} w_{e,f,k',i} n^{x_I}_{e,f,k'} \Delta S_{e,f,k'}, \tag{2.43}$$

and similarly with respect to each neighboring element degree of freedom, $h_{e',j}$ to get

$$\frac{\partial(\int_{\partial\Omega_e} \hat{h} n^{x_I} w_i dS)}{\partial h_{e',j}} = \sum_{k'} \frac{\partial \hat{h}}{\partial h_{e',f,k'}} w_{e',f,k',j} w_{e,f,k',i} n^{x_I}_{e,f,k'} \Delta S_{e,f,k'} \tag{2.44}$$

$$= \frac{1}{2} w_{e',f,k',j} w_{e,f,k',i} \mathbf{n}^{x_I}_{e,f,k'} \Delta S_{e,f,k'}. \tag{2.45}$$

The fully discrete element integral with the density term, assuming we know that mass fraction values at the quadrature points from the transport equation, is given by

$$\int_{\Omega_e} \hat{\rho} \delta_{I3} w_i dV = \sum_k \hat{\rho}(c_{e,k}) \delta_{I3} w_{e,k,i} \Delta V_{e,k}, \tag{2.46}$$

where $\Delta V_{e,k}$ are the element quadrature weights. Differentiation with respect to the freshwater head element degrees of freedom gives

$$\frac{\partial\big(\int_{\Omega_e}\hat{\rho}\delta_{I3}w_i dV\big)}{\partial h_{e,j}} = 0.$$

The last fully discrete element integral is given by

$$\int_{\Omega_e} h\frac{\partial w_i}{\partial x_I}dV = \sum_k \big(\sum_j h_{e,j}w_{e,k,j}\frac{\partial w_{e,k,i}}{\partial x_I}\Delta V_{e,k}\big),$$

and differentiating we obtain

$$\begin{aligned}\frac{\partial(\int_{\Omega_e} h\frac{\partial w_i}{\partial x_I}dV)}{\partial h_{e,j}} &= \sum_k \frac{\partial h}{\partial h_{e,j}}w_{e,k,j}\frac{\partial w_{e,k,i}}{\partial x_I}\Delta V_{e,k}\\ &= \sum_k w_{e,k,j}\frac{\partial w_{e,k,i}}{\partial x_I}\Delta V_{e,k}. \end{aligned} \tag{2.47}$$

Combining these rules we obtain the fully discrete $\mathbf{b}(h)$ and $\frac{\partial \mathbf{b}_I}{\partial h_{e,j}}$ for each element e and $\frac{\partial \mathbf{b}_I}{\partial h_{e',j}}$ for each e' sharing a face with e given as

$$\begin{aligned}\mathbf{b}_I(h) &= \sum_{k'}\hat{h}\big(\sum_j h_{e,j}w_{e,f,k',j}, \sum_j h_{e',f}w_{e',f,k',j}\big)w_{e,f,k',i}\mathbf{n}^{x_I}_{e,f,k'}\Delta S_{e,f,k'}\\ &\quad+\sum_k\bigg(-\hat{\rho}(c_{e,k})\delta_{I3}w_{e,k,i}\Delta V_{e,k}+\sum_j h_{e,j}w_{e,k,j}\frac{\partial w_{e,k,i}}{\partial x_I}\Delta V_{e,k}\bigg),\\ \frac{\partial \mathbf{b}_I}{\partial h_{e,j}} &= \sum_k w_{e,k,j}\frac{\partial w_{e,k,i}}{\partial x_I}\Delta V_{e,k}+\frac{1}{2}\sum_{k'}w_{e,f,k',j}w_{e,f,k',i}\mathbf{n}^{x_I}_{e,f,k'}\Delta S_{e,f,k'},\\ \frac{\partial \mathbf{b}_I}{\partial h_{e',j}} &= \frac{1}{2}\sum_{k'}w_{e',f,k',j}w_{e,f,k',i}\mathbf{n}^{x_I}_{e,f,k'}\Delta S_{e,f,k'},\end{aligned}$$

for $i = 1, ..., \dim(W_h)$. Next we get

$$\frac{\partial \bar{U}_{j,I}}{\partial h_{e,\tilde{j}}} = \left[A_I^{-1}\frac{\partial \mathbf{b}_I}{\partial h_{e,\tilde{j}}}\right]_j, \quad I = 1,2,3, \tag{2.48}$$

and likewise for each e'. Since $\bar{\mathbf{u}}_{e,f,k} = \sum_j \bar{U}_j w_{e,f,k,j}$, we obtain

$$\begin{aligned}\frac{\partial \bar{\mathbf{u}}_{e,f,k}}{\partial h_{e,\tilde{j}}} &= \sum_j \frac{\partial \bar{U}_{j,I}}{\partial h_{e,\tilde{j}}} w_{e,f,k,j} \\ &= \sum_j \left[A_I^{-1} \frac{\partial b_I}{\partial h_{e,\tilde{j}}} \right]_j w_{e,f,k,j}.\end{aligned}$$

Using the properties of $\tilde{\mathbf{a}}$, we compute

$$\begin{aligned}\frac{\partial (\{\!\{\tilde{\mathbf{a}}\bar{\mathbf{u}}\}\!\})_{e,f,k}}{\partial h_{e,\tilde{j}}} &= \frac{\partial (\{\!\{\tilde{\mathbf{a}}\bar{\mathbf{u}}\}\!\})_{e,f,k}}{\partial (\tilde{\mathbf{a}}\bar{\mathbf{u}})_{e,f,k}} \left(\frac{\partial \tilde{\mathbf{a}}}{\partial h_{e,\tilde{j}}} \bar{\mathbf{u}}_{e,f,k} + \tilde{\mathbf{a}} \frac{\partial \bar{\mathbf{u}}_{e,f,k}}{\partial h_{e,\tilde{j}}} \right) \\ &= \frac{\partial (\{\!\{\tilde{\mathbf{a}}\bar{\mathbf{u}}\}\!\})_{e,f,k}}{\partial (\tilde{\mathbf{a}}\bar{\mathbf{u}})_{e,f,k}} \tilde{\mathbf{a}}(c_{e,f,k}) \sum_j \left[A_I^{-1} \frac{\partial b_I}{\partial h_{e,\tilde{j}}} \right]_j w_{e,f,k,j} \qquad (2.49) \\ &= \frac{1}{2} \tilde{\mathbf{a}}(c_{e,f,k}) \sum_j \left[A_I^{-1} \frac{\partial b_I}{\partial h_{e,\tilde{j}}} \right]_j w_{e,f,k,j}, \qquad (2.50)\end{aligned}$$

and likewise for e'. Utilizing these results and the definition of the numerical flux, we build the flux and element integrals for the global residual and Jacobian in terms of the single head variable which are used in the Newton interative method.

2.3.4.2 Iterative Solution Method

As discussed previously, we utilize a modified Newton method to solve the simplified non-linear system. Using Equations 2.34 and 2.35, we define the following discrete weak residuals:

$$\begin{aligned}\boldsymbol{\mathcal{R}}_F^k(\mathbf{C},\mathbf{H}) &= \mathbf{M}_{h,1}(\mathbf{C}^{n+1,k}) \frac{\mathbf{H}^{n+1,k} - \mathbf{H}^{n+1,0}}{\Delta t} \\ &\quad + (\mathbf{M}_{h,2} + \mathbf{A}_1(\mathbf{C}^{n+1,k}) \mathbf{M}_u^{-1} \mathbf{A}_1^T(\mathbf{C}^{n+1,k})) \mathbf{H}^{n+1,k} \\ &\quad - \mathbf{G}_1(\mathbf{C}^{n+1,k}) - \mathbf{A}_1(\mathbf{C}^{n+1,k}) \mathbf{M}_u^{-1} \mathbf{G}_2, \\ \boldsymbol{\mathcal{R}}_T^k(\mathbf{C},\mathbf{U},\mathbf{H}) &= \frac{\Theta(\mathbf{C}^{n+1,k}) - \Theta(\mathbf{C}^{n+1,0})}{\Delta t} \\ &\quad + \mathbf{A}_3(\mathbf{C}^{n+1,k}, \mathbf{U}^{n+1,k}, \mathbf{H}^{n+1,k}) \mathbf{C}^{n+1,k} - \mathbf{G}_3,\end{aligned}$$

where n is the current time level and the system residual at iteration k is given by $\boldsymbol{\mathcal{R}}^k(\mathbf{H},\mathbf{U},\mathbf{C}) = [\boldsymbol{\mathcal{R}}_F^k, \boldsymbol{\mathcal{R}}_T^k]^T$. We also define our Jacobian matrices, $\boldsymbol{\mathcal{J}}_*^k$ with entries given as

$$\mathcal{J}_{H,i,j}^k(H,C) = \frac{\partial \mathcal{R}_{F,j}^k}{\partial H_i^{n+1,k}},$$
$$\mathcal{J}_{C,i,j}^k(C,H,\mathbf{U}) = \frac{\partial \mathcal{R}_{C,j}^k}{\partial C_i^{n+1,k}}.$$

Finally, defining our Newton iterates $\delta\mathbf{H} \equiv \mathbf{H}^{n+1,k+1} - \mathbf{H}^{n+1,k}$ and $\delta\mathbf{C} \equiv \mathbf{C}^{n+1,k+1} - \mathbf{C}^{n+1,k}$, the coupling algorithm consists of the following steps:

1. Initialize Iteration Values: $\boldsymbol{\rho}^{n+1,0} = \boldsymbol{\rho}(\mathbf{C}^n)$, $\mathbf{H}^{n+1,0} = \mathbf{H}^n$,and $\mathbf{C}^{n+1,0} = \mathbf{C}^n$.

2. For $k = 1, 2...$ until convergence:

    i. Solve the linearized flow system for $\delta\mathbf{H}$:

        a. Solve for the degrees of freedom of $\mathbf{U}$ in terms of $\mathbf{H}$ to get Equation 2.34.

        b. Solve the linear system for $\delta\mathbf{H}$:

$$\boldsymbol{\mathcal{J}}_H^k(H^{n+1,k}, C^{n+1,k})\delta\mathbf{H} = -\boldsymbol{\mathcal{R}}_F^k(\mathbf{C}^{n+1,k}, \mathbf{H}^{n+1,k}). \tag{2.51}$$

    ii. Update the head: $\mathbf{H}^{n+1,k+1} = \delta\mathbf{H} + \mathbf{H}^{n+1,k}$.

    iii. Update $\mathbf{U}^{n+1,k+1}$ utilizing $\mathbf{H}^{n+1,k+1}, \mathbf{C}^{n+1,k}$.

    iv. Solve linearized transport system for $\delta\mathbf{C}$ using $\mathbf{U}^{n+1,k+1}, \mathbf{H}^{n+1,k+1}$, $\boldsymbol{\rho}^{n+1,k}$:

$$\boldsymbol{\mathcal{J}}_C^k(\mathbf{C}^{n+1,k}, \mathbf{U}^{n+1,k+1})\delta C = -\boldsymbol{\mathcal{R}}_T^k(C^{n+1,k}, \mathbf{U}^{n+1,k+1}). \tag{2.52}$$

v. Update the mass fraction, $\mathbf{C}^{n+1,k+1} = \delta\mathbf{C} + \mathbf{C}^{n+1,k}$.

vi. Update the density, $\boldsymbol{\rho}^{n+1,k+1} = \boldsymbol{\rho}(\mathbf{C}^{n+1,k+1})$.

vii. Test for Convergence by testing $\|\boldsymbol{\mathcal{R}}^{k+1}\| < \tau_s$ for some suitable error tolerances τ_s.

2.3.5 Implementation Software

The numerical model is implemented using the Proteus Computational Mechanics Toolkit software (Proteus) developed at the USACE Engineer Research and Development Center Coastal and Hydraulics Lab (ERDC-CHL) [78]. Proteus is a Python package designed for rapidly developing computer models and numerical methods. Its primary focus is on models of continuum mechanical processes described by partial differential equations and on discretizations and solvers for computing approximate solutions to these equations. It contains a collection of Python modules implemented in C, C++, Fortran and Python. It has the ability to generate irregular triangular and tetrahedral meshes with different material properties using the Triangle and TETGEN software which can be used to implement block heterogeneity of a porous medium. The code is parallelized using the Message Passing Interface (MPI) and the Portable, Extensible Toolkit for Scientific Computation (PETSc).

For our numerical method, the algebraic system of equations in the solution algorithm is built and solved using Proteus. Element integrals in all problems are approximated using Gaussian quadrature that is exact for the integrand of highest polynomial order in the weak formulation. The weak residuals and Jacobian ma-

trices are constructed for the Newton Solver and the linear systems of equations (2.51 and 2.52) are solved using several different linear solvers. For 2D and smaller 3D problems, a sparse matrix solver from PETSc [13, 14, 15] was utilized (for single processor runs we used SuperLU and for parallel cases we used SuperLU_DIST [51, 90]). For large 3D problems, because the transport system is non-symmetric, the PETSc stabilized, bi-conjugate gradient method (bcgsl) linear solver with an additive Schwarz method preconditioner was utilized. It was also applied to the flow system for convenience. A fixed time step was utilized for simulations and both unstructured and structured spatial meshes were utilized and are annotated in each of the following problems. Simulations were run in serial and parallel on multiple platforms to include the Texas Advanced Computing Center Sun Constellation Cluster "Ranger" and the Linux Cluster "Lonestar". We discuss the numerical results in Chapter 4. In the next chapter, we will analyze some of the properties of the coupled DG method.

Chapter 3

Method Analysis

This chapter contains an analysis of the coupled DG approximation. Separately, the LDG method and the NIPG method have been analyzed in a number of works as previously discussed in Section 1.2.3. In this section, we will show several properties of the continuous-in-time coupled DG formulation: consistency, compatibility and convergence rates. All of these properties are essential to the performance of the method. We will begin by looking at the consistency of the method.

3.1 Consistency Analysis

If the DG formulation is *consistent*, then the true solution to the IBVP will also satisfy the DG formulation. We show here that the conservative formulation is consistent and the proof for the non-conservative formulation is similar.

Lemma 3.1.1. *If* $(h, \mathbf{u}, c) \in H^1(0,T;H^2(\Omega_e)) \times H^1(0,T;H^2(\Omega_e))^d \times H^1(0,T;H^2(\Omega_e))$, *is the solution to the IBVP (2.15-2.17), then* $(h, \mathbf{u}, c)$ *satisfies the semi-discrete DG formulation (2.30).*

Proof. The consistency of the formulation follows from the consistency of the numerical fluxes. Assume that $(h, \mathbf{u}, c) \in H^1(0,T;H^2(\Omega_e)) \times H^1(0,T;H^2(\Omega_e))^d \times H^1(0,T;H^2(\Omega_e))$ is a solution to (2.15-2.17) and let $(w, v, \tilde{w}) \in W \times \mathbf{V} \times W$ be test

functions. Looking at our semi-discrete method, we have:

$$\begin{aligned}
(\rho S h_t, w)_\Omega + \mathcal{A}_1(h, \mathbf{u}, w; c) &= \mathcal{L}_1(w; c), \quad \forall w \in \tilde{W}(\Omega), \\
\mathcal{A}_2(h, \mathbf{u}, c; \mathbf{v}) &= \mathcal{L}_2(\mathbf{v}; c), \quad \forall \mathbf{v} \in \tilde{\mathbf{V}}(\Omega), \\
((\rho\phi c)_t, w)_\Omega + \mathcal{B}(c, w; \mathbf{u}, h) &= \mathcal{L}(w), \quad \forall w \in \tilde{W}(\Omega).
\end{aligned}$$

The continuity of $(h, \mathbf{u}, c)$ gives $c^u = c$, $\{\!\{c\}\!\} = \mathbf{c}$ and $[\![c]\!] = 0$ (and likewise for $\mathbf{u}, h$). Using this, the definition of the time derivative

$$(\rho\phi)_t = \rho S h_t + \phi \frac{\partial \rho}{\partial c} c_t \tag{3.1}$$

and that our solution satisfies the boundary conditions, the formulation simplifies to:

$$\begin{aligned}
((\rho\phi)_t, w)_\Omega - (\rho\mathbf{u}, \nabla w)_\Omega + \langle \rho\mathbf{u}, [\![w]\!] \rangle_{\mathcal{E}_i} + \langle (\rho\mathbf{u}) \cdot \mathbf{n}, w \rangle_{\Gamma_D} &= (\rho_s Q_s, w)_\Omega \\
&\quad - \langle \rho u^b, w \rangle_{\Gamma_N}, \\
(\mathbf{K}^{-1}\mathbf{u}, \mathbf{v})_\Omega - (h, \nabla \cdot \mathbf{v})_\Omega + \langle h, [\![\mathbf{v}]\!] \rangle_{\mathcal{E}_i} + \langle h, \mathbf{v} \cdot \mathbf{n} \rangle_{\Gamma_N} &= -(\hat{\rho}\mathbf{e}_z, \mathbf{v})_{\Omega_e} \\
&\quad - \langle h^b, \mathbf{v} \cdot \mathbf{n} \rangle_{\Gamma_D}, \\
((\rho\phi c)_t, w)_\Omega - (c\rho\mathbf{u}, \nabla w)_\Omega + (\rho\mathbf{D}\nabla c, \nabla w)_\Omega + \langle \rho c\mathbf{u}, [\![w]\!] \rangle_{\mathcal{E}_i} & \\
+ \langle c_I \hat{\mathbf{q}}, w \rangle_{\Gamma_+} - \langle \rho\mathbf{D}\nabla c, [\![w]\!] \rangle_{\mathcal{E}_i} &= (c_s \rho_s Q_s, w)_\Omega \\
&\quad - \langle c_I \hat{\mathbf{q}}, w \rangle_{\Gamma_-},
\end{aligned}$$

or on each element we have

$$\begin{aligned}
(\rho S h_t, w)_{\Omega_e} - (\rho\mathbf{u}, \nabla w)_{\Omega_e} + \langle \rho\mathbf{u} \cdot \mathbf{n}, w \rangle_{\partial\Omega_e} &= (\rho_s Q_s, w)_{\Omega_e}, \\
(\mathbf{K}^{-1}\mathbf{u}, \mathbf{v})_{\Omega_e} - (h, \nabla \cdot \mathbf{v})_{\Omega_e} + \langle h, \mathbf{v} \cdot \mathbf{n} \rangle_{\partial\Omega_e} &= -(\hat{\rho}\mathbf{e}_z, \mathbf{v})_{\Omega_e}, \\
((\rho\phi c)_t, w)_{\Omega_e} - (c\rho\mathbf{u} - \rho\mathbf{D}\nabla c, \nabla w)_{\Omega_e} + \langle (\rho c\mathbf{u} - \rho\mathbf{D}\nabla c) \cdot \mathbf{n}, w \rangle_{\partial\Omega_e} &= (c_s \rho_s Q_s, w)_{\Omega_e}.
\end{aligned}$$

Applying Green's theorem on each element Ω_e gives

$$(\rho S h_t + \nabla \cdot \rho \mathbf{u} - f, w)_{\Omega_e} = 0,$$

$$(\mathbf{K}^{-1}\mathbf{u} + \nabla h + \hat{\rho}\mathbf{e}_z, \mathbf{v})_{\Omega_e} = 0,$$

$$((\rho\phi c)_t + \nabla \cdot (c\rho\mathbf{u} - \rho\mathbf{D}\nabla c) - c_s\rho_s Q_s, w)_{\Omega_e} = 0,$$

which is satisfied by assumption. The initial conditions are trivially satisfied. □

3.2 Flow and Transport Model Compatibility

If the flow and transport algorithms are not compatible, a loss of accuracy and/or a loss of global conservation can occur[49]. We define "global conservation" in the following sense. Let $(\mathbf{u}, h, c)$ be the smooth solution to the IBVP (2.15-2.17). Integrating the transport equation (2.17) over $\Omega \times (0, T]$, applying the divergence theorem to the divergence term and applying the boundary conditions, we have:

$$\int_0^T \int_\Omega (\rho\phi c)_t dx dt + \int_0^T \int_{\Gamma_+} \rho c \mathbf{u} \cdot \mathbf{n} ds dt + \int_0^T \int_{\partial\Gamma_-} c_I \rho \mathbf{u} \cdot \mathbf{n} ds dt = \int_0^T \int_\Omega c_s \rho_s Q_s dx dt,$$

or

$$\int_\Omega \rho(c(x,T))\phi(x)c(x,T)dx + \int_0^T \int_{\Gamma_+} c\rho\mathbf{u} \cdot \mathbf{n} ds dt = \int_\Omega \rho(x,0)\phi(x)c(x,0)dx - \int_0^T \int_{\Gamma_-} c_I \rho \mathbf{u} \cdot \mathbf{n} ds dt + \int_0^T \int_\Omega \rho_s c_s Q_s(x,t) dx dt, \tag{3.2}$$

which says that mass is conserved globally for all time.

Now, for the transport DG formulation (2.23), if we let $w \equiv 1$ and introduce

the true flow solution, $(\mathbf{u}, h)$, we have

$$((\rho(C)\phi C)_t, 1)_\Omega + (\rho(C)C\mathbf{u}\cdot\mathbf{n}, 1)_{\Gamma_+} + (\rho(C)C\mathbf{u}\cdot\mathbf{n}, 1)_{\Gamma_-} = (c_s\rho_s Q_s, 1)_\Omega. \quad (3.3)$$

Integrating over $(0, T]$, we recover (3.2):

$$\begin{aligned}\int_\Omega \rho(C(x,T))\phi(x)C(x,T)dx + \int_0^T \int_{\Gamma_+} \rho C\mathbf{u}\cdot\mathbf{n} ds dt \\ = \int_\Omega \rho(C(x,0))\phi(x)C(x,0)dx - \int_0^T \int_{\Gamma_-} c_I\rho_I\mathbf{u}\cdot\mathbf{n} ds dt + \int_0^T \int_\Omega \rho_s c_s Q_s dx dt.\end{aligned} \quad (3.4)$$

If we replace $(\mathbf{U}, H) \approx (\mathbf{u}, h)$ in our scheme, do we still have the accuracy and conservation properties? We follow Dawson and coauthors [49] where they define a flow and transport formulation as compatible if the two criteria are met:

- The transport formulation is globally conservative in the sense of (3.4) when we have an approximate velocity U from the flow formulation.
- The method is *zeroth-order* accurate, i.e., if the true concentration solution is identically a constant, the method gives a constant solution.

In [49], the authors showed these results for several different numerical schemes for linear flow and transport without coupling. In this case, the existence of a constant transport solution implied uniqueness. However, in the case of the coupled, non-linear system, we will relax the definition of zeroth order accuracy due to the difficulties in proving the constant solution's uniqueness. Our result is restricted to the case where the flow approximation space is contained in the transport space and where the concentration boundary conditions and initial conditions are the same

constant value. In this case, we show that if the flow field satisfies the LDG formulation, then the transport formulation will admit a constant solution. In simpler terms, under the specific conditions, the method produces the "right" type of solution, a constant concentration solution, but we do not show the uniqueness of this solution. Using this relaxed definition, we have the following compatibility result.

Lemma 3.2.1. *The semi-discrete DG transport formulation and the LDG flow formulation are compatible.*

Proof. Let $u \equiv \mathbf{U}$ as defined by the approximation from the LDG flow method and assume that the flow approximation space is contained in the transportation approximation space. Then, in the DG transport formulation, we have:

$$\begin{aligned}((\rho(C)\phi C)_t, w)_\Omega + (\rho(C)C\mathbf{U} - \rho(C)\mathbf{D}\nabla C, \nabla w)_\Omega + \langle C^u\hat{\mathbf{q}}, [\![w]\!]\rangle_{\mathcal{E}_i} \\ - \langle \{\!\{\rho(C)\mathbf{D}\nabla C\}\!\}, [\![w]\!]\rangle_{\mathcal{E}_i} + \langle [\![C]\!], [\![w]\!]\rangle_{\mathcal{E}_i} \\ + \langle C\hat{\mathbf{q}}, w\rangle_{\Gamma^+} + \langle C_I\hat{\mathbf{q}}, w\rangle_{\Gamma^-} = (c_s\rho_s Q_s, w)_\Omega. \end{aligned} \tag{3.5}$$

If we define $w \equiv 1$, we have

$$((\rho(C)\phi C)_t, 1)_\Omega + \langle C\hat{\mathbf{q}}, 1\rangle_{\Gamma^+} + \langle C_I\hat{\mathbf{q}}, 1\rangle_{\Gamma^-} = (c_s\rho_s Q_s, 1)_\Omega \tag{3.6}$$

and integrating over the time interval $[0, T]$, we have

$$\begin{aligned}((\rho(C(T))\phi C(T), 1)_\Omega + \int_0^T \langle C\hat{\mathbf{q}}, w\rangle_{\Gamma^+} = (\rho(C(0))\phi C(0), 1)_\Omega - \int_0^T \langle C_I\hat{\mathbf{q}}, 1\rangle_{\Gamma^-} \\ + \int_0^T (c_s\rho_s Q_s, 1)_\Omega, \end{aligned} \tag{3.7}$$

which gives the global conservation independent of how $\mathbf{U}$ is computed.

To show the modified zeroth order accuracy result, we first let $c_I = c_s \equiv$

$\bar{C}$, where $\bar{C}$ is a non-zero, constant concentration. Under these conditions, the concentration true solution should be identically a constant, $\bar{C}$. Applying these conditions to the flow formulation gives

$$(\rho(C)SH_t + \phi\frac{\partial\rho}{\partial C}C_t, w)_\Omega + (\rho(C)\mathbf{U}, \nabla w)_\Omega + \langle\hat{\mathbf{q}}, [\![w]\!]\rangle_{\mathcal{E}_i} + \langle\hat{\mathbf{q}}, w\rangle_{\Gamma^D} + \langle\hat{\mathbf{q}}, w\rangle_{\Gamma^N} = (\rho_s(\bar{C})Q_s, w)_\Omega, \tag{3.8}$$

where C is the approximate solution. Multiplying Equation (3.8) by $\bar{C}$, we have

$$\begin{aligned}(\bar{C}\rho(C)SH_t + \bar{C}\phi\frac{\partial\rho}{\partial C}C_t, w)_\Omega + (\bar{C}\rho(C)\mathbf{U}, \nabla w)_\Omega + \langle\bar{C}\hat{\mathbf{q}}, [\![w]\!]\rangle_{\mathcal{E}_i} \\ + \langle\bar{C}\hat{\mathbf{q}}, w\rangle_{\Gamma^D} + \langle\bar{C}\hat{\mathbf{q}}, w\rangle_{\Gamma^N} \\ = (\bar{C}\rho_s(\bar{C})Q_s, w)_\Omega.\end{aligned} \tag{3.9}$$

Now, turning to the transport weak formulation, with the given initial and boundary conditions, we have

$$\begin{aligned}((\rho(C)\phi C)_t, w)_\Omega - (C\rho(C)\mathbf{U}, \nabla w)_\Omega + (\rho(C)\mathbf{D}\nabla C, \nabla w)_\Omega + \langle C^u\hat{\mathbf{q}}, [\![w]\!]\rangle_{\mathcal{E}_i} \\ - \langle\{\!\{\rho(C)\mathbf{D}\nabla C\}\!\}, [\![w]\!]\rangle_{\mathcal{E}_i} \\ + \langle\sigma_c [\![C]\!], [\![w]\!]\rangle_{\mathcal{E}_i} + \langle C\hat{\mathbf{q}}, w\rangle_{\Gamma_+} + \langle\{\!\{\rho\mathbf{D}\nabla w\}\!\}, [\![C]\!]\rangle_{\mathcal{E}_i} \\ = (\bar{C}\rho_s Q_s, w)_\Omega - \langle\bar{C}\hat{\mathbf{q}}, w\rangle_{\Gamma_-}.\end{aligned} \tag{3.10}$$

Letting $C = \bar{C}$ and substituting into Equation (3.10) gives

$$\begin{aligned}((\rho(\bar{C})\phi\bar{C})_t, w)_\Omega - (\bar{C}\rho(\bar{C})\mathbf{u}, \nabla w)_\Omega + (\rho(\bar{C})\mathbf{D}\nabla C, \nabla w)_\Omega \\ + \langle\bar{C}\hat{\mathbf{q}}, [\![w]\!]\rangle_{\mathcal{E}_i} - \langle\{\!\{\rho(\bar{C})\mathbf{D}\nabla\bar{C}\}\!\}, [\![w]\!]\rangle_{\mathcal{E}_i} \\ + \langle\sigma_c [\![\bar{C}]\!], [\![w]\!]\rangle_{\mathcal{E}_i} + \langle\bar{C}\hat{\mathbf{q}}, w\rangle_{\Gamma_+} + \langle\{\!\{\rho(\bar{C})\mathbf{D}\nabla w\}\!\}, [\![\bar{C}]\!]\rangle_{\mathcal{E}_i} \\ = (\bar{C}\rho_s Q_s, w)_\Omega - \langle\bar{C}\hat{\mathbf{q}}, w\rangle_{\Gamma_-}\end{aligned} \tag{3.11}$$

or

$$((\rho(\bar{C})\phi\bar{C})_t, w)_\Omega - (\bar{C}\rho(\bar{C})\mathbf{u}, \nabla w)_\Omega + \langle \bar{C}\hat{\mathbf{q}}, [\![w]\!]\rangle_{\mathcal{E}_i} + \langle \bar{C}\hat{\mathbf{q}}, w\rangle_{\Gamma_+} - \langle \bar{C}\hat{\mathbf{q}}, w\rangle_{\Gamma_-}$$
$$= (\bar{C}\rho_s Q_s, w)_\Omega. \tag{3.12}$$

If we apply the definition of the flow mass time derivative (3.1) with $\bar{C}$ constant, we arrive at

$$(\bar{C}\rho(\bar{C})SH_t, w)_\Omega + (\bar{C}\rho(\bar{C})\mathbf{U}, \nabla w)_\Omega + \langle \bar{C}\hat{\mathbf{q}}, [\![w]\!]\rangle_{\mathcal{E}_i} + \langle \bar{C}\hat{\mathbf{q}}, w\rangle_{\Gamma^+} + \langle \bar{C}\hat{\mathbf{q}}, w\rangle_{\Gamma^-}$$
$$- (\bar{C}\rho_s(\bar{C})Q_s, w)_\Omega = 0. \tag{3.13}$$

Comparing Equations (3.9) and (3.13), we see if the flow system is satisfied with a constant concentration solution, then the transport equation is satisfied and we have our result. □

3.3 An *a Priori* Error Estimate

In this section, we analyze the error in the continuous in time coupled DG approximation. We develop the error equations and then prove an *a priori* error bound for the coupled DG formulation. Since this is the first formulation to our knowledge of a couple DG formulation for the variable density system, there is no analysis of this specific formulation. However, Sun and Wheeler in [119] analyzed a coupled, continuous in time DG method for the ground water flow and reactive transport system. We use a similar method, using a velocity cut-off operator to treat the coupling of the flow and transport. However, unlike the system they analyzed, the flow equation is not in primal form so there is no velocity post-processing step which allows the opportunity to get a velocity error bound. As a result, we use a

different approach. Also, because of the non-linearity of the system, the error bound that is proved is dependent on the primary coupling parameter in the system, the density constract ϵ. In this section, we initially present a modified formulation of the model to assist in the analysis and state assumptions on the solution and coefficients. We develop the error equations and state the error estimate with a sketch of the proof here and then present the detailed proof in Appendix 1. We begin with some preliminaries and reiterate some notation presented earlier.

3.3.1 Preliminaries

Let $\Omega \in \mathbb{R}^d$ with boundary $\partial\Omega$. Let $\{\mathcal{T}_\Delta\}_{\Delta>0}$ be a family of regular quasi-uniform, possibly non-conforming, partitions of Ω such that no individual element crosses $\partial\Omega$. For $d = 2$, $\mathcal{T}_\Delta$ will contain triangles and for $d = 3$, tetrahedra. Let Δ_e denote the element diameter of $\Omega_e \in \mathcal{T}_\Delta$ with Δ signifying the maximum diameter over all $\Omega_e \in \mathcal{T}_\Delta$. We assume that each triangulation is locally quasi-uniform in the following sense. There exists a $\tau \geq 0$ such that $\Delta/\Delta_e \leq \tau$ for all $\Delta_e \in \mathcal{T}_\Delta$.
We use the previously defined function spaces which we reiterate with some additional notation. If we define $W_{\Omega_e} = H^s(\Omega_e)$, $s \geq 1$ and $\mathbf{V}_{\Omega_e} = (W_{\Omega_e})^d$, then we can define the standard DG function spaces

$$W = \{w \in L^2(\Omega) : \text{ on each } \Omega_e \in \mathcal{T}_\Delta, w \in W_{\Omega_e}\},$$
$$\mathbf{V} = \{\mathbf{v} \in (L^2(\Omega))^d : \text{ on each } \Omega_e \in \mathcal{T}_\Delta, \mathbf{v} \in \mathbf{V}_{\Omega_e}\}.$$

We seek approximations $(H, \mathbf{U}, C)$ to our solutions $(h, \mathbf{u}, c)$ in the finite element space $\tilde{W} \times \tilde{\mathbf{V}} \times \tilde{W}$ given by

$$\tilde{\mathbf{V}} \subset \mathbf{V} = \{\tilde{\mathbf{v}} \in L^2(\Omega)^d : \tilde{\mathbf{v}}|_{\Omega_e} \in (\mathcal{P}^{k_e}(\Omega_e))^d, \forall \Omega_e \in \mathcal{T}_\Delta\},$$
$$\tilde{W} \subset W = \{\tilde{w} \in L^2(\Omega) : \tilde{w}|_{\Omega_e} \in \mathcal{P}^{k_e}(\Omega_e), \forall \Omega_e \in \mathcal{T}_\Delta\},$$

where $k_e \geq 1$ can vary on each element. Let $(\cdot, \cdot)_{\Omega_e}$ denote the $L_2(\Omega_e)$ scalar (or $L_2(\Omega_e)^d$ vector) inner product, $\langle \cdot, \cdot \rangle_{\partial\Omega_e}$ the $L_2(\partial\Omega_e)$ scalar (or $L_2(\partial\Omega_e)^d$ vector) inner product and $\|\cdot\|_{0,\Omega_e}$ corresponding $L_2(\Omega_e)$ norm. For simplicity, we use similar notation for the "broken" norm over the entire space, $\|\cdot\|_{0,\Omega} = \sum_{\Omega_e \in \mathcal{T}_\Delta} \|\cdot\|_{0,\Omega_e}$. For $\mathbf{u} \in (L_2(\Omega))^d$, we define the vector norm

$$\|\mathbf{u}\|_{(L_2(\Omega))^d} \equiv \| |\mathbf{u}| \|_{0,\Omega}\,, \tag{3.14}$$

where $|\mathbf{u}| = (\mathbf{u} \cdot \mathbf{u})^{1/2}$ is the standard vector norm. For matrix valued functions $\mathbf{D}(\mathbf{u}) \in (L_2(\Omega))^{d \times d}$, we define the norm

$$\|\mathbf{D}\|_{(L_2(\Omega))^{d\times d}} \equiv \| \|\mathbf{D}\|_2 \|_{0,\Omega}\,, \tag{3.15}$$

where $\|\mathbf{D}\|_2 \equiv \sup_{|\mathbf{v}|=1} |\mathbf{D}\mathbf{v}|$, the matrix norm consistent with the defined vector norm. For simplicity, we will use the same notation for scalar, vector and matrix norms where the appropriate form is understood by the argument of the norm. Let $[0, T]$ denote a time interval where $T > 0$ is a fixed constant.

To facilitate the proof, we introduce an auxiliary variable, $\mathbf{q} \equiv \rho(c)\mathbf{u}$, the Darcy *mass* velocity, and the equivalent approximation $\mathbf{Q} = \rho(C)\mathbf{U}$. Using this auxiliary variable, our semi-discrete DG formulation is given by:

Find approximations $(H(\cdot,t),\mathbf{Q}(\cdot,t),C(\cdot,t)) \approx (h,\mathbf{q},c)$ such that for $t=0$

$$\begin{cases} (H(\cdot,0)-h^0(\cdot),\tilde{w})_\Omega = 0, & \forall \tilde{w}\in\tilde{W}, \\ (C(\cdot,0)-c^0(\cdot),w)_\Omega = 0, & \forall w\in\tilde{W}, \end{cases}$$

and for $t>0$:

$$\begin{cases} (\rho(C)SH_t,\tilde{w})_\Omega - (\mathbf{Q},\nabla\tilde{w})_\Omega + \left\langle \{\!\{\mathbf{Q}\}\!\}, [\![\tilde{w}]\!] \right\rangle_{\mathcal{E}_i} + \left\langle \sigma_h [\![H]\!], [\![\tilde{w}]\!] \right\rangle_{\mathcal{E}_i} \\ \qquad + \left\langle \mathbf{Q}\cdot\mathbf{n},\tilde{w}\right\rangle_{\Gamma_D} + \left\langle \sigma_h H,\tilde{w}\right\rangle_{\Gamma_D} \\ \qquad = (\rho_s Q_s - \phi\frac{\partial\rho}{\partial C}C_t,\tilde{w})_\Omega + \left\langle \sigma_h h^b,\tilde{w}\right\rangle_{\Gamma_D} - \left\langle \rho(C)u^b,\tilde{w}\right\rangle_{\Gamma_N}, & \forall\tilde{w}\in\tilde{W}(\Omega), \\ \\ (\rho(C)^{-1}\mathbf{K}^{-1}\mathbf{Q},\tilde{\mathbf{v}})_\Omega - (H,\nabla\cdot\tilde{\mathbf{v}})_\Omega + \left\langle \{\!\{H\}\!\}, [\![\tilde{\mathbf{v}}]\!] \right\rangle_{\mathcal{E}_i} + \left\langle H,\tilde{\mathbf{v}}\cdot\mathbf{n}\right\rangle_{\Gamma_N} \\ \qquad = -(\hat{\rho}\mathbf{e}_z,\tilde{\mathbf{v}})_\Omega - \left\langle h^b,\tilde{\mathbf{v}}\cdot n\right\rangle_{\Gamma_D}, & \forall\tilde{\mathbf{v}}\in\tilde{\mathbf{V}}(\Omega), \\ \\ ((\rho(C)\phi C)_t,w)_\Omega - (C\mathbf{Q}-\mathbf{D}_q(\mathbf{Q})\nabla C,\nabla w)_\Omega + \left\langle C^u\hat{\mathbf{q}}, [\![w]\!] \right\rangle_{\mathcal{E}_i} \\ \qquad - \left\langle \{\!\{\mathbf{D}_q(\mathbf{Q})\nabla C\}\!\}, [\![w]\!] \right\rangle_{\mathcal{E}_i} + \left\langle \sigma_c [\![C]\!], [\![w]\!] \right\rangle_{\mathcal{E}_i} \\ \qquad + \left\langle \{\!\{\mathbf{D}_q(\mathbf{Q})\nabla w\}\!\}, [\![C]\!] \right\rangle_{\mathcal{E}_i} + \left\langle C\hat{\mathbf{q}},w\right\rangle_{\Gamma_+} \\ \qquad = (c_s\rho_s Q_s,w)_\Omega - \left\langle c_I\hat{\mathbf{q}},w\right\rangle_{\Gamma_-}, & \forall w\in\tilde{W}(\Omega), \end{cases}$$

where $\hat{\mathbf{q}}$ is the numerical flux as previously defined and the dispersion tensor is now defined in terms of $\mathbf{q}$ and is given by:

$$\begin{aligned} \mathbf{D}_q \equiv \rho(c)\mathbf{D}(\mathbf{u}) &= \rho(c)\mathbf{D}_{mol} + \mathbf{D}_{mech}(\mathbf{q}) \\ &= \rho(c)\phi D_m\mathbf{I} + (\alpha_L-\alpha_T)\frac{\mathbf{q}\otimes\mathbf{q}}{|\mathbf{q}|} + \alpha_T|\mathbf{q}|\mathbf{I}. \end{aligned} \tag{3.16}$$

In the following development, unless otherwise noted, we will refer to $\mathbf{D}_q$ as $\mathbf{D}$ to reduce notation.

3.3.2 Assumptions

We now make several assumptions to facilitate the analysis. With the nonlinear coupling of the system and the nonlinearities in the transport equation, it is necessary to make assumptions on the coefficients and data to arrive at an estimate.

We make these assumptions explicit here for further use later in the development of our proof.

(A1) There exist positive numbers $\rho_*, \rho^*, \phi_*, \phi^*, S^*, S_*, D_{m,*}, D_m^*$ such that

$$\rho_* \leq \rho(c) \leq \rho^*,$$

$$\phi_* \leq \phi(x) \leq \phi^*,$$

$$S_* \leq S(x) \leq S^*,$$

$$D_{m,*} \leq D_m \leq D_m^*,$$

for all c and $x \in \Omega$. We also assume our reference density, $\rho_0 = \rho_*$.

(A2) The density constitutive equation is given by $\rho(c) = \rho_0(1+\epsilon c)$ where $\epsilon = \frac{\rho_1 - \rho_0}{\rho_0}$.

(A3) The porosity, $\phi(x)$ and specific storage $S(x)$ can be functions of space but are independent of the freshwater hydraulic head.

(A4) The bulk fluid mass, $\rho\phi$ and its time derivative, $(\rho\phi)_t$, as well as $(\rho S)_t$, are bounded.

(A5) The initial conditions, $c_0(x,0)$ and $h_0(x,0)$ are continuous on Ω and are non-negative.

(A6) We assume the following regularity on our functions and their time derivatives:

$$h \in W^{1,\infty}(0,T; H^{s_{flow}}(\Omega)),$$

$$\mathbf{u} \in (L^{\infty}(0,T; H^{s_{vel}}(\Omega)))^d,$$

$$c \in W^{1,\infty}(0,T; H^{s_{trans}}),$$

where d is the spatial dimension, $s_{flow}, s_{vel}, s_{trans} \geq 1$. Also, since c represents a normalized mass fraction, we have $\|c\|_{\infty,\Omega}, \|\pi c\|_{\infty,\Omega} \leq 1$, where πc is a projection into our approximation space that will be defined later.

(A7) The hydraulic conductivity tensor, $\mathbf{K}$, is uniformly positive definite so that $\mathbf{K}^{1/2}$ and $\mathbf{K}^{-1}$ are well defined and also that

$$\max_{ij} \mathbf{K}_{ij} \leq k^*,$$

$$\min_{ij} \mathbf{K}_{ij} \geq k_*,$$

where $k^*, k_* \in \mathbb{R}^+ \setminus \{0\}$. The viscosity μ does not vary with concentration so $\mathbf{K}$ is constant.

(A8) We assume homogeneous boundary conditions ($h_b = u_b = c_I = 0$). We also assume $\Gamma^+ \subset \Gamma^N$, which is slightly less restrictive requirement than $\partial\Omega \equiv \Gamma^N$, which was used in [119].

(A9) The penalty terms on an element edge (face) for each of the formulations is given by $\sigma_{h,\gamma} = \frac{\sigma_{h,0}}{|\gamma|^{\beta_h}}$ and $\sigma_{c,\gamma} = \frac{\sigma_{c,0}}{|\gamma|^{\beta_c}}$, where $|\gamma|$ is the length of the edge in 2D and the area of the face in 3D, the penalty power, $\beta_* \geq 1$, and the penalty constant, $\sigma_{*,0} > 0$. On any face γ in the mesh $\mathcal{T}_\Delta$, let E_γ denote the set of elements sharing the face, and Δ_γ be the maximum element diameter over all the elements in E_γ. We will assume that

$$\sigma_*\big|_\gamma = \mathcal{O}(\Delta_\gamma^{-1}).$$

(A10) The hydrodynamic dispersion tensor, $\mathbf{D}_q$, is uniformly positive definite as given by the following two lemmas. Proofs of the lemmas for $\mathbf{D}(\mathbf{u})$ are presented

in [119] and are easily extended to account for the current definition of the dispersion tensor, $\mathbf{D}_q$.

Lemma 3.3.1. *Uniform positive definiteness of* $\mathbf{D}_q(\mathbf{q}, c)$. *Let* $\mathbf{D}_q$ *be defined as previous, where* $D_m(x) \geq 0$, $\alpha_L(x) \geq 0$ *and* $\alpha_T(x) \geq 0$ *are non-negative functions of* $x \in \Omega$. *Then*

$$\mathbf{D}_q(\mathbf{q}, c)\nabla c \cdot \nabla c \geq (\rho_* \phi_* D_m + min(\alpha_L, \alpha_T) |\mathbf{q}|) |\nabla c|^2 .$$

If, in addition, $D_m(x) \geq D_{m,*} > 0$ *uniformly in the domain* Ω, *then* $\mathbf{D}_q$ *is uniformly positive definite in* Ω*:*

$$\mathbf{D}_q(\mathbf{q}, c)\nabla c \cdot \nabla c \geq \rho_* \phi_* D_{m,*} |\nabla c|^2 .$$

Lemma 3.3.2. *Uniform Lipschitz continuity of* $\mathbf{D}_{mech}(\mathbf{q})$. *Let* $\mathbf{D}_{mech}(\mathbf{q})$ *be as previously above, where* $\alpha_L(x) \geq 0$ *and* $\alpha_T(x) \geq 0$ *are non-negative for* $x \in \Omega$, *and the dispersivities* α_L *and* α_T *are uniformly bounded, i.e.,* $\alpha_L(x) \leq \alpha_L^*$ *and* $\alpha_T(x) \leq \alpha_T^*$. *Then*

$$\|\mathbf{D}_{mech}(\mathbf{u}) - \mathbf{D}_{mech}(\mathbf{v})\|_{(L_2(\Omega)^{d\times d})} \leq Z^D \|\mathbf{u} - \mathbf{v}\|_{(L_2(\Omega))^d} , \tag{3.17}$$

where $Z^D = (7\alpha_T^* + 6\alpha_L^*)d^{3/2}$ *is a fixed number (*$d = 2$ *or* 3 *is the dimension of domain* Ω*).*

(A11) In the transport equation, on an element Ω_e, we will define the mass velocity $\mathbf{Q}$ as the following:

$$\mathbf{Q}(x) = \begin{cases} \mathbf{Q}(x), & x \in \Omega_e, \\ \hat{\mathbf{q}}(x), & x \in \partial\Omega_e, \end{cases}$$

where $\hat{\mathbf{q}}$ is the numerical flux from the LDG formulation. We also define a cut-off function for $\mathbf{Q}$ similar to [119]:

$$\mathcal{M}(\mathbf{Q}(x)) = \begin{cases} \mathbf{Q}(x), & |\mathbf{Q}(x)| < M, \\ M\frac{\mathbf{Q}(x)}{|\mathbf{Q}(x)|}, & |\mathbf{Q}(x)| \geq M. \end{cases} \tag{3.18}$$

Selecting a large enough value of M for the cutoff function provides control over the $\mathbf{Q}$ in the transport equation. In the following analysis, we define $\mathcal{M}(\mathbf{Q}) = \mathbf{Q}^M$. Although this assumes stability of the method, it does allow an estimate on the error.

(A12) Given (A1) and (A11), we also have that, for large enough M in the cutoff function

$$\left\|\mathbf{D}(\mathbf{Q}^M)\right\|_{0,\Omega} \leq Z^M,$$

where Z^M is a Δ-independent constant.

3.3.2.1 Basic Inequalities

In the following analysis, unless otherwise noted, Z and ε represent generic, positive constants that are independent of Δ that take different values at different places. We use a number of standard inequalities that we present here without proofs. We will use the following inequalities repeatedly to bound inner products and norms:

Lemma 3.3.3. *Young's Inequality. Let $a \geq 0$ and $b \geq 0$. Then, for any $\varepsilon \geq 0$,*

$$ab \leq \frac{\varepsilon}{2}a^2 + \frac{1}{2\varepsilon}b^2.$$

Lemma 3.3.4. *Cauchy-Schwarz Inequality. Let $f, g \in L_2(\Omega)$, then*

$$(f, g)_\Omega \leq \|f\|_{L_2(\Omega)} \|g\|_{L_2(\Omega)}.$$

Since we are proving a bound for the semi-discrete, time dependent problem, we employ the continuous in time Grönwall inequality as presented in [110]:

Lemma 3.3.5. *Continuous Grönwall's Inequality. Let f, g, h be piecewise continuous non-negative functions defined on (a, b). Assume that g is nondecreasing. Assume that there is a positive constant, C, independent of t, such that*

$$f(t) + h(t) \leq g(t) + C \int_a^t f(s)ds, \quad \forall t \in [a, b].$$

Then

$$f(t) + h(t) \leq e^{C(t-a)} g(t), \quad \forall t \in [a, b].$$

Let $\pi h, \pi c \in \tilde{W}$ and $\pi \mathbf{u} \in \tilde{\mathbf{V}}$ be the L_2 projection of h, c and $\mathbf{u}$ into their respective approximation spaces, i.e.,

$$\begin{aligned}
(h - \pi h, w)_\Omega &= 0, \quad \forall w \in \tilde{W}, \\
(\mathbf{u} - \pi \mathbf{u}, \mathbf{v})_\Omega &= 0, \quad \forall v \in \tilde{\mathbf{V}}, \\
(c - \pi c, \tilde{w})_\Omega &= 0, \quad \forall \tilde{w} \in \tilde{W}.
\end{aligned} \tag{3.19}$$

By the assumptions on our approximation spaces, we also have the following:

$$\begin{aligned}
\mathbf{v} \in \tilde{\mathbf{V}}, &\qquad \nabla \cdot \mathbf{v} \in \tilde{W}, \\
w \in \tilde{W}, &\qquad \nabla w \in \tilde{\mathbf{V}}.
\end{aligned} \tag{3.20}$$

We have the following estimate for our projections:

Lemma 3.3.6. *Projection Error Bound. Let πw denote the $L_2(\Omega_e)$ -projection of $w \in H^r(\Omega_e)$ into the space $\mathcal{P}^k(\Omega_e)$. Then there exists a constant, Z^p, independent of Δ_e, such that*

$$\|w - \pi w\|_{l,\Omega_e} \leq Z^p \Delta_e^{\min(s,k+1)-l} \|w\|_{s,\Omega_e}, \tag{3.21}$$

where $0 \leq l \leq min(s, k+1)$.

We define $e_h = H - h$, $e_h^I = h - \pi h$ and $e_h^A = H - \pi h = e_h + e_h^I$ (where I and A represent interpolation and approximation errors) and similarly for $\mathbf{u}$ and c. We will utilize the following trace estimate [26] in the analysis:

Lemma 3.3.7. *Trace Inequality. Suppose that an element Ω_e has a Lipschitz boundary. Then there exists a constant $Z^{tr,e}$ such that*

$$\|w\|_{0,\partial\Omega_e} \leq Z^{tr,e} \|w\|_{0,\Omega_e}^{1/2} \|w\|_{1,\Omega_e}^{1/2} \tag{3.22}$$

for every $w \in H^1(\Omega_e)$.

If we define the trace constant $Z^{tr} = \sup_\Delta \max_e Z^{tr,e}$, then it can be shown to be finite for regular meshes, including triangular and tetrahedral meshes. Using this, we have the following bound for $w \in W$:

$$\|w\|_{0,\mathcal{E}_i}^2 \leq \sum_{\Omega_e} \|w\|_{0,\partial\Omega_e}^2 \leq (Z^{tr})^2 \sum_{\Omega_e} \|w\|_{0,\Omega_e} \|w\|_{1,\Omega_e}. \tag{3.23}$$

For functions in the approximation spaces, we have the following inverse estimate.

Lemma 3.3.8. *Inverse Estimate. For a regular, quasi-uniform mesh, there exists a constant Z^{inv} independent of Δ_e such that*

$$\|w\|_{1,\Omega_e} \leq Z^{inv} \Delta_e^{-1} \|w\|_{0,\Omega_e} \tag{3.24}$$

for every $w \in \tilde{W}$.

Combining, (3.24) and (3.22) gives the modified trace estimate for functions in the approximation space:

$$\begin{aligned} \|w\|_{0,\partial\Omega_e} &\leq Z^{tr,e} \|w\|_{0,\Omega_e}^{1/2} \|w\|_{1,\Omega_e}^{1/2} \\ &\leq Z^{tr,e} (Z^{inv})^{1/2} \Delta_e^{-1/2} \|w\|_{0,\Omega_e} . \end{aligned} \tag{3.25}$$

Combining the previous results and using the regularity requirement on our mesh, we have the following global result for functions in our approximation space which we will use extensively to bound our approximation error in our analysis:

$$\sum_{\Omega_e} \|w\|_{0,\partial\Omega_e}^2 \leq \frac{\tau (Z^{tr})^2 Z^{inv}}{\Delta} \sum_{\Omega_e} \|w\|_{0,\Omega_e}^2 = \frac{\tau (Z^{tr})^2 Z^{inv}}{\Delta} \|w\|_{0,\Omega}^2 . \tag{3.26}$$

For brevity, we use $Z^{tr,1} \equiv \tau (Z^{tr})^2 Z^{inv}$ when we apply (3.26).

3.3.3 Error Equations

Flow Error Equation. Since we defined the auxiliary variable $\mathbf{q} = \rho(c)\mathbf{u}$, we must define a suitable projection of $\mathbf{q}$ into the approximation space, $\tilde{\mathbf{V}}$. So, let $\mathbf{Q} \equiv \pi_Q(\rho(C)\mathbf{U}) \in \tilde{\mathbf{V}}$ where we define the projection π_Q as

$$(\rho(C)^{-1}\mathbf{K}^{-1}(\mathbf{Q} - \rho(C)\mathbf{U}), \mathbf{v})_\Omega = 0, \qquad \forall \mathbf{v} \in \tilde{\mathbf{V}}. \tag{3.27}$$

We define the error, $\mathbf{e}_q = \mathbf{Q} - \mathbf{q}$, and then, subtracting the mixed weak formulation with the exact solution from the flow mixed DG formulation with $(H, \mathbf{Q}, C)$, we

have the following:

$$\begin{aligned}((\rho(C)Se_{h,t},w)_\Omega + \mathcal{A}_1(e_h,\mathbf{e}_q,w) &= ((\rho(C)-\rho(c))Sh_t,w)_\Omega - \left\langle(\rho(C)-\rho)u^b,w\right\rangle_{\Gamma_N} \\ &\quad - (\phi\rho_0\epsilon C_t - \phi\rho_0\epsilon c_t,w)_\Omega, \\ \mathcal{A}_2(\mathbf{e}_q,e_h,\mathbf{v};C) &= -((\rho(C)^{-1}-\rho(c)^{-1})\mathbf{K}^{-1}\mathbf{q},\mathbf{v})_\Omega \\ &\quad - ((\hat{\rho}(C)-\hat{\rho}(c))\mathbf{e}_z,\mathbf{v})_\Omega, \end{aligned} \tag{3.28}$$

where we define

$$\begin{aligned}\mathcal{A}_1(h,\mathbf{q},w) &\equiv -(\mathbf{q},\nabla w)_\Omega + \left\langle\, \{\!\{\mathbf{q}\}\!\}\,,[\![w]\!]\,\right\rangle_{\mathcal{E}_i} \\ &\quad + \left\langle \mathbf{q}\cdot\mathbf{n},w\right\rangle_{\Gamma_D} + \left\langle \sigma_h\,[\![h]\!]\,,[\![w]\!]\,\right\rangle_{\mathcal{E}_i} + \left\langle\sigma_h h,w\right\rangle_{\Gamma_D}, \\ \mathcal{A}_2(h,\mathbf{q},\mathbf{v};c) &\equiv (\rho(c)^{-1}\mathbf{K}^{-1}\mathbf{q},\mathbf{v})_\Omega - (h,\nabla\cdot\mathbf{v})_\Omega + \left\langle\, \{\!\{h\}\!\}\,,[\![\mathbf{v}]\!]\,\right\rangle_{\mathcal{E}_i} + \left\langle h,\mathbf{v}\cdot\mathbf{n}\right\rangle_{\Gamma_N}. \end{aligned}$$

We introduce the projection $\pi_q\mathbf{q} = \pi_q(\rho(c)\mathbf{u})$ into the approximation space using a similar projection to (3.27) defined as

$$(\rho(c)^{-1}\mathbf{K}^{-1}(\pi_q\mathbf{q} - \rho(c)\mathbf{u}),\mathbf{v})_\Omega = 0, \qquad \forall\mathbf{v}\in\tilde{\mathbf{V}}. \tag{3.29}$$

Using this projection, we introduce $\mathbf{e}_q = \mathbf{e}_q^A - \mathbf{e}_q^I$ combined with $e_h = e_h^A - e_h^I$ to get the following equations:

$$\begin{aligned}(\rho(C)Se_{h,t}^A,w)_\Omega + \mathcal{A}_1(e_h^A,\mathbf{e}_q^A,w) &= (\rho(C)Se_{h,t}^I,w)_\Omega + ((\rho(C)-\rho(c))Sh_t,w)_\Omega \\ &\quad + \mathcal{A}_1(e_h^I,\mathbf{e}_q^I,w) - \left\langle(\rho(C)-\rho)u^b,w\right\rangle_{\Gamma_N} \\ &\quad - (\phi\rho_0\epsilon C_t - \phi\rho_0\epsilon c_t,w)_\Omega, \\ \mathcal{A}_2(\mathbf{e}_q^A,e_h^A,\mathbf{v};C) &= \mathcal{A}_2(\mathbf{e}_q^I,e_h^I,\mathbf{v};C) - ((\rho(C)^{-1}-\rho(c)^{-1})\mathbf{K}^{-1}\mathbf{q},\mathbf{v})_\Omega \\ &\quad - ((\hat{\rho}(C)-\hat{\rho}(c))\mathbf{e}_z,\mathbf{v})_\Omega. \end{aligned} \tag{3.30}$$

Using integration by parts, we can rewrite $\mathcal{A}_2$ as

$$\mathcal{A}_2(h, \mathbf{q}, \mathbf{v}; c) = (\rho(c)^{-1}\mathbf{K}^{-1}\mathbf{q}, \mathbf{v})_\Omega + (\nabla h, \mathbf{v})_\Omega - \left\langle \left[\!\left[h\right]\!\right], \{\!\{\mathbf{v}\}\!\} \right\rangle_{\mathcal{E}_i} - \left\langle h, \mathbf{v}\cdot\mathbf{n}\right\rangle_{\Gamma_D}.$$

Using this representation for the bilinear form, if we let $w \equiv e_h^A$ and $\mathbf{v} \equiv \mathbf{e}_q^A$, we have

$$\begin{aligned}\mathcal{A}_1(e_h^A, \mathbf{e}_q^A, e_h^A) + \mathcal{A}_2(e_h^A, \mathbf{e}_q^A, \mathbf{e}_q^A; C) = (\rho(C)^{-1}\mathbf{K}^{-1}\mathbf{e}_q^A, \mathbf{e}_q^A)_\Omega \\ + \left\langle \sigma_h \left[\!\left[e_h^A\right]\!\right], \left[\!\left[e_h^A\right]\!\right] \right\rangle_{\mathcal{E}_i} + \left\langle \sigma_h e_h^A, e_h^A \right\rangle_{\Gamma_D},\end{aligned}$$

and using this we get the flow error equation:

$$\begin{aligned}(\rho(C)Se_{h,t}^A, e_h^A)_\Omega + \left\|\rho(C)^{-1/2}\mathbf{K}^{-1/2}\mathbf{e}_q^A\right\|_{0,\Omega}^2 + \left\|\sigma_h^{1/2}\left[\!\left[e_h^A\right]\!\right]\right\|_{0,\mathcal{E}_i}^2 + \left\|\sigma_h^{1/2}e_h^A\right\|_{0,\Gamma_D}^2 \\ = \mathcal{A}_1(e_h^I, \mathbf{e}_q^I, \mathbf{e}_q^A) + \mathcal{A}_2(\mathbf{e}_q^I, e_h^I, \mathbf{e}_h^A; C) + (\rho(C)Se_{h,t}^I, e_h^A)_\Omega \\ + ((\rho(C) - \rho(c))Sh_t, e_h^A)_\Omega - \left\langle (\rho(C) - \rho(c))u^b, e_h^A \right\rangle_{\Gamma_N} \\ - ((\rho(C)^{-1} - \rho(c)^{-1})\mathbf{K}^{-1}\mathbf{q}, \mathbf{e}_q^A)_\Omega - ((\hat{\rho}(C) - \hat{\rho}(c))\mathbf{e}_z, \mathbf{e}_q^A)_\Omega \\ - (\phi\rho_0\epsilon e_{c,t}, e_h^A)_\Omega. \qquad (3.31)\end{aligned}$$

Transport Error Equation. The transport error equation follows a straight forward development. If we subtract the weak formulation of the transport equation with the exact solution from our semi-discrete transport DG formulation and introduce the $\mathbf{Q}^M = \mathcal{M}(\mathbf{Q})$, we have

$$((\rho(C)\phi C - \rho(c)\phi c)_t, \tilde{w})_\Omega + \mathcal{B}(e_c, \tilde{w}; \mathbf{Q}^M) = \mathcal{B}(c, \tilde{w}; \mathbf{q}) - \mathcal{B}(c, \tilde{w}; \mathbf{Q}^M), \qquad (3.32)$$

where

$$\begin{aligned}\mathcal{B}(c,w;\mathbf{q}) = &-(c\mathbf{q},\nabla w)_\Omega + (\mathbf{D}(\mathbf{q})\nabla c,\nabla w)_\Omega + \left\langle c^u\hat{\mathbf{q}},[\![c]\!]\right\rangle_{\mathcal{E}_i}\\ &-\left\langle \{\!\{\mathbf{D}(\mathbf{q})\nabla w\}\!\},[\![w]\!]\right\rangle_{\mathcal{E}_i} + \left\langle \sigma_c[\![c]\!],[\![w]\!]\right\rangle_{\mathcal{E}_i}\\ &+\left\langle c\hat{\mathbf{q}},w\right\rangle_{\Gamma_+} + \left\langle \{\!\{\mathbf{D}(\mathbf{q})\nabla w\}\!\},[\![c]\!]\right\rangle_{\mathcal{E}_i}.\end{aligned}$$

Introducing $e_c = e_c^A - e_c^I$ and setting $\tilde{w} \equiv e_c^A \in \tilde{W}$ we have the transport error equation:

$$\begin{aligned}((\rho(C)\phi e_c^A)_t, e_c^A)_\Omega + \mathcal{B}(e_c^A, e_c^A; \mathbf{Q}^M) = &-((\rho(C)\phi\pi c - \rho(c)\phi c)_t, e_c^A)_\Omega + \mathcal{B}(e_c^I, e_c^A; \mathbf{Q}^M)\\ &+ \mathcal{B}(c, e_c^A; \mathbf{q}) - \mathcal{B}(c, e_c^A; \mathbf{Q}^M). \qquad (3.33)\end{aligned}$$

3.3.4 Error Estimate

We now present the primary result from this section.

Theorem 3.3.9 (Coupled System Error Estimate)**.** *Assume (A1)-(A12). If the constant M for the cut-off operator and the penalty constants are sufficiently large*

and if the density contrast, ϵ, is sufficiently small, then we have the estimate:

$$
\begin{aligned}
&\left\|\rho(C(\cdot,T))^{1/2}\phi^{1/2}e_c^A(\cdot,T)\right\|_{0,\Omega}^2 \\
&\quad+\left\|\rho(C(\cdot,T))^{1/2}S^{1/2}e_h^A(\cdot,T)\right\|_{0,\Omega}^2 \\
&\quad+\int_0^T\Big[\left\|\mathbf{D}^{1/2}(\mathbf{Q}^M)\nabla e_c^A\right\|_{0,\Omega}^2+\left\|\rho(C)^{-1/2}\mathbf{K}^{-1/2}\mathbf{e}_q^A\right\|_{0,\Omega}^2 \\
&\quad+\left\|\sigma_c^{1/2}\left[\left[e_c^A\right]\right]\right\|_{0,\mathcal{E}_i}^2+\left\|\sigma_h^{1/2}\left[\left[e_h^A\right]\right]\right\|_{0,\mathcal{E}_i}^2+\left\|\sigma_h^{1/2}e_h^A\right\|_{0,\Gamma_D}^2\Big] \\
&\leq Z(t)\Bigg[\left(\Delta^{2min(s_{flow},1k+1)}+\Delta^{2min(s_{flow},k+1)-2}\right)\|h\|^2_{L^2(0,T;H^{s_{flow}}(\Omega))} \\
&\quad+\Delta^{2min(s_{flow},k+1)}\|h_t\|^2_{L^2(0,T;H^{s_{flow}}(\Omega))} \\
&\quad+\left(\Delta^{2min(s_{vel},k+1)}+\Delta^{2min(s_{vel},k+1)-2}\right)\|\mathbf{q}\|^2_{L^2(0,T;H^{s_{vel}}(\Omega))} \\
&\quad+\Delta^{2min(s_{trans},k+1)-2}\|c\|^2_{L^2(0,T;H^{s_{trans}}(\Omega))} \\
&\quad+\Delta^{2min(s_{trans},k+1)}\|c_t\|^2_{L^2(0,T;H^{s_{trans}}(\Omega))}\Bigg],
\end{aligned}
$$

where $Z(t)=e^{Ct}$ with C a mesh and time -independent positive constant.

We present a sketch of the proof here with the full detailed proof in Appendix 1. The general outline for the proof is as follows:

1. Derive an estimate for the head and velocity L_2 error in which the bound will include the mass fraction error time derivative.

2. Derive an estimate for the transport error in which the bound will include the L_2 velocity error.

3. Derive an estimate for the mass fraction time derivative by utilizing the transport error equation with $\tilde{w} \equiv e_h^A$. This bound will include the head error

gradient and the velocity error but will be multiplied by the density constrast ϵ.

4. Derive an estimate for the head gradient L_2 error utilizing the Darcy Error equation with $\tilde{\mathbf{v}} \equiv \nabla e_h^A$ and utilize this bound to eliminate the head gradient L_2 error from (3).

5. Combine the inequalities from (1) and (2), apply the bound from (4) to eliminate the mass fraction time derivative term and utilize the penalty constant and ϵ factor to hide terms on the left hand side of the inequality.

6. Apply Grönwall's inequality to (5) to get the final error bound.

Following this outline, turning to the first step, it is straight forward to derive the following bound for flow error equation (3.31):

$$
\begin{aligned}
&\frac{1}{2}\left\|\rho(C(\cdot,T)^{1/2}S^{1/2}e_h^A(\cdot,T)\right\|_{0,\Omega}^2 \\
&\quad + \frac{1}{2}\int_0^T \Big[\left\|\rho(C)^{-1/2}\mathbf{K}^{-1/2}\mathbf{e}_q^A\right\|_{0,\Omega}^2 + \left\|\sigma_h^{1/2}\left[\left[e_h^A\right]\right]\right\|_{0,\mathcal{E}_i}^2 + \left\|\sigma_h^{1/2}e_h^A\right\|_{0,\Gamma_D}^2\Big] \\
&\leq Z_1\big[(\Delta^{2\min(s_{flow},k+1)} + \Delta^{2\min(s_{flow},k+1)-2})\left\|h\right\|^2_{L^2(0,T;H^{s_{flow}}(\Omega))} \\
&\quad + \Delta^{2\min(s_{flow},k+1)}\left\|h_t\right\|^2_{L^2(0,T;H^{s_{flow}}(\Omega))} + \Delta^{2\min(s_{trans},k+1)}\left\|c\right\|^2_{L^2(0,T;H^{s_{trans}}(\Omega))} \\
&\quad + (\Delta^{2\min(s_{vel},k+1)} + \Delta^{2\min(s_{vel},k+1)-2})\left\|\mathbf{q}\right\|^2_{L^2(0,T;H^{s_{vel}}(\Omega))}\big] \\
&\quad + Z_2\int_0^T \Big[\left\|\rho(C)^{1/2}S^{1/2}e_h^A\right\|_{0,\Omega}^2 + \left\|\rho(C)^{1/2}\phi^{1/2}e_c^A\right\|_{0,\Omega}^2\Big] \\
&\quad + \int_0^T \left|(\phi\rho_0\epsilon e_{c,t}, e_h^A)_\Omega\right|, \qquad (3.34)
\end{aligned}
$$

where Z_1, Z_2 are Δ-independent, positive constants. This also gives an estimate on the $L_2(L_2(\Omega))$ velocity error. Note that these bounds depend on the mass frac-

tion and mass fraction time derivative error. Using the same methodology for the transport error equation (3.33), it is straight forward to derive the bound

$$\begin{aligned}\frac{1}{4}\left\|\rho(C(\cdot,T))^{1/2}\phi^{1/2}e_c^A(\cdot,T)\right\|_{0,\Omega}^2 &+ \frac{1}{2}\int_0^T\Big[\left\|\mathbf{D}^{1/2}(\mathbf{Q}^M)\nabla e_c^A\right\|_{0,\Omega}^2 \\ &+ \left\|\sigma_c^{1/2}\left[\left[e_c^A\right]\right]\right\|_{0,\mathcal{E}_i}^2\Big] \\ &\leq Z_1\Big[(\Delta^{2\min(s_{trans},k+1)-2})\left\|c\right\|^2_{L^2(0,T;H^{s_{trans}}(\Omega))} \\ &\quad+(\Delta^{2\min(s_{trans},k+1)})\left\|c_t\right\|^2_{L^2(0,T;H^{s_{trans}}(\Omega))} \\ &\quad+(\Delta^{2\min(s_{trans},k+1)})\left\|\mathbf{q}\right\|^2_{L^2(0,T;H^{s_{vel}}(\Omega))}\Big] \\ &\quad+Z_2\int_0^T\left\|\rho(C)^{1/2}\phi^{1/2}e_c^A\right\|_{0,\Omega}^2 \\ &\quad+Z^{q,1}\int_0^T\left\|\rho(C)^{-1/2}\mathbf{K}^{-1/2}\mathbf{e}_q^A\right\|_{0,\Omega}^2, \qquad (3.35)\end{aligned}$$

with $Z^{q,1}=\sum_{i=1}^4 Z_i^q$ and Z_i^q defined as

$$\begin{aligned}Z_1^q &= \rho^* k^*\left\|\mathbf{D}(\mathbf{Q}^M)^{-1/2}\right\|_{0,\Omega}^2, \\ Z_2^q &= (Z^D)^2\rho^* k^*\left\|\mathbf{D}(\mathbf{Q}^M)^{-1/2}\right\|_{0,\Omega}^2\left\|\nabla c\right\|_{0,\Omega}^2, \\ Z_3^q &= \frac{(Z^{tr,1})^2\rho^* k^*}{\sigma_{c,0}}, \\ Z_4^q &= \frac{(Z^{tr,1}Z^D)^2\rho^* k^*}{\sigma_{c,0}}\left\|\nabla c\right\|_{0,\Omega}^2\left\|\nabla c\right\|_{1,\Omega}^2.\end{aligned}$$

Z_1, Z_2 are positive constants and $Z^{tr,1}, Z^D$ are as previously defined.

We use Equation 3.32 to get a bound on $(\rho_0\epsilon\phi e_{c,t}, e_h^A)_\Omega$. Setting $\tilde{w}=e_h^A$ in Equation 3.32, we have

$$\begin{aligned}((\rho(C)\phi C-\rho(c)\phi c)_t, e_h^A)_\Omega+\mathcal{B}(e_c^A,e_h^A;\mathbf{Q}^M) &= \mathcal{B}(e_c^I,e_h^A;\mathbf{Q}^M)+\mathcal{B}(c,e_h^A;\mathbf{q}) \\ &\quad-\mathcal{B}(c,e_h^A;\mathbf{Q}^M). \qquad (3.36)\end{aligned}$$

Since bounding the time derivative is a key part of the proof, we present it here. Expanding the time derivative and using our constitutive equation for the density gives

$$\begin{aligned}((\rho(C)\phi C - \rho(c)\phi c)_t, e_h^A)_\Omega = ((\rho(C)\phi)_t e_c, e_h^A)_\Omega + (\rho(C)\phi e_{c,t}, e_h^A)_\Omega \\ + (\phi\rho_0\epsilon e_c c_t, e_h^A)_\Omega + (\phi\rho_0\epsilon e_{c,t} c, e_h^A)_\Omega,\end{aligned}$$

and combining this with Equation 3.36 we arrive at the bound

$$\begin{aligned}\left|(\rho(C)\phi e_{c,t}, e_h^A)_\Omega\right| \leq \left|((\rho(C)\phi)_t e_c, e_h^A)_\Omega\right| + \left|(\phi\rho_0\epsilon e_c c_t, e_h^A)_\Omega\right| + \left|(\phi\rho_0\epsilon e_{c,t} c, e_h^A)_\Omega\right| \\ + \left|\mathcal{B}(e_c^A, e_h^A; \mathbf{Q}^M)\right| + \left|\mathcal{B}(e_c^I, e_h^A; \mathbf{Q}^M)\right| \\ + \left|\mathcal{B}(c, e_h^A; \mathbf{q}) - \mathcal{B}(c, e_h^A; \mathbf{Q}^M)\right|.\end{aligned}$$

Since $\rho_0 \leq \rho(C)$ for all C, we have

$$\begin{aligned}\left|(\rho_0\epsilon\phi e_{c,t}, e_h^A)_\Omega\right| &\leq \epsilon\left|(\rho(C)\phi e_{c,t}, e_h^A)_\Omega\right| \\ &\leq \epsilon\Big[\left|((\rho(C)\phi)_t e_c, e_h^A)_\Omega\right| + \left|(\phi\rho_0\epsilon e_c c_t, e_h^A)_\Omega\right| + \left|(\phi\rho_0\epsilon e_{c,t} c, e_h^A)_\Omega\right| \\ &\quad + \left|\mathcal{B}(e_c^A, e_h^A; \mathbf{Q}^M)\right| + \left|\mathcal{B}(e_c^I, e_h^A; \mathbf{Q}^M)\right| \\ &\quad + \left|\mathcal{B}(c, e_h^A; \mathbf{q}) - \mathcal{B}(c, e_h^A; \mathbf{Q}^M)\right|\Big],\end{aligned}$$

and using (A6), we have $\left|(\phi\rho_0\epsilon e_{c,t} c, e_h^A)_\Omega\right| \leq \left|(\phi\rho_0\epsilon e_{c,t}, e_h^A)_\Omega\right|$ which gives the estimate

$$\begin{aligned}\left|(\rho_0\epsilon\phi e_{c,t}, e_h^A)_\Omega\right| \leq \frac{\epsilon}{1-\epsilon}\Big[\left|((\rho(C)\phi)_t e_c, e_h^A)_\Omega\right| + \left|(\phi\rho_0\epsilon e_c c_t, e_h^A)_\Omega\right| \\ + \left|\mathcal{B}(e_c^A, e_h^A; \mathbf{Q}^M)\right| + \left|\mathcal{B}(e_c^I, e_h^A; \mathbf{Q}^M)\right| \\ + \left|\mathcal{B}(c, e_h^A; \mathbf{q}) - \mathcal{B}(c, e_h^A; \mathbf{Q}^M)\right|\Big].\end{aligned} \tag{3.37}$$

Bounding each term on the right hand side of Equation 3.37 gives the following estimate

$$
\begin{aligned}
&\left|(\rho_0 \epsilon \phi e_{c,t,}, e_h^A)_\Omega\right| \\
&\qquad \leq \frac{\epsilon}{1-\epsilon}\Bigg[Z_5 \left\| \rho(C)^{1/2} \phi^{1/2} e_c^A \right\|_{0,\Omega}^2 + Z_6 \left\| \rho(C)^{1/2} S^{1/2} e_h^A \right\|_{0,\Omega}^2 \\
&\qquad + Z^{q,2} \left\| \rho(C)^{-1/2} \mathbf{K}^{-1/2} \mathbf{e}_q^A \right\|_{0,\Omega}^2 + \left\| \sigma_h^{1/2} \left[[e_h^A] \right] \right\|_{0,\mathcal{E}_i}^2 \\
&\qquad + \frac{4}{5} \left\| \sigma_c^{1/2} \left[[e_c^A] \right] \right\|_{0,\mathcal{E}_i}^2 \\
&\qquad + \left(\frac{Z^{tr}}{\sigma_{h,0}} \left\| \mathbf{D}(\mathbf{Q}^M)^{1/2} \right\|_{0,\Omega}^2 + \left\| \mathbf{D}(\mathbf{Q}^M)^{1/2} \right\|_{0,\Omega}^2 \right) \left\| \mathbf{D}(\mathbf{Q}^M)^{1/2} \nabla e_c^A \right\|_{0,\Omega}^2 \\
&\qquad + \left(3 + \frac{5 (Z^{tr,1})^2 \left\| \mathbf{D}(\mathbf{Q}^M) \right\|_{0,\Omega}^2}{\sigma_{c,0}} \right) \left\| \nabla e_h^A \right\|_{0,\Omega}^2 \\
&\qquad + Z_7 \Big[\left(\Delta^{2\min(s_{trans}, k+1)-2} + \Delta^{2\min(s_{trans}, k+1)} \right) \|c\|_{H^{s_{trans}}(\Omega)}^2 \\
&\qquad + \Delta^{2\min(s_{vel}, k+1)} \|\mathbf{q}\|_{H^{s_{vel}}(\Omega)}^2 \Big] \Bigg],
\end{aligned}
\tag{3.38}
$$

where $Z_5 - Z_7$ are Δ-independent constants and $Z^{q,2} = \sum_{i=5}^{8} Z_i^q$ with:

$$
\begin{aligned}
Z_5^q &= \frac{\rho^* k^*}{4}, \\
Z_6^q &= \frac{1}{4} (Z^D)^2 \rho^* k^* \left\| \nabla c \right\|_{0,\Omega}^2, \\
Z_7^q &= \frac{(Z^{tr,1})^2 \rho^* k^*}{\sigma_{h,0}}, \\
Z_8^q &= \frac{15 (Z^D Z^{tr,1})^2 \rho^* k^*}{\sigma_{h,0}} \left\| \nabla c \right\|_{0,\Omega}^2 \left\| \nabla c \right\|_{1,\Omega}^2.
\end{aligned}
$$

To get an estimate for $\left\| \nabla e_h^A \right\|_{0,\Omega}$ in Equation 3.38, we start off with the error equation derived from Darcy's equation in its original form (Equation 3.30). Defining our test function $\mathbf{v} \equiv \nabla e_h^A \in \tilde{\mathbf{V}}$ and applying the homogenous boundary conditions

assumption (A8), we arrive at the expression:

$$(\nabla e_h, \nabla e_h^A)_\Omega = -(\rho(C)^{-1}\mathbf{K}^{-1}\mathbf{e}_q, \nabla e_h^A)_\Omega + \left\langle \left[\!\left[e_h \right]\!\right], \left\{\!\left\{ \nabla e_h^A \right\}\!\right\} \right\rangle_{\mathcal{E}_i} + \left\langle e_h, \nabla e_h^A \right\rangle_{\Gamma_D}$$
$$- ((\rho(C)^{-1} - \rho^{-1}(c))\mathbf{K}^{-1}\mathbf{q}, \nabla e_h^A)_\Omega - ((\hat{\rho}(C) - \hat{\rho}(c))\mathbf{e}_z, \nabla e_h^A)_\Omega.$$

Using the orthogonality of our interpolant, the left side becomes

$$(\nabla e_h, \nabla e_h^A)_\Omega = \left\| \nabla e_h^A \right\|_{0,\Omega}^2.$$

Bounding each term on the right hand side, we have

$$\begin{aligned}
\left\| \nabla e_h^A \right\|_{0,\Omega}^2 \leq\ & Z_9^q \left\| \rho(c)^{-1/2}\mathbf{K}^{-1/2}\mathbf{e}_q^A \right\|_{0,\Omega}^2 + \frac{1}{2}\left\| \sigma_h^{1/2}\left[\!\left[e_h^A \right]\!\right] \right\|_{0,\mathcal{E}_i}^2 \\
& + Z_1 \left\| \rho(C)^{1/2}\phi^{1/2} e_c^A \right\|_{0,\Omega}^2 + \frac{1}{2}\left\| \sigma_h^{1/2} e_h^A \right\|_{0,\Gamma_D}^2 \\
& + Z_2\big[\Delta^{2\min(s_{flow},k+1)-2}\left\| h \right\|_{H^{s_{flow}}(\Omega)}^2 \\
& + \Delta^{2\min(s_{vel},k+1)}\left\| \mathbf{q} \right\|_{H^{s_{vel}}(\Omega)}^2 + \Delta^{2\min(s_{trans},k+1)}\left\| c \right\|_{H^{s_{trans}}(\Omega)}^2\big], \quad (3.39)
\end{aligned}$$

where $Z_9^q = \frac{7}{\rho_* k_*}$, Z_1, Z_2 are positive, Δ-independent constants and where we have gained the constraint on our penalty constant that $\sigma_{h,0} \geq 14 Z^{tr,1}$.

Using Equation 3.39 to bound the gradient of the head error in Equation 3.38 and

combining terms gives

$$
\begin{aligned}
&\left|(\rho_0\epsilon\phi e_{c,t}, e_h^A)_\Omega\right| \\
&\quad\leq \frac{\epsilon}{1-\epsilon}\Bigg[Z_5\left\|\rho(C)^{1/2}\phi^{1/2}e_c^A\right\|_{0,\Omega}^2 + Z_6\left\|\rho(C)^{1/2}S^{1/2}e_h^A\right\|_{0,\Omega}^2 \\
&\qquad + (Z^{q,2} + 3Z_9^q + Z_9^q\frac{5(Z^{tr,1})^2\left\|\mathbf{D}(\mathbf{Q}^M)\right\|_{0,\Omega}^2}{\sigma_{c,0}})\left\|\rho(c)^{-1}\mathbf{K}^{-1}\mathbf{e}_q^A\right\|_{0,\Omega}^2 \\
&\qquad + \frac{4}{5}\left\|\sigma_c^{1/2}\left[\left[e_c^A\right]\right]\right\|_{0,\mathcal{E}_i}^2 \\
&\qquad + (\frac{Z^{tr,1}}{\sigma_{h,0}}\left\|\mathbf{D}(\mathbf{Q}^M)^{1/2}\right\|_{0,\Omega}^2 + \left\|\mathbf{D}(\mathbf{Q}^M)^{1/2}\right\|_{0,\Omega}^2)\left\|\mathbf{D}(\mathbf{Q}^M)^{1/2}\nabla e_c^A\right\|_{0,\Omega}^2 \\
&\qquad + (\frac{5}{2} + \frac{5(Z^{tr,1})^2\left\|\mathbf{D}(\mathbf{Q}^M)\right\|_{0,\Omega}^2}{2\sigma_{c,0}})\left\|\sigma_h^{1/2}\left[\left[e_h^A\right]\right]\right\|_{0,\mathcal{E}_i}^2 \\
&\qquad + (\frac{3}{2} + \frac{5(Z^{tr,1})^2\left\|\mathbf{D}(\mathbf{Q}^M)\right\|_{0,\Omega}^2}{2\sigma_{c,0}})\left\|\sigma_h^{1/2}e_h^A\right\|_{0,\Gamma_D}^2 \\
&\qquad + Z\big[(\Delta^{2\min(s_{flow},k+1)-2})\left\|h\right\|_{H^{s_{flow}}(\Omega)}^2 + \Delta^{2\min(s_{vel},k+1)}\left\|\mathbf{q}\right\|_{H^{s_{vel}}(\Omega)}^2 \\
&\qquad + (\Delta^{2\min(s_{trans},k+1)-2})\left\|c\right\|_{H^{s_{trans}}(\Omega)}^2\big]\Bigg].
\end{aligned}
\tag{3.40}
$$

Leaving this estimate for now, we use the velocity error estimate derived from Equation 3.34 to eliminate the velocity error term from Equation 3.35 and rearrange terms to get

$$
\begin{aligned}
&\frac{1}{2}\left\|\rho(C(\cdot,T))^{1/2}\phi^{1/2}e_c^A(\cdot,T)\right\|_{0,\Omega}^2 + \frac{1}{2}\int_0^T\left[\left\|\mathbf{D}^{1/2}(\mathbf{Q}^M)\nabla e_c^A\right\|_{0,\Omega}^2 + \left\|\sigma_c^{1/2}\left[\left[e_c^A\right]\right]\right\|_{0,\mathcal{E}_i}^2\right] \\
&\quad\leq Z_\Delta + Z_2\int_0^T\left\|\rho(C)^{1/2}\phi^{1/2}e_c^A\right\|_{0,\Omega}^2 + Z_3\int_0^T\left[\left\|\rho(C)^{1/2}S^{1/2}e_h^A\right\|_{0,\Omega}^2\right. \\
&\qquad + Z^{q,1}\int_0^T\left|(\phi\rho_0\epsilon e_{c,t}, e_h^A)_\Omega\right|,
\end{aligned}
\tag{3.41}
$$

where Z_1, Z_2 and Z_3 are new positive constants and $Z^{q,1}$ is as previously defined

and

$$
\begin{aligned}
Z_\Delta =& Z\Big[(\Delta^{2\min(s_{flow},1k+1)} + \Delta^{2\min(s_{flow},k+1)-2}) \left\|h\right\|^2_{L^2(0,T;H^{s_{flow}}(\Omega))} \\
&+ \Delta^{2\min(s_{flow},k+1)} \left\|h_t\right\|^2_{L^2(0,T;H^{s_{flow}}(\Omega))} \\
&+ (\Delta^{2\min(s_{vel},k+1)} + \Delta^{2\min(s_{vel},k+1)-2}) \left\|\mathbf{q}\right\|^2_{L^2(0,T;H^{s_{vel}}(\Omega))} \\
&+ \Delta^{2\min(s_{trans},k+1)-2} \left\|c\right\|^2_{L^2(0,T;H^{s_{trans}}(\Omega))} \\
&+ \Delta^{2\min(s_{trans},k+1)} \left\|c_t\right\|^2_{L^2(0,T;H^{s_{trans}}(\Omega))}\Big].
\end{aligned}
$$

Adding Equation 3.41 to Equation 3.34 gives

$$
\begin{aligned}
&\frac{1}{2}\left\|\rho(C(\cdot,T))^{1/2}\phi^{1/2}e_c^A(\cdot,T)\right\|^2_{0,\Omega} + \frac{1}{2}\left\|\rho(C(\cdot,T))^{1/2}S^{1/2}e_h^A(\cdot,T)\right\|^2_{0,\Omega} \\
&\quad + \frac{1}{2}\int_0^T \Big[\left\|\mathbf{D}^{1/2}(\mathbf{Q}^M)\nabla e_c^A\right\|^2_{0,\Omega} + \left\|\rho(C)^{-1/2}\mathbf{K}^{-1/2}\mathbf{e}_q^A\right\|^2_{0,\Omega} \\
&\quad + \left\|\sigma_c^{1/2}\left[\left[e_c^A\right]\right]\right\|^2_{0,\mathcal{E}_i} + \left\|\sigma_h^{1/2}\left[\left[e_h^A\right]\right]\right\|^2_{0,\mathcal{E}_i} + \left\|\sigma_h^{1/2}e_h^A\right\|^2_{0,\Gamma_D}\Big] \\
&\quad \leq Z_\Delta + Z_2\int_0^T \left\|\rho(C)^{1/2}\phi^{1/2}e_c^A\right\|^2_{0,\Omega} + Z_3\int_0^T \left\|\rho(C)^{1/2}S^{1/2}e_h^A\right\|^2_{0,\Omega} \\
&\qquad + (1+Z^{q,1})\int_0^T \left|(\phi\rho_0\epsilon e_{c,t}, e_h^A)_\Omega\right|. \qquad (3.42)
\end{aligned}
$$

Finally, we use the mass fraction error time derivative estimate (Equation 3.40) to

bound the mass fraction error time derivative term in Equation 3.42:

$$
\begin{aligned}
&\frac{1}{2}\left\|\rho(C(\cdot,T))^{1/2}\phi^{1/2}e_c^A(\cdot,T)\right\|_{0,\Omega}^2+\frac{1}{2}\left\|\rho(C(\cdot,T))^{1/2}S^{1/2}e_h^A(\cdot,T)\right\|_{0,\Omega}^2\\
&\quad+\frac{1}{2}\int_0^T\Bigg[\left\|\mathbf{D}^{1/2}(\mathbf{Q}^M)\nabla e_c^A\right\|_{0,\Omega}^2+\left\|\rho(C)^{-1/2}\mathbf{K}^{-1/2}\mathbf{e}_q^A\right\|_{0,\Omega}^2\\
&\quad+\left\|\sigma_c^{1/2}\left[\left[e_c^A\right]\right]\right\|_{0,\mathcal{E}_i}^2+\left\|\sigma_h^{1/2}\left[\left[e_h^A\right]\right]\right\|_{0,\mathcal{E}_i}^2+\left\|\sigma_h^{1/2}e_h^A\right\|_{0,\Gamma_D}^2\Bigg]\\
&\quad\le Z_\Delta+Z_2\int_0^T\left\|\rho(C)^{1/2}\phi^{1/2}e_c^A\right\|_{0,\Omega}^2+Z_3\int_0^T\left\|\rho(C)^{1/2}S^{1/2}e_h^A\right\|_{0,\Omega}^2\\
&\quad+(1+Z^{q,1})\int_0^T\frac{\epsilon}{1-\epsilon}\Bigg[Z_5\left\|\rho(C)^{1/2}\phi^{1/2}e_c^A\right\|_{0,\Omega}^2+Z_6\left\|\rho(C)^{1/2}S^{1/2}e_h^A\right\|_{0,\Omega}^2\\
&\quad+(Z^{q,2}+3Z_9^q+Z_9^q\frac{5(Z^{tr,1})^2\left\|\mathbf{D}(\mathbf{Q}^M)\right\|_{0,\Omega}^2}{\sigma_{c,0}})\left\|\rho(c)^{-1}\mathbf{K}^{-1}\mathbf{e}_q^A\right\|_{0,\Omega}^2\\
&\quad+\frac{4}{5}\left\|\sigma_c^{1/2}\left[\left[e_c^A\right]\right]\right\|_{0,\mathcal{E}_i}^2\\
&\quad+(\frac{Z^{tr,1}}{\sigma_{h,0}}\left\|\mathbf{D}(\mathbf{Q}^M)^{1/2}\right\|_{0,\Omega}^2+\left\|\mathbf{D}(\mathbf{Q}^M)^{1/2}\right\|_{0,\Omega}^2)\left\|\mathbf{D}(\mathbf{Q}^M)^{1/2}\nabla e_c^A\right\|_{0,\Omega}^2\\
&\quad+(\frac{5}{2}+\frac{5(Z^{tr,1})^2\left\|\mathbf{D}(\mathbf{Q}^M)\right\|_{0,\Omega}^2}{2\sigma_{c,0}})\left\|\sigma_h^{1/2}\left[\left[e_h^A\right]\right]\right\|_{0,\mathcal{E}_i}^2\\
&\quad+(\frac{3}{2}+\frac{5(Z^{tr,1})^2\left\|\mathbf{D}(\mathbf{Q}^M)\right\|_{0,\Omega}^2}{2\sigma_{c,0}})\left\|\sigma_h^{1/2}e_h^A\right\|_{0,\Gamma_D}^2\\
&\quad+Z\big[(\Delta^{2\min(s_{flow},k+1)-2})\left\|h\right\|_{H^{s_{flow}}(\Omega)}^2+\Delta^{2\min(s_{vel},k+1)}\left\|\mathbf{q}\right\|_{H^{s_{vel}}(\Omega)}^2\\
&\quad+(\Delta^{2\min(s_{trans},k+1)-2})\left\|c\right\|_{H^{s_{trans}}(\Omega)}^2\big]\Bigg].
\end{aligned}
\tag{3.43}
$$

Rearranging terms, we have

$$\begin{aligned}
&\frac{1}{2}\left\|\rho(C(\cdot,T))^{1/2}\phi^{1/2}e_c^A(\cdot,T)\right\|_{0,\Omega}^2+\frac{1}{2}\left\|\rho(C(\cdot,T))^{1/2}S^{1/2}e_h^A(\cdot,T)\right\|_{0,\Omega}^2\\
&\quad+\frac{1}{2}\int_0^T\Big[\left\|\mathbf{D}^{1/2}(\mathbf{Q}^M)\nabla e_c^A\right\|_{0,\Omega}^2+\left\|\rho(C)^{-1/2}\mathbf{K}^{-1/2}\mathbf{e}_q^A\right\|_{0,\Omega}^2\\
&\quad+\left\|\sigma_c^{1/2}\left[\left[e_c^A\right]\right]\right\|_{0,\mathcal{E}_i}^2+\left\|\sigma_h^{1/2}\left[\left[e_h^A\right]\right]\right\|_{0,\mathcal{E}_i}^2+\left\|\sigma_h^{1/2}e_h^A\right\|_{0,\Gamma_D}^2\Big]\\
&\leq Z_\Delta+Z_2\int_0^T\left\|\rho(C)^{1/2}\phi^{1/2}e_c^A\right\|_{0,\Omega}^2+Z_3\int_0^T\left\|\rho(C)^{1/2}S^{1/2}e_h^A\right\|_{0,\Omega}^2\\
&\quad+G_1\int_0^T\left\|\rho(C)^{-1/2}\mathbf{K}^{-1/2}\mathbf{e}_q^A\right\|_{0,\Omega}^2+G_2\int_0^T\left\|\sigma_h^{1/2}e_h^A\right\|_{0,\Gamma_D}^2\\
&\quad+G_3\int_0^T\left\|\sigma_c^{1/2}\left[\left[e_c^A\right]\right]\right\|_{0,\mathcal{E}_i}^2+G_4\int_0^T\left\|\mathbf{D}(\mathbf{Q}^M)^{1/2}\nabla e_c^A\right\|_{0,\Omega}^2\\
&\quad+G_5\int_0^T\left\|\sigma_c^{1/2}\left[\left[e_h^A\right]\right]\right\|_{0,\mathcal{E}_i}^2,
\end{aligned}\tag{3.44}$$

where Z_1, Z_2, and Z_3 are positive constants independent of Δ and where we have the revised coefficients

$$\begin{aligned}
G_1&=(1+Z^{q,1})\frac{\epsilon}{1-\epsilon}(Z^{q,2}+3Z_9^q+Z_9^q\frac{5(Z^{tr,1})^2\left\|\mathbf{D}(\mathbf{Q}^M)\right\|_{0,\Omega}^2}{\sigma_{c,0}})\\
&=(1+Z^{q,1})\frac{Z^{q,2}\epsilon}{1-\epsilon}+(1+Z^{q,1})\frac{3Z_9^q\epsilon}{1-\epsilon}+(1+Z^{q,1})\frac{\epsilon}{1-\epsilon}Z_9^q\frac{5(Z^{tr})^2\left\|\mathbf{D}(\mathbf{Q}^M)\right\|_{0,\Omega}^2}{\sigma_{c,0}}\\
&=G_{1,a}+G_{1,b}+G_{1,c},\\
G_2&=(1+Z^{q,1})\frac{\epsilon}{1-\epsilon}(\frac{3}{2}+\frac{5(Z^{tr,1})^2\left\|\mathbf{D}(\mathbf{Q}^M)\right\|_{0,\Omega}^2}{2\sigma_{c,0}})\\
&=(1+Z^{q,1})\frac{3\epsilon}{2(1-\epsilon)}+(1+Z^{q,1})\frac{\epsilon}{1-\epsilon}\frac{5(Z^{tr,1})^2\left\|\mathbf{D}(\mathbf{Q}^M)\right\|_{0,\Omega}^2}{2\sigma_{c,0}}\\
&=G_{2,a}+G_{2,b},
\end{aligned}$$

$$
\begin{aligned}
G_3 &= (1+Z^{q,1})\frac{\epsilon}{1-\epsilon}\big(\frac{3}{2}+\frac{(Z^{tr,1})^2\left\|\mathbf{D}(\mathbf{Q}^M)\right\|_{0,\Omega}^2}{2\sigma_{c,0}}\big)\\
&= (1+Z^{q,1})\frac{3\epsilon}{2(1-\epsilon)}+(1+Z^{q,1})\frac{\epsilon}{1-\epsilon}\big(\frac{(Z^{tr,1})^2\left\|\mathbf{D}(\mathbf{Q}^M)\right\|_{0,\Omega}^2}{2\sigma_{c,0}}\big)\\
&= G_{3,a}+G_{3,b},\\
G_4 &= (1+Z^{q,1})\frac{\epsilon}{1-\epsilon}\big(\frac{Z^{tr,1}}{\sigma_{h,0}}\left\|\mathbf{D}(\mathbf{Q}^M)^{1/2}\right\|_{0,\Omega}^2+\left\|\mathbf{D}(\mathbf{Q}^M)^{1/2}\right\|_{0,\Omega}^2\big)\\
&= (1+Z^{q,1})\frac{\epsilon}{1-\epsilon}\frac{Z^{tr,1}}{\sigma_{h,0}}\left\|\mathbf{D}(\mathbf{Q}^M)^{1/2}\right\|_{0,\Omega}^2+(1+Z^{q})\frac{\epsilon}{1-\epsilon}\left\|\mathbf{D}(\mathbf{Q}^M)^{1/2}\right\|_{0,\Omega}^2\\
&= G_{4,a}+G_{4,b},\\
G_5 &= \frac{4\epsilon}{5(1-\epsilon)}(1+Z^{q,1}).
\end{aligned}
$$

For small enough ϵ and large enough penalty constants, $\sigma_{c,0}, \sigma_{h,0}$, we can hide the terms with G_* coefficients on the left hand side of the equation. Using this, we arrive at

$$
\begin{aligned}
&\frac{1}{2}\left\|\rho(C(\cdot,T))^{1/2}\phi^{1/2}e_c^A(\cdot,T)\right\|_{0,\Omega}^2+\frac{1}{4}\left\|\rho(C(\cdot,T))^{1/2}S^{1/2}e_h^A(\cdot,T)\right\|_{0,\Omega}^2\\
&\quad+\frac{1}{4}\int_0^T\Big[\left\|\mathbf{D}^{1/2}(\mathbf{Q}^M)\nabla e_c^A\right\|_{0,\Omega}^2+\left\|\rho(C)^{-1/2}\mathbf{K}^{-1/2}\mathbf{e}_q^A\right\|_{0,\Omega}^2+\left\|\sigma_c^{1/2}\left[\left[e_c^A\right]\right]\right\|_{0,\mathcal{E}_i}^2\\
&\quad+\left\|\sigma_h^{1/2}\left[\left[e_h^A\right]\right]\right\|_{0,\mathcal{E}_i}^2+\left\|\sigma_h^{1/2}e_h^A\right\|_{0,\Gamma_D}^2\Big]\\
&\leq Z_\Delta+Z_2\int_0^T\left\|\rho(C)^{1/2}\phi^{1/2}e_c^A\right\|_{0,\Omega}^2+Z_3\int_0^T\left\|\rho(C)^{1/2}S^{1/2}e_h^A\right\|_{0,\Omega}^2. \qquad (3.45)
\end{aligned}
$$

Applying Gronwall's inequality gives the final result.

Chapter 4

Numerical Results

As discussed in Section 1, due to the non-linear nature of the model, few analytical solutions exist to the VDFT problem and those that do exist are very narrow in scope. As a result, verification of numerical codes and validation of models for VDFT has been a challenge. Most verification and validation has been done primarily through comparison to existing numerical codes on established numerical problems. As part of the code verification process, we conducted a convergence study of our numerical methods where we looked at both the uncoupled models and the coupled model. We also explored model performance on the following benchmark problems:

1. Vertical Interface Between Fresh and Saline Groundwater,
2. Modified Henry SWI Problem,
3. 2D SWI problem of Goswami and Clement,
4. 3D Saltpool Problem.

We utilized these benchmark problems to show the method effectively captures the physics of variable density flow and solute transport from experimental results (vali-

dation) and achieves similar results as existing proven numerical codes (verification). We begin with the convergence study.

4.1 A Convergence Study

The purpose of the convergence study is to verify numerically the Δ-convergence of the method. Due to the difficulty in implementing the method of manufactured solutions (MMS) for the non-linear system, we conducted a hierarchical grid convergence study for the coupled system. However, a convergence study using MMS was conducted separately for the the LDG method and the NIPG method to show that each method separately achieved the established rate of convergence prior to analyzing the coupled system. In the rest of this section, we detail the separate convergence studies and the coupled hierarchical grid convergence study.

4.1.1 LDG Method

The LDG method convergence study utilized the flow equation:

$$\begin{cases} -\nabla \cdot \mathbf{A}\mathbf{v} = f, & x \in \Omega, \\ \mathbf{v} = \nabla u, \end{cases}$$

$$\begin{cases} \mathbf{v} \cdot \mathbf{n} = \mathbf{v}_b, & x \in \partial\Omega, \\ u = u_b \end{cases}$$

where $\Omega = [0,1] \times [0,1]$. We look at two cases. For the first case, the analytic solution is not in the approximation space while for the second, the analytic solution is in the approximation space for quadratic approximations.

For Case 1, setting

$$\mathbf{A}(x,y) = \begin{bmatrix} x^2+5 & 0 \\ 0 & y^2+5 \end{bmatrix}$$

and using the MMS with the analytical solution

$$\begin{aligned} u_a(x,y) &= \sin^2(2\pi x) + \cos^2(2\pi y) + x^2 + y^2, \\ \mathbf{v}_a(x,y) &= \nabla u_a = \begin{bmatrix} 1 + 4\pi\cos(2\pi x) * \sin(2\pi x) \\ 1 - 4\pi\cos(2\pi y) * \sin(2\pi y) \end{bmatrix}, \end{aligned}$$

gives a source function defined as

$$\begin{aligned} f(x,y) = &-2x(1 + 4\pi\cos(2\pi x) * \sin(2\pi x)) \\ &- (5 + x^2)8\pi^2(\cos^2(2\pi x) - \sin^2(2\pi x)) \\ &- 2y(1 - 4\pi\cos(2\pi y) * \sin(2\pi y) \\ &- (5 + y^2)8\pi^2(-\cos^2(2\pi y) + \sin^2(2\pi y)). \end{aligned}$$

The following boundary conditions were imposed using the analytical solutions:

$$\begin{aligned} \mathbf{v}_b &= \mathbf{v}_a \cdot \mathbf{n}, \qquad && (x,y) \in (x,1), \\ u_b &= u_a, && (x,y) \in (0,y) \cup (1,y) \cup (x,1). \end{aligned}$$

For Case 2, if we define

$$\mathbf{A}(x,y) = \begin{bmatrix} x+5 & 0 \\ 0 & y+5 \end{bmatrix}$$

and use the analytical solution

$$\begin{aligned} u_a(x,y) &= x^2 + y^2, \\ \mathbf{v}_a(x,y) &= \nabla u_a = \begin{bmatrix} 2x \\ 2y \end{bmatrix}, \end{aligned}$$

we have the source term defined as

$$f(x,y) = -2x - 2(5 + x) - 2y - 2(5 + y)).$$

The following boundary conditions are imposed using the analytic solutions:

$$\mathbf{v}_b = \mathbf{v}_a \cdot \mathbf{n}, \qquad (x, y) \in (1, y),$$

$$u_b = u_a, \qquad (x, y) \in (0, y) \cup (x, 1) \cup (x, 0).$$

Figure 4.1 shows the convergence results for Case 1. The method exhibits $p + 1$

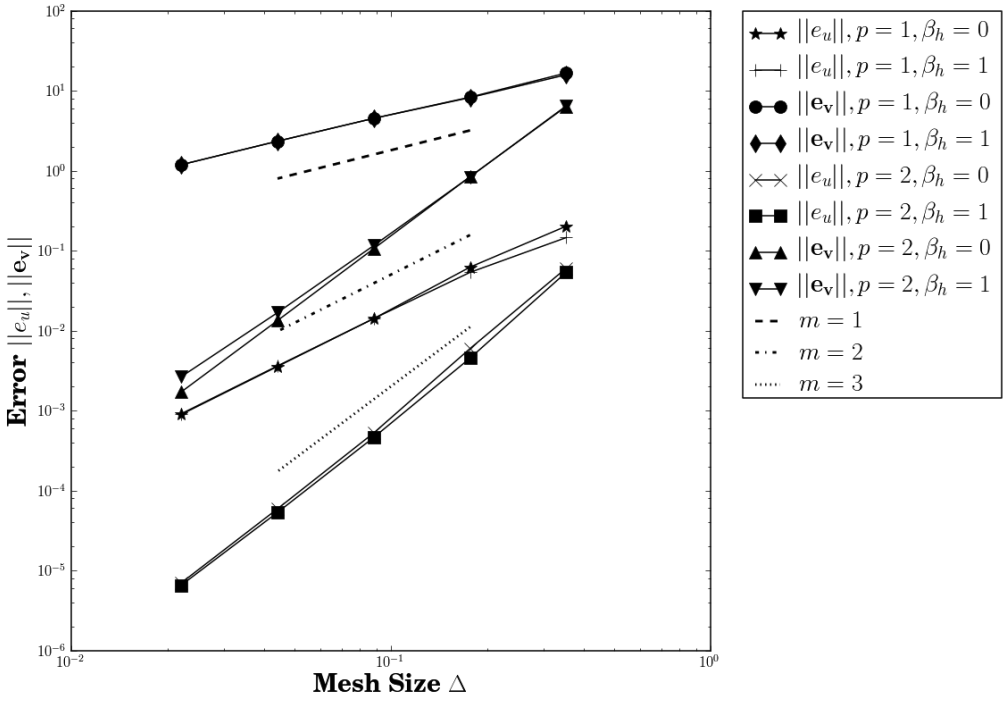

Figure 4.1: Convergence Results: LDG Only Case 1 for $p = 1, 2$ and $\beta_h = 0, 1$.

convergence for the potential, u, and better than p convergence for the velocity, which is expected. The order of the penalty parameter did not seem to affect the order of convergence. For Case 2, we achieved the same convergence rates for $p = 1$ and for $p = 2$ the error was less that 10^{-12} for both the potential and the

velocity. This is expected because the analytical solution is in the approximation space. Overall, the LDG method performed as expected on these problems.

4.1.2 NIPG Method

The NIPG formulation with standard upwinding was tested using a linear advection diffusion equation:

$$\begin{aligned} \partial_t c + \nabla \cdot (c\mathbf{u} - \mathbf{D}\nabla c) &= f(x,y,t), \quad && (x,y) \in \Omega, \\ (c\mathbf{u} - \mathbf{D}\nabla c) \cdot \mathbf{n} &= c_b u_b, && (x,y) \in \Gamma_-, \\ \mathbf{D}\nabla c \cdot n &= 0, && (x,y) \in \Gamma_+, \end{aligned}$$

where $\partial\Omega = \Gamma_+ \cup \Gamma_-$ are the inflow and outflow boundaries, respectively. We look at both the steady state and transient solutions. Again, we use MMS. Setting

$$\mathbf{D} = \begin{bmatrix} .01 & 0 \\ 0 & .01 \end{bmatrix}$$

and $\mathbf{u} = [1,0]^T$, defining the analytical solution as

$$c(x,y,t) = 2 + \cos(2\pi x) + \cos(2\pi y) + \cos(\frac{\pi}{2}t),$$

gives the source term

$$f(x,y,t) = -\frac{\pi}{2}\sin(\frac{\pi}{2}t) - 2\pi\sin(2\pi x) + .01(2\pi)^2\cos(2\pi x) + .01(2\pi)^2\cos(2\pi y).$$

We note, the gradient of the solution is zero on the boundary in order to comply with our boundary conditions. For the steady state analysis, we disregard the time dependent term. We utilize the NIPG formulation with inflow/outflow boundary conditions only. The boundary conditions on the inflow were set using the time

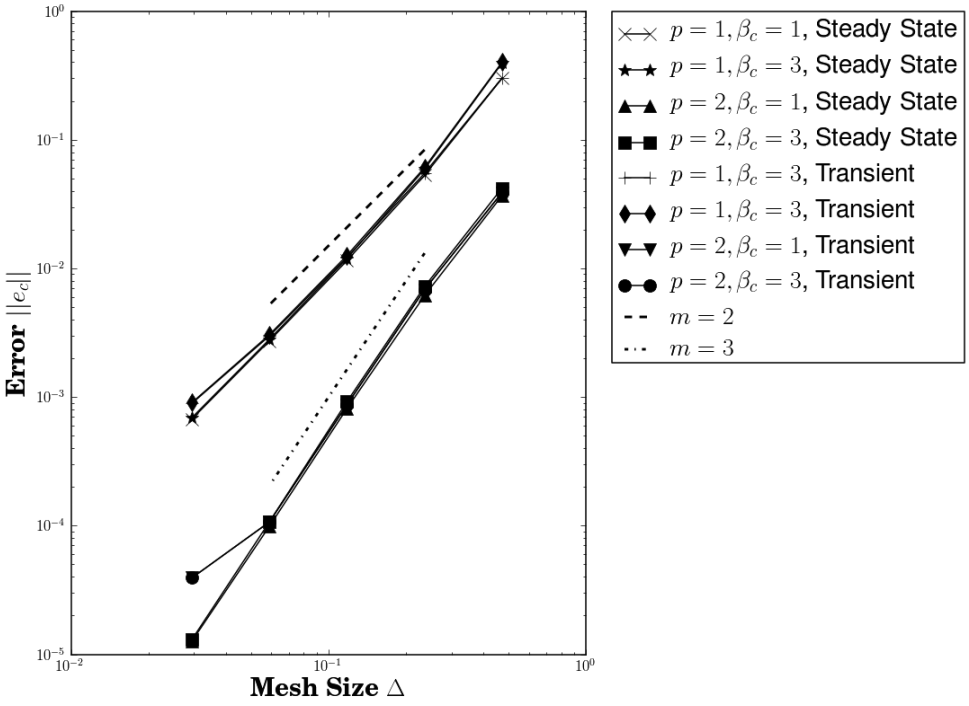

Figure 4.2: NIPG Only Convergence Results: Steady State and Transient Convergence results for $p = 1, 2$ and $\beta_c = 1, 3$.

dependent analytic solution. Figure 4.2 shows the results for both the transient and steady state case for different approximation orders $p = 1, 2$. For both $p = 1$ and $p = 2$, the method exhibits a convergence rate of $p + 1$. Simulations were run with $\sigma_c = \mathcal{O}(|e|^{-\beta})$ for $\beta = 1, 3$ (where $|e|$ is the boundary measure). There was no major difference between implementing different penalty parameters. For the transient case, a first order Backward Euler time discretization was utilized. For the $p = 2$ case, an extremely small timestep $\Delta t = .001$s was utilized to eliminate temporal error but at the highest discretization it appears that the temporal error dominated and we lost the desired convergence rates. However, utilizing a higher

order fixed leading order, backward difference formula (FLCBDF) method with error adaptation, we were able to recover the convergence rates for $p = 1$ and $p = 2$ at the finer discretizations.

4.1.3 Coupled Model Convergence Analysis

To analyze the convergence of the coupled system, we devised a problem with boundary conditions that did not involve a changing inflow/outflow seaside boundary condition. The problem consisted of an initial saltwater pocket in the center of the domain which is transported under the fluid velocity field. The domain was a 2×1m rectangular domain with no flow conditions on the top and bottom of the domain. On the left side of the domain, a constant freshwater inflow was applied and on the outflow, a zero freshwater head was established. For the transport equation, a freshwater inflow condition on the left boundary was established with $c = 0$ and a zero diffusive flux condition was established on the outflow. An initial condition corresponding to a zero freshwater head and a mass fraction initial condition defined as

$$c(x, y, 0) = e^{-50(x-1)^2-50(y-1/2)^2}$$

was used. We studied the convergence of the method for this problem using a hierarchical grid error analysis. We ran simulations with 6 grid refinements. The finest level in each case served as the "true" solution and at each level, the error was evaluated by projecting the coarse solution to the finest mesh quadrature points and then evaluated the L_2 error integrals on the fine mesh. Each of the runs utilized the Backward Euler time discretization with $dt = .01$s. Several different simulations

were run for $p = 1, 2$ with combinations of penalty powers ($\beta_h = 1, \beta_c = 1, 3$) and the results are displayed in Figure 4.3. For both linear and quadratic approximating functions, the value of the penalty parameter for the transport formulation did not impact the order of convergence. For $p = 1$, first order convergence was achieved which corroborated the error estimate proved in Section 3. For $p = 2$, we achieved a higher rate of convergence than the estimate in Section 3. The method showed third order convergence for the head and mass fraction with second order convergence for the velocity.

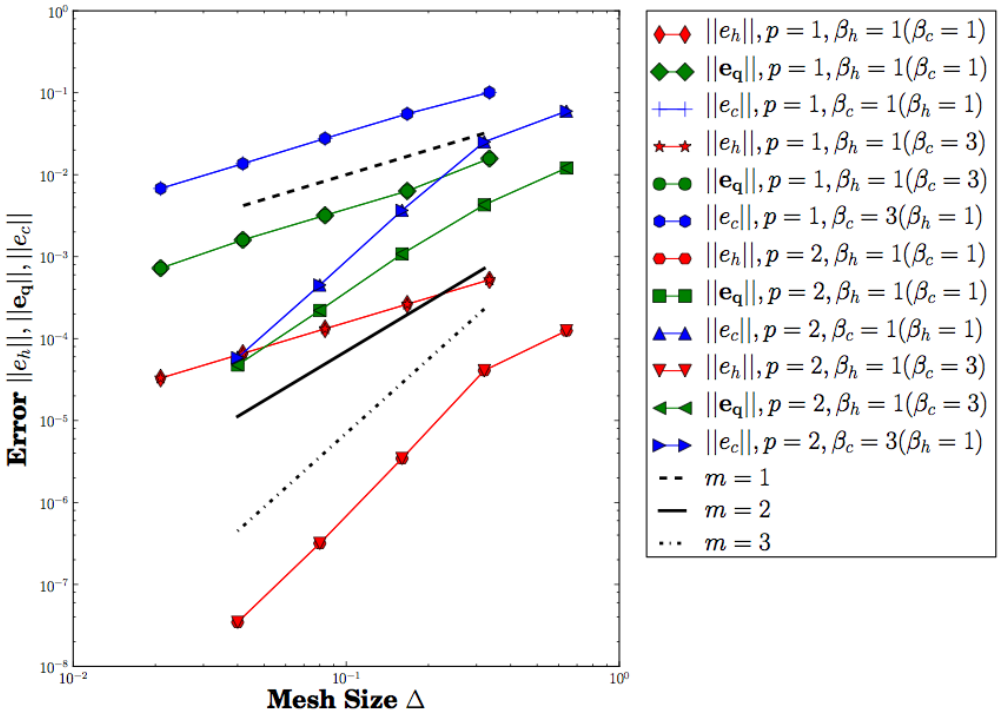

Figure 4.3: Coupled Flow and Transport Hierarchical Grid Convergence ($p = 1, 2$, $\beta_c = 1, 3, \beta_h = 1$).

4.2 Vertical Interface Between Fresh and Saline Groundwater

In the first example, we look at a problem with simple geometry to explore groundwater flow in response to density differences. The primary objective is to show that the method captures the gravity-driven flow characteristics under simple geometry and boundary conditions. This helps eliminate implementation issues and boundary error that can arise when using complex boundary conditions. The general geometry for the problem is presented in Figure 4.4. Assuming a sharp interface between freshwater and saltwater and the flow is primarily horizontal, the model for a gravity current spreading due to buoyancy effects in a confined porous layer can be written as [20]

$$\frac{\partial \psi}{\partial t} = \Lambda \frac{\partial}{\partial z}(\psi(1-\psi)\frac{\partial \psi}{\partial z}, \tag{4.1}$$

where $\psi = H/h$, the dimensionless thickness of the dense current propagating along the base of the domain and

$$\Lambda = \frac{k\Delta\rho g}{\mu\phi} \tag{4.2}$$

is the characteristic spreading of the gravity current. This model has been applied in several different physical situations to derive analytical solutions and we look at two of these situations. The first application is a model for flow in two reservoirs of differing densities connected by a long, vertically confined aquifer of constant porosity, ϕ, permeability k and thickness H. One reservoir contains less-dense freshwater ρ_f while the other contains saltwater ρ_s with each having a constant viscosity, μ (which is reasonable for small density differences). The difference in the densities causes

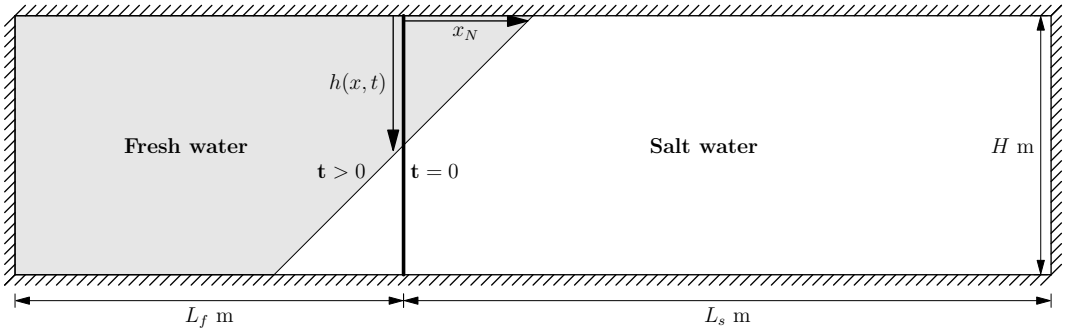

Figure 4.4: Vertical Interface Problem Setup.

the less-dense freshwater to flow over the denser saltwater. We refer to this case as the *Long Channel Case*. The second application of the model is a gravity current spreading with respect to an initial finite volume of freshwater in a porous medium. We refer to this as the *Confined Case*. Both cases exhibit different behaviors and we will show the numerical method captures these behaviors. For the second case, there are recent experimental results to compare with the numerical results.

4.2.1 Case 1: Long Channel

The first problem is presented in [20, 73] and looks at gravity-driven flow between two porous, long reservoirs containing fluids of different densities and at different pressures. Huppert and Woods [73] showed that Equation 4.1 admits a similarity solution with similarity variable $\xi = x/(\Lambda t)^{1/2}$. This showed the movement of the nose of the interface x_N at the top and bottom of the domain (see Figure 4.4) should obey the power law $x_N \approx t^{1/2}$. These analytical results corroborated earlier numerical results of Bear [20]. We look to see if our numerical method gives this result.

Parameter	Description	Value		Units
		Case 1	Case 2	
ϕ	porosity	.1	$(.42, .44, .45)^*$	[-]
ρ_0	density (freshwater)	1000	1000	$\mathrm{kg \cdot m^{-3}}$
ρ_1	density (saltwater)1025		1007.52	$\mathrm{kg \cdot m^{-3}}$
μ	dynamic viscosity	1.0×10^{-3}	8.94×10^{-4}	$\mathrm{Pa \cdot s}$
$c(\rho_0)$	mass fraction (freshwater)	0	0	kg sol/kg water
$c(\rho_1)$	mass fraction (saltwater)	1	1	kg sol/kg water
$\Delta\rho$	density contrast	25	7.62	$\mathrm{kg \cdot m^{-3}}$
D^*_{mol}	molecular diffusion coefficient	0	1.0×10^{-9}	$\mathrm{m^2 \cdot s^{-1}}$
α_L	longitudinal dispersivity	0	(0.1,0.2,0.3)	mm
α_T	transverse dispersivity	0	$.1\alpha_L$	mm
k	permeability	-	$(1.2, 5.7, 15) \times 10^{-5}$	$\mathrm{cm^2}$
K	hydraulic conductivity	1×10^{-3}	-	$\mathrm{m \cdot s^{-1}}$
S	specific mass storativity	6.87×10^{-4}	6.87×10^{-4}	$\mathrm{m^{-1}}$
H	channel height	.5	.14	m
$L_f + L_s$	channel length	4.0	1.0	m
L_f	freshwater zone initial width	2.0	.09	m

* (Case 2-1,Case 2-2, Case 2-3)

Table 4.1: Simulation Parameters for the Vertical Interface problem.

Numerical Setup. Problem parameters utilized in simulations are contained in Table 4.1. The parameters were selected to satisfy Equation 4.2. No dispersion is used making the transport equation hyperbolic so both stabilization and shock-capturing were used in the transport formulation. No flow boundary conditions were specified on the top and bottom of the domain. To simulate the long channel flow, an extended domain with no flow conditions on the left and right domain boundaries was used to reduce the boundary effects. Initial conditions corresponding to freshwater ($c = 0$) in the left part of the domain and saltwater ($c = 1$) in the right part of the domain with a sharp interface between the two fluids were established for the transport equation. For the flow equation, a corresponding equivalent freshwater head was established for each half of the domain corresponding to the different fluid densities.

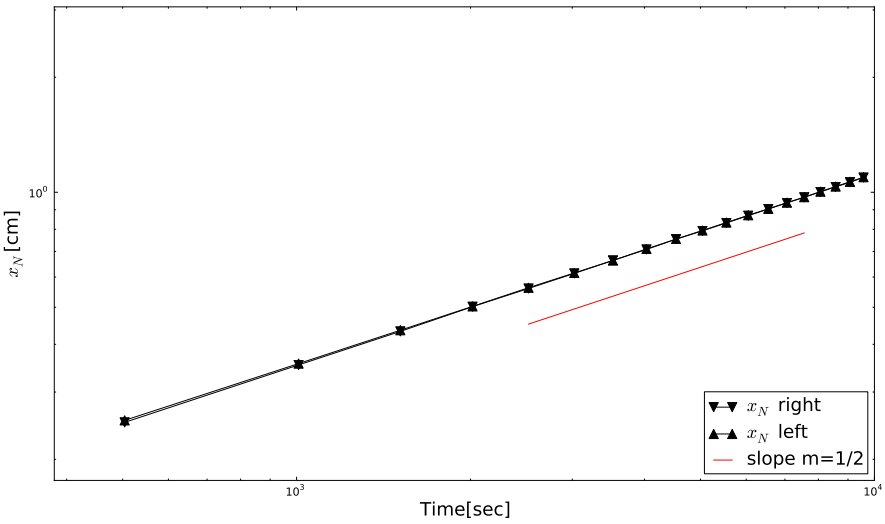

Figure 4.5: Case 1: Log-Log Plot of Nose Positions (left and right) over time.

Numerical Results Simulations were run with structured triangular meshes of 401×51 nodes. A fixed time step of $\Delta t = 10$s was utilized. Figure 4.5 displays a log-log plot of the left and right nose positions x_N over time. The nose positions were determined by the intersection of the .5 isochlor and the top (for the right) and bottom (for the left) domain boundary. As can be seen from Figure 4.5, the movement of the front obeys the proposed power law.

4.2.2 Case 2: Confined Aquifer

MacMinn and co-authors [92] recently conducted experiments in the exploration of spreading and convective dissolution of CO_2 in vertically confined, horizontal aquifers. As part of their exploration, they conducted an experiment where they

looked at gravity driven flow from an initially sharp interface between freshwater and saltwater. They utilized an asymptotic solution developed by Barenblatt [16], to determine the hydraulic conductivity of the experimental porous medium to be used in later results. We look at this experiment as a benchmark problem.

Numerical Setup. The experimental setup consisted of a $1 \times 0.15 \times .01$m flow cell filled with glass beads that was open on the top of the cell. For each experiment, a uniform bead size was selected. Initially, a gate was placed at $x = .09$m and the left side of the flow cell was filled with dyed freshwater and the right side was filled with saltwater of a given density. The gate was removed and the fluid flow was captured using a digitial camera. The porosity of flow cell was estimated using the bulk volume of fluid added to the cell. The permeability was indirectly measured via the spreading of the gravity current and the previously described theoretical model for the problem in Equation 4.1. Using this model, they treated the permeability as a fitting parameter to best fit the analytical model to the experimental results. They also present the permeability values as measured by the Kozeny-Carman (K-C) relation.

We model the physical experiment as a two-dimensional problem in a $1 \times .014$m domain to account for the unsaturated part of the domain along the top boundary and to attain the necessary volume of freshwater in the left half of the domain. Simulation parameters are highlighted in Table 4.1. All parameters that were explicitly specified in the experiment were utilized. For dispersion tensor parameters, we took the longitudinal dispersity to be the average grain size diameter

following [64] with a transverse dispersivity of 1/10 the size of the longitudinal dispersivity [100]. We utilized both the fitted permeability values as well as the K-C determined values to compare results.

Numerical Results. Using an asymptotic solution due to Barenblatt [16] for a dimensionless form of the model in Equation 4.1, MacMinn and coauthors showed that the position x_N of the nose of the freshwater plume will asymptotically approach the power law

$$\tilde{x}_N = (9\tilde{t})^{1/3},$$

where the scaled variables are defined as:

$$\tilde{x} = \frac{x}{L},$$
$$\tilde{t} = \frac{\kappa H}{L^2} t.$$

We would expect the numerical results to obey this power law. We ran numerical simulations for three different cases corresponding to the different bead sizes in Figure 4.1 using both the fitted and K-C permeability values. A structured, triangular grid of 201×29 nodes was utilized with a fixed time step of $\Delta t = 10$s. Both stabilization and shock capturing were used for the transport equation because of the small longitudinal dispersivities. Figure 4.6 compares the nose position x_N over time with the experimental results. Because the numerical results are for a transition zone model, we show both the .5 and .9 isochlor locations for the numerical freshwater nose. Figure 4.6 also displays the log-log plot of the nose position (as tracked by the .9 isochlor) versus time for each of the three bead diameters. For

reference, we display the velocity field in the vicinity of the transition zone for Case 1 in Figure 4.7. For all of the cases, the movement of the nose as tracked by the .9 isochlor obeys the expected power law. For Case 1, the numerical results are close to the experimental results. This can also be seen in Figure 4.8 which shows the experimental pictures of the current together with the numerical results as tracked by the numerical .1,.5 and .9 isochlors. However, the results get worse as the bead size increases (higher effective porosities and dispersivities). There are a number of reasons why this may have occured. The permeability in the experiments of MacMinn was not measured directly, but fitted in the context of the simplified model. The full 2D simulations performed here fit the observed nose positions best if standard Kozeny Carman permeability values are chosen. The systematic discrepancy between the KC permeabilities and those fitted by MacMinn is an indication that the simplified model introduces a systematic bias. Also, for larger grain sizes, the larger permeabilities and grain sizes lead to higher velocity values which may be outside of the regime where Darcy's law is valid.

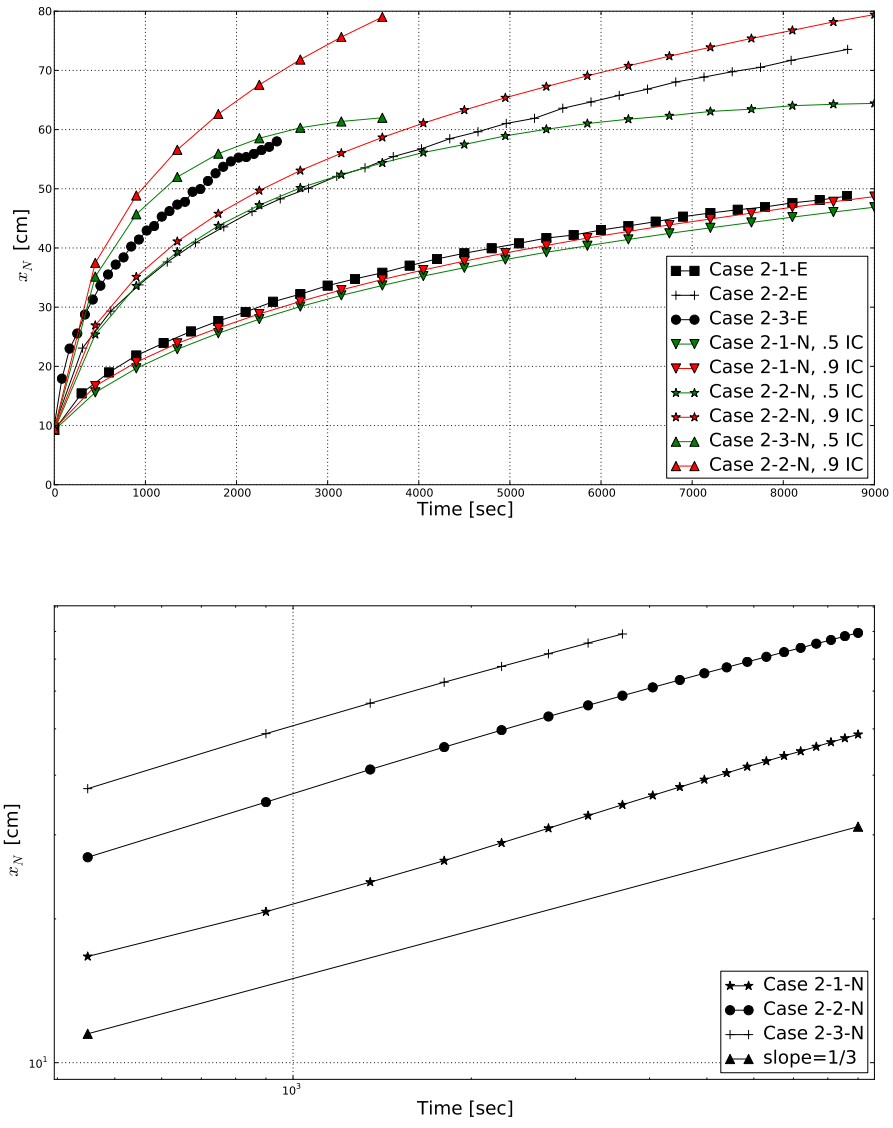

Figure 4.6: Vertical Interface Case 2: Experimental (E) and Numerical (N) Nose Positions over time for 1mm (Case 2-1), 2mm (Case 2-2) and 3mm (Case 2-3) bead experiments (top). Nose Location vs. Time Log-Log Plots (bottom).

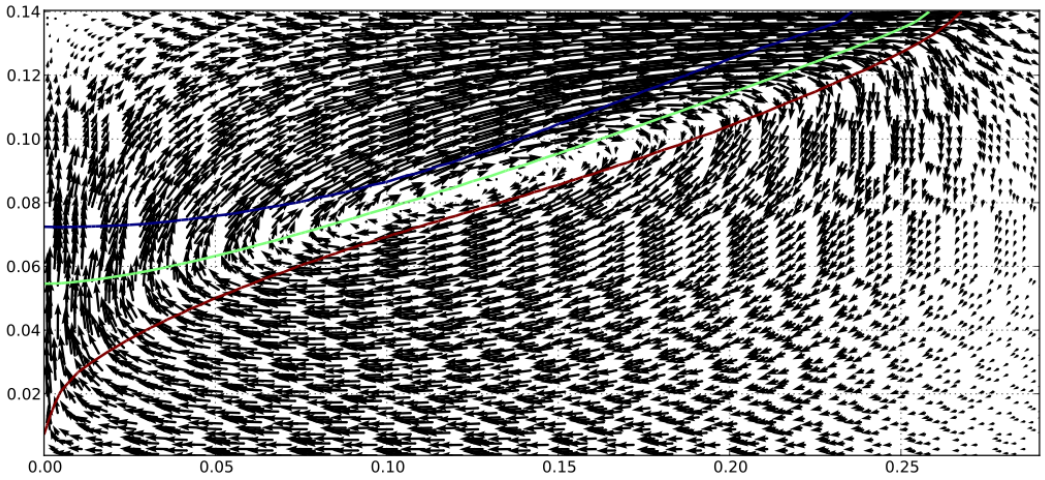

Figure 4.7: Vertical Interface Case 2-1: Velocity Field around transition zone at $t = 2250$s with .1,.5,.9 Isochlors.

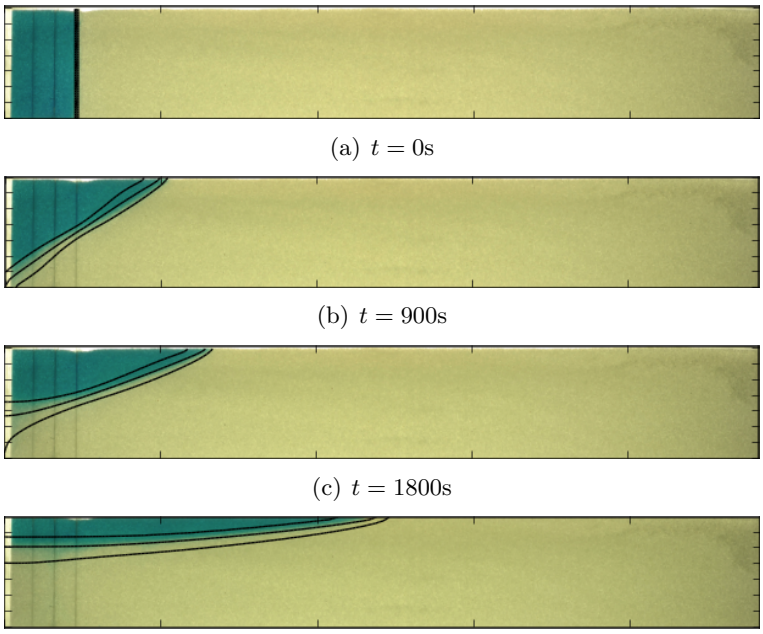

(a) $t = 0$s

(b) $t = 900$s

(c) $t = 1800$s

(d) $t = 8800$s

Figure 4.8: Case 2 Comparison: .1,.5,.9 Numerical isochlors and experimental comparison

4.3 The Modified Henry Problem

The first model for saltwater intrusion was presented by H. Henry [67] and has been the most commonly used benchmark problem for saltwater intrusion simulators. The original problem is a steady-state saltwedge in a rectangular, saturated, confined, two-dimensional aquifer. Henry presented an analytic solution for the problem and over the years, numerous researchers tried to reproduce the result with numerical models (see [118] for a review of this history). Throughout this exploration, the problem was revised and improved. We will utilize a modified version of Henry's problem proposed by Arbarca and co-authors [1] which utilizes the hydrodynamic dispersion tensor, anisotropic hydraulic conductivity tensor and implements more physical inflow/outflow sea-side boundary conditions than posed in Henry's original work. The use of a velocity dependent dispersion tensor creates more physical transition zones and, unlike the original Henry problem, the inflow/outflow seaside boundary condition makes the problem sensitive to density dependence in the domain which makes it a suitable VDFT benchmark [1]. Although Arbarca does a detailed analysis of the sensitivity of the problem to diffusion and mechanical dispersion by varying several dimensionless parameters in the problem, we only use their diffusive and dispersive reference cases and the low dispersivity case to compare code performance.

4.3.1 Numerical Setup

The problem parameters are listed in Table 4.2. For boundary conditions, a no flow condition was set at the top and bottom of the domain. On the freshwater

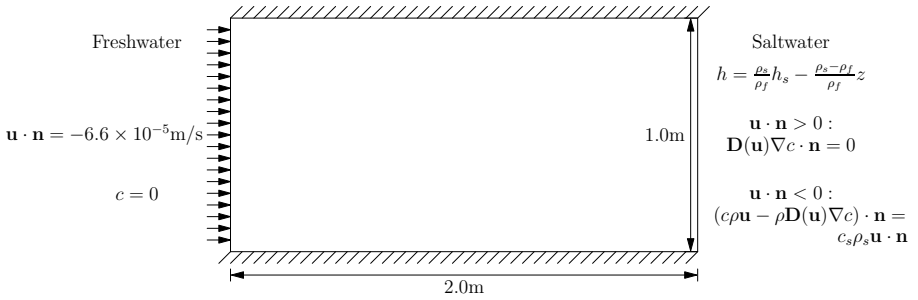

Figure 4.9: Modified Henry Problem Setup.

inflow portion of the domain, a flux corresponding to freshwater with a velocity of $\mathbf{u} = 6.6 \times 10^{-5}$ m/s was set. A concentration was set corresponding to a freshwater mass fraction. On the seaside boundary, an equivalent freshwater head corresponding to seawater density was used for the flow equation and inflow-outflow conditions were set for the transport equation. Although the original Henry problem was a steady state problem, we utilized a transient model and run simulations until they reach steady state. Initial conditions of freshwater mass fraction (c=0) and a constant freshwater head of $h = 0$ were established.

4.3.2 Numerical Results

Simulations for the diffusive and dispersive reference cases were run on a structured 40×20 node triangular grid. For the lower dispersivity case, a structured triangular grid consisting of 201×101 nodes was utilized. As a result of the parameters and the refined mesh for the lower dispersivity case, no stabilization or shock capturing was needed in the transport model. A fixed time step of $t = 10$s was utilized for each of the simulations. Figure 4.10 displays the DG model performance

Parameter	Description	Value	Units
ϕ	porosity	.35	[-]
ρ_0	density (freshwater)	1000	$\mathrm{kg} \cdot \mathrm{m}^{-3}$
ρ_1	density (saltwater)	1025	$\mathrm{kg} \cdot \mathrm{m}^{-3}$
$c(\rho_0)$	mass fraction (freshwater)	0	kg sol/kg water
$c(\rho_1)$	mass fraction (saltwater)	1	kg sol/kg water
ϵ	density contrast	.025	[-]
D_{mol}	molecular diffusion coefficient	$(18.8571 \times 10^{-6}, 0)^*$	$\mathrm{m}^2 \cdot \mathrm{s}^{-1}$
α_L	longitudinal dispersivity	(0, 0.1/.01)	m
α_T	transverse dispersivity	$(0, .1\alpha_L)$	m
K_x	hydraulic conductivity	0.01244	$\mathrm{m} \cdot \mathrm{s}^{-1}$
K_z	hydraulic conductivity	$.66K_x$	$\mathrm{m} \cdot \mathrm{s}^{-1}$
S	specific mass storativity with respect to head changes	6.87×10^{-4}	m^{-1}

* (Diffusive Case, Dispersive Case)

Table 4.2: Simulation Parameters for the dispersive Henry problem (pure diffusion and dispersion cases).

for the three simulations. For the two reference cases, the numerical results compare closely with Figure 4 from [1]. Their results were attained using the finite element simulator Saturated-Unsaturated Transport (SUTRA [122]) with a structured mesh of 256×128 elements. The low dispersivity case, compares well to the corresponding results in Figure 6 from [1], except that the dispersion zone extends slightly further than our numerical results.

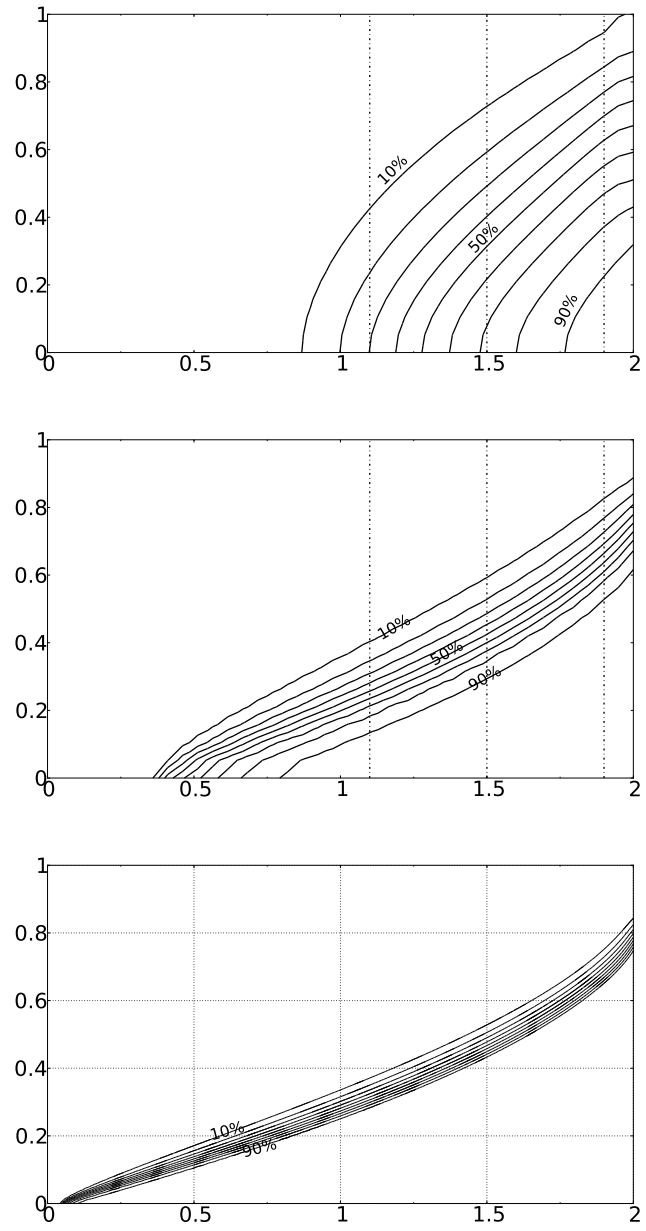

Figure 4.10: Modified Henry Problem Numerical Results: Transition zone isochlor plot for Diffusive Case (Top), Dispersive Case, $\alpha_L = .1$ (Middle), and Dispersive Case, $\alpha_L = .01$ (bottom).

4.4 Goswami-Clement Saltwater Intrusion Problem

Since the Henry problem was originally designed as a steady state saltwater intrusion problem, it cannot be used to verify the performance of a transient solution. Goswami and Clement [64] devised a laboratory experiment in which they attempted to replicate the physics of a time dependent saltwater wedge receding and intruding in a homogeneous, isotropic porous medium. They compared the experimental data to the numerical results from several well known numerical models showing good results. We utilize this experiment as one of our benchmark problems.

4.4.1 Experimental Setup

The original experiment was conducted using a rectangular flow tank with a $53 \times 30.5 \times 2.7$cm porous medium region which contained a homogeneous packing of uniform silica beads of average diameter 1.1mm. Fluid flow was forced through the flow tank using two constant-head chambers located on either side of the tank, one with saltwater and one with freshwater. Heads were set to induce a flow of freshwater through the domain while allowing a saltwater wedge to intrude into the domain. Relevant material properties for the porous medium (e.g. conductivity and porosity), were measured using several experimental methods. These parameters were used as input to the numerical model and are contained in Table 4.3. The physical experiment consisted of applying a freshwater head $h_f = 26.7$cm to the right side of the domain with a constant equivalent freshwater head corresponding to a saltwater hydraulic head of $h_s = 25.5$cm. These conditions were maintained until the saltwater wedge reached the first steady state condition (SS-1). At this

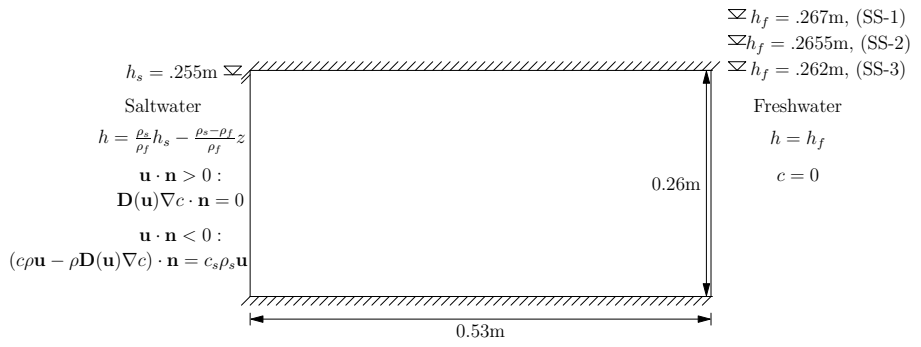

Figure 4.11: Goswami-Clement Problem Setup.

point, the right side freshwater head was reduced to $h_f = 26.2$cm and the system was allowed to evolve until it reached the second steady state condition (SS-2). Finally, the freshwater head was increased to $h_f = 26.7$cm which caused the saltwater wedge to recede and the system was allowed to evolve until the last steady state condition (SS-3). Measurements for the location of the salt wedge as well as flow measurements were taken at specified times. These measurements were developed into benchmark datasets to which we compare our numerical results.

Parameter	Description	Value	Units
ϕ	porosity	.385	[-]
μ	dynamic viscosity of freshwater	1.0×10^{-3}	$\mathrm{kgm^{-1}s^{-1}}$
g	gravitational constant	9.81	$\mathrm{m \cdot s^{-2}}$
ρ_f	density (freshwater)	998.2	$\mathrm{kg \cdot m^{-3}}$
ρ_s	density (saltwater)	1026	$\mathrm{kg \cdot m^{-3}}$
$c(\rho_f)$	reference mass fraction (freshwater)	0	kg sol/kg water
$c(\rho_s)$	normalized mass fraction (corresponding to $\omega_{\max}$)	1	kg sol/kg water
ϵ	density contrast	.026	[-]
D_{mol}	molecular diffusion coefficient	1.0×10^{-9}	$\mathrm{m^2 \cdot s^{-1}}$
α_L	transverse dispersivity	.001	m
α_T	longitudinal dispersivity	$.1\alpha_L$	m
K	hydraulic conductivity	.0122	$\mathrm{m \cdot s^{-1}}$
S	specific mass storativity with respect to head changes	1.0×10^{-5}	$\mathrm{m^{-1}}$

Table 4.3: Simulation Parameters for the Goswami-Clement Saltwater Intrusion Problem.

4.4.2 Numerical Setup

Figure 4.11 describes the domain geometry and boundary conditions. For the numerical simulations, an assumption of a fully saturated, confined porous media was made in order to apply the fully-saturated DG formulation. This was not exactly the experimental setup but is a suitable approximation since head gradients are small. An initial condition of zero concentration and corresponding constant freshwater head was established in the domain. No flow boundary conditions were set at the top and bottom of the domain as well as the upper most portion of the saltwater (left) side of the domain. Freshwater boundary conditions were set on the right side of domain as a constant freshwater hydraulic head condition and a constant concentration ($c = 0$) corresponding to freshwater. On the left side boundary, an inflow-outflow condition was set for the transport equation in which saltwater enters the lower (inflow) portion of the domain and water of variable salt concentration exits the domain on the upper (outflow) portion of the boundary. For the flow condition, a freshwater hydraulic head corresponding to a constant saltwater hydraulic head was set. This conversion to an equivalent freshwater head was given by the relation [105]

$$h = \frac{\rho_s}{\rho_f} h_s - \frac{\rho_s - \rho_f}{\rho_f} z,$$

where $h_s = 0.255$cm is the salt water hydraulic head corresponding to a pure salt water column on the left side of the domain. The distance, z, is measured from the bottom of the tank in our numerical setup.

4.4.3 Numerical Results

Goswami and Clement used several existing numerical models to simulate the experiment and presented the results which closely matched the experimental results. The primary model for which they present the results was SEAWAT [85], which utilized a fully implicit finite difference package for the flow coupled with the TVD (total-variation diminishing) advection package for the transport. They utilized a fixed time step of $\Delta t = 1$s and used several mesh sizes, presenting most results for $\Delta = .5$cm. They also utilized the SUTRA code and a modified version of the MODFLOW cell-centered finite difference model with sharp interface package Sea Water Intrusion (SWI) to simulate the experiment and noted similar results to the SEAWAT simulations.

The DG simulations were run utilizing structured, triangular grids of both 266×131 and 107×53 nodes with linear Lagrangian basis functions. To allow us to utilize a similar discretization to the published numerical results, stabilization and shock capturing were used. The small dispersivities in the transport equation required a mesh size of $\Delta x \leq .002$mm to attain mesh Peclét numbers below one. Fixed times steps of $\Delta t = 10$s were utilized. We outline the results for the different parts of the experiment.

Steady State Tests

For this part of the verification, each of the different head differentials corresponding to the three steady states were set up and the solution was evolved from the initial conditions until they reached steady state. Figure 4.12 compares the .5

salt mass isochlors for each of the steady state runs against the experimental data from the experiment. Figure 4.13 displays the transition zone widths as measured by the .1, .5 and .9 mass fraction isochlors for SS-1 (for both coarse and refined discretizations) and SS-2 (for the coarse discretization). The two steady state cases,

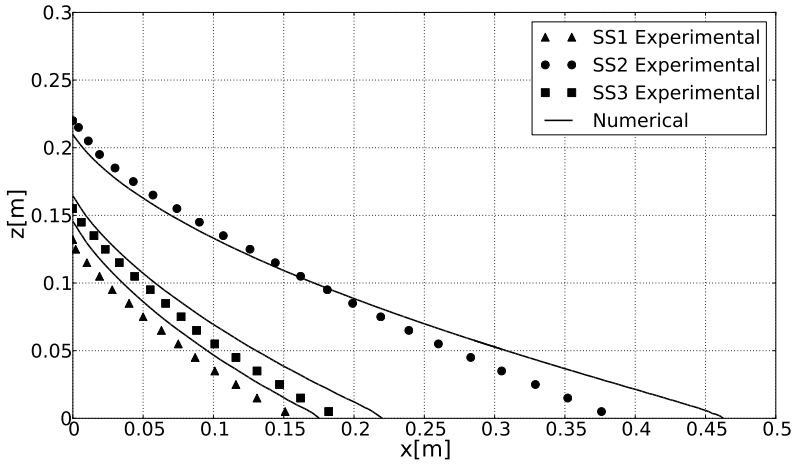

Figure 4.12: Steady State Saltwedge Comparison: Numerical .5 Isochlor Comparison with Experimental Results.

SS-1 and SS-3, are comparable to the published SEAWAT code performance in Figure 5 in [64] although they intrude slightly further into the domain. However, for the smallest head differentials (SS-2), the saltwedge intrudes further than both the experimental results and the published SEAWAT results. The DG results also have a wider transition zone which can be attributed to the numerical diffusion introduced by the stabilization. The transition zone width decreases with grid refinement as can be seen in Figure 4.13.

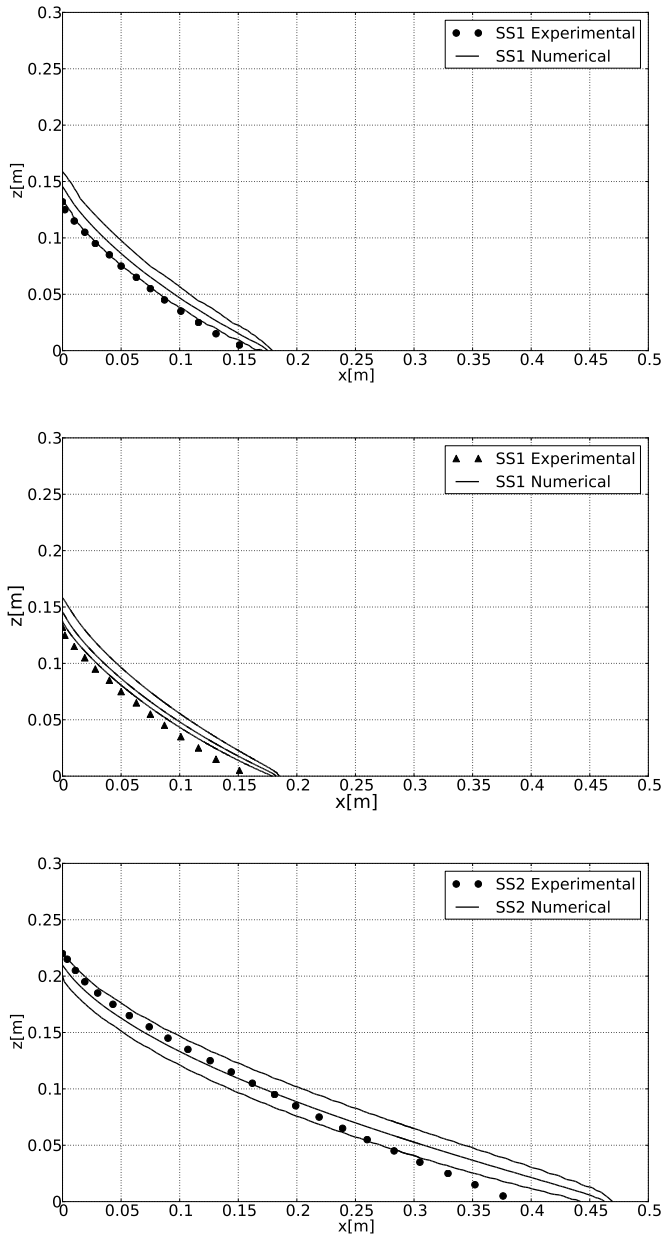

Figure 4.13: SS-1 Coarse Grid (top) and Refined Grid (middle) and SS-2 Coarse Grid (bottom) Isochlors (.1,.5,.9) with experimental data.

Flux Test

The flux test measures the flux of freshwater entering the right side of the domain at steady state. Table 4.4 presents the measured results, the variable density results from SEAWAT and Proteus as well as the numerical results for the freshwater flux for an equivalent freshwater system with no density dependence. The freshwater fluxes were computed with a zero density contrast to give non-density dependent Darcy flow. The DG results match the SEAWAT results for the freshwater flows. However, for the variable density cases, the fluxes were less than the experimental results for all three cases but were close to the SEAWAT results for the SS-1 and SS-3 cases in terms of difference from the experimental values. However, for the SS-2 case, the DG results differ significantly from the SEAWAT results which is consistent with the results from the steady state case.

	SS-1	SS-2	SS-3
Experimental Data*	1.42	0.59	1.19
Proteus Variable Density	1.37	0.563	01.125
Proteus Difference (%)	3.5	4.6	5.5
SEAWAT Variable Density	1.46	0.59	1.13
SEAWAT Difference (%)	2.8	0	5.0
SEAWAT Pure Freshwater Flow	1.94	1.12	1.69
Proteus Pure Freshwater Flow	1.93	1.12	1.69

*All units are in centimeters per second.

Table 4.4: Comparison of Measured and Model-Predicted Freshwater Flows Under Steady State Conditions.

Transient Test

The performance of the transient model is analyzed using this test. For each part of this test, advancing and receding salt wedges, simulations were initially run for sufficient time until the solution reached steady state. Then, new simulations were run with the initial freshwater head settings until the system reached the steady

state time and maintained at steady state for an additional 1000s. The freshwater boundary condition was then adjusted for the specific case and results were archived at the times used in the experiment. Figure 4.14 compare the advancing and receding salt wedge numerical results to the experimental data. Based on the steady state conditions, the movement of the salt wedge for each of the cases is comparable to the experimental results. The advancing saltwedge results are somewhat better than the receding saltwedge results due to the better match of the initial conditions.

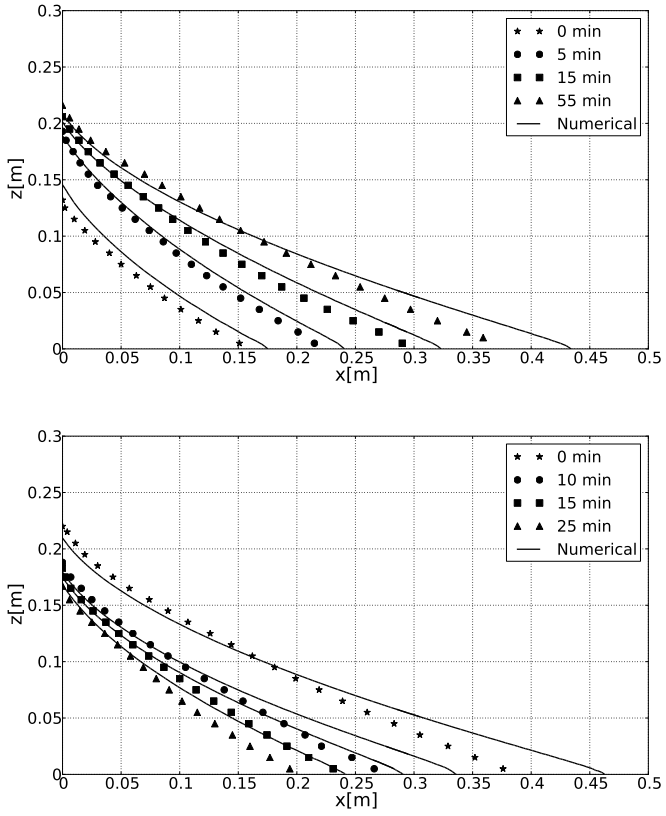

Figure 4.14: Goswami-Clement Problem Transient Results: Advancing (top) and Receding (bottom) Saltwedge Comparison: Numerical .5 Isochlors with experimental results.

4.5 3D Saltpool Problem

The Salt Pool Verification problem is based on an experiment conducted by Oswald and Kinzelbach [100] which replicates the saltwater upconing phenomena around freshwater wells in unconstrained aquifers and was designed to be a benchmark for variable density flow and transport codes. The benchmark is a necessary and sufficient test for the physics of 3D steady-state stable convection [123]. A thorough analysis and numerical simulation of the experiment was conducted by Johannsen and coauthors [75] where they conducted parameter fitting and extremely refined vertical discretization to capture the experimental results. We follow much of their work in setting up our new numerical benchmark problem.

4.5.1 Experiment Setup

The original experiment was conducted in a $0.2 \times 0.2 \times 0.2$m cube with four $.001 \times .001$ m openings at the corners of the top boundary of the cube and an opening of the same size in the middle of the bottom domain (see Figure 4.15 for the geometry of Phase 3 of the problem). The experiment consisted of three phases:

1. Phase 1: Injection of salt water through the bottom opening with outflow through the top two holes.

2. Phase 2: All openings are closed and the system is allowed to achieve a stable configuration.

3. Phase 3: Salt water is injected into the domain through one of the top openings with outflow through the top opening diagonally across from the inflow.

Experiments were conducted with 1% (Case 1) and 10 % (Case 2) salt mass fractions. For our benchmark problem, we only simulated Case 1 starting at the beginning of Phase 2 with a stable freshwater/saltwater configuration. Simulation parameters were the calibrated Case 1 parameters from the numerical simulations in [75] and are specified in Table 4.5.

4.5.2 Numerical Setup

Initial conditions again were chosen to match [75], using a stable freshwater zone overlying a saltwater zone with an 8mm wide transition zone centered at z=.06m. In the transition zone, the mass fraction varied linearly from c=0 at the top boundary to c=1 at the bottom boundary. A corresponding initial freshwater head field was constructed from the mass fraction profile. Boundary conditions were implemented using two different methods. First, following the method utilized in [75], the inflow and outflow conditions were modeled utilizing source (inlet) and sink (outlet) terms to provide the equivalent freshwater flux into and out of the domain. Numerically, this was done by implementing source/sink terms in elements contained within a cubic volume with edge size equal to the discretization, Δ_x. In this method, no flow boundary conditions were used on the entire domain. The second method was a geometric implementation of the inlet/outlet conditions where the flow equation inlet boundary condition was modeled using a normal flux Neumann condition defined as $\mathbf{Q}\rho_0$, where $\mathbf{Q}$ is the inflow flux and ρ_0 the inflow (freshwater) density. A Dirichlet freshwater head condition corresponding to a pressure value of zero was used at the outlet. On all other parts of the domain, no flow (zero normal

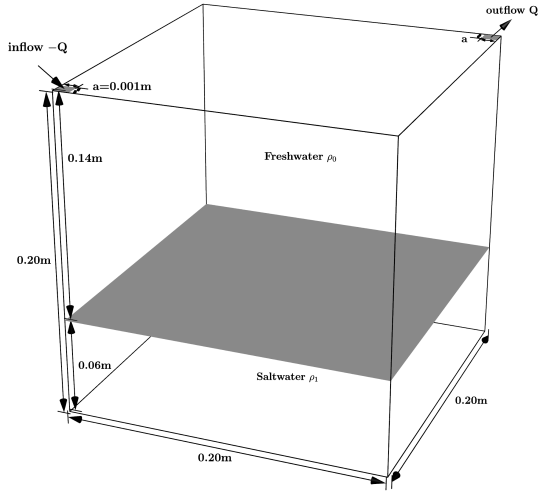

Figure 4.15: 3D Saltpool Problem Definition.

velocity) conditions were used. For the transport equation, a zero normalized mass fraction corresponding to freshwater inflow is specified for the inlet. At the outlet, a zero diffusive normal flux boundary condition is set and on the rest of the boundary, a zero total normal flux boundary condition is set. We present the results for the former inlet/outlet representation.

4.5.3 Numerical Results

For the simulations, a fixed time step of Δt=1s was used for both the flow and transport models. Both stabilization and shock-capturing were used in the transport equation because of the small dispersivities. A structured, tetrahedral mesh consisting of 64,000 nodes was used with linear Langrangian basis functions. The linear system equations were solved using the PETSc stabilized biconjugate gradient linear solver with additive Schwarz preconditioner. The simulation was run using 504 cores on the TACC Linux cluster "Lonestar". Results were compared against

the experimental Case 1 results in [100] and the numerical results of [75] which were attained using the variable density flow and transport package d^{3}f. This package employs a fully implicit/fully coupled solution technique for a vertex-centered finite volume discretization with a consistent velocity discretization. Continuous, piecewise trilinear functions were utilized and no stabilization was employed in the transport equation. A second order, implicit Runge-Kutta time integration scheme was utilized. The authors noted that they attained a qualitatively good approximation with a grid level of $4,413$ grid points.

Figure 4.17 shows the DG simulation salt mass fraction isosurfaces. Comparing

Parameter	Description	Value	Units
ϕ	porosity	.37	[-]
μ	dynamic viscosity of freshwater	1.0×10^{-3}	$\mathrm{kgm^{-1}s^{-1}}$
g	gravitational constant	9.81	$\mathrm{m \cdot s^{-2}}$
ρ_0	density (freshwater)	998.2	$\mathrm{kg \cdot m^{-3}}$
ρ_1	density (saltwater)	1007.6	$\mathrm{kg \cdot m^{-3}}$
$\omega_{\max}$	maximum salt mass fraction	.01, .1	kg sol/kg water
$c(\rho_0)$	reference mass fraction (freshwater)	0	kg sol/kg water
$c(\rho_1)$	normalized mass fraction (corresponding to $\omega_{\max}$)	1	kg sol/kg water
ϵ	density contrast	.0076	[-]
D_{mol}	molecular diffusion coefficient	1.0×10^{-9}	$\mathrm{m^2 \cdot s^{-1}}$
α_T	transverse dispersivity	1.2×10^{-3}	m
α_L	longitudinal dispersivity	$.12 \times 10^{-3}$	m
k	permeability	9.8×10^{-10}	$\mathrm{m^2}$
K	hydraulic conductivity	9.773×10^{-3}	m/s
β	fluid compressibility	0.0	$\mathrm{Pa^{-1}}$
S	specific mass storativity	6.87×10^{-4}	$\mathrm{m^{-1}}$
Q	inflow and outflow flux	1.89×10^{-6}	$\mathrm{m^3/s}$

Table 4.5: Simulation Parameters for the 3D Saltpool Problem.

to the experimental results of Figure 4 in [100], we see that the qualitative behavior of our simulation is close to the experimental results except in the corners of the domain. Figure 4.16 displays a diagonal slice of the domain with the mass fraction contours from our simulation. The results compare with the experimental results for Case 1 in Figure 3 of [100]. Except for a slightly wider transition zone, we have

a good qualitative match. Figure 4.18 shows the mass fraction break-out curves at the outlet for the experimental Case 1 (as presented in Table 2 of [75]) compared to our Case 1 simulation at different points along the diagonal bisecting the outlet. The DG simulation mass fraction break-out curves are higher starting at the corner of the outlet but are close to the experimental results in the center of the outlet. The higher mass fraction values at the corner of the domain are consistent with the earlier numerical results. The qualitative behavior is a good match, capturing the time of the maximum mass fraction value. Overall, our numerical method performance of the code on the Case 1 Saltpool Problem is good though a much finer grid was needed to capture the behavior compared to the published results in [75].

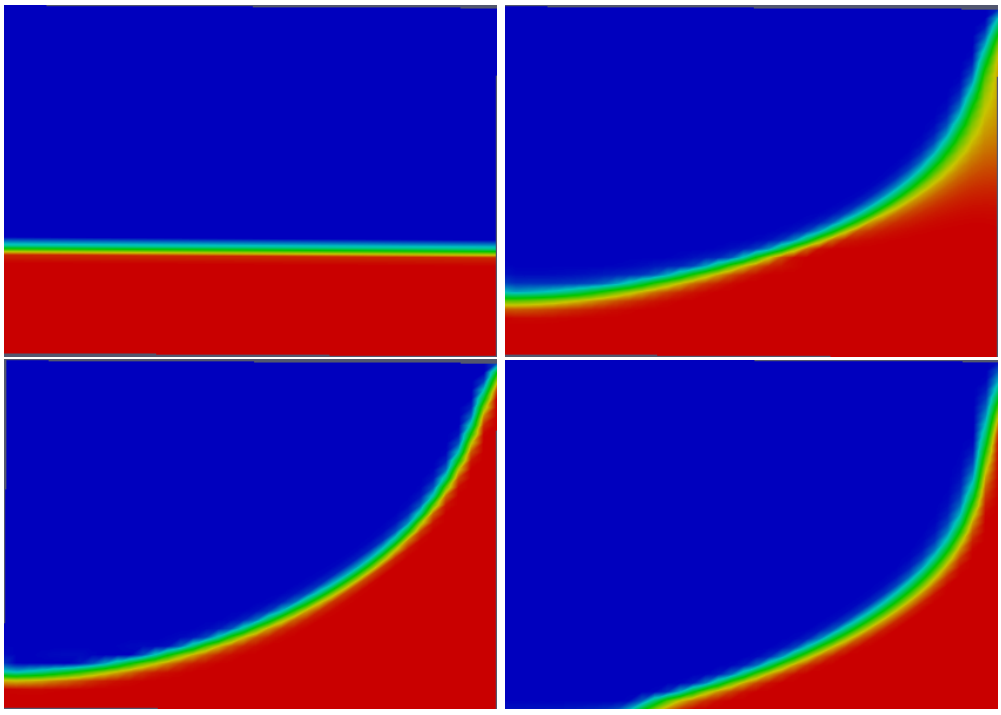

Figure 4.16: Diagonal Mass Fraction Contours: DG Numerical Results at $t = 0, 480, 1360, 8500$s (from left to right and down).

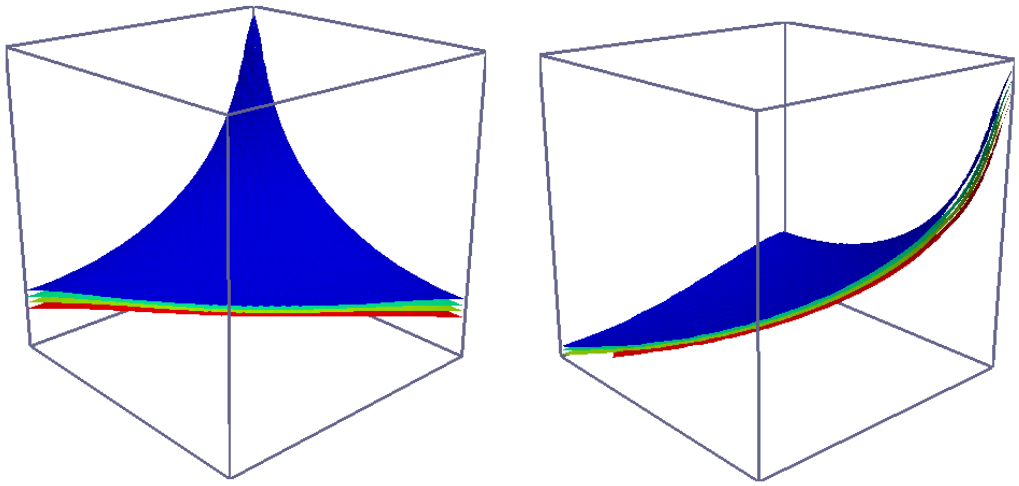

Figure 4.17: 3D view of concentration isosurfaces (Saltpool Case 1, mf=.2,.4,.6 and .8,t = 77 min).

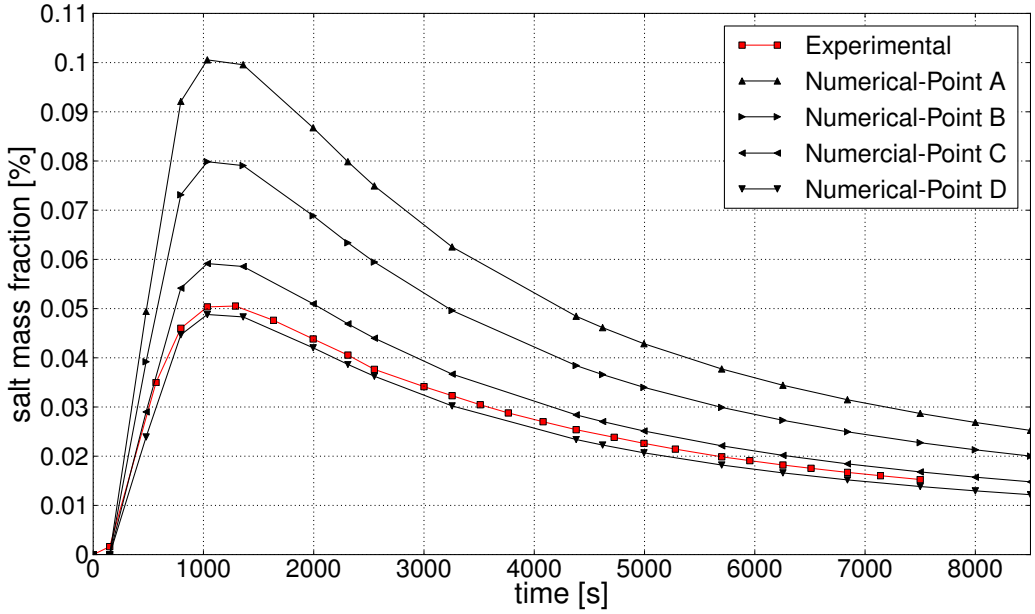

Figure 4.18: Saltpool Diagonal Mass Fraction Breakout Curve. Experimental Case 1 Results [75], and Numerical Results at $\mathbf{x}_A = [.2, .2, .2], \mathbf{x}_B = [.199, .199, .2], \mathbf{x}_C = [.198, .198, .2], \mathbf{x}_D = [.1975, .1975, .2]$.

Chapter 5

Concluding Remarks and Future Research

In this final chapter, we provide some general remarks on the previously discussed analytical and numerical results. This is followed by some future research directions and goals that arose during our exploration that were not accomplished during this disseration.

5.1 Concluding Remarks

The major aim of this dissertation was the development, analysis and implementation of a fully discontinuous formulation for the variable density flow and transport system that models salt water intrusion. For conclusions, we highlight the following:

- We implemented the proposed numerical method using the DoD Proteus Toolkit software. This implementation is flexible in that the parallel capabilities and the use of structured and unstructured triangular/tetrahedral meshes give the capability to model saltwater intrusion in large, complex domains.
- The method performed well on a number of benchmark numerical and experimental problems. In diffusion dominated problems such as the modified Henry problem, performance was similar to the published numerical results.

The method was able to capture much of the variable density flow and transport physics as demonstrated by its performance on the sharp interface and Saltpool problems. Performance on the Goswami-Clement problem was mixed, performing well on the higher head differentials cases but not at the smallest head differentials. This may be a result of the confined flow approximation and implementation of the variably saturated model as discussed below is needed.

- In problems such as the Goswami-Clement and Saltpool 3D problems with small diffusion coefficients and dispersivities where advection was dominant, the stabilization mechanisms within the NIPG transport formulation were not sufficient to reduce non-physical oscillations in the solution. Additional stabilization and shock capturing were required in the transport formulation to reduce overshoot and undershoot. This introduced numerical diffusion and led to a slightly wider transition zone.

- The analysis of Section 3 showed that the method should achieve suboptimal convergence under certain assumptions. Specifically, in deriving this error estimate, homogenous zero boundary conditions and a restriction on the density contrast was assumed. The numerical convergence study in Section 4 showed that the uncoupled formulations for the LDG and NIPG methods achieved proven convergence rates for each method. The coupled convergence study agreed with the analytical findings for linear approximating functions. For the case of quadratic approximating functions, the method achieved second order convergence for the velocity which agreed with the analytical results but achieved a higher convergence rate for the head and mass fraction. The

value of the penalty power in the transport penalty term also did not affect the convergence rates which was atypical of the NIPG method. The increased order of convergence may be a result of the non-linear coupling of the system and further investigation needs to be made into this issue.

5.2 Future Research

There are several tasks that were originally planned for this dissertation as well as a number of areas that arose during the research that will be a focus for future research. We highlight several of the areas.

- Analysis and numerical implementation was focused on the DG spatial discretization with a lesser emphasis placed on the time integration methods. A more detailed analysis of the fully discrete model to show flow and transport compatibility is still needed. Also, only first order time integration methods were applied in this work. However, to increase the temporal accuracy and the overall efficiency of the method, higher order time integration methods with adaptive capabilities are needed. Implementation of higher order fixed leading coefficient backward difference formulas (for which the backward Euler method is a subset) such as in [60] will increase the efficiency and temporal accuracy.

- As discussed previously, for advection dominated problems, the stabilization and shock capturing method in the transport formulation introduced numerical diffusion into the solution that reduced overshoot/undershoot but also led

to transition zones that were wider than the experimental results. A more detailed analysis of the stabilization formulation and the form of the stabilization parameter is needed but was beyond the current scope of this dissertation.

- Convergence rates for the coupled system in this work were determined using a hierarchical grid method. A manufactured solution for the coupled system is problematic because of the non-linearity of the coupled system but would be extremely beneficial and although it was not developed for this work, we look to develop one for future works to assist in verification of numerical codes.

- DG methods are computationally more expensive than other methods because of the increased number of degrees of freedom. To fully take advantage of the unique qualities provided by DG methods, adaptivity in mesh size and polynomial approximation order is needed. The saltwater intrusion problem, where strong physics occur only in a small, localized portion of the domain, is a strong candidate for this adaptivity. Future work in this area will make the method more computationally efficient and accurate. Ideally, this would also reduce the need for stabilization and shock capturing, better allowing the method to capture the sharp transition zones.

- Most of the benchmark problems chosen for this work were problems with a low density contrast for which a linear density constitutive relation is valid. We would like to explore model performance on problems involving higher density contrasts such as Case 2 of the saltpool problem from Section 4 in order to test method performance.

- The saturated model can be applied in the case of confined aquifers and specific cases with unconfined aquifers but to model saltwater intrusion in general cases, a model that takes into account variable saturation to account for water flow through the unsaturated zone must be used. Several models exist in the literature for the variably-saturated density-dependent model, we will implement a modified Richard's equation for the flow model and standard constitutive equations for the relative hydraulic conductivity and saturation similar to the model presented by Boufadel and coauthors [25]. This implementation will remove the need for the boundary condition between the saturated and unsaturated zones as highlighted in Section 2.

Appendices

Appendix A

Error Analysis

In this appendix, we provide the details to the proof of Theorem 3.3.9 from Section 3.3.4. We refer the reader to the preliminaries stated in Section 3.3.1-3.3.2.1 to provide the background for the proof. Specifically, we will make reference to Assumptions (A1)-(A12) and the inequalities and estimates outlined in those sections. The proof will proceed according to the following outline:

1. Derive an estimate for the head and velocity L_2 error in which the bound will include the mass fraction error time derivative.

2. Derive an estimate for the transport error in which the bound will include the L_2 velocity error.

3. Derive an estimate for the mass fraction time derivative by utilizing the transport error equation with $\tilde{w} \equiv e_h^A$. This bound will include the head error gradient and the velocity error but will be multiplied by the density constrast ϵ.

4. Derive an estimate for the head gradient L_2 error utilizing the Darcy Error equation with $\tilde{\mathbf{v}} \equiv \nabla e_h^A$ and utilize this bound to eliminate the head gradient L_2 error from (3).

5. Combine the inequalities from (1) and (2), apply the bound from (4) to eliminate the mass fraction time derivative term and utilize the penalty constant and ϵ factor to hide terms on the left hand side of the inequality.

6. Apply Grönwall's inequality to (5) to get the final error bound.

Head and Velocity L_2 Error Estimate. We first get an estimate for the flow error equation, Equation 3.31:

$$\begin{aligned}(\rho(C)Se^A_{h,t}, e^A_h)_\Omega + \left\|\rho(C)^{-1/2}\mathbf{K}^{-1/2}\mathbf{e}^A_q\right\|^2_{0,\Omega} + \left\|\sigma_h^{1/2}\left[\left[e^A_h\right]\right]\right\|^2_{0,\mathcal{E}_i} + \left\|\sigma_h^{1/2}e^A_h\right\|^2_{0,\Gamma_D} \\ = \mathcal{A}_1(e^I_h, \mathbf{e}^I_q, \mathbf{e}^A_q) + \mathcal{A}_2(\mathbf{e}^I_q, e^I_h, \mathbf{e}^A_h; C) + ((\rho(C)Se^I_{h,t}, e^A_h)_\Omega \\ + ((\rho(C)-\rho(c))Sh_t, e^A_h)_\Omega - \left\langle(\rho(C)-\rho(c))u^b, e^A_h\right\rangle_{\Gamma_N} \\ - ((\rho(C)^{-1}-\rho^{-1}(c))\mathbf{K}^{-1}\mathbf{q}, \mathbf{e}^A_q)_\Omega - ((\hat{\rho}(C)-\hat{\rho}(c))\mathbf{e}_z, \mathbf{e}^A_q)_\Omega \\ - (\phi\rho_0\epsilon e_{c,t}, e^A_h)_\Omega \\ = \mathcal{A}_1(e^I_h, \mathbf{e}^I_q, \mathbf{e}^A_q) + \mathcal{A}_2(\mathbf{e}^I_q, e^I_h, \mathbf{e}^A_h; C) + \sum_{i=1}^{6} T^F_i. \end{aligned} \tag{A.1}$$

Looking at the time derivative term on the left of Equation A.1, integrating over $[0,T]$ and then integrating by parts, we have

$$\begin{aligned}\int_0^T (\rho(C)Se^A_{h,t}, e^A_h)_\Omega &= \frac{1}{2}\int_0^T (\rho(C)S\partial_t(e^A_h)^2)_\Omega \\ &= \frac{1}{2}\left\|\rho(C)^{1/2}S^{1/2}e^A_h\right\|_{0,\Omega}\Big|_0^T - \frac{1}{2}\int_0^T (\rho(C)S)_t e^A_h, e^A_h)_\Omega, \end{aligned} \tag{A.2}$$

where we have

$$\begin{aligned}|\frac{1}{2}\int_0^T (\rho(C)S)_t e^A_h, e^A_h)_\Omega| &\le \frac{\|(\rho(C)S)_t\|_{\infty,\Omega}}{2}\int_0^T (e^A_h, e^A_h)_\Omega \\ &\le Z\int_0^T \left\|\rho(C)^{1/2}S^{1/2}e^A_h\right\|^2_{0,\Omega} \end{aligned} \tag{A.3}$$

applying (A4). Turning to the right side of the equation, we have

$$\begin{aligned}\left|T_1^F\right| &= |(\rho(C)Se_{h,t}^I, e_h^A)_\Omega| \\ &\leq Z \left\|e_{h,t}^I\right\|_{0,\Omega}^2 + \varepsilon \left\|\rho(C)^{1/2}S^{1/2}e_h^A\right\|_{0,\Omega}^2 \end{aligned} \tag{A.4}$$

using (A1). Next, we have

$$\begin{aligned}\left|T_2^F\right| &= |((\rho(C)-\rho(c))Sh_t, e_h^A)_\Omega| \\ &= \left|(\rho_0\epsilon Se_c h_t, e_h^A)_\Omega\right| \\ &\leq Z_1 \left\|\rho(C)^{1/2}\phi^{1/2}e_c^A\right\|_{0,\Omega}^2 + Z_2 \left\|e_c^I\right\|_{0,\Omega}^2 \\ &\quad \varepsilon \left\|\rho(C)^{1/2}S^{1/2}e_h^A\right\|_{0,\Omega}^2 \end{aligned} \tag{A.5}$$

where we have applied (A1,A2,A6). Using the homogeneous boundary conditions (A8), we have

$$\left|T_3^F\right| = |\left\langle(\rho(C)-\rho(c))u^b, e_h^A\right\rangle_{\Gamma_N}| = 0. \tag{A.6}$$

Applying (A1,A6,A7), we have the bound:

$$\begin{aligned}\left|T_F^4\right| &= |((\rho(C)^{-1}-\rho(c)^{-1})\mathbf{K}^{-1}\mathbf{q}, \mathbf{e}_q^A)_\Omega| \\ &= |(\frac{(\rho(c)-\rho(C))}{\rho(C)^{1/2}\rho(c)}\mathbf{K}^{-1/2}\mathbf{q}, \rho(C)^{-1/2}\mathbf{K}^{-1/2}\mathbf{e}_q^A)_\Omega| \\ &\leq Z_1 \left\|\rho(C)^{1/2}\phi^{1/2}e_c^A\right\|_{0,\Omega}^2 + Z_2 \left\|e_c^I\right\|_{0,\Omega}^2 \\ &\quad + \varepsilon \left\|\rho(C)^{-1/2}\mathbf{K}^{-1/2}\mathbf{e}_q^A\right\|_{0,\Omega}^2. \end{aligned} \tag{A.7}$$

Finally, using (A1,A7) and applying the definition of $\hat{\rho}$, we get

$$\begin{aligned}
\left|T_5^F\right| &= |((\hat{\rho}(C) - \hat{\rho}(c))\mathbf{e}_z, \mathbf{e}_q^A)_\Omega| \\
&= |(\epsilon e_c \mathbf{e}_z, \mathbf{e}_q^A)_\Omega| \\
&\leq Z_1 \left\| \rho(C)^{1/2} \phi^{1/2} e_c^A \right\|_{0,\Omega}^2 + Z_2 \left\| e_c^I \right\|_{0,\Omega}^2 \\
&+ \quad \varepsilon \left\| \rho(C)^{-1/2} \mathbf{K}^{-1/2} \mathbf{e}_q^A \right\|_{0,\Omega}^2 .
\end{aligned} \tag{A.8}$$

We leave the time derivative term T_6^F for now. We will later employ the transport error equation to get a bound on this term. Turning to the first bilinear form on the left in Equation A.1, we have

$$\begin{aligned}
\mathcal{A}_1(e_h^I, \mathbf{e}_q^I, e_h^A) &= -(\mathbf{e}_q^I, \nabla e_h^A)_\Omega + \left\langle \left\{\!\!\left\{ \mathbf{e}_q^I \right\}\!\!\right\}, \left[\!\left[e_h^A \right]\!\right] \right\rangle_{\mathcal{E}_i} + \left\langle \mathbf{e}_q^I \cdot \mathbf{n}, e_h^A \right\rangle_{\Gamma_D} \\
&\quad + \left\langle \sigma_h \left[\!\left[e_h^I \right]\!\right], \left[\!\left[e_h^A \right]\!\right] \right\rangle_{\mathcal{E}_i} + \left\langle \sigma_h e_h^I, e_h^A \right\rangle_{\Gamma_D} \\
&\equiv \sum_{i=7}^{11} T_i^F
\end{aligned} \tag{A.9}$$

and for the second bilinear form, we have

$$\begin{aligned}
\mathcal{A}_2(e_h^I, \mathbf{e}_q^I, \mathbf{e}_q^A; C) &= (\rho(C)^{-1} \mathbf{K}^{-1} \mathbf{e}_q^I, \mathbf{e}_q^A)_\Omega - (e_h^I, \nabla \cdot \mathbf{e}_q^A)_\Omega \\
&\quad + \left\langle \left\{\!\!\left\{ e_h^I \right\}\!\!\right\}, \left[\!\left[\mathbf{e}_q^A \right]\!\right] \right\rangle_{\mathcal{E}_i} + \left\langle e_h^I, \mathbf{e}_q^A \cdot \mathbf{n} \right\rangle_{\Gamma_N} \\
&\equiv \sum_{i=12}^{15} T_i^F .
\end{aligned} \tag{A.10}$$

We will bound each of the terms. First, using the inverse estimate, Equation 3.24, and applying (A1), we have

$$\begin{aligned}
\left|T_7^F\right| &= |(\mathbf{e}_q^I, \nabla e_h^A)_\Omega| \\
&\leq Z\Delta^{-1} \left\|\mathbf{e}_q^I\right\|_{0,\Omega} \Delta \left\|\rho(C)^{1/2} S^{1/2} \nabla e_h^A\right\|_{0,\Omega} \\
&\leq Z_1\Delta^{-1} \left\|\mathbf{e}_q^I\right\|_{0,\Omega} \left\|\rho(C)^{1/2} S^{1/2} e_h^A\right\|_{0,\Omega} \\
&\leq Z_2\Delta^{-2} \left\|\mathbf{e}_q^I\right\|_{0,\Omega}^2 + \varepsilon \left\|\rho(C)^{1/2} S^{1/2} e_h^A\right\|_{0,\Omega}^2 .
\end{aligned} \tag{A.11}$$

For the boundary terms, $T_8^F - T_{11}^F$, we will employ the trace estimates, Equations 3.23 and 3.26, and the definition of our penalty parameter (A10). Using these, we have

$$\begin{aligned}
\left|T_8^F\right| + \left|T_9^F\right| &= \left\langle \left\{\!\!\left\{\mathbf{e}_q^I\right\}\!\!\right\}, \left[\!\left[e_h^A\right]\!\right] \right\rangle_{\mathcal{E}_i} + |\langle \mathbf{e}_q^I \cdot \mathbf{n}, e_h^A \rangle_{\Gamma_D}| \\
&= |\langle \sigma_h^{-1/2} \left\{\!\!\left\{\mathbf{e}_q^I\right\}\!\!\right\}, \sigma_h^{1/2} \left[\!\left[e_h^A\right]\!\right] \rangle_{\mathcal{E}_i}| + |\langle \sigma_h^{-1/2} \mathbf{e}_q^I \cdot \mathbf{n}, \sigma_h^{1/2} e_h^A \rangle_{\Gamma_D}| \\
&\leq Z\Big[\left\|\sigma_h^{-1/2} \left\{\!\!\left\{\mathbf{e}_q^I\right\}\!\!\right\}\right\|_{0,\mathcal{E}_i}^2 + \left\|\sigma_h^{-1/2} \mathbf{e}_q^I\right\|_{0,\Gamma_D}^2 \Big] \\
&\quad + \varepsilon\Big[\left\|\sigma_h^{1/2} \left[\!\left[e_h^A\right]\!\right]\right\|_{0,\mathcal{E}_i}^2 + \left\|\sigma_h^{1/2} e_h^A\right\|_{0,\Gamma_D}^2 \Big] \\
&\leq Z \sum_{\Omega_e} \Delta_e \left\|\mathbf{e}_q^I\right\|_{0,\Omega_e} \left\|\mathbf{e}_q^I\right\|_{1,\Omega_e} \\
&\quad + \varepsilon\Big[\left\|\sigma_h^{1/2} \left[\!\left[e_h^A\right]\!\right]\right\|_{0,\mathcal{E}_i}^2 + \left\|\sigma_h^{1/2} e_h^A\right\|_{0,\Gamma_D}^2 \Big]
\end{aligned} \tag{A.12}$$

and

$$\begin{aligned}
\left|T_{10}^F\right| + \left|T_{11}^F\right| &= \left|\left\langle \sigma_h \left[\left[e_h^I\right]\right], \left[\left[e_h^A\right]\right] \right\rangle_{\mathcal{E}_i}\right| + \left|\left\langle \sigma_h e_h^I, e_h^A \right\rangle_{\Gamma_D}\right| \\
&= \left|\left\langle \sigma_h^{1/2} \left[\left[e_h^I\right]\right], \sigma_h^{1/2} \left[\left[e_h^A\right]\right] \right\rangle_{\mathcal{E}_i}\right| + \left|\left\langle \sigma_h^{1/2} e_h^I, \sigma_h^{1/2} e_h^A \right\rangle_{\Gamma_D}\right| \\
&\leq Z\big[\left\|\sigma_h^{1/2} \left[\left[e_h^I\right]\right]\right\|_{0,\mathcal{E}_i}^2 + \left\|\sigma_h^{1/2} e_h^I\right\|_{0,\Gamma_D}^2 \big] \\
&\quad + \varepsilon\big[\left\|\sigma_h^{1/2} \left[\left[e_h^A\right]\right]\right\|_{0,\mathcal{E}_i}^2 + \left\|\sigma_h^{1/2} e_h^A\right\|_{0,\Gamma_D}^2 \big] \\
&\leq Z \sum_{\Omega_e} \Delta_e^{-1} \left\|e_h^I\right\|_{0,\Omega_e} \left\|e_h^I\right\|_{1,\Omega_e} \\
&\quad + \varepsilon\big[\left\|\sigma_h^{1/2} \left[\left[e_h^A\right]\right]\right\|_{0,\mathcal{E}_i}^2 + \left\|\sigma_h^{1/2} e_h^A\right\|_{0,\Gamma_D}^2 \big].
\end{aligned} \tag{A.13}$$

Next, applying (A1,A7), we have

$$\begin{aligned}
\left|T_{12}^F\right| &= |(\rho(C)^{-1}\mathbf{K}^{-1}\mathbf{e}_q^I, \mathbf{e}_q^A)_\Omega| \\
&= |(\rho(C)^{-1/2}\mathbf{K}^{-1/2}\mathbf{e}_q^I, \rho(C)^{-1/2}\mathbf{K}^{-1/2}\mathbf{e}_q^A)_\Omega| \\
&\leq Z \left\|\mathbf{e}_q^I\right\|_{0,\Omega}^2 + \varepsilon \left\|\rho(C)^{-1/2}\mathbf{K}^{-1/2}\mathbf{e}_q^A\right\|_{0,\Omega}^2.
\end{aligned} \tag{A.14}$$

Since $\nabla \cdot \mathbf{e}_q^A \in \tilde{W}$, the orthogonality properties of the interpolant gives

$$\left|T_{13}^F\right| = |(e_h^I, \nabla \cdot \mathbf{e}_q^A)_\Omega| = 0. \tag{A.15}$$

For the next two terms, we apply (A1,A7), the trace estimates, Equation 3.23 and

3.26, and the definition of the penalty parameters (A9) to arrive at the bounds

$$\begin{aligned}
|T_{14}^F| + |T_{15}^F| &= \left| \left\langle \left\{\!\!\left\{ e_h^I \right\}\!\!\right\}, [\![\mathbf{e}_q^A]\!] \right\rangle_{\mathcal{E}_i} \right| + \left| \left\langle e_h^I, \mathbf{e}_q^A \cdot \mathbf{n} \right\rangle_{\Gamma_N} \right| \\
&\leq Z_1 \left\| \sigma_h^{1/2} \left\{\!\!\left\{ e_h^I \right\}\!\!\right\} \right\|_{0,\mathcal{E}_i} \left\| \sigma_h^{-1/2} \rho(C)^{-1/2} \mathbf{K}^{-1/2} [\![\mathbf{e}_q^A]\!] \right\|_{0,\mathcal{E}_i} \\
&\quad + Z_2 \left\| \sigma_h^{1/2} e_h^I \right\|_{0,\Gamma_N} \left\| \sigma_h^{-1/2} \rho(C)^{-1/2} \mathbf{K}^{-1/2} \mathbf{e}_q^A \right\|_{0,\Gamma_N} \\
&\leq Z \sum_{\Omega_e} \Delta_e^{-1} \left\| e_h^I \right\|_{0,\Omega_e} \left\| e_h^I \right\|_{1,\Omega_e} \\
&\quad + \varepsilon \left\| \rho(C)^{-1/2} \mathbf{K}^{-1/2} \mathbf{e}_q^A \right\|_{0,\Omega}. \qquad \text{(A.16)}
\end{aligned}$$

We apply the following result for the projection error, e_*^I using Equation 3.21 and using the mesh quasi-uniformity property:

$$\begin{aligned}
\sum_{\Omega_e} \left\| e_h^I \right\|_{0,\Omega_e} \left\| e_h^I \right\|_{1,\Omega_e} &\leq \sum_{\Omega_e} (Z^{p,e})^2 \Delta_e^{\min(s_{flow},k+1)} \Delta_e^{\min(s_{flow},k+1)-1} \left\| h \right\|_{s_{flow},\Omega_e}^2 \\
&\leq \max_{\Omega_e} (Z^{p,e})^2 \Delta^{2\min(s_{flow},k+1)-1} \left\| h \right\|_{s_{flow},\Omega}^2. \qquad \text{(A.17)}
\end{aligned}$$

Using this estimate with our previous results, applying (A5), integrating the appropriate terms in time and choosing the appropriate constants to hide terms on the left hand side, we arrive at our flow error estimate:

$$\begin{aligned}
&\frac{1}{2} \left\| \rho(C(\cdot,T))^{1/2} S^{1/2} e_h^A(\cdot,T) \right\|_{0,\Omega}^2 \\
&\quad + \frac{1}{2} \int_0^T \Big[\left\| \rho(C)^{-1/2} \mathbf{K}^{-1/2} \mathbf{e}_q^A \right\|_{0,\Omega}^2 + \left\| \sigma_h^{1/2} [\![e_h^A]\!] \right\|_{0,\mathcal{E}_i}^2 + \left\| \sigma_h^{1/2} e_h^A \right\|_{0,\Gamma_D}^2 \Big] \\
&\leq Z_1 \big[(\Delta^{2\min(s_{flow},k+1)} + \Delta^{2\min(s_{flow},k+1)-2}) \left\| h \right\|_{L^2(0,T;H^{s_{flow}}(\Omega))}^2 \\
&\quad + \Delta^{2\min(s_{flow},k+1)} \left\| h_t \right\|_{L^2(0,T;H^{s_{flow}}(\Omega))}^2 + \Delta^{2\min(s_{trans},k+1)} \left\| c \right\|_{L^2(0,T;H^{s_{trans}}(\Omega))}^2 \\
&\quad + (\Delta^{2\min(s_{vel},k+1)} + \Delta^{2\min(s_{vel},k+1)-2}) \left\| \mathbf{q} \right\|_{L^2(0,T;H^{s_{vel}}(\Omega))}^2 \big] \\
&\quad + Z_2 \int_0^T \Big[\left\| \rho(C)^{1/2} S^{1/2} e_h^A \right\|_{0,\Omega}^2 + \left\| \rho(C)^{1/2} \phi^{1/2} e_c^A \right\|_{0,\Omega}^2 \Big] \\
&\quad + \int_0^T \left| (\phi \rho_0 \epsilon e_{c,t}, e_h^A)_\Omega \right|, \qquad \text{(A.18)}
\end{aligned}$$

where Z_* are Δ-independent, positive constants. From this, we also get an $L_2(L_2)$ estimate on the velocity error:

$$\begin{aligned}
\frac{1}{2}\int_0^T \big[\left\| \rho(C)^{-1/2}\mathbf{K}^{-1/2}\mathbf{e}_q^A \right\|_{0,\Omega}^2 \\
&\leq Z_1\big[(\Delta^{2\min(s_{flow},k+1)} + \Delta^{2\min(s_{flow},k+1)-2})\left\|h\right\|^2_{L^2(0,T;H^{s_{flow}}(\Omega))} \\
&\quad + \Delta^{2\min(s_{flow},k+1)}\left\|h_t\right\|^2_{L^2(0,T;H^{s_{flow}}(\Omega))} \\
&\quad + \Delta^{2\min(s_{trans},k+1)}\left\|c\right\|^2_{L^2(0,T;H^{s_{trans}}(\Omega))} \\
&\quad + (\Delta^{2\min(s_{vel},k+1)} + \Delta^{2\min(s_{vel},k+1)-2})\left\|\mathbf{q}\right\|^2_{L^2(0,T;H^{s_{vel}}(\Omega))}\big] \\
&\quad + Z_2\int_0^T \big[\left\| \rho(C)^{1/2}S^{1/2}e_h^A \right\|_{0,\Omega}^2 + \left\| \rho(C)^{1/2}\phi^{1/2}e_c^A \right\|_{0,\Omega}^2 \big] \\
&\quad + \int_0^T \left| (\phi\rho_0\epsilon e_{c,t}, e_h^A)_\Omega \right|. \qquad \text{(A.19)}
\end{aligned}$$

Mass Fraction Estimates. We now turn to the transport equation to derive several estimates. We utilize the equation

$$\begin{aligned}
((\rho(C)\phi e_c^A)_t, \tilde{w})_\Omega + \mathcal{B}(e_c^A, \tilde{w}; \mathbf{Q}) = -((\rho(C)\phi\pi c - \rho(c)\phi c)_t, \tilde{w})_\Omega + \mathcal{B}(e_c^I, \tilde{w}; \mathbf{Q}) \\
+ \mathcal{B}(c, \tilde{w}; \mathbf{q}) - \mathcal{B}(c, \tilde{w}; \mathbf{Q}) \qquad \text{(A.20)}
\end{aligned}$$

and let $\tilde{w} \equiv e_c^A$ and $\tilde{w} \equiv e_h^A$, to arrive at two estimates. We note that both test functions are contained in our approximation space, $\tilde{W}$. We first start with the standard error equation.

Mass Fraction L_2 Error Estimate. Introducing $e_c = e_c^A - e_c^I$ and defining $\tilde{w} \equiv e_c^A \in \tilde{W}$ and letting $\mathbf{Q} \equiv \mathbf{Q}^M$, we have the transport error equation

$$\begin{aligned}
((\rho(C)\phi e_c^A)_t, e_c^A)_\Omega + \mathcal{B}(e_c^A, e_c^A; \mathbf{Q}^M) = -((\rho(C)\phi\pi c - \rho(c)\phi c)_t, e_c^A)_\Omega + \mathcal{B}(e_c^I, e_c^A; \mathbf{Q}^M) \\
+ \mathcal{B}(c, e_c^A; \mathbf{q}) - \mathcal{B}(c, e_c^A; \mathbf{Q}^M). \qquad \text{(A.21)}
\end{aligned}$$

We first turn to the left side of Equation A.21. For the first term, integrating over the interval $[0,T]$ and integrating by parts in time gives:

$$\int_0^T \left((\rho(C)\phi e_c^A)_t, e_c^A\right)_\Omega = \frac{1}{2}\int_0^T \left((\rho(C)\phi)_t e_c^A, e_c^A\right)_\Omega + \frac{1}{2}\left\|\rho(C)^{1/2}\phi^{1/2}e_c^A\right\|_{0,\Omega}^2 \Big|_0^T, \tag{A.22}$$

where, using (A1,A4), we have

$$|\frac{1}{2}\int_0^T \left((\rho(C)\phi)_t e_c^A, e_c^A\right)_\Omega| \le Z\int_0^T \left\|\rho(C)^{1/2}\phi^{1/2}e_c^A\right\|_{0,\Omega}^2. \tag{A.23}$$

Turning to $\mathcal{B}(e_c^A, e_c^A; \mathbf{Q}^M)$, we have

$$\begin{aligned}
\mathcal{B}_c(e_c^A, e_c^A; \mathbf{Q}^M) &= -(e_c^A\mathbf{Q}^M, \nabla e_c^A)_\Omega + (\mathbf{D}(\mathbf{Q}^M)\nabla e_c^A, \nabla e_c^A)_\Omega + \left\langle e_c^{A,u}\mathbf{Q}^M, [\![e_c^A]\!]\right\rangle_{\mathcal{E}_i} \\
&\quad - \left\langle \{\!\{\mathbf{D}(\mathbf{Q}^M)\nabla e_c^A\}\!\}, [\![e_c^A]\!]\right\rangle_{\mathcal{E}_i} + \left\langle \sigma_c [\![e_c^A]\!], [\![e_c^A]\!]\right\rangle_{\mathcal{E}_i} \\
&\quad + \left\langle e_c^A\mathbf{Q}^M, e_c^A\right\rangle_{\Gamma_+} + \left\langle \{\!\{\mathbf{D}(\mathbf{Q}^M)\nabla e_c^A\}\!\}, [\![e_c^A]\!]\right\rangle_{\mathcal{E}_i} \\
&= -(e_c^A\mathbf{Q}^M, \nabla e_c^A)_\Omega + (\mathbf{D}(\mathbf{Q}^M)\nabla e_c^A, \nabla e_c^A)_\Omega \\
&\quad + \left\langle e_c^{A,u}\mathbf{Q}^M, [\![e_c^A]\!]\right\rangle_{\mathcal{E}_i} + \left\langle \sigma_c [\![e_c^A]\!], [\![e_c^A]\!]\right\rangle_{\mathcal{E}_i} + \left\langle e_c^A\mathbf{Q}^M, e_c^A\right\rangle_{\Gamma_+} \\
&\equiv \sum_{i=1}^5 T_i^{TL}.
\end{aligned} \tag{A.24}$$

By (A9,A10) and the velocity definition on an outflow boundary, we have that T_2^{TL}, T_4^{TL}, and T_5^{TL} are all non-negative. We look at each term. Using (A1,A10) and for large enough M in the cut-off operator, we have

$$\begin{aligned}
\left|T_1^{TL}\right| &= |(e_c^A\mathbf{Q}^M, \nabla e_c^A)_\Omega| \\
&= \left|(\mathbf{D}(\mathbf{Q}^M)^{-1/2}e_c^A\mathbf{Q}^M, \mathbf{D}(\mathbf{Q}^M)^{1/2}\nabla e_c^A)_\Omega\right| \\
&\le \left\|\mathbf{D}(\mathbf{Q}^M)^{-1/2}e_c^A\mathbf{Q}^M\right\|_{0,\Omega}\left\|\mathbf{D}(\mathbf{Q}^M)^{1/2}\nabla e_c^A\right\|_{0,\Omega} \\
&\le Z\left\|\rho(C)^{1/2}\phi^{1/2}e_c^A\right\|_{0,\Omega}^2 + \varepsilon\left\|\mathbf{D}(\mathbf{Q}^M)^{1/2}\nabla e_c^A\right\|_{0,\Omega}^2.
\end{aligned} \tag{A.25}$$

Using (A10), we have

$$\begin{aligned}\left|T_2^{TL}\right| &= (\mathbf{D}(\mathbf{Q}^M)\nabla e_c^A, \nabla e_c^A)_\Omega \\ &= \left\|\mathbf{D}^{1/2}(\mathbf{Q}^M)\nabla e_c^A\right\|_{0,\Omega}^2. \end{aligned} \tag{A.26}$$

Next, applying the trace estimate, Equation 3.26, (A9) and for large enough M, we have

$$\begin{aligned}\left|T_3^{TL}\right| &= |\left\langle e_c^{A,u}\mathbf{Q}^M, [[e_c^A]]\right\rangle_{\mathcal{E}_i}| \\ &\leq \left\|\sigma_c^{-1/2}e_c^{A,u}\mathbf{Q}^M\right\|_{0,\mathcal{E}_i}\left\|\sigma_c^{1/2}\,[[e_c^A]]\right\|_{0,\mathcal{E}_i} \\ &\leq Z\left\|\sigma_c^{-1/2}e_c^{A,u}\mathbf{Q}^M\right\|_{0,\mathcal{E}_i}^2 + \varepsilon\left\|\sigma_c^{1/2}\,[[e_c^A]]\right\|_{0,\mathcal{E}_i}^2 \\ &\leq Z_1\sum_{\Omega_e}\left\|\sigma_c^{-1/2}e_c^A\right\|_{0,\partial\Omega_e}^2 + \varepsilon\left\|\sigma_c^{1/2}\,[[e_c^A]]\right\|_{0,\mathcal{E}_i}^2 \\ &\leq Z_2\left\|\rho(C)^{1/2}\phi^{1/2}e_c^A\right\|_{0,\Omega}^2 + \varepsilon\left\|\sigma_c^{1/2}\,[[e_c^A]]\right\|_{0,\mathcal{E}_i}^2. \end{aligned} \tag{A.27}$$

Using (A9), we have

$$\left|T_4^{TL}\right| = \left\|\sigma_c^{1/2}\,[[e_c^A]]\right\|_{0,\mathcal{E}_i}^2. \tag{A.28}$$

Finally, by the definition of $\mathbf{Q}^M$ on an outflow boundary, we have

$$\begin{aligned}\left|T_5^{TL}\right| &= \left\langle e_c^A\mathbf{Q}^M, e_c^A\right\rangle_{\Gamma_+} \\ &= \left\langle \mathbf{Q}^M, (e_c^A)^2\right\rangle_{\Gamma_+} \geq 0, \end{aligned} \tag{A.29}$$

and as a result, we will drop this term in our final estimate. Turning to the right side of Equation A.21, for the time derivative term, we have

$$\begin{aligned}-((\rho(C)\phi\pi c - \rho(c)\phi c)_t, e_c^A)_\Omega &= -((\phi(\rho(C)-\rho(c))\pi c)_t, e_c^A)_\Omega + ((\phi\rho(c)e_c^I)_t, e_c^A)_\Omega \\ &= -((\phi\rho_0\epsilon e_c\pi c)_t, e_c^A)_\Omega + ((\phi\rho(c)e_c^I)_t, e_c^A)_\Omega. \end{aligned} \tag{A.30}$$

Looking at the first term on the left in Equation A.30, if we expand the time derivative term, apply the definition of the error, e_c, and use (A2) we have

$$\begin{aligned}((\phi\rho_0\epsilon e_c\pi c)_t, e_c^A)_\Omega &= (\phi\rho_0\epsilon e_c\pi c_t, e_c^A)_\Omega + (\phi\rho_0\epsilon e_{c,t}\pi c, e_c^A)_\Omega \\ &= (\phi\rho_0\epsilon e_c^A\pi c_t, e_c^A)_\Omega - (\phi\rho_0\epsilon e_c^I\pi c_t, e_c^A)_\Omega \\ &\quad + (\phi\rho_0\epsilon e_{c,t}^A\pi c, e_c^A)_\Omega - (\phi\rho_0\epsilon e_{c,t}^I\pi c, e_c^A)_\Omega, \end{aligned} \tag{A.31}$$

where we have for the first term

$$|(\phi\rho_0\epsilon e_c^A\pi c_t, e_c^A)_\Omega| \leq Z \left\| \rho(C)^{1/2}\phi^{1/2}e_c^A \right\|_{0,\Omega}^2, \tag{A.32}$$

applying (A1,A6). For the second and third terms, applying (A1,A6), we have

$$\begin{aligned}|(\phi\rho_0\epsilon e_c^I\pi c_t, e_c^A)_\Omega - (\phi\rho_0\epsilon e_{c,t}^I\pi c, e_c^A)_\Omega| &\leq Z\left[\left\|e_c^I\right\|_{0,\Omega}^2 + \left\|e_{c,t}^I\right\|_{0,\Omega}^2 \right] \\ &\quad + \varepsilon \left\| \rho(C)^{1/2}\phi^{1/2}e_c^A \right\|_{0,\Omega}^2. \end{aligned} \tag{A.33}$$

Finally, for the last term, integrating in time and applying (A1,A6) gives

$$\begin{aligned}\int_0^T (\phi\rho_0\epsilon e_{c,t}^A\pi c, e_c^A)_\Omega &= \int_0^T (\phi\rho_0\epsilon\pi c, \partial_t(e_c^A)^2)_\Omega \\ &= \left\| (\phi\rho_0\epsilon\pi c)^{1/2}e_c^A \right\|_{0,\Omega}^2 |_0^T \\ &\leq \epsilon \left\| (\phi^{1/2}\rho(C)^{1/2}e_c^A(\cdot,T) \right\|_{0,\Omega}^2 \\ &\leq \frac{1}{4} \left\| (\phi^{1/2}\rho(C)^{1/2}e_c^A(\cdot,T) \right\|_{0,\Omega}^2. \end{aligned} \tag{A.34}$$

for $\epsilon < 1/4$. For the second term in Equation A.30, using (A1,A4), we have

$$\begin{aligned}|((\phi\rho(c)e_c^I)_t, e_c^A)_\Omega| &= |(\phi\rho(c)e_{c,t}^I, e_c^A)_\Omega + ((\phi\rho(c))_t e_c^I, e_c^A)_\Omega| \\ &\leq Z\left[\left\|e_c^I\right\|_{0,\Omega}^2 + \left\|e_{c,t}^I\right\|_{0,\Omega}^2 \right] + \varepsilon \left\| \rho(C)^{1/2}\phi^{1/2}e_c^A \right\|_{0,\Omega}^2. \end{aligned} \tag{A.35}$$

Turning to $\mathcal{B}(e_c^I, e_c^A; \mathbf{Q}^M)$, we have

$$\begin{aligned}\mathcal{B}(e_c^I, e_c^A; \mathbf{Q}^M) \equiv & -(e_c^I \mathbf{Q}^M, \nabla e_c^A)_\Omega + (\mathbf{D}(\mathbf{Q}^M)\nabla e_c^I, \nabla e_c^A)_\Omega + \left\langle e_c^{I,u}\mathbf{Q}^M, [[e_c^A]] \right\rangle_{\mathcal{E}_i} \\ & - \left\langle \{\{\mathbf{D}(\mathbf{Q}^M)\nabla e_c^I\}\}, [[e_c^A]] \right\rangle_{\mathcal{E}_i} + \left\langle \sigma_c [[e_c^I]], [[e_c^A]] \right\rangle_{\mathcal{E}_i} \\ & + \left\langle e_c^I \mathbf{Q}^M, e_c^A \right\rangle_{\Gamma_+} + \left\langle \{\{\mathbf{D}(\mathbf{Q}^M)\nabla e_c^A\}\}, [[e_c^I]] \right\rangle_{\mathcal{E}_i} \\ \equiv & \sum_{i=1}^{7} T_i^{TR}. \end{aligned} \tag{A.36}$$

We bound each one of the terms. For large enough M and using (A10), we have

$$\begin{aligned}\left|T_1^{TR}\right| &= |(e_c^I \mathbf{Q}^M, \nabla e_c^A)_\Omega| \\ &\leq Z \left\|e_c^I\right\|_{0,\Omega}^2 + \varepsilon \left\|\mathbf{D}(\mathbf{Q}^M)^{1/2}\nabla e_c^A\right\|_{0,\Omega}^2. \end{aligned} \tag{A.37}$$

Using (A10), we have

$$\begin{aligned}\left|T_2^{TR}\right| &= |(\mathbf{D}(\mathbf{Q}^M)\nabla e_c^I, \nabla e_c^A)_\Omega| \\ &\leq Z \left\|\nabla e_c^I\right\|_{0,\Omega}^2 + \varepsilon \left\|\mathbf{D}(\mathbf{Q}^M)^{1/2}\nabla e_c^A\right\|_{0,\Omega}^2. \end{aligned} \tag{A.38}$$

For the boundary terms $T_3^{TR} - T_7^{TR}$, we employ the trace estimates, Equations 3.23 and 3.26 and the penalty parameter assumptions (A9). So, for large enough M and using (A9,A10), we have

$$\begin{aligned}\left|T_3^{TR}\right| + \left|T_6^{TR}\right| &= \left|\left\langle e_c^{I,u}\mathbf{Q}^M, [[e_c^A]] \right\rangle_{\mathcal{E}_i}\right| + \left|\left\langle e_c^I \mathbf{Q}^M, e_c^A \right\rangle_{\Gamma_+}\right| \\ &= \left|\left\langle \sigma_c^{-1/2} e_c^{I,u}\mathbf{Q}^M, \sigma_c^{1/2} [[e_c^A]] \right\rangle_{\mathcal{E}_i}\right| + \left|\left\langle \sigma_c^{1/2} e_c^I \mathbf{Q}^M, \sigma_c^{-1/2} e_c^A \right\rangle_{\Gamma_+}\right| \\ &\leq \left\|\sigma_c^{-1/2} e_c^{I,u}\mathbf{Q}^M\right\|_{0,\mathcal{E}_i} \left\|\sigma_c^{1/2} [[e_c^A]]\right\|_{0,\mathcal{E}_i} \\ &\quad + \left\|\sigma_c^{1/2} e_c^I \mathbf{Q}^M\right\|_{0,\Gamma_+} \left\|\sigma_c^{-1/2} e_c^A\right\|_{0,\Gamma_+} \\ &\leq Z \sum_{\Omega_e} \left[\Delta_e^{-1} \left\|e_c^I\right\|_{0,\Omega_e} \left\|e_c^I\right\|_{1,\Omega_e} + \Delta_e \left\|e_c^I\right\|_{0,\Omega_e} \left\|e_c^I\right\|_{1,\Omega_e}\right] \\ &\quad + \varepsilon_1 \left\|\rho(C)^{1/2}\phi^{1/2} e_c^A\right\|_{0,\Omega}^2 + \varepsilon_2 \left\|\sigma_c^{1/2} [[e_c^A]]\right\|_{0,\mathcal{E}_i}^2. \end{aligned} \tag{A.39}$$

Using (A9), Equation 3.23 and for large enough M, we have

$$\begin{aligned}
\left|T_4^{TR}\right| &= |\langle \left\{\!\!\left\{\mathbf{D}(\mathbf{Q}^M)\nabla e_c^I\right\}\!\!\right\}, \left[\!\left[e_c^A\right]\!\right] \rangle_{\mathcal{E}_i}| \\
&\leq \left\|\sigma_c^{-1/2} \left\{\!\!\left\{\mathbf{D}(\mathbf{Q}^M)\nabla e_c^I\right\}\!\!\right\}\right\|_{0,\mathcal{E}_i} \left\|\sigma_c^{1/2} \left[\!\left[e_c^A\right]\!\right]\right\|_{0,\mathcal{E}_i} \\
&\leq Z \sum_{\Omega_e} \Delta_e \left\|\nabla e_c^I\right\|_{0,\Omega_e} \left\|\nabla e_c^I\right\|_{1,\Omega_e} \\
&\quad + \varepsilon \left\|\sigma_c^{1/2} \left[\!\left[e_c^A\right]\!\right]\right\|_{0,\mathcal{E}_i}^2 . \qquad \text{(A.40)}
\end{aligned}$$

Again, using (A9) and Equation 3.23, we have

$$\begin{aligned}
\left|T_5^{TR}\right| &= |\langle \sigma_c \left[\!\left[e_c^I\right]\!\right], \left[\!\left[e_c^A\right]\!\right] \rangle_{\mathcal{E}_i}| \\
&\leq \left\|\sigma_c^{1/2} \left[\!\left[e_c^I\right]\!\right]\right\|_{0,\mathcal{E}_i} \left\|\sigma_c^{1/2} \left[\!\left[e_c^A\right]\!\right]\right\|_{0,\mathcal{E}_i} \\
&\leq Z \sum_{\Omega_e} \Delta_e^{-1} \left\|e_c^I\right\|_{0,\Omega_e} \left\|e_c^I\right\|_{1,\Omega_e} + \varepsilon \left\|\sigma_c^{1/2} \left[\!\left[e_c^A\right]\!\right]\right\|_{0,\mathcal{E}_i}^2 . \qquad \text{(A.41)}
\end{aligned}$$

For the last term, applying (A10) and for large enough M, we have

$$\begin{aligned}
\left|T_7^{TR}\right| &= |\langle \left\{\!\!\left\{\mathbf{D}(\mathbf{Q}^M)\nabla e_c^A\right\}\!\!\right\}, \left[\!\left[e_c^I\right]\!\right] \rangle_{\mathcal{E}_i}| \\
&\leq \left\|\sigma_c^{-1/2} \left\{\!\!\left\{\mathbf{D}(\mathbf{Q}^M)\nabla e_c^A\right\}\!\!\right\}\right\|_{0,\mathcal{E}_i} \left\|\sigma_c^{1/2} \left[\!\left[e_c^I\right]\!\right]\right\|_{0,\mathcal{E}_i} \\
&\leq \varepsilon \left\|\mathbf{D}(\mathbf{Q}^M)^{1/2}\nabla e_c^A\right\|_{0,\Omega}^2 + Z \sum_{\Omega_e} \Delta_e^{-1} \left\|e_c^I\right\|_{0,\Omega_e}^2 \left\|e_c^I\right\|_{1,\Omega_e}^2 . \qquad \text{(A.42)}
\end{aligned}$$

Finally, we turn to $\mathcal{B}(c, e_c^A; \mathbf{q}) - \mathcal{B}(c, e_c^A; \mathbf{Q}^M)$:

$$\begin{aligned}
\mathcal{B}(c, e_c^A; \mathbf{q}) - \mathcal{B}(c, e_c^A; \mathbf{Q}^M) &= -((\mathbf{q} - \mathbf{Q}^M)c, \nabla e_c^A)_\Omega + ((\mathbf{D}(\mathbf{q}) - \mathbf{D}(\mathbf{Q}^M)\nabla c, \nabla e_c^A)_\Omega \\
&\quad + \left\langle c(\mathbf{q} - \mathbf{Q}^M), \left[\!\left[e_c^A\right]\!\right] \right\rangle_{\mathcal{E}_i} \\
&\quad - \left\langle \left\{\!\!\left\{\mathbf{D}(\mathbf{q}) - \mathbf{D}(\mathbf{Q}^M)\nabla c\right\}\!\!\right\}, \left[\!\left[e_c^A\right]\!\right] \right\rangle_{\mathcal{E}_i} \\
&\quad + \left\langle c(\mathbf{q} - \mathbf{Q}^M), e_c^A \right\rangle_{\Gamma_+} \\
&\equiv \sum_{i=8}^{12} T_i^{TR}. \qquad \text{(A.43)}
\end{aligned}$$

We bound each of the terms. For the first term, using (A1,A7,A10) and for large enough M, we have

$$\begin{aligned}
\left|T_8^{TR}\right| &\leq \left|((\mathbf{e}_q^A c, \nabla e_c^A)_\Omega\right| + \left|(\mathbf{e}_q^I c, \nabla e_c^A)_\Omega\right| \\
&= \left|(\rho(C)^{1/2}\mathbf{K}^{1/2}\rho(C)^{-1/2}\mathbf{K}^{-1/2}\mathbf{e}_q^A, \mathbf{D}(\mathbf{Q}^M)^{-1/2}\mathbf{D}(\mathbf{Q}^M)^{1/2}\nabla e_c^A)_\Omega\right| \\
&\quad + \left|(\mathbf{e}_q^I, \mathbf{D}(\mathbf{Q}^M)^{-1/2}\mathbf{D}(\mathbf{Q}^M)^{1/2}\nabla e_c^A)_\Omega\right| \\
&\leq \frac{Z_1^q}{2\varepsilon}\left\|\rho(C)^{-1/2}\mathbf{K}^{-1/2}\mathbf{e}_q^A\right\|_{0,\Omega}^2 + Z\left\|\mathbf{e}_q^I\right\|_{0,\Omega}^2 \\
&\quad + \frac{\varepsilon}{2}\left\|\mathbf{D}(\mathbf{Q}^M)^{1/2}\nabla e_c^A\right\|_{0,\Omega}^2, \qquad \text{(A.44)}
\end{aligned}$$

where $Z_1^q = \rho^* k^* \left\|\mathbf{D}(\mathbf{Q}^M)^{-1/2}\right\|_{0,\Omega}^2$.

Using the definition of the hydrodynamic dispersion tensor, Equation 3.16, the second term can be written as

$$\begin{aligned}
\left|T_9^{TR}\right| &= \left|((\mathbf{D}_{mech}(\mathbf{q}) - \mathbf{D}_{mech}(\mathbf{Q}^M))\nabla c, \nabla e_c^A)_\Omega\right. \\
&\quad \left. + (\mathbf{D}_{mol}(\rho(c) - \rho(C))\nabla c, \nabla e_c^A)_\Omega\right|. \\
&\leq \left|((\mathbf{D}_{mech}(\mathbf{q}) - \mathbf{D}_{mech}(\pi\mathbf{q})\nabla c, \nabla e_c^A)_\Omega\right| \\
&\quad + \left|((\mathbf{D}_{mech}(\pi\mathbf{q}) - \mathbf{D}_{mech}(\mathbf{Q}^M)\nabla c, \nabla e_c^A)_\Omega\right| \\
&\quad + \left|(\mathbf{D}_{mol}(\rho(c) - \rho(C))\nabla c, \nabla e_c^A)_\Omega\right|. \\
&\equiv \left|T_{9a}^{TR}\right| + \left|T_{9b}^{TR}\right| + \left|T_{9c}^{TR}\right|. \qquad \text{(A.45)}
\end{aligned}$$

Looking at the first term on the right in Equation A.45, applying (A6,A10) and

Equation 3.17, we have

$$\begin{aligned}
\left|T_{9a}^{TR}\right| &= \left|((\mathbf{D}_{mech}(\mathbf{q}) - \mathbf{D}_{mech}(\pi\mathbf{q}))\nabla c, \nabla e_c^A)_\Omega\right| \\
&\leq \|\nabla c\|_{0,\Omega} \|\mathbf{D}_{mech}(\mathbf{q}) - \mathbf{D}_{mech}(\pi\mathbf{q})\|_{0,\Omega} \left\|\mathbf{D}(\mathbf{Q}^M)^{-1/2}\mathbf{D}(\mathbf{Q}^M)^{1/2}\nabla e_c^A\right\|_{0,\Omega} \\
&\leq Z^D \|\nabla c\|_{0,\Omega} \left\|\mathbf{e}_q^I\right\|_{0,\Omega} \left\|\mathbf{D}(\mathbf{Q}^M)^{-1/2}\right\|_{0,\Omega} \left\|\mathbf{D}(\mathbf{Q}^M)^{1/2}\nabla e_c^A\right\|_{0,\Omega} \\
&\leq Z \left\|\mathbf{e}_q^I\right\|_{0,\Omega}^2 + \varepsilon \left\|\mathbf{D}(\mathbf{Q}^M)^{1/2}\nabla e_c^A\right\|_{0,\Omega}^2. \qquad \text{(A.46)}
\end{aligned}$$

For the second term on the right in Equation A.45, applying (A6,A10) and Equation 3.17, we have

$$\begin{aligned}
\left|T_{9b}^{TR}\right| &= \left|((\mathbf{D}_{mech}(\pi\mathbf{q}) - \mathbf{D}_{mech}(\mathbf{Q}^M))\nabla c, \nabla e_c^A)_\Omega\right| \\
&\leq \|\nabla c\|_{0,\Omega} \left\|\mathbf{D}_{mech}(\pi\mathbf{q}) - \mathbf{D}_{mech}(\mathbf{Q}^M)\right\|_{0,\Omega} \left\|\mathbf{D}(\mathbf{Q}^M)^{-1/2}\mathbf{D}(\mathbf{Q}^M)^{1/2}\nabla e_c^A\right\|_{0,\Omega} \\
&\leq Z^D \|\nabla c\|_{0,\Omega} \left\|\rho(C)^{1/2}\mathbf{K}^{1/2}\rho(C)^{-1/2}\mathbf{K}^{-1/2}\mathbf{e}_q^A\right\|_{0,\Omega} * \\
&\quad \left\|\mathbf{D}(\mathbf{Q}^M)^{-1/2}\right\|_{0,\Omega} \left\|\mathbf{D}(\mathbf{Q}^M)^{1/2}\nabla e_c^A\right\|_{0,\Omega} \\
&\leq \frac{Z_2^q}{2\varepsilon} \left\|\rho(C)^{-1/2}\mathbf{K}^{-1/2}\mathbf{e}_q^A\right\|_{0,\Omega}^2 + \frac{\varepsilon}{2} \left\|\mathbf{D}(\mathbf{Q}^M)^{1/2}\nabla e_c^A\right\|_{0,\Omega}^2 \qquad \text{(A.47)}
\end{aligned}$$

where $Z_2^q = (Z^D)^2\rho^* k^* \left\|\mathbf{D}(\mathbf{Q}^M)^{-1/2}\right\|_{0,\Omega}^2 \|\nabla c\|_{0,\Omega}^2$.

Looking at the last term on the right in Equation A.45, using (A1,A2,A10), we have

$$\begin{aligned}
\left|T_{9c}^{TR}\right| &\leq \left|(\mathbf{D}_{mol}(\rho_0\epsilon e_c^A)\nabla c, \nabla e_c^A)_\Omega\right| + \left|(\phi\mathbf{D}_{mol}(\rho_0\epsilon e_c^I)\nabla c, \nabla e_c^A)_\Omega\right| \\
&\leq Z_1 \left\|\rho(C)^{1/2}\phi^{1/2}e_c^A\right\|_{0,\Omega}^2 + \varepsilon_1 \left\|\mathbf{D}(\mathbf{Q}^M)^{1/2}\nabla e_c^A\right\|_{0,\Omega}^2 \\
&\quad Z_2 \left\|e_c^I\right\|_{0,\Omega}^2 + \varepsilon_2 \left\|\mathbf{D}(\mathbf{Q}^M)^{1/2}\nabla e_c^A\right\|_{0,\Omega}^2. \qquad \text{(A.48)}
\end{aligned}$$

Using (A1,A7,A9), the trace estimates Equations 3.23 and 3.26 gives

$$\begin{aligned}
\left|T_{10}^{TR}\right| &= |\left\langle c(\mathbf{q}-\mathbf{Q}^M), \left[\left[e_c^A\right]\right] \right\rangle_{\mathcal{E}_i}| \\
&\leq |\left\langle \sigma_c^{-1/2}\mathbf{e}_q^A, \sigma_c^{1/2}\left[\left[e_c^A\right]\right] \right\rangle_{\mathcal{E}_i}| + |\left\langle \sigma_c^{-1/2}\mathbf{e}_q^I, \sigma_c^{1/2}\left[\left[e_c^A\right]\right] \right\rangle_{\mathcal{E}_i}| \\
&\leq Z \left\|\sigma_c^{-1/2}\rho(C)^{1/2}\mathbf{K}^{1/2}\rho(C)^{-1/2}\mathbf{K}^{-1/2}\mathbf{e}_q^A\right\|_{0,\mathcal{E}_i} \left\|\sigma_c^{1/2}\left[\left[e_c^A\right]\right]\right\|_{0,\mathcal{E}_i} \\
&\quad + \left\|\sigma_c^{-1/2}\mathbf{e}_q^I\right\|_{0,\mathcal{E}_i} \left\|\sigma_c^{1/2}\left[\left[e_c^A\right]\right]\right\|_{0,\mathcal{E}_i} \\
&\leq \frac{Z_3^q\varepsilon_1}{2}\left\|\rho(C)^{-1/2}\mathbf{K}^{-1/2}\mathbf{e}_q^A\right\|_{0,\Omega}^2 + \frac{1}{2\varepsilon_1}\left\|\sigma_c^{1/2}\left[\left[e_c^A\right]\right]\right\|_{0,\mathcal{E}_i}^2 \\
&\quad + Z\sum_{\Omega_e}\Delta_e \left\|\mathbf{e}_q^I\right\|_{0,\Omega_e}\left\|\mathbf{e}_q^I\right\|_{1,\Omega_e} + \varepsilon_2\left\|\sigma_c^{1/2}\left[\left[e_c^A\right]\right]\right\|_{0,\mathcal{E}_i}^2, \qquad \text{(A.49)}
\end{aligned}$$

where $Z_3^q = \frac{(Z^{tr,1})^2\rho^* k^*}{\sigma_{c,0}}$. For T_{11}^{TR}, we use the definition of the dispersion tensor to get

$$\begin{aligned}
\left|T_{11}^{TR}\right| &\leq \left|\left\langle \left\{\!\!\left\{(\mathbf{D}_{mech}(\mathbf{q}) - \mathbf{D}_{mech}(\pi\mathbf{q}))\nabla c\right\}\!\!\right\}, \left[\left[e_c^A\right]\right] \right\rangle_{\mathcal{E}_i}\right| \\
&\quad \left|\left\langle \left\{\!\!\left\{(\mathbf{D}_{mech}(\pi\mathbf{q}) - \mathbf{D}_{mech}(\mathbf{Q}^M))\nabla c\right\}\!\!\right\}, \left[\left[e_c^A\right]\right] \right\rangle_{\mathcal{E}_i}\right| \\
&\quad + \left|\left\langle \left\{\!\!\left\{\mathbf{D}_{mol}(\rho(C) - \rho(c))\nabla c\right\}\!\!\right\}, \left[\left[e_c^A\right]\right] \right\rangle_{\mathcal{E}_i}\right| \\
&\equiv \left|T_{11a}^{TR}\right| + \left|T_{11b}^{TR}\right| + \left|T_{11c}^{TR}\right|. \qquad \text{(A.50)}
\end{aligned}$$

For the first term on the right in Equation A.50, using (A9,10) and Equation 3.23

we have

$$\begin{aligned}
\left|T_{11a}^{TR}\right| &= \left|\left\langle \left\{\!\!\left\{(\mathbf{D}_{mech}(\mathbf{q}) - \mathbf{D}_{mech}(\pi\mathbf{q}))\nabla c\right\}\!\!\right\}, \left[\!\left[e_c^A\right]\!\right] \right\rangle_{\mathcal{E}_i}\right| \\
&\leq \left\|\sigma_c^{-1/2} \left\{\!\!\left\{(\mathbf{D}_{mech}(\mathbf{q}) - \mathbf{D}_{mech}(\pi\mathbf{q}))\nabla c\right\}\!\!\right\}\right\|_{0,\mathcal{E}_i} \left\|\sigma_c^{1/2} \left[\!\left[e_c^A\right]\!\right]\right\|_{0,\mathcal{E}_i} \\
&\leq \frac{\varepsilon}{2} \left\|\sigma_c^{-1/2} \left\{\!\!\left\{(\mathbf{D}_{mech}(\mathbf{q}) - \mathbf{D}_{mech}(\pi\mathbf{q}))\nabla c\right\}\!\!\right\}\right\|_{0,\mathcal{E}_i}^2 + \frac{1}{2\varepsilon} \left\|\sigma_c^{1/2} \left[\!\left[e_c^A\right]\!\right]\right\|_{\mathcal{E}_i}^2 \\
&\leq \frac{\varepsilon}{2} \sum_{\Omega_e} \left\|\sigma_c^{-1/2} (\mathbf{D}_{mech}(\mathbf{q}) - \mathbf{D}_{mech}(\pi\mathbf{q}))\nabla c\right\|_{0,\partial\Omega_e}^2 + \frac{1}{2\varepsilon} \left\|\sigma_c^{1/2} \left[\!\left[e_c^A\right]\!\right]\right\|_{0,\mathcal{E}_i} \\
&= Z \sum_{\Omega_e} \Delta_e \left\|\mathbf{e}_q^I\right\|_{0,\Omega_e} \left\|\mathbf{e}_q^I\right\|_{1,\Omega_e} + \frac{1}{2\varepsilon} \left\|\sigma_c^{1/2} \left[\!\left[e_c^A\right]\!\right]\right\|_{0,\mathcal{E}_i}. \qquad \text{(A.51)}
\end{aligned}$$

Next, using (A9,10) and Equation 3.26 we have

$$\begin{aligned}
\left|T_{11b}^{TR}\right| &= \left|\left\langle \left\{\!\!\left\{(\mathbf{D}_{mech}(\mathbf{q}) - \mathbf{D}_{mech}(\mathbf{Q}^M))\nabla c\right\}\!\!\right\}, \left[\!\left[e_c^A\right]\!\right] \right\rangle_{\mathcal{E}_i}\right| \\
&\leq \left\|\sigma_c^{-1/2} \left\{\!\!\left\{(\mathbf{D}_{mech}(\pi\mathbf{q}) - \mathbf{D}_{mech}(\mathbf{Q}^M))\nabla c\right\}\!\!\right\}\right\|_{0,\mathcal{E}_i} \left\|\sigma_c^{1/2} \left[\!\left[e_c^A\right]\!\right]\right\|_{0,\mathcal{E}_i} \\
&\leq \frac{\varepsilon}{2} \left\|\sigma_c^{-1/2} \left\{\!\!\left\{(\mathbf{D}_{mech}(\pi\mathbf{q}) - \mathbf{D}_{mech}(\mathbf{Q}^M))\nabla c\right\}\!\!\right\}\right\|_{0,\mathcal{E}_i}^2 + \frac{1}{2\varepsilon} \left\|\sigma_c^{1/2} \left[\!\left[e_c^A\right]\!\right]\right\|_{\mathcal{E}_i}^2 \\
&\leq \frac{\varepsilon}{2} \sum_{\Omega_e} \left\|\sigma_c^{-1/2} (\mathbf{D}_{mech}(\pi\mathbf{q}) - \mathbf{D}_{mech}(\mathbf{Q}^M))\nabla c\right\|_{0,\partial\Omega_e}^2 + \frac{1}{2\varepsilon} \left\|\sigma_c^{1/2} \left[\!\left[e_c^A\right]\!\right]\right\|_{0,\mathcal{E}_i} \\
&\leq \frac{Z_4^q \varepsilon}{2} \left\|\rho(C)^{-1/2} \mathbf{K}^{-1/2} \mathbf{e}_q^A\right\|_{0,\partial\Omega_e}^2 + \frac{1}{2\varepsilon} \left\|\sigma_c^{1/2} \left[\!\left[e_c^A\right]\!\right]\right\|_{0,\mathcal{E}_i}, \qquad \text{(A.52)}
\end{aligned}$$

where we define $Z_4^q = \frac{(Z^{tr,1} Z^D)^2 \rho^* k^*}{\sigma_{c,0}} \|\nabla c\|_{0,\Omega}^2 \|\nabla c\|_{1,\Omega}^2$.

Turning to the last term in Equation A.50, using (A1,A6,A9) and the trace estimates

Equations 3.23 and 3.26, we have

$$
\begin{aligned}
\left|T_{11c}^{TR}\right| &\leq \left|\left\langle \left\{\left\{\phi\rho_0\varepsilon\mathbf{D}_{mol}e_c^A\nabla c\right\}\right\}, \left[\left[e_c^A\right]\right]\right\rangle_{\mathcal{E}_i}\right| + \left|\left\langle \left\{\left\{\phi\rho_0\varepsilon\mathbf{D}_{mol}e_c^I\nabla c\right\}\right\}, \left[\left[e_c^A\right]\right]\right\rangle_{\mathcal{E}_i}\right| \\
&\leq \frac{\varepsilon}{2}\left[\left\|\sigma_c^{-1/2}\left\{\left\{\phi\rho_0\epsilon e_c^I\nabla c\right\}\right\}\right\|_{0,\mathcal{E}_i}^2 + \left\|\sigma_c^{-1/2}\left\{\left\{\phi\rho_0\epsilon e_c^A\nabla c\right\}\right\}\right\|_{0,\mathcal{E}_i}^2\right] \\
&\quad + \frac{1}{2\varepsilon}\left\|\sigma_c^{1/2}\left[\left[e_c^A\right]\right]\right\|_{0,\mathcal{E}_i}^2 \\
&\leq \frac{\varepsilon}{2}\sum_{\Omega_e}\left[\left\|\sigma_c^{-1/2}\phi\rho_0\epsilon e_c^I\nabla c\right\|_{0,\partial\Omega_e}^2 + \left\|\sigma_c^{-1/2}\phi\rho_0\epsilon e_c^A\nabla c\right\|_{0,\partial\Omega_e}^2\right] \\
&\quad + \frac{1}{2\varepsilon}\left\|\sigma_c^{1/2}\left[\left[e_c^A\right]\right]\right\|_{0,\mathcal{E}_i}^2 \\
&\leq \frac{Z\varepsilon}{2}\left[\sum_{\Omega_e}\Delta_e\left\|e_c^I\right\|_{0,\Omega_e}\left\|e_c^I\right\|_{1,\Omega_e} + \left\|\rho(C)^{1/2}\phi^{1/2}e_c^A\right\|_{0,\Omega}^2\right] \\
&\quad + \frac{1}{2\varepsilon}\left\|\sigma_c^{1/2}\left[\left[e_c^A\right]\right]\right\|_{0,\mathcal{E}_i}^2 .
\end{aligned} \tag{A.53}
$$

Finally, for T_{12}^{TR}, we have

$$
\left|\left\langle c(\mathbf{q}-\mathbf{Q}^M), e_c^A\right\rangle_{\Gamma_+}\right| = 0 \tag{A.54}
$$

using (A8) since $\mathbf{q} \equiv \mathbf{Q}^M$ for $x \in \Gamma_+$ for large enough constant M in the cutoff function.

Combining terms, choosing appropriate constants to hide terms on the left and

introducing the projection error estimates, we have

$$\begin{aligned}\frac{1}{4}\left\|\rho(C(\cdot,T))^{1/2}\phi^{1/2}e_c^A(\cdot,T)\right\|_{0,\Omega}^2 + \frac{1}{2}\int_0^T \Bigg[&\left\|\mathbf{D}^{1/2}(\mathbf{Q}^M)\nabla e_c^A\right\|_{0,\Omega}^2 \\ &+ \left\|\sigma_c^{1/2}\left[\left[e_c^A\right]\right]\right\|_{0,\mathcal{E}_i}^2\Bigg] \\ &\leq Z_1\Bigg[(\Delta^{2\min(s_{trans},k+1)-2})\left\|c\right\|^2_{L^2(0,T;H^{s_{trans}}(\Omega))} \\ &\quad + (\Delta^{2\min(s_{trans},k+1)})\left\|c_t\right\|^2_{L^2(0,T;H^{s_{trans}}(\Omega))} \\ &\quad + (\Delta^{2\min(s_{vel},k+1)})\left\|\mathbf{q}\right\|^2_{L^2(0,T;H^{s_{vel}}(\Omega))}\Bigg] \\ &\quad + Z_2\int_0^T\left\|\rho(C)^{1/2}\phi^{1/2}e_c^A\right\|_{0,\Omega}^2 \\ &\quad + Z^{q,1}\int_0^T\left\|\rho(C)^{-1/2}\mathbf{K}^{-1/2}\mathbf{e}_q^A\right\|_{0,\Omega}^2, \qquad \text{(A.55)}\end{aligned}$$

where $Z^{q,1} = \sum_{i=1}^4 Z_i^q$ from previously defined constants and Z_1, Z_2 are positive constants.

Mass fraction time derivative estimate. We now use Equation A.20 with $\tilde{w} \equiv e_h^A$ to get a bound on $(\rho_0\epsilon\phi e_{c,t}, e_h^A)_\Omega$. Setting $\tilde{w} = e_h^A$ in Equation A.20, we have

$$\begin{aligned}((\rho(C)\phi C - \rho(c)\phi c)_t, e_h^A)_\Omega + \mathcal{B}(e_c^A, e_h^A; \mathbf{Q}^M) = \mathcal{B}(e_c^I, e_h^A; \mathbf{Q}^M) + \mathcal{B}(c, e_h^A; \mathbf{q}) \\ - \mathcal{B}(c, e_h^A; \mathbf{Q}^M). \qquad \text{(A.56)}\end{aligned}$$

Expanding the time derivative, applying (A2) and using the definition of the error, e_c, gives

$$\begin{aligned}((\rho(C)\phi C - \rho(c)\phi c)_t, e_h^A)_\Omega = ((\rho(C)\phi)_t e_c, e_h^A)_\Omega + (\rho(C)\phi e_{c,t}, e_h^A)_\Omega \\ + (\phi\rho_0\epsilon e_c c_t, e_h^A)_\Omega + (\phi\rho_0\epsilon e_{c,t}c, e_h^A)_\Omega \qquad \text{(A.57)}\end{aligned}$$

and using this in Equation A.56 gives

$$\begin{aligned}\left|(\rho(C)\phi e_{c,t},e_h^A)_\Omega\right| \leq & \left|((\rho(C)\phi)_t e_c, e_h^A)_\Omega\right| + \left|(\phi\rho_0\epsilon e_c c_t, e_h^A)_\Omega\right| + \left|(\phi\rho_0\epsilon e_{c,t} c, e_h^A)_\Omega\right| \\ & + \left|\mathcal{B}(e_c^A, e_h^A; \mathbf{Q}^M)\right| + \left|\mathcal{B}(e_c^I, e_h^A; \mathbf{Q}^M)\right| \\ & + \left|\mathcal{B}(c, e_h^A; \mathbf{q}) - \mathcal{B}(c, e_h^A; \mathbf{Q}^M)\right|. \end{aligned} \tag{A.58}$$

Since $\rho_0 \leq \rho(C)$ for all C, we have

$$\left|(\rho_0\epsilon\phi e_{c,t}, e_h^A)_\Omega\right| \leq \epsilon \left|(\rho(C)\phi e_{c,t}, e_h^A)_\Omega\right| \tag{A.59}$$

$$\begin{aligned} \leq \epsilon \Bigg[& \left|((\rho(C)\phi)_t e_c, e_h^A)_\Omega\right| + \left|(\phi\rho_0\epsilon e_c c_t, e_h^A)_\Omega\right| + \left|(\phi\rho_0\epsilon e_{c,t} c, e_h^A)_\Omega\right| \\ & + \left|\mathcal{B}(e_c^A, e_h^A; \mathbf{Q}^M)\right| + \left|\mathcal{B}(e_c^I, e_h^A; \mathbf{Q}^M)\right| \\ & + \left|\mathcal{B}(c, e_h^A; \mathbf{q}) - \mathcal{B}(c, e_h^A; \mathbf{Q}^M)\right| \Bigg]. \end{aligned} \tag{A.60}$$

Using (A6), we have $\left|(\phi\rho_0\epsilon e_{c,t} c, e_h^A)_\Omega\right| \leq \left|(\phi\rho_0\epsilon e_{c,t}, e_h^A)_\Omega\right|$ and finally arrive at the estimate

$$\begin{aligned}\left|(\rho_0\epsilon\phi e_{c,t}, e_h^A)_\Omega\right| \leq \frac{\epsilon}{1-\epsilon} \Bigg[& \left|((\rho(C)\phi)_t e_c, e_h^A)_\Omega\right| + \left|(\phi\rho_0\epsilon e_c c_t, e_h^A)_\Omega\right| \\ & + \left|\mathcal{B}(e_c^A, e_h^A; \mathbf{Q}^M)\right| + \left|\mathcal{B}(e_c^I, e_h^A; \mathbf{Q}^M)\right| \\ & + \left|\mathcal{B}(c, e_h^A; \mathbf{q}) - \mathcal{B}(c, e_h^A; \mathbf{Q}^M)\right| \Bigg]. \end{aligned} \tag{A.61}$$

We bound each of the terms in turn. For the first term, using the definition of the error and (A1,A4), we have

$$\begin{aligned}\left|((\rho(C)\phi)_t e_c, e_h^A)_\Omega\right| \leq & Z_1 \left\|(\rho(C)^{1/2}\phi^{1/2} e_c^A\right\|_{0,\Omega}^2 \\ & + Z_2 \left\|\rho(C)^{1/2} S^{1/2} e_h^A\right\|_{0,\Omega}^2 + Z_3 \left\|e_c^I\right\|_{0,\Omega}^2. \end{aligned} \tag{A.62}$$

Similarly, for the second term, we have

$$\left|(\phi\rho_0\epsilon e_c c_t, e_h^A)_\Omega\right| \leq Z_1 \left\|\phi^{1/2}\rho(C)^{1/2}e_c^A\right\|_{0,\Omega}^2 + Z_2 \left\|\rho(C)^{1/2}S^{1/2}e_h^A\right\|_{0,\Omega}^2 + Z_3 \left\|e_c^I\right\|_{0,\Omega}^2 \tag{A.63}$$

using (A1,A4). Turning to the bilinear forms, for $\mathcal{B}(e_c^A, e_h^A; \mathbf{Q}^M)$, we have

$$\begin{aligned}\mathcal{B}_c(e_c^A, e_h^A; \mathbf{Q}^M) &= -(e_c^A\mathbf{Q}^M, \nabla e_h^A)_\Omega + (\mathbf{D}(\mathbf{Q}^M)\nabla e_c^A, \nabla e_h^A)_\Omega + \left\langle e_c^{A,u}\mathbf{Q}^M, \left[\left[e_h^A\right]\right]\right\rangle_{\mathcal{E}_i} \\ &\quad - \left\langle \left\{\left\{\mathbf{D}(\mathbf{Q}^M)\nabla e_c^A\right\}\right\}, \left[\left[e_h^A\right]\right]\right\rangle_{\mathcal{E}_i} + \left\langle \sigma_c\left[\left[e_c^A\right]\right], \left[\left[e_h^A\right]\right]\right\rangle_{\mathcal{E}_i} \\ &\quad + \left\langle e_c^A\mathbf{Q}^M, e_h^A\right\rangle_{\Gamma_+} + \left\langle \left\{\left\{\mathbf{D}(\mathbf{Q}^M)\nabla e_h^A\right\}\right\}, \left[\left[e_c^A\right]\right]\right\rangle_{\mathcal{E}_i} \\ &\equiv \sum_{i=1}^{7} T_i^{THL}.\end{aligned} \tag{A.64}$$

For the first term, for large enough M and using (A1), we have

$$\begin{aligned}\left|T_1^{THL}\right| &= \left|(e_c^A\mathbf{Q}^M, \nabla e_h^A)_\Omega\right| \\ &\leq Z\left\|\rho(C)^{1/2}\phi^{1/2}e_c^A\right\|_{0,\Omega}^2 + \varepsilon\left\|\nabla e_h^A\right\|_{0,\Omega}^2.\end{aligned} \tag{A.65}$$

Next, using (A10) gives

$$\begin{aligned}\left|T_2^{THL}\right| &= \left|(\mathbf{D}(\mathbf{Q}^M)\nabla e_c^A, \nabla e_h^A)_\Omega\right| \\ &\leq \left\|\mathbf{D}(\mathbf{Q}^M)^{1/2}\right\|_{0,\Omega}^2 \left\|\mathbf{D}(\mathbf{Q}^M)^{1/2}\nabla e_c^A\right\|_{0,\Omega}^2 + \varepsilon\left\|\nabla e_h^A\right\|_{0,\Omega}^2.\end{aligned} \tag{A.66}$$

For the boundary terms, $T_3^{THL} - T_7^{THL}$, we will apply the trace estimate to get our bounds. For the first, for large enough M and using (A1,A9) with the trace estimate Equation 3.26, we have

$$\begin{aligned}\left|T_3^{THL}\right| &= \left|\left\langle e_c^{A,u}\mathbf{Q}^M, \left[\left[e_h^A\right]\right]\right\rangle_{\mathcal{E}_i}\right| \\ &= \left|\left\langle \sigma_h^{-1/2}e_c^{A,u}\mathbf{Q}^M, \sigma_h^{1/2}\left[\left[e_h^A\right]\right]\right\rangle_{\mathcal{E}_i}\right| \\ &\leq Z\left\|\rho(C)^{1/2}\phi^{1/2}e_c^A\right\|_{0,\Omega}^2 + \varepsilon\left\|\sigma_h^{1/2}\left[\left[e_h^A\right]\right]\right\|_{0,\mathcal{E}_i}^2.\end{aligned} \tag{A.67}$$

For the second, using (A9,A10) and the trace estimate Equation 3.26, we have

$$\begin{aligned}
\left|T_4^{THL}\right| &= \left|\left\langle \left\{\left\{\mathbf{D}(\mathbf{Q}^M)\nabla e_c^A\right\}\right\}, \left[\left[e_h^A\right]\right] \right\rangle_{\mathcal{E}_i}\right| \\
&= \left|\left\langle \sigma_h^{-1/2}\left\{\left\{\mathbf{D}(\mathbf{Q}^M)\nabla e_c^A\right\}\right\}, \sigma_h^{1/2}\left[\left[e_h^A\right]\right] \right\rangle_{\mathcal{E}_i}\right| \\
&\leq \left\|\sigma_h^{-1/2}\left\{\left\{\mathbf{D}(\mathbf{Q}^M)\nabla e_c^A\right\}\right\}\right\|_{0,\mathcal{E}_i} \left\|\sigma_h^{1/2}\left[\left[e_h^A\right]\right]\right\|_{0,\mathcal{E}_i} \\
&\leq \frac{Z^{tr,1}}{\sigma_{h,0}}\left\|\mathbf{D}(\mathbf{Q}^M)^{1/2}\right\|_{0,\Omega}^2 \left\|\mathbf{D}(\mathbf{Q}^M)^{1/2}\nabla e_c^A\right\|_{0,\Omega}^2 + \frac{1}{4}\left\|\sigma_h^{1/2}\left[\left[e_h^A\right]\right]\right\|_{0,\mathcal{E}_i}^2. \quad \text{(A.68)}
\end{aligned}$$

For the third term, with (A9), we have

$$\begin{aligned}
\left|T_5^{THL}\right| &= \left|\left\langle \sigma_c\left[\left[e_c^A\right]\right], \left[\left[e_h^A\right]\right] \right\rangle_{\mathcal{E}_i}\right| \\
&\leq \frac{3}{4}\left\|\sigma_c^{1/2}\left[\left[e_c^A\right]\right]\right\|_{0,\mathcal{E}_i}^2 + \frac{1}{3}\left\|\sigma_h^{1/2}\left[\left[e_h^A\right]\right]\right\|_{0,\mathcal{E}_i}^2, \quad \text{(A.69)}
\end{aligned}$$

where we will have to relate the penalty constants to hide the second error term ($\sigma_{c,0} \leq \sigma_{h,0}$). For the next term, we have

$$\left|T_6^{THL}\right| = \left|\left\langle e_c^A\mathbf{Q}^M, e_h^A\right\rangle_{\Gamma_+}\right| = 0 \quad \text{(A.70)}$$

after applying (A8).

Finally, similar to T_4^{THL}, we have

$$\begin{aligned}
\left|T_7^{THL}\right| &= \left|\left\langle \left\{\left\{\mathbf{D}(\mathbf{Q}^M)\nabla e_h^A\right\}\right\}, \left[\left[e_c^A\right]\right] \right\rangle_{\mathcal{E}_i}\right| \\
&= \left|\left\langle \sigma_c^{-1/2}\left\{\left\{\mathbf{D}(\mathbf{Q}^M)\nabla e_h^A\right\}\right\}, \sigma_c^{1/2}\left[\left[e_c^A\right]\right] \right\rangle_{\mathcal{E}_i}\right| \\
&\leq \left\|\sigma_c^{-1/2}\left\{\left\{\mathbf{D}(\mathbf{Q}^M)\nabla e_h^A\right\}\right\}\right\|_{0,\mathcal{E}_i} \left\|\sigma_c^{1/2}\left[\left[e_c^A\right]\right]\right\|_{0,\mathcal{E}_i} \\
&\leq \frac{5(Z^{tr,1}\left\|\mathbf{D}(\mathbf{Q}^M)\right\|_{0,\Omega})^2}{\sigma_{c,0}}\left\|\nabla e_h^A\right\|_{0,\Omega}^2 + \frac{1}{20}\left\|\sigma_c^{1/2}\left[\left[e_c^A\right]\right]\right\|_{0,\mathcal{E}_i}^2. \quad \text{(A.71)}
\end{aligned}$$

For the second bilinear form, we have

$$\begin{aligned}\mathcal{B}(e_c^I, e_h^A; \mathbf{Q}^M) \equiv & -(e_c^I \mathbf{Q}^M, \nabla e_h^A)_\Omega + (\mathbf{D}(\mathbf{Q}^M)\nabla e_c^I, \nabla e_h^A)_\Omega + \left\langle e_c^{I,u}\mathbf{Q}^M, \left[\left[e_h^A\right]\right] \right\rangle_{\mathcal{E}_i} \\ & - \left\langle \left\{\left\{\mathbf{D}(\mathbf{Q}^M)\nabla e_c^I\right\}\right\}, \left[\left[e_h^A\right]\right] \right\rangle_{\mathcal{E}_i} + \left\langle \sigma_c \left[\left[e_c^I\right]\right], \left[\left[e_h^A\right]\right] \right\rangle_{\mathcal{E}_i} \\ & + \left\langle e_c^I \mathbf{Q}^M, e_h^A \right\rangle_{\Gamma_+} + \left\langle \left\{\left\{\mathbf{D}(\mathbf{Q}^M)\nabla e_h^A\right\}\right\}, \left[\left[e_c^I\right]\right] \right\rangle_{\mathcal{E}_i} \\ \equiv & \sum_{i=1}^{7} T_i^{THR}. \end{aligned} \tag{A.72}$$

Starting with the first two terms, for large enough M, we have

$$\begin{aligned}\left|T_1^{THR}\right| &= \left|(e_c^I \mathbf{Q}^M, \nabla e_h^A)_\Omega\right| \\ &\leq Z \left\|e_c^I\right\|_{0,\Omega}^2 + \varepsilon \left\|\nabla e_h^A\right\|_{0,\Omega}^2 \end{aligned} \tag{A.73}$$

and

$$\begin{aligned}\left|T_2^{THR}\right| &= \left|(\mathbf{D}(\mathbf{Q}^M)\nabla e_c^I, \nabla e_h^A)_\Omega\right| \\ &\leq Z \left\|\nabla e_c^I\right\|_{0,\Omega}^2 + \varepsilon \left\|\nabla e_h^A\right\|_{0,\Omega}^2. \end{aligned} \tag{A.74}$$

Again, for the boundary terms T_3^{THR}-T_7^{THR} we will employ the trace estimates to get our bounds. So, for large enough M and using (A9) and Equation 3.23, we have

$$\begin{aligned}\left|T_3^{THR}\right| &= \left|\left\langle e_c^{I,u}\mathbf{Q}^M, \left[\left[e_h^A\right]\right] \right\rangle_{\mathcal{E}_i}\right| \\ &= \left|\left\langle \sigma_h^{-1/2} e_c^{I,u}\mathbf{Q}^M, \sigma_h^{1/2} \left[\left[e_h^A\right]\right] \right\rangle_{\mathcal{E}_i}\right| \\ &\leq Z \sum_{\Omega_e} \Delta_e \left\|e_c^I\right\|_{0,\Omega_e} \left\|e_c^I\right\|_{1,\Omega_e} + \varepsilon \left\|\sigma_h^{1/2} \left[\left[e_h^A\right]\right]\right\|_{0,\mathcal{E}_i}^2. \end{aligned} \tag{A.75}$$

Next, applying (A9,A10) and Equation 3.23, we have

$$\begin{aligned}\left|T_4^{THR}\right| &= \left|\left\langle \left\{\left\{\mathbf{D}(\mathbf{Q}^M)\nabla e_c^I\right\}\right\}, \left[\left[e_h^A\right]\right]\right\rangle_{\mathcal{E}_i}\right| \\ &= \left\|\sigma_h^{-1/2}\left\{\left\{\mathbf{D}(\mathbf{Q}^M)\nabla e_c^I\right\}\right\}\right\|_{0,\mathcal{E}_i}\left\|\sigma_h^{1/2}\left[\left[e_h^A\right]\right]\right\|_{0,\mathcal{E}_i} \\ &\leq Z\sum_{\Omega_e}\Delta_e\left\|\nabla e_c^I\right\|_{0,\Omega_e}\left\|\nabla e_c^I\right\|_{1,\Omega_e} + \varepsilon\left\|\sigma_h^{1/2}\left[\left[e_h^A\right]\right]\right\|_{0,\mathcal{E}_i}^2. \end{aligned} \tag{A.76}$$

Using (A9) and Equation 3.23, we have

$$\begin{aligned}\left|T_5^{THR}\right| &= \left|\left\langle \sigma_c\left[\left[e_c^I\right]\right], \left[\left[e_h^A\right]\right]\right\rangle_{\mathcal{E}_i}\right| \\ &= \left|\left\langle \sigma_h^{1/2}\left[\left[e_c^I\right]\right], \sigma_c^{1/2}\left[\left[e_h^A\right]\right]\right\rangle_{\mathcal{E}_i}\right| \\ &\leq \left\|\sigma_c^{1/2}e_c^I\right\|_{0,\mathcal{E}_i}\left\|\sigma_c^{1/2}\left[\left[e_h^A\right]\right]\right\|_{0,\mathcal{E}_i} \\ &\leq Z\sum_{\Omega_e}\Delta_e^{-1}\left\|e_c^I\right\|_{0,\Omega_e}\left\|e_c^I\right\|_{1,\Omega_e} + \varepsilon\left\|\sigma_h^{1/2}\left[\left[e_h^A\right]\right]\right\|_{0,\mathcal{E}_i}^2. \end{aligned} \tag{A.77}$$

We have

$$\left|T_6^{THR}\right| = \left|\left\langle e_c^I\mathbf{Q}^M, e_h^A\right\rangle_{\Gamma_+}\right| = 0 \tag{A.78}$$

using (A8). Finally, using (A9), Equations 3.23 and 3.26 and for large enough M in the cutoff operator, we have

$$\begin{aligned}\left|T_7^{THR}\right| &= \left|\left\langle \left\{\left\{\mathbf{D}(\mathbf{Q}^M)\nabla e_h^A\right\}\right\}, \left[\left[e_c^I\right]\right]\right\rangle_{\mathcal{E}_i}\right| \\ &\leq \left\|\sigma_c^{-1/2}\left\{\left\{\mathbf{D}(\mathbf{Q}^M)\nabla e_h^A\right\}\right\}\right\|_{0,\mathcal{E}_i}\left\|\sigma_c^{1/2}\left[\left[e_c^I\right]\right]\right\|_{0,\mathcal{E}_i} \\ &\leq \varepsilon\left\|\nabla e_h^A\right\|_{0,\Omega}^2 + Z\sum_{\Omega_e}\Delta_e^{-1}\left\|e_c^I\right\|_{0,\Omega_e}\left\|e_c^I\right\|_{1,\Omega_e}. \end{aligned} \tag{A.79}$$

Finally, we turn to $\mathcal{B}(c, e_h^A; \mathbf{q}) - \mathcal{B}(c, e_h^A; \mathbf{Q}^M)$:

$$\begin{aligned}\mathcal{B}(c, e_h^A; \mathbf{q}) - \mathcal{B}(c, e_h^A; \mathbf{Q}^M) &= -((\mathbf{q} - \mathbf{Q}^M)c, \nabla e_h^A)_\Omega + ((\mathbf{D}(\mathbf{q}) - \mathbf{D}(\mathbf{Q}^M)\nabla c, \nabla e_h^A)_\Omega \\ &\quad + \left\langle c(\mathbf{q} - \mathbf{Q}^M), [[e_h^A]] \right\rangle_{\mathcal{E}_i} \\ &\quad - \left\langle \{\{\mathbf{D}(\mathbf{q}) - \mathbf{D}(\mathbf{Q}^M)\nabla c\}\}, [[e_h^A]] \right\rangle_{\mathcal{E}_i} \\ &\quad + \left\langle c(\mathbf{q} - \mathbf{Q}^M), e_h^A \right\rangle_{\Gamma_+} \\ &\equiv \sum_{i=8}^{12} T_i^{THR}. \end{aligned} \tag{A.80}$$

For the first term, using (A1,A6,A7), we have

$$\begin{aligned}\left|T_8^{THR}\right| &\leq \left|(\mathbf{e}_q^A c, \nabla e_h^A)_\Omega\right| + \left|(\mathbf{e}_q^I c, \nabla e_h^A)_\Omega\right| \\ &\leq \left|(\rho(C)^{1/2}\mathbf{K}^{1/2}\rho(C)^{-1/2}\mathbf{K}^{-1/2}\mathbf{e}_q, \nabla e_h^A)_\Omega\right| + \left|(\mathbf{e}_q^I c, \nabla e_h^A)_\Omega\right| \\ &\leq Z_5^q \left\|\rho(C)^{-1/2}\mathbf{K}^{-1/2}\mathbf{e}_q^A\right\|_{0,\Omega}^2 + Z\left\|\mathbf{e}_q^I\right\|_{0,\Omega} + \left\|\nabla e_h^A\right\|_{0,\Omega}, \end{aligned} \tag{A.81}$$

where, $Z_5^q = \frac{\rho^* k^*}{4}$. For the next term, we expand the term using the definition of the dispersion tensor to get:

$$\begin{aligned}\left|T_9^{THR}\right| &= \left|((\mathbf{D}(\mathbf{q}) - \mathbf{D}(\mathbf{Q}^M))\nabla c, \nabla e_h^A)_\Omega\right| \\ &= \left|((\mathbf{D}_{mol}(\rho(c) - \rho(C))\nabla c, \nabla e_h^A)_\Omega\right| \\ &\quad + \left|((\mathbf{D}_{mech}(\mathbf{q}) - \mathbf{D}_{mech}(\mathbf{Q}^M))\nabla c, \nabla e_h^A)_\Omega\right| \\ &\equiv \left|T_{9,a}^{THR}\right| + \left|T_{9,b}^{THR}\right|. \end{aligned} \tag{A.82}$$

For the first term, using (A1,A2,A6) and the definition of the error, we have:

$$\begin{aligned}\left|T_{9,a}^{THR}\right| &= \left|((\mathbf{D}_{mol}(\rho(c) - \rho(C))\nabla c, \nabla e_h^A)_\Omega\right| \\ &= \left|((\mathbf{D}_{mol}\rho_0\epsilon e_c\nabla c, \nabla e_h^A)_\Omega\right| \\ &\leq Z\left[\left\|\rho(C)^{1/2}\phi^{1/2}e_c^A\right\|_{0,\Omega}^2 + \left\|e_c^I\right\|_{0,\Omega}^2\right] + \left\|\nabla e_h^A\right\|_\Omega^2. \end{aligned} \tag{A.83}$$

For the second term, we use (A1,A7,A10) which gives

$$\begin{aligned}
\left|T_{9,b}^{THR}\right| &\leq \left|((\mathbf{D}(\mathbf{q})-\mathbf{D}(\pi\mathbf{q}))\nabla c, \nabla e_h^A)_\Omega\right| + \left|((\mathbf{D}(\pi\mathbf{q})-\mathbf{D}(\mathbf{Q}^M))\nabla c, \nabla e_h^A)_\Omega\right| \\
&\leq \|\mathbf{D}(\mathbf{q})-\mathbf{D}(\pi\mathbf{q})\|_{0,\Omega} \|\nabla c\|_{0,\Omega} \left\|\nabla e_h^A\right\|_{0,\Omega} \\
&\quad + \left\|\mathbf{D}(\pi\mathbf{q})-\mathbf{D}(\mathbf{Q}^M)\right\|_{0,\Omega} \|\nabla c\|_{0,\Omega} \left\|\nabla e_h^A\right\|_{0,\Omega} \\
&\leq Z \left\|\mathbf{e}_q^I\right\|_{0,\Omega} \left\|\nabla e_h^A\right\|_{0,\Omega} \\
&\quad + Z^D(\rho^* k^*)^{1/2} \left\|\rho(C)^{-1/2}\mathbf{K}^{-1/2}\mathbf{e}_q^A\right\|_{0,\Omega} \|\nabla c\|_{0,\Omega} \left\|\nabla e_h^A\right\|_{\Omega} \\
&\leq Z_6^q \left\|\rho(C)^{-1/2}\mathbf{K}^{-1/2}\mathbf{e}_q^A\right\|_{0,\Omega}^2 + Z \left\|\mathbf{e}_q^I\right\|_{0,\Omega}^2 + \varepsilon \left\|\nabla e_h^A\right\|_{0,\Omega}^2, \qquad \text{(A.84)}
\end{aligned}$$

where $Z_6^q = \frac{1}{4}(Z^D)^2\rho^* k^* \|\nabla c\|_{0,\Omega}^2$. Next, employing (A1,A7,A9), and Equations 3.23 and 3.26, we have

$$\begin{aligned}
\left|T_{10}^{THR}\right| &= \left|\left\langle c(\mathbf{q}-\mathbf{Q}^M), [[e_h^A]] \right\rangle_{\mathcal{E}_i}\right| \\
&\leq \left|\left\langle \sigma_h^{-1/2}\mathbf{e}_q^A, \sigma_h^{1/2} [[e_h^A]] \right\rangle_{\mathcal{E}_i}\right| + \left|\left\langle \sigma_h^{-1/2}\mathbf{e}_q^I, \sigma_h^{1/2} [[e_h^A]] \right\rangle_{\mathcal{E}_i}\right| \\
&\leq \left\|\sigma_h^{-1/2}(\mathbf{q}-\mathbf{Q}^M)\right\|_{0,\mathcal{E}_i} \left\|\sigma_h^{1/2} [[e_h^A]]\right\|_{0,\mathcal{E}_i} \\
&\leq Z_7^q \left\|\rho(C)^{-1/2}\mathbf{K}^{-1/2}\mathbf{e}_q^A\right\|_{0,\Omega}^2 + Z\sum_{\Omega_e} \Delta_e \left\|\mathbf{e}_q^I\right\|_{0,\Omega_e} \left\|\mathbf{e}_q^I\right\|_{1,\Omega_e} \\
&\quad + \frac{1}{4}\left\|\sigma_h^{1/2} [[e_h^A]]\right\|_{0,\mathcal{E}_i}^2, \qquad \text{(A.85)}
\end{aligned}$$

where $Z_7^q = \frac{(Z^{tr,1})^2\rho^* k^*}{\sigma_{h,0}}$. For the next term, similar to T_9^{THR}, we expand the term using the definition of the dispersion tensor to get

$$\begin{aligned}
\left|T_{11}^{THR}\right| &= \left|\left\langle \left\{\!\!\left\{(\mathbf{D}(\mathbf{q})-\mathbf{D}(\mathbf{Q}^M))\nabla c\right\}\!\!\right\}, [[e_h^A]] \right\rangle_{\mathcal{E}_i}\right| \\
&\leq \left|\left\langle \left\{\!\!\left\{\phi\mathbf{D}_{mol}(\rho(c)-\rho(C))\nabla c\right\}\!\!\right\}, [[e_h^A]] \right\rangle_{\mathcal{E}_i}\right| \\
&\quad + \left|\left\langle \left\{\!\!\left\{\mathbf{D}_{mech}(\mathbf{q})-\mathbf{D}_{mech}(\mathbf{Q}^M)\nabla c\right\}\!\!\right\}, [[e_h^A]] \right\rangle_{\mathcal{E}_i}\right| \\
&\equiv \left|T_{11,a}^{THR}\right| + \left|T_{11,b}^{THR}\right|. \qquad \text{(A.86)}
\end{aligned}$$

For the first term on the right, applying the trace estimates Equation 3.23 and 3.26 with (A1,A6,A9,A10), we have

$$\begin{aligned}
\left|T_{11,a}^{THR}\right| &= \left|\left\langle \left\{\!\!\left\{\phi \mathbf{D}_{mol}(\rho(c)-\rho(C))\nabla c\right\}\!\!\right\}, \left[\!\left[e_h^A\right]\!\right] \right\rangle_{\mathcal{E}_i}\right| \\
&\leq \left|\left\langle \left\{\!\!\left\{D_m\rho_0\epsilon e_c^A\nabla c\right\}\!\!\right\}, \left[\!\left[e_h^A\right]\!\right] \right\rangle_{\mathcal{E}_i}\right| \\
&\quad + \left|\left\langle \left\{\!\!\left\{D_m\rho_0\epsilon e_c^I\nabla c\right\}\!\!\right\}, \left[\!\left[e_h^A\right]\!\right] \right\rangle_{\mathcal{E}_i}\right| \\
&\leq \left\|\sigma_h^{-1/2}\left\{\!\!\left\{D_m\rho_0\epsilon e_c^A\nabla c\right\}\!\!\right\}\right\|_{0,\mathcal{E}_i} \left\|\sigma_h^{1/2}\left[\!\left[e_h^A\right]\!\right]\right\|_{0,\mathcal{E}_i} \\
&\quad + \left\|\sigma_h^{-1/2}\left\{\!\!\left\{D_m\rho_0\epsilon e_c^I\nabla c\right\}\!\!\right\}\right\|_{0,\mathcal{E}_i} \left\|\sigma_h^{1/2}\left[\!\left[e_h^A\right]\!\right]\right\|_{0,\mathcal{E}_i} \\
&\leq Z_1\left\|\rho(C)^{1/2}\phi^{1/2}e_c^A\right\|_{0,\Omega}^2 + \varepsilon_1\left\|\sigma_h^{1/2}\left[\!\left[e_h^A\right]\!\right]\right\|_{0,\mathcal{E}_i}^2 \\
&\quad + Z_2\sum_{\Omega_e}\Delta_e\left\|e_c^I\right\|_{0,\Omega_e}\left\|e_c^I\right\|_{1,\Omega_e} + \varepsilon_2\left\|\sigma_h^{1/2}\left[\!\left[e_h^A\right]\!\right]\right\|_{0,\mathcal{E}_i}^2
\end{aligned} \tag{A.87}$$

and for the second term, again using (A1,A9,A10) with the trace estimates, we have

$$\begin{aligned}
\left|T_{11,b}^{THR}\right| &= \left|\left\langle \left\{\!\!\left\{(\mathbf{D}_{mech}(\mathbf{q})-\mathbf{D}_{mech}(\pi\mathbf{q}))\nabla c\right\}\!\!\right\}, \left[\!\left[e_h^A\right]\!\right] \right\rangle_{\mathcal{E}_i}\right| \\
&\quad + \left|\left\langle \left\{\!\!\left\{(\mathbf{D}_{mech}(\pi\mathbf{q})-\mathbf{D}_{mech}(\mathbf{Q}^M))\nabla c\right\}\!\!\right\}, \left[\!\left[e_h^A\right]\!\right] \right\rangle_{\mathcal{E}_i}\right| \\
&\leq \left\|\sigma_h^{-1/2}\left\{\!\!\left\{(\mathbf{D}_{mech}(\mathbf{q})-\mathbf{D}_{mech}(\pi\mathbf{q}))\nabla c\right\}\!\!\right\}\right\|_{0,\mathcal{E}_i} \left\|\sigma_h^{1/2}\left[\!\left[e_h^A\right]\!\right]\right\|_{0,\mathcal{E}_i} \\
&\quad + \left\|\sigma_h^{-1/2}\left\{\!\!\left\{(\mathbf{D}_{mech}(\pi\mathbf{q})-\mathbf{D}_{mech}(\mathbf{Q}^M))\nabla c\right\}\!\!\right\}\right\|_{0,\mathcal{E}_i} \left\|\sigma_h^{1/2}\left[\!\left[e_h^A\right]\!\right]\right\|_{0,\mathcal{E}_i} \\
&\leq Z_8^q\left\|\rho(C)^{-1/2}\mathbf{K}^{-1/2}\mathbf{e}_q^A\right\|_{0,\Omega}^2 + Z\sum_{\Omega_e}\Delta_e\left\|\mathbf{e}_q^I\right\|_{0,\Omega_e}\left\|\mathbf{e}_q^I\right\|_{1,\Omega_e} \\
&\quad + \frac{1}{30}\left\|\sigma_h^{1/2}\left[\!\left[e_h^A\right]\!\right]\right\|_{0,\mathcal{E}_i}^2,
\end{aligned} \tag{A.88}$$

where $Z_8^q = \frac{15(Z^D Z^{tr,1})^2\rho^* k^*}{\sigma_{h,0}}\left\|\nabla c\right\|_{0,\Omega}^2\left\|\nabla c\right\|_{1,\Omega}^2$. Finally, we have:

$$\left|T_{12}^{THR}\right| = \left|\left\langle c(\mathbf{q}-\mathbf{Q}^M), e_h^A\right\rangle_{\Gamma_+}\right| = 0 \tag{A.89}$$

applying (A8).

Combining the previous results, choosing appropriate constants and using the projection approximations, we arrive at the following bound:

$$
\begin{aligned}
&\left|(\rho(C)\phi e_{c,t}, e_h^A)_\Omega\right| \\
&\qquad \leq \frac{\epsilon}{1-\epsilon}\Bigg[Z_5 \left\|\rho(C)^{1/2}\phi^{1/2} e_c^A\right\|_{0,\Omega}^2 + Z_6 \left\|\rho(C)^{1/2} S^{1/2} e_h^A\right\|_{0,\Omega}^2 \\
&\qquad\quad + Z^{q,2} \left\|\rho(C)^{-1/2}\mathbf{K}^{-1/2}\mathbf{e}_q^A\right\|_{0,\Omega}^2 + \left\|\sigma_h^{1/2}\left[\!\left[e_h^A\right]\!\right]\right\|_{0,\mathcal{E}_i}^2 \\
&\qquad\quad + \frac{4}{5}\left\|\sigma_c^{1/2}\left[\!\left[e_c^A\right]\!\right]\right\|_{0,\mathcal{E}_i}^2 \\
&\qquad\quad + \Big(\frac{Z^{tr}}{\sigma_{h,0}}\left\|\mathbf{D}(\mathbf{Q}^M)^{1/2}\right\|_{0,\Omega}^2 + \left\|\mathbf{D}(\mathbf{Q}^M)^{1/2}\right\|_{0,\Omega}^2\Big)\left\|\mathbf{D}(\mathbf{Q}^M)^{1/2}\nabla e_c^A\right\|_{0,\Omega}^2 \\
&\qquad\quad + \Big(3 + \frac{5(Z^{tr,1})^2\left\|\mathbf{D}(\mathbf{Q}^M)\right\|_{0,\Omega}^2}{\sigma_{c,0}}\Big)\left\|\nabla e_h^A\right\|_{0,\Omega}^2 \\
&\qquad\quad + Z_7\big[\big(\Delta^{2\min(s_{trans},k+1)-2} + \Delta^{2\min(s_{trans},k+1)}\big)\|c\|_{H^{s_{trans}}(\Omega)}^2 \\
&\qquad\quad + \Delta^{2\min(s_{vel},k+1)}\|\mathbf{q}\|_{H^{s_{vel}}(\Omega)}^2\big]\Bigg],
\end{aligned}
\tag{A.90}
$$

where $Z^{q,2} = \sum_{i=6}^{9} Z_i^q$ as previously defined and Z_5, Z_6, Z_7 are positive, Δ-independent constants.

An estimate for $\left\|\nabla e_h^A\right\|_{0,\Omega}$. To get an estimate for $\left\|\nabla e_h^A\right\|_{0,\Omega}$, we start off with the error equation derived from Darcy's equation in its original form but with $\mathbf{v} \equiv \nabla e_h^A \in \tilde{\mathbf{V}}$. Using (A8), we arrive at the expression

$$
\begin{aligned}
(\nabla e_h, \nabla e_h^A)_\Omega &= -(\rho(C)^{-1}\mathbf{K}^{-1}\mathbf{e}_q, \nabla e_h^A)_\Omega + \left\langle \left[\!\left[e_h\right]\!\right], \left\{\!\left\{\nabla e_h^A\right\}\!\right\}\right\rangle_{\mathcal{E}_i} + \left\langle e_h, \nabla e_h^A\right\rangle_{\Gamma_D} \\
&\quad - ((\rho(C)^{-1} - \rho^{-1}(c))\mathbf{K}^{-1}\mathbf{q}, \nabla e_h^A)_\Omega - ((\hat{\rho}(C) - \hat{\rho}(c))\mathbf{e}_z, \nabla e_h^A)_\Omega \\
&\equiv \sum_{i=1}^{5} T_i^{FD}.
\end{aligned}
\tag{A.91}
$$

Using the orthogonality of our interpolant, the left side becomes

$$(\nabla e_h, \nabla e_h^A)_\Omega = \left\|\nabla e_h^A\right\|_{0,\Omega}^2. \tag{A.92}$$

We now bound the right hand side to get our estimate. Using (A1) and the definition of the error, we have

$$\begin{aligned}
\left|T_1^{FD}\right| &\leq \left|(\rho(C)^{-1/2}\mathbf{K}^{-1/2}\mathbf{e}_q^A, \nabla e_h^A)_\Omega\right| + \left|(\rho(C)^{-1/2}\mathbf{K}^{-1/2}\mathbf{e}_q^I, \nabla e_h^A)_\Omega\right| \\
&\leq \frac{1}{2} Z_9^q \left\|\rho(c)^{-1/2}\mathbf{K}^{-1/2}\mathbf{e}_q^A\right\|_{0,\Omega}^2 + Z\left\|\mathbf{e}_q^I\right\|_{0,\Omega}^2 \\
&\quad + \frac{1}{14}\left\|\nabla e_h^A\right\|_{0,\Omega}^2,
\end{aligned} \tag{A.93}$$

with $Z_9^q = \frac{7}{\rho_* k_*}$. Applying the error definition, the second term becomes

$$\begin{aligned}
\left|T_2^{FD}\right| &= \left\langle \left[\!\left[e_h\right]\!\right], \left\{\!\left\{\nabla e_h^A\right\}\!\right\} \right\rangle_{\mathcal{E}_i} \\
&\leq \left|\left\langle \left[\left[e_h^A\right]\right], \left\{\!\left\{\nabla e_h^A\right\}\!\right\} \right\rangle_{\mathcal{E}_i}\right| + \left|\left\langle \left[\left[e_h^I\right]\right], \left\{\!\left\{\nabla e_h^A\right\}\!\right\} \right\rangle_{\mathcal{E}_i}\right| \\
&\equiv T_{2,a}^{FD} + T_{2,b}^{FD}.
\end{aligned} \tag{A.94}$$

Applying the trace estimates Equation 3.26 and (A9), the first term is bounded by

$$\begin{aligned}
\left|T_{2,a}^{FD}\right| &= \left|\left\langle \left[\left[e_h^A\right]\right], \left\{\!\left\{\nabla e_h^A\right\}\!\right\} \right\rangle_{\mathcal{E}_i}\right| \\
&\leq \left\|\sigma_h^{1/2}\left[\left[e_h^A\right]\right]\right\|_{0,\mathcal{E}_i} \left\|\sigma_h^{-1/2}\left\{\!\left\{\nabla e_h^A\right\}\!\right\}\right\|_{0,\mathcal{E}_i} \\
&\leq \frac{1}{4}\left\|\sigma_h^{1/2}\left[\left[e_h^A\right]\right]\right\|_{0,\mathcal{E}_i}^2 + \frac{Z^{tr,1}}{\sigma_{h,0}}\left\|\nabla e_h^A\right\|_{0,\Omega}^2.
\end{aligned} \tag{A.95}$$

Applying the trace estimates Equation 3.23 and 3.26 gives a bound on the second term:

$$\begin{aligned}\left|T_{2,a}^{FD}\right| &= \left|\left\langle\, [[e_h^I]]\,,\, \{\{\nabla e_h^A\}\}\,\right\rangle_{\mathcal{E}_i}\right| \\ &\leq \left\|\sigma_h^{1/2}\,[[e_h^I]]\right\|_{0,\mathcal{E}_i} \left\|\sigma_h^{-1/2}\,\{\{\nabla e_h^A\}\}\right\|_{0,\mathcal{E}_i} \\ &\leq Z\sum_{\Omega_e}\Delta_e^{-1}\left\|e_h^I\right\|_{0,\Omega_e}\left\|e_h^I\right\|_{1,\Omega_e} + \frac{1}{14}\left\|\nabla e_h^A\right\|_{0,\Omega}^2. \end{aligned} \tag{A.96}$$

Next, we have

$$\begin{aligned}\left|T_3^{FD}\right| &= \left|\left\langle e_h, \nabla e_h^A\right\rangle_{\Gamma_D}\right| \\ &\leq \left|\left\langle e_h^A, \nabla e_h^A\right\rangle_{\Gamma_D}\right| + \left|\left\langle e_h^I, \nabla e_h^A\right\rangle_{\Gamma_D}\right| \end{aligned} \tag{A.97}$$

where we apply the trace estimate Equation 3.26 and 3.23 and (A9) to get the bounds

$$\begin{aligned}\left|\left\langle e_h^A, \nabla e_h^A\right\rangle_{\Gamma_D}\right| &\leq \left\|\sigma_h^{1/2} e_h^A\right\|_{0,\Gamma_D}\left\|\sigma_h^{-1/2}\nabla e_h^A\right\|_{0,\Gamma_D} \\ &\leq \frac{1}{4}\left\|\sigma_h^{1/2} e_h^A\right\|_{0,\Gamma_D}^2 + \frac{Z^{tr,1}}{\sigma_{h,0}}\left\|\nabla e_h^A\right\|_{0,\Omega}^2 \end{aligned} \tag{A.98}$$

and

$$\begin{aligned}\left|\left\langle e_h^I, \nabla e_h^A\right\rangle_{\Gamma_D}\right| &\leq \left\|\sigma_h^{1/2} e_h^I\right\|_{0,\Gamma_D}\left\|\sigma_h^{-1/2}\nabla e_h^A\right\|_{0,\Gamma_D} \\ &\leq Z\sum_{\Omega_e}\Delta_e^{-1}\left\|e_h^I\right\|_{0,\Omega_e}\left\|e_h^I\right\|_{1,\Omega_e} + \frac{1}{14}\left\|\nabla e_h^A\right\|_{0,\Omega}^2. \end{aligned} \tag{A.99}$$

Using (A1,A6), we have

$$\begin{aligned}\left|T_4^{FD}\right| &= \left|((\rho(C)^{-1} - \rho^{-1}(c))\mathbf{K}^{-1}\mathbf{q}, \nabla e_h^A)_\Omega\right| \\ &\leq Z_1\left\|\rho(C)^{1/2}\phi^{1/2} e_c^A\right\|_{0,\Omega}^2 + Z_2\left\|e_c^I\right\|_{0,\Omega}^2 + \frac{1}{14}\left\|\nabla e_h^A\right\|_{0,\Omega}^2. \end{aligned} \tag{A.100}$$

Finally, we apply (A1,A4) to get the bound:

$$\begin{aligned}\left|T_5^{FD}\right| &= \left|((\hat{\rho}(C)-\hat{\rho}(c))\mathbf{e}_z, \nabla e_h^A)_\Omega\right| \\ &= \left|\rho_0 \epsilon e_c \mathbf{e}_z, \nabla e_h^A)_\Omega\right| \\ &\leq Z \left\|\rho(C)^{1/2}\phi^{1/2} e_c^A\right\|_{0,\Omega}^2 + Z_2 \left\|e_c^I\right\|_{0,\Omega}^2 + \frac{1}{14}\left\|\nabla e_h^A\right\|_{0,\Omega}^2 . \end{aligned} \tag{A.101}$$

Combining the previous results and using the approximation results gives our final estimate:

$$\begin{aligned}\left\|\nabla e_h^A\right\|_{0,\Omega}^2 \leq Z_9^q \left\|\rho(c)^{-1/2}\mathbf{K}^{-1/2}\mathbf{e}_q^A\right\|_{0,\Omega}^2 + \frac{1}{2}\left\|\sigma_h^{1/2}\left[\left[e_h^A\right]\right]\right\|_{0,\mathcal{E}_i}^2 + Z_1\left\|\rho(C)^{1/2}\phi^{1/2}e_c^A\right\|_{0,\Omega}^2 \\ + \frac{1}{2}\left\|\sigma_h^{1/2}e_h^A\right\|_{0,\Gamma_D}^2 + Z_2\big[\Delta^{2\min(s_{flow},k+1)-2}\left\|h\right\|_{H^{s_{flow}}(\Omega)}^2 \\ + \Delta^{2\min(s_{vel},k+1)}\left\|\mathbf{q}\right\|_{H^{s_{vel}}(\Omega)}^2 + \Delta^{2\min(s_{trans},k+1)}\left\|c\right\|_{H^{s_{trans}}(\Omega)}^2\big].\end{aligned} \tag{A.102}$$

where Z_1, Z_2 are positive, mesh independent constants and were we have gained the constraint on our penalty constant that $\sigma_{h,0} \geq 14Z^{tr,1}$.

Combined Estimate To get an estimate for the coupled system, we first use (A.102) to bound the gradient of the head error in (A.90) and combine terms to get

$$\begin{aligned}
&\left|(\rho(C)\phi e_{c,t}, e_h^A)_\Omega\right| \\
&\quad\leq \frac{\epsilon}{1-\epsilon}\Bigg[Z_5\left\|\rho(C)^{1/2}\phi^{1/2}e_c^A\right\|_{0,\Omega}^2 + Z_6\left\|\rho(C)^{1/2}S^{1/2}e_h^A\right\|_{0,\Omega}^2 \\
&\qquad + (Z^{q,2} + 3Z_9^q + Z_9^q\frac{5(Z^{tr,1})^2\left\|\mathbf{D}(\mathbf{Q}^M)\right\|_{0,\Omega}^2}{\sigma_{c,0}})\left\|\rho(c)^{-1}\mathbf{K}^{-1}\mathbf{e}_q^A\right\|_{0,\Omega}^2 \\
&\qquad + \frac{4}{5}\left\|\sigma_c^{1/2}\left[\left[e_c^A\right]\right]\right\|_{0,\mathcal{E}_i}^2 \\
&\qquad + (\frac{Z^{tr,1}}{\sigma_{h,0}}\left\|\mathbf{D}(\mathbf{Q}^M)^{1/2}\right\|_{0,\Omega}^2 + \left\|\mathbf{D}(\mathbf{Q}^M)^{1/2}\right\|_{0,\Omega}^2)\left\|\mathbf{D}(\mathbf{Q}^M)^{1/2}\nabla e_c^A\right\|_{0,\Omega}^2 \\
&\qquad + (\frac{5}{2} + \frac{5(Z^{tr,1})^2\left\|\mathbf{D}(\mathbf{Q}^M)\right\|_{0,\Omega}^2}{2\sigma_{c,0}})\left\|\sigma_h^{1/2}\left[\left[e_h^A\right]\right]\right\|_{0,\mathcal{E}_i}^2 \\
&\qquad + (\frac{3}{2} + \frac{5(Z^{tr,1})^2\left\|\mathbf{D}(\mathbf{Q}^M)\right\|_{0,\Omega}^2}{2\sigma_{c,0}})\left\|\sigma_h^{1/2}e_h^A\right\|_{0,\Gamma_D}^2 \\
&\qquad + Z\big[(\Delta^{2\min(s_{flow},k+1)-2})\left\|h\right\|_{H^{s_{flow}}(\Omega)}^2 + \Delta^{2\min(s_{vel},k+1)}\left\|\mathbf{q}\right\|_{H^{s_{vel}}(\Omega)}^2 \\
&\qquad + (\Delta^{2\min(s_{trans},k+1)-2})\left\|c\right\|_{H^{s_{trans}}(\Omega)}^2\big]\Bigg].
\end{aligned} \tag{A.103}$$

Leaving this estimate for now, we use the velocity error estimate (A.19) to eliminate the velocity error term from the transport equation and rearrange terms gives

$$\begin{aligned}
&\frac{1}{2}\left\|\rho(C(\cdot,T))^{1/2}\phi^{1/2}e_c^A(\cdot,T)\right\|_{0,\Omega}^2 + \frac{1}{2}\int_0^T\big[\left\|\mathbf{D}^{1/2}(\mathbf{Q}^M)\nabla e_c^A\right\|_{0,\Omega}^2 + \left\|\sigma_c^{1/2}\left[\left[e_c^A\right]\right]\right\|_{0,\mathcal{E}_i}^2\big] \\
&\quad\leq Z_\Delta + Z_2\int_0^T\left\|\rho(C)^{1/2}\phi^{1/2}e_c^A\right\|_{0,\Omega}^2 + Z_3\int_0^T\big[\left\|\rho(C)^{1/2}S^{1/2}e_h^A\right\|_{0,\Omega}^2 \\
&\qquad + Z^{q,1}\int_0^T\left|(\phi\rho_0\epsilon e_{c,t}, e_h^A)_\Omega\right|
\end{aligned} \tag{A.104}$$

where Z_1, Z_2 and Z_3 are new positive constants and $Z^{q,1}$ is as previously defined

and where

$$
\begin{aligned}
Z_\Delta =& Z\Big[(\Delta^{2\min(s_{flow},1k+1)} + \Delta^{2\min(s_{flow},k+1)-2}) \left\|h\right\|^2_{L^2(0,T;H^{s_{flow}}(\Omega))} \\
&+ \Delta^{2\min(s_{flow},k+1)} \left\|h_t\right\|^2_{L^2(0,T;H^{s_{flow}}(\Omega))} \\
&+ (\Delta^{2\min(s_{vel},k+1)} + \Delta^{2\min(s_{vel},k+1)-2}) \left\|\mathbf{q}\right\|^2_{L^2(0,T;H^{s_{vel}}(\Omega))} \\
&+ \Delta^{2\min(s_{trans},k+1)-2} \left\|c\right\|^2_{L^2(0,T;H^{s_{trans}}(\Omega))} \\
&+ \Delta^{2\min(s_{trans},k+1)} \left\|c_t\right\|^2_{L^2(0,T;H^{s_{trans}}(\Omega))}\Big].
\end{aligned}
$$

We now add (A.104) to (A.18) to get

$$
\begin{aligned}
&\frac{1}{2}\left\|\rho(C(\cdot,T))^{1/2}\phi^{1/2}e_c^A(\cdot,T)\right\|^2_{0,\Omega} + \frac{1}{2}\left\|\rho(C(\cdot,T))^{1/2}S^{1/2}e_h^A(\cdot,T)\right\|^2_{0,\Omega} \\
&\quad + \frac{1}{2}\int_0^T \Big[\left\|\mathbf{D}^{1/2}(\mathbf{Q}^M)\nabla e_c^A\right\|^2_{0,\Omega} + \Big[\left\|\rho(C)^{-1/2}\mathbf{K}^{-1/2}\mathbf{e}_q^A\right\|^2_{0,\Omega} \\
&\quad + \left\|\sigma_c^{1/2}\left[\left[e_c^A\right]\right]\right\|^2_{0,\mathcal{E}_i} + \left\|\sigma_h^{1/2}\left[\left[e_h^A\right]\right]\right\|^2_{0,\mathcal{E}_i} + \left\|\sigma_h^{1/2}e_h^A\right\|^2_{0,\Gamma_D}\Big] \\
&\quad \leq Z_\Delta + Z_2\int_0^T \left\|\rho(C)^{1/2}\phi^{1/2}e_c^A\right\|^2_{0,\Omega} + Z_3\int_0^T \left\|\rho(C)^{1/2}S^{1/2}e_h^A\right\|^2_{0,\Omega} \\
&\qquad + (1+Z^{q,1})\int_0^T \left|(\phi\rho_0\epsilon e_{c,t}, e_h^A)_\Omega\right|. \qquad \text{(A.105)}
\end{aligned}
$$

In our last step, we use our mass fraction error time derivative estimate (A.103) to

bound the time derivative to get

$$
\begin{aligned}
&\frac{1}{2}\left\|\rho(C(\cdot,T))^{1/2}\phi^{1/2}e_c^A(\cdot,T)\right\|_{0,\Omega}^2+\frac{1}{2}\left\|\rho(C(\cdot,T))^{1/2}S^{1/2}e_h^A(\cdot,T)\right\|_{0,\Omega}^2\\
&\quad+\frac{1}{2}\int_0^T\Big[\left\|\mathbf{D}^{1/2}(\mathbf{Q}^M)\nabla e_c^A\right\|_{0,\Omega}^2+\left\|\rho(C)^{-1/2}\mathbf{K}^{-1/2}\mathbf{e}_q^A\right\|_{0,\Omega}^2\\
&\quad+\left\|\sigma_c^{1/2}\left[\left[e_c^A\right]\right]\right\|_{0,\mathcal{E}_i}^2+\left\|\sigma_h^{1/2}\left[\left[e_h^A\right]\right]\right\|_{0,\mathcal{E}_i}^2+\left\|\sigma_h^{1/2}e_h^A\right\|_{0,\Gamma_D}^2\Big]\\
&\quad\le Z_\Delta+Z_2\int_0^T\left\|\rho(C)^{1/2}\phi^{1/2}e_c^A\right\|_{0,\Omega}^2+Z_3\int_0^T\left\|\rho(C)^{1/2}S^{1/2}e_h^A\right\|_{0,\Omega}^2\\
&\quad+(1+Z^{q,1})\int_0^T\frac{\epsilon}{1-\epsilon}\Big[Z_5\left\|\rho(C)^{1/2}\phi^{1/2}e_c^A\right\|_{0,\Omega}^2+Z_6\left\|\rho(C)^{1/2}S^{1/2}e_h^A\right\|_{0,\Omega}^2\\
&\quad+(Z^{q,2}+3Z_9^q+Z_9^q\frac{5(Z^{tr,1})^2\left\|\mathbf{D}(\mathbf{Q}^M)\right\|_{0,\Omega}^2}{\sigma_{c,0}})\left\|\rho(c)^{-1}\mathbf{K}^{-1}\mathbf{e}_q^A\right\|_{0,\Omega}^2\\
&\quad+\frac{4}{5}\left\|\sigma_c^{1/2}\left[\left[e_c^A\right]\right]\right\|_{0,\mathcal{E}_i}^2\\
&\quad+(\frac{Z^{tr,1}}{\sigma_{h,0}}\left\|\mathbf{D}(\mathbf{Q}^M)^{1/2}\right\|_{0,\Omega}^2+\left\|\mathbf{D}(\mathbf{Q}^M)^{1/2}\right\|_{0,\Omega}^2)\left\|\mathbf{D}(\mathbf{Q}^M)^{1/2}\nabla e_c^A\right\|_{0,\Omega}^2\\
&\quad+(\frac{5}{2}+\frac{5(Z^{tr,1})^2\left\|\mathbf{D}(\mathbf{Q}^M)\right\|_{0,\Omega}^2}{2\sigma_{c,0}})\left\|\sigma_h^{1/2}\left[\left[e_h^A\right]\right]\right\|_{0,\mathcal{E}_i}^2\\
&\quad+(\frac{3}{2}+\frac{5(Z^{tr,1})^2\left\|\mathbf{D}(\mathbf{Q}^M)\right\|_{0,\Omega}^2}{2\sigma_{c,0}})\left\|\sigma_h^{1/2}e_h^A\right\|_{0,\Gamma_D}^2\\
&\quad+Z\big[(\Delta^{2\min(s_{flow},k+1)-2})\left\|h\right\|_{H^{s_{flow}}(\Omega)}^2+\Delta^{2\min(s_{vel},k+1)}\left\|\mathbf{q}\right\|_{H^{s_{vel}}(\Omega)}^2\\
&\quad+(\Delta^{2\min(s_{trans},k+1)-2})\left\|c\right\|_{H^{s_{trans}}(\Omega)}^2\big]\Big].
\end{aligned}
\tag{A.106}
$$

Rearranging terms, we arrive at

$$\begin{aligned}
&\frac{1}{2}\left\|\rho(C(\cdot,T))^{1/2}\phi^{1/2}e_c^A(\cdot,T)\right\|_{0,\Omega}^2+\frac{1}{2}\left\|\rho(C(\cdot,T))^{1/2}S^{1/2}e_h^A(\cdot,T)\right\|_{0,\Omega}^2\\
&\quad+\frac{1}{2}\int_0^T\Big[\left\|\mathbf{D}^{1/2}(\mathbf{Q}^M)\nabla e_c^A\right\|_{0,\Omega}^2+\left\|\rho(C)^{-1/2}\mathbf{K}^{-1/2}\mathbf{e}_q^A\right\|_{0,\Omega}^2\\
&\quad+\left\|\sigma_c^{1/2}\left[\left[e_c^A\right]\right]\right\|_{0,\mathcal{E}_i}^2+\left\|\sigma_h^{1/2}\left[\left[e_h^A\right]\right]\right\|_{0,\mathcal{E}_i}^2+\left\|\sigma_h^{1/2}e_h^A\right\|_{0,\Gamma_D}^2\Big]\\
&\leq Z_\Delta+Z_2\int_0^T\left\|\rho(C)^{1/2}\phi^{1/2}e_c^A\right\|_{0,\Omega}^2+Z_3\int_0^T\left\|\rho(C)^{1/2}S^{1/2}e_h^A\right\|_{0,\Omega}^2\\
&\quad+G_1\int_0^T\left\|\rho(C)^{-1/2}\mathbf{K}^{-1/2}\mathbf{e}_q^A\right\|_{0,\Omega}^2+G_2\int_0^T\left\|\sigma_h^{1/2}e_h^A\right\|_{0,\Gamma_D}^2\\
&\quad+G_3\int_0^T\left\|\sigma_c^{1/2}\left[\left[e_c^A\right]\right]\right\|_{0,\mathcal{E}_i}^2+G_4\int_0^T\left\|\mathbf{D}(\mathbf{Q}^M)^{1/2}\nabla e_c^A\right\|_{0,\Omega}^2\\
&\quad++G_5\int_0^T\left\|\sigma_c^{1/2}\left[\left[e_h^A\right]\right]\right\|_{0,\mathcal{E}_i}^2,
\end{aligned}\tag{A.107}$$

where Z_1, Z_2, and Z_3 are positive constants independent of Δ and where we have the revised coefficients

$$\begin{aligned}
G_1&=(1+Z^{q,1})\frac{\epsilon}{1-\epsilon}(Z^{q,2}+3Z_9^q+Z_9^q\frac{5(Z^{tr,1})^2\left\|\mathbf{D}(\mathbf{Q}^M)\right\|_{0,\Omega}^2}{\sigma_{c,0}})\\
&=(1+Z^{q,1})\frac{Z^{q,2}\epsilon}{1-\epsilon}+(1+Z^{q,1})\frac{3Z_9^q\epsilon}{1-\epsilon}+(1+Z^{q,1})\frac{\epsilon}{1-\epsilon}Z_9^q\frac{5(Z^{tr})^2\left\|\mathbf{D}(\mathbf{Q}^M)\right\|_{0,\Omega}^2}{\sigma_{c,0}}\\
&=G_{1,a}+G_{1,b}+G_{1,c},
\end{aligned}\tag{A.108}$$

$$\begin{aligned}
G_2&=(1+Z^{q,1})\frac{\epsilon}{1-\epsilon}(\frac{3}{2}+\frac{5(Z^{tr,1})^2\left\|\mathbf{D}(\mathbf{Q}^M)\right\|_{0,\Omega}^2}{2\sigma_{c,0}})\\
&=(1+Z^{q,1})\frac{3\epsilon}{2(1-\epsilon)}+(1+Z^{q,1})\frac{\epsilon}{1-\epsilon}\frac{5(Z^{tr,1})^2\left\|\mathbf{D}(\mathbf{Q}^M)\right\|_{0,\Omega}^2}{2\sigma_{c,0}}\\
&=G_{2,a}+G_{2,b},
\end{aligned}\tag{A.109}$$

$$
\begin{aligned}
G_3 &= (1+Z^{q,1})\frac{\epsilon}{1-\epsilon}\big(\frac{3}{2}+\frac{(Z^{tr,1})^2\left\|\mathbf{D}(\mathbf{Q}^M)\right\|_{0,\Omega}^2}{2\sigma_{c,0}}\big)\\
&= (1+Z^{q,1})\frac{3\epsilon}{2(1-\epsilon)}+(1+Z^{q,1})\frac{\epsilon}{1-\epsilon}\big(\frac{(Z^{tr,1})^2\left\|\mathbf{D}(\mathbf{Q}^M)\right\|_{0,\Omega}^2}{2\sigma_{c,0}}\big)\\
&= G_{3,a}+G_{3,b}, \qquad \text{(A.110)}\\
G_4 &= (1+Z^{q,1})\frac{\epsilon}{1-\epsilon}\big(\frac{Z^{tr,1}}{\sigma_{h,0}}\left\|\mathbf{D}(\mathbf{Q}^M)^{1/2}\right\|_{0,\Omega}^2+\left\|\mathbf{D}(\mathbf{Q}^M)^{1/2}\right\|_{0,\Omega}^2\big)\\
&= (1+Z^{q,1})\frac{\epsilon}{1-\epsilon}\frac{Z^{tr,1}}{\sigma_{h,0}}\left\|\mathbf{D}(\mathbf{Q}^M)^{1/2}\right\|_{0,\Omega}^2+(1+Z^{q})\frac{\epsilon}{1-\epsilon}\left\|\mathbf{D}(\mathbf{Q}^M)^{1/2}\right\|_{0,\Omega}^2\\
&= G_{4,a}+G_{4,b},\\
G_5 &= \frac{4\epsilon}{5(1-\epsilon)}(1+Z^{q,1}). \qquad \text{(A.111)}
\end{aligned}
$$

We wish to show that with small enough ϵ and large enough penalty constants, we can hide the terms with G_i coefficients on the right side. So, we want to choose our penalty constants and restriction on ϵ such that $G_i \leq 1/4$ for $i = 1,2,3,4,5$. For the terms involving the penalty constant $(G_{1,c}, G_{2,b}, G_{3,b}, G_{4,a})$, we will take a large enough penalty constants to get a desired bound and then place a restriction on the density contrast, ϵ, to provide another bound. Again, the constants are defined as

$$
\begin{aligned}
Z^{q,1} &= \rho^* k^* \left\|\mathbf{D}(\mathbf{Q}^M)^{-1/2}\right\|_{0,\Omega}^2+(Z^D)^2\rho^* k^*\left\|\mathbf{D}(\mathbf{Q}^M)^{-1/2}\right\|_{0,\Omega}^2\|\nabla c\|_{0,\Omega}^2\\
&\quad+\frac{(Z^{tr,1})^2\rho^* k^*}{\sigma_{c,0}}+\frac{(Z^{tr,1}Z^D)^2\rho^* k^*}{\sigma_{c,0}}\|\nabla c\|_{0,\Omega}^2\|\nabla c\|_{1,\Omega}^2,\\
Z^{q,2} &= \frac{\rho^* k^*}{4}+\frac{1}{4}(Z^D)^2\rho^* k^*\|\nabla c\|_{0,\Omega}^2+\frac{(Z^{tr,1})^2\rho^* k^*}{\sigma_{h,0}}\\
&\quad+\frac{15(Z^D Z^{tr,1})^2\rho^* k^*}{\sigma_{h,0}}\|\nabla c\|_{0,\Omega}^2\|\nabla c\|_{1,\Omega}^2,\\
Z_9^q &= \frac{7}{\rho_* k_*}.
\end{aligned}
$$

For G_1, we wish to find $G_{1,a}, G_{1,b} \leq 1/10$ and choose a large enough penalty con-

stants such that $G_{1,c} \leq 3/20$. For $G_{1,a}$, we have

$$\begin{aligned} G_{1,a} &= \frac{\epsilon}{1-\epsilon}(Z^{q,2} + Z^{q,2}Z^{q,1}) \\ &= \frac{\epsilon}{4(1-\epsilon)}\Bigg[\rho^* k^* + (Z^D)^2\rho^* k^* \left\|\nabla c\right\|_{0,\Omega}^2 + \rho^* k^* \left\|\mathbf{D}(\mathbf{Q}^M)^{-1/2}\right\|_{0,\Omega}^2 \\ &\quad + 2(\rho^* k^*)^2 \left\|\mathbf{D}(\mathbf{Q}^M)^{-1/2}\right\|_{0,\Omega}^2 (Z^D)^2 \left\|\nabla c\right\|_{0,\Omega}^2 \\ &\quad + (Z^D)^4(\rho^* k^*)^2 \left\|\mathbf{D}(\mathbf{Q}^M)^{-1/2}\right\|_{0,\Omega}^2 \left\|\nabla c\right\|_{0,\Omega}^4 \Bigg] \\ &\quad + \frac{\epsilon}{1-\epsilon}\Bigg[\textit{penalty constant terms}\Bigg]. \end{aligned} \tag{A.112}$$

Similarly, for $G_{1,b}$ we have

$$\begin{aligned} G_{1,b} &= \frac{3\epsilon}{1-\epsilon}(Z_9^q + Z_9^q Z^{q,1}) \\ &= \frac{3\epsilon}{1-\epsilon}\Bigg[\frac{7}{\rho_* k_*} + \frac{7}{\rho_* k_*}\rho^* k^* \left\|\mathbf{D}(\mathbf{Q}^M)^{-1/2}\right\|_{0,\Omega}^2 \\ &\quad + \frac{7}{\rho_* k_*}(Z^D)^2\rho^* k^* \left\|\mathbf{D}(\mathbf{Q}^M)^{-1/2}\right\|_{0,\Omega}^2 \left\|\nabla c\right\|_{0,\Omega}^2 \Bigg] \\ &\quad + \frac{\epsilon}{1-\epsilon}\Bigg[\textit{penalty constant terms}\Bigg]. \end{aligned} \tag{A.113}$$

Assuming large enough penalty constants such that each of the penalty constant terms in Equation A.112 and A.113 are less than 1/20, then for $G_{1,a}, G_{1,b} \leq 1/10$ we have the following restrictions on ϵ:

$$\epsilon \leq \begin{cases} \frac{1}{Z_{G_{1,a}}} \\ \frac{1}{Z_{G_{1,b}}} \end{cases}$$

where we have

$$\begin{aligned} Z_{G_{1,a}} &= 1 + 5\Bigg[\rho^* k^* + (Z^D)^2\rho^* k^* \left\|\nabla c\right\|_{0,\Omega}^2 + \rho^* k^* \left\|\mathbf{D}(\mathbf{Q}^M)^{-1/2}\right\|_{0,\Omega}^2 \\ &\quad + 2(\rho^* k^*)^2 \left\|\mathbf{D}(\mathbf{Q}^M)^{-1/2}\right\|_{0,\Omega}^2 (Z^D)^2 \left\|\nabla c\right\|_{0,\Omega}^2 \\ &\quad + (Z^D)^4(\rho^* k^*)^2 \left\|\mathbf{D}(\mathbf{Q}^M)^{-1/2}\right\|_{0,\Omega}^2 \left\|\nabla c\right\|_{0,\Omega}^4 \Bigg] \end{aligned} \tag{A.114}$$

and

$$Z_{G_{1,b}} = 1 + 420\Big[\frac{1}{\rho_* k_*} + \frac{1}{\rho_* k_*}\rho^* k^* \left\|\mathbf{D}(\mathbf{Q}^M)^{-1/2}\right\|_{0,\Omega}^2 + \frac{1}{\rho_* k_*}(Z^D)^2\rho^* k^* \left\|\mathbf{D}(\mathbf{Q}^M)^{-1/2}\right\|_{0,\Omega}^2 \|\nabla c\|_{0,\Omega}^2\Big]. \tag{A.115}$$

For G_2, we will choose a large enough penalty constant such that $G_{2,b} \leq 1/8$ and then we have the following restrictions on ϵ such that $G_{2,a} \leq 1/8$:

$$\begin{aligned} G_{2,a} &= (1 + Z^{q,1})\frac{4\epsilon}{1-\epsilon} \\ &= \frac{4\epsilon}{1-\epsilon}\big[\rho^* k^* \left\|\mathbf{D}(\mathbf{Q}^M)^{-1/2}\right\|_{0,\Omega}^2 \\ &\quad + (Z^D)^2\rho^* k^* \left\|\mathbf{D}(\mathbf{Q}^M)^{-1/2}\right\|_{0,\Omega}^2 \|\nabla c\|_{0,\Omega}^2\big] \\ &\quad + \frac{4\epsilon}{1-\epsilon}\big[\frac{(Z^{tr,1})^2\rho^* k^*}{\sigma_{c,0}} + \frac{(Z^{tr,1}Z^D)^2\rho^* k^*}{\sigma_{c,0}}\|\nabla c\|_{0,\Omega}^2 \|\nabla c\|_{1,\Omega}^2\big]. \end{aligned} \tag{A.116}$$

We choose a large enough penalty constant such that the second term is less than $1/16$ and then we have the following restrictions on ϵ such that the first term is less than $1/16$:

$$\epsilon \leq \frac{1}{1 + 64\big[(Z^D)^2\rho^* k^* \left\|\mathbf{D}(\mathbf{Q}^M)^{-1/2}\right\|_{0,\Omega}^2 \|\nabla c\|_{0,\Omega}^2 + \rho^* k^* \left\|\mathbf{D}(\mathbf{Q}^M)^{-1/2}\right\|_{0,\Omega}^2\big]}. \tag{A.117}$$

Similarly, for G_3, we choose a large enough penalty constant such that $G_{3,b} \leq 1/8$ and then we need to analyze $G_{3,a}$:

$$\begin{aligned} G_{3,a} &= (1 + Z^{q,1})\frac{3\epsilon}{2(1-\epsilon)} \\ &= \frac{3\epsilon}{2(1-\epsilon)}\Big[1 + \rho^* k^* \left\|\mathbf{D}(\mathbf{Q}^M)^{-1/2}\right\|_{0,\Omega}^2 \\ &\quad + (Z^D)^2\rho^* k^* \left\|\mathbf{D}(\mathbf{Q}^M)^{-1/2}\right\|_{0,\Omega}^2 \|\nabla c\|_{0,\Omega}^2\Big] \\ &\quad + \frac{3\epsilon}{2(1-\epsilon)}\Big[\frac{(Z^{tr,1})^2\rho^* k^*}{\sigma_{c,0}} + \frac{(Z^{tr,1}Z^D)^2\rho^* k^*}{\sigma_{c,0}}\|\nabla c\|_{0,\Omega}^2 \|\nabla c\|_{1,\Omega}^2\Big]. \end{aligned} \tag{A.118}$$

We choose a large enough penalty constant such that the second term is less than 1/16 and then we have the following restrictions on ϵ such that the first term is less than 1/16:

$$\epsilon \leq \frac{2}{17 + 48\big[(Z^D)^2\rho^* k^* \left\|\mathbf{D}(\mathbf{Q}^M)^{-1/2}\right\|_{0,\Omega}^2 \|\nabla c\|_{0,\Omega}^2 + \rho^* k^* \left\|\mathbf{D}(\mathbf{Q}^M)^{-1/2}\right\|_{0,\Omega}^2\big]}. \tag{A.119}$$

For G_4, we choose a large enough penalty constant such that $G_{4,b} \leq 1/8$ and then we analyze:

$$\begin{aligned} G_{4,b} &= (1 + Z^{q,1})\frac{\epsilon}{4(1-\epsilon)} \left\|\mathbf{D}(\mathbf{Q}^M)^{1/2}\right\|_{0,\Omega}^2 \\ &= \frac{\epsilon \left\|\mathbf{D}(\mathbf{Q}^M)^{1/2}\right\|_{0,\Omega}^2}{4(1-\epsilon)} \Bigg[1 + \rho^* k^* \left\|\mathbf{D}(\mathbf{Q}^M)^{-1/2}\right\|_{0,\Omega}^2 \\ &\quad + (Z^D)^2\rho^* k^* \left\|\mathbf{D}(\mathbf{Q}^M)^{-1/2}\right\|_{0,\Omega}^2 \|\nabla c\|_{0,\Omega}^2 \Bigg] \\ &\quad + \frac{\epsilon \left\|\mathbf{D}(\mathbf{Q}^M)^{1/2}\right\|_{0,\Omega}^2}{4(1-\epsilon)} \left[\frac{(Z^{tr,1})^2\rho^* k^*}{\sigma_{c,0}} + \frac{(Z^{tr,1}Z^D)^2\rho^* k^*}{\sigma_{c,0}} \|\nabla c\|_{0,\Omega}^2 \|\nabla c\|_{1,\Omega}^2 \right]. \end{aligned} \tag{A.120}$$

Again, we choose a large enough penalty constant such that the second term is less than 1/16 and then we have the following restrictions on ϵ such that the first term is less than 1/16:

$$\epsilon \leq \frac{4}{Z_{G_4}}, \tag{A.121}$$

where

$$\begin{aligned} Z_{G_4} = 4 + 16\Bigg[&\left\|\mathbf{D}(\mathbf{Q}^M)^{1/2}\right\|_{0,\Omega}^2 + \left\|\mathbf{D}(\mathbf{Q}^M)^{1/2}\right\|_{0,\Omega}^2 \rho^* k^* \left\|\mathbf{D}(\mathbf{Q}^M)^{-1/2}\right\|_{0,\Omega}^2 \\ &+ \left\|\mathbf{D}(\mathbf{Q}^M)^{1/2}\right\|_{0,\Omega}^2 (Z^D)^2\rho^* k^* \left\|\mathbf{D}(\mathbf{Q}^M)^{-1/2}\right\|_{0,\Omega}^2 \|\nabla c\|_{0,\Omega}^2 \Bigg]. \end{aligned} \tag{A.122}$$

Finally, for G_5, we have

$$\begin{aligned}
G_5 &= \frac{4\epsilon}{5(1-\epsilon)}(1+Z^{q,1}) \\
&= \frac{4\epsilon}{5(1-\epsilon)}\left[1+\rho^*k^*\left\|\mathbf{D}(\mathbf{Q}^M)^{-1/2}\right\|_{0,\Omega}^2+(Z^D)^2\rho^*k^*\left\|\mathbf{D}(\mathbf{Q}^M)^{-1/2}\right\|_{0,\Omega}^2\|\nabla c\|_{0,\Omega}^2\right] \\
&\quad+\frac{4\epsilon}{5(1-\epsilon)}(1+Z^{q,1})\left[\frac{(Z^{tr,1})^2\rho^*k^*}{\sigma_{c,0}}+\frac{(Z^{tr,1}Z^D)^2\rho^*k^*}{\sigma_{c,0}}\|\nabla c\|_{0,\Omega}^2\|\nabla c\|_{1,\Omega}^2\right].
\end{aligned} \tag{A.123}$$

We choose a large enough penalty constant such that the second term is less than 1/8 and then we have the following restrictions on ϵ such that the first term is less than 1/8:

$$\epsilon \leq \frac{5}{37+32\left[\left\|\mathbf{D}(\mathbf{Q}^M)^{-1/2}\right\|_{0,\Omega}^2\rho^*k^*+(Z^D)^2\rho^*k^*\left\|\mathbf{D}(\mathbf{Q}^M)^{-1/2}\right\|_{0,\Omega}^2\|\nabla c\|_{0,\Omega}^2\right.}. \tag{A.124}$$

So, assuming a large enough penalty constant, a density contrast that meets the restrictions of (A.114)-(A.124) and a large enough constant, M in our velocity cutoff function, we have

$$\begin{aligned}
&\frac{1}{2}\left\|\rho(C(\cdot,T))^{1/2}\phi^{1/2}e_c^A(\cdot,T)\right\|_{0,\Omega}^2+\frac{1}{4}\left\|\rho(C(\cdot,T))^{1/2}S^{1/2}e_h^A(\cdot,T)\right\|_{0,\Omega}^2 \\
&\qquad+\frac{1}{4}\int_0^T\left[\left\|\mathbf{D}^{1/2}(\mathbf{Q}^M)\nabla e_c^A\right\|_{0,\Omega}^2+\left\|\rho(C)^{-1/2}\mathbf{K}^{-1/2}\mathbf{e}_q^A\right\|_{0,\Omega}^2\right. \\
&\qquad\left.+\left\|\sigma_c^{1/2}\left[\left[e_c^A\right]\right]\right\|_{0,\mathcal{E}_i}^2+\left\|\sigma_h^{1/2}\left[\left[e_h^A\right]\right]\right\|_{0,\mathcal{E}_i}^2+\left\|\sigma_h^{1/2}e_h^A\right\|_{0,\Gamma_D}^2\right] \\
&\qquad\leq Z_\Delta+Z_2\int_0^T\left\|\rho(C)^{1/2}\phi^{1/2}e_c^A\right\|_{0,\Omega}^2+Z_3\int_0^T\left\|\rho(C)^{1/2}S^{1/2}e_h^A\right\|_{0,\Omega}^2.
\end{aligned} \tag{A.125}$$

Applying Grönwall's inequality gives us our final results.

Bibliography

[1] E. Abarca, J. Carrera, X. Sánchez-Vila, and M. Dentz. Anisotropic dispersive Henry problem. *Adv. Water Resour.*, 30:913–926, 2007.

[2] P. Ackerer and A. Younes. Efficient approximations for the simulation of density driven flow in porous media. *Adv. Water Resour.*, 31:15–27, 2008.

[3] P. Ackerer, A. Younes, and M. Mancip. A new coupling algorithm for density-driven flow in porous media. *Geophys. Res. Lett.*, 31:1–4, 2004.

[4] P. Ackerer, A. Younes, and R. Mose. Modeling variable density flow and solute transport in porous medium: 1. Numerical model and verification. *Transp. Porous Media*, 35:345–373, 1999.

[5] P. Ackerer, A. Younes, S.E. Oswald, and W. Kinzelbach. On modelling of density driven flow. *Calibration and Reliability in Groundwater Modelling (Proceedings of the ModelCARE 99 Conference held at Zurich, Switzerland, September 1999)*, IAHS Publ. No. 265:377–384, 2000.

[6] V. Aizinger, C. Dawson, B. Cockburn, and P. Castillo. The local discontinuous Galerkin method for contaminant transport. *Adv. Water Resour.*, 24:73–87, 2001.

[7] D.N. Arnold. An interior penalty finite element method with discontinuous elements. *SIAM J. Numer. Anal.*, 4:742–760, 1982.

[8] D.N. Arnold, F. Brezzi, B. Cockburn, and L.D. Marini. Unified analysis of discontinuous Galerkin methods for elliptic problems. *SIAM J. Numer. Anal.*, 39(5):1749–1779, 2002.

[9] UN Atlas of the Oceans. Human settlements on the coast, 2012. Retrieved May 20, 2012 from http://www.oceansatlas.org.

[10] I. Babuška. The finite element method with inner penalty. *Math. Comp.*, 27:221–228, 1973.

[11] I. Babuška, C.E. Baumann, and J.T. Oden. A discontinuous hp finite element method for diffusion problems: 1-d analysis. *Comput. Methods Appl. Mech. Engrg.*, 37(9):103–122, 1999.

[12] I. Babuška and M. Zlámal. Nonconforming elements in the finite element method with penalty. *SIAM J. Numer. Anal.*, 10:863–875, 1973.

[13] Satish Balay, Jed Brown, , Kris Buschelman, Victor Eijkhout, William D. Gropp, Dinesh Kaushik, Matthew G. Knepley, Lois Curfman McInnes, Barry F. Smith, and Hong Zhang. PETSc users manual. Technical Report ANL-95/11 - Revision 3.2, Argonne National Laboratory, 2011.

[14] Satish Balay, Jed Brown, Kris Buschelman, William D. Gropp, Dinesh Kaushik, Matthew G. Knepley, Lois Curfman McInnes, Barry F. Smith, and Hong Zhang. PETSc Web page, 2011. http://www.mcs.anl.gov/petsc.

[15] Satish Balay, William D. Gropp, Lois Curfman McInnes, and Barry F. Smith. Efficient management of parallelism in object oriented numerical software li-

braries. In E. Arge, A. M. Bruaset, and H. P. Langtangen, editors, *Modern Software Tools in Scientific Computing*, pages 163–202. Birkhäuser Press, 1997.

[16] G. I. Barenblatt. On some unsteady motions of fluids and gases in a porous medium. *Applied Mathematics and Mechanics (PMM)*, 16(1):67–78, 1952. in Russian.

[17] F. Bassi and S. Rebay. A high-order accurate discontinuous finite element method for the numerical solution of the compressible Navier-Stokes equations. *J. Comput. Phys.*, 131:267–279, 1997.

[18] C.E. Baumann. *An h-p Adaptive Discontinuous Finite Element Method of Computational Fluid Dynamics.* PhD thesis, The University of Texas at Austin, Austin, 1997.

[19] C.E. Baumann and J.T. Oden. A discontinuous *hp* finite element method for convection-diffusion problems. *Comput. Methods Appl. Mech. Engrg.*, 175:311–341, 1999.

[20] J. Bear. *Dynamics of Fluids in Porous Media.* American Elsevier Publishing Company, Inc., 1988.

[21] J. Bear and A.H.-D. Cheng. *Theory and Applications of Transport in Porous Media: Modeling Groundwater Flow and Contaminant Transport.* Springer, 2010.

[22] J. Bear, A.H.-D. Cheng, S. Sorek, D. Ouazar, and I. Herrera, editors. *Theory and Applications of Transport in Porous Media: Seawater Intrusion in Coastal Aquifers - Concepts, Methods and Practices*, chapter 5. Kluwer Academic Publishers, 1999.

[23] J. Bear, Q. Zhou, and J. Bensabat. Three dimensional simulation of seawater intrusion in heterogeous aquifers, with application to the coastal aquifer of Israel. In *First International Conference on Saltwater Intrusion and Coastal Aquifers - Monitoring, Modeling, and Management. Essaouira, Morocco*, April 2001.

[24] A.G. Bobba. Mathematical models for saltwater intrusion in coastal aquifers. *Water Resour. Manag.*, 7:3–37, 1993.

[25] M.C. Boufadel, M.T. Suidan, and A.D. Venosa. Density-dependent flow in one-dimensional variably-saturated media. *J. Hydrol.*, 202:280–301, 1997.

[26] S.C. Brenner and L.R. Scott. *The Mathematical Theory of Finite Element Methods*. Springer, 2008.

[27] F. Brezzi, B. Cockburn, L.D. Marini, and E. Süli. Stabilization mechanisms in discontinuous Galerkin finite element methods. *Comput. Methods Appl. Mech. Engrg.*, 195:3293–3310, 2006.

[28] A. N. Brooks and T. J. R. Hughes. Streamline upwind/petrov-galerkin formulations for convection dominated flows with particular emphasis on the incompressible naviar-stokes equations. *Comput. Methods Appl. Mech. Engrg.*,

32:199–259, 1982.

[29] M.A. Buès and C. Oltean. Numerical simulations for saltwater intrusion by the mixed hybrid finite element method and discontinuous finite element method. *Transp. Porous Media*, 40:171–200, 2000.

[30] A. Buffa, T.J.R. Hughes, and G. Sangalli. Analysis of a multiscale discontinuous Galerkin method for convection-diffusion problems. *SIAM J. Numer. Anal.*, 44(4):1420–1440, 2007.

[31] C. W. Carlston. An early american statement of the badon ghyben-herzberg principle of static fresh-water-salt-water balance. *Am. J. Sci.*, 261:88–91, 1963.

[32] P. Castillo. Performance of discontinuous Galerkin methods for elliptic PDEs. *SIAM J. Sci. Comput.*, 24(2):524–547, 2002.

[33] P. Castillo, B. Cockburn, I. Perugia, and D. Schötzau. An a priori analysis of the local discontinuous Galerkin method for elliptic problems. *SIAM J. Numer. Anal.*, 38:1676–1706, 2001.

[34] P. Castillo, B. Cockburn, D. Schötzau, and C. Schwab. Optimal a priori error estimates for the *hp*-version of the local discontinuous Galerkin method for convection-diffusion problems. *Math. Comp.*, 71(238):455–478, 2002.

[35] B. Cockburn and C. Dawson. Some extensions of the local discontinuous Galerkin method for convection-diffusion equations in multidimensions. In

J. Whiteman, editor, *The Proceedings of the Conference on the Mathematics of Finite Elements and Applications: MAFELAP X*, Amsterdam, 2000. Elsevier.

[36] B. Cockburn, S. Hou, and C.-W. Shu. The Runge-Kutta local projection discontinuous Galerkin finite element method for conservation laws IV: The multidimensional case. *Math. Comp.*, 54(190):545–581, 1990.

[37] B. Cockburn, S.-Y. Lin, and C.-W. Shu. TVB Runge-Kutta local projection discontinuous Galerkin finite element method for conservation laws III: One-dimensional systems. *J. Comp. Phys.*, 84(1):90–113, 1989.

[38] B. Cockburn and C.-W. Shu. The Runge-Kutta local projection discontinuous Galerkin finite element method for conservation laws II: General framework. *Math. Comp.*, 52(186):411–435, 1989.

[39] B. Cockburn and C.-W. Shu. The Runge-Kutta local projection P^1-discontinuous Galerkin finite element method for scalar conservation laws. *RAIRO Modél. Math. Anal. Numér*, 25(3):337–361, 1991.

[40] B. Cockburn and C.-W. Shu. The local discontinuous Galerkin methods for time-dependent convection-diffusion systems. *SIAM J. Numer. Anal.*, 35:2440–2463, 1998.

[41] B. Cockburn and C.-W. Shu. The Runge-Kutta local projection discontinuous Galerkin finite element method for conservation laws V: Multidimensional systems. *J. Comp. Phys.*, 141:199–224, 1998.

[42] R. Codina and J. Blasco. Analysis of a stabilized finite element approximation of the transient convection-diffusion-reaction equation using orthogonal subscales. *Computing and Visualization in Science*, 4(3):167–174, 2002.

[43] A.E. Croucher and M.J. O'Sullivan. The Henry problem for saltwater intrusion. *Water Resour. Res.*, 18:159–170, 1995.

[44] C. Dawson. Godunov-mixed methods for advection-diffusion equations in multidimensions. *SIAM J. Numer. Anal.*, 30(5):1315–1332, 1993.

[45] C. Dawson. Analysis of an upwind-mixed finite element method for nonlinear contaminant transport equations. *SIAM J. Numer. Anal.*, 35(5):1709–1724, 1998.

[46] C. Dawson. Coupling local discontinuous and continuous Galerkin methods for flow problems. *Adv. Water Resour.*, 28:729–744, 2005.

[47] C. Dawson. Analysis of discontinuous finite element methods for groundwater/surface water coupling. *SIAM J. Numer. Anal.*, 44(4):1375–1404, 2006.

[48] C. Dawson and J. Proft. *A Priori* estimates for interior penalty versions of the local discontinuous Galerkin method applied to transport equations. *Num. Meth. Part. D. E.*, 17(6):545–564, 2001.

[49] C. Dawson, S. Sun, and M.F. Wheeler. Compatible algorithms for coupled flow and transport. *Comput. Methods Appl. Mech. Engrg.*, 193:2565–2580, 2004.

[50] C.N. Dawson. Godunov-mixed methods for advective flow problems in one space dimension. *SIAM J. Numer. Anal.*, 28(5):1282–1309, 1991.

[51] James W. Demmel, Stanley C. Eisenstat, John R. Gilbert, Xiaoye S. Li, and Joseph W. H. Liu. A supernodal approach to sparse partial pivoting. *SIAM J. Matrix Anal. A.*, 20(3):720–755, 1999.

[52] M. Dentz, D.M. Tartakovsky, E. Abarca, A. Guadagnini, X. Sanchez-Vila, and J. Carrera. Variable-density flow in porous media. *J. Fluid Mech.*, 561:209–235, 2006.

[53] H.-J.G Diersch. FEFLOW finite element subsurface flow and transport simulation system - User's manual/reference manual/white papers. Release 5.0. *WASY Ltd, Berlin*, 2002.

[54] H.-J.G. Diersch and O. Kolditz. Variable-density flow and transport in porous media: Approaches and challenges. *Adv. Water Resour.*, 25:899–944, 2002.

[55] J. Douglas and T. Dupont. Interior penalty procedures for elliptic and parabolic Galerkin methods. *Lecture Notes in Physics*, 58:207–216, 1976.

[56] J.W. Elder. Steady free convection in a porous medium heated from below. *J. Fluid Mech.*, 27:29–48, 1967.

[57] J.W. Elder. Transient convection in a porous medium. *J. Fluid Mech.*, 27:609–623, 1967.

[58] G.H.P. Oude Essink. Improving fresh groundwater supply - problems and solutions. *Ocean Coast. Manage.*, 44:429–449, 2001.

[59] G.H.P. Oude Essink. Salt water intrusion in a three-dimensional groundwater system in the Netherlands: A numerical study. *Transp. Porous Media*, 43:137–158, 2001.

[60] M. W. Farthing, C.E. Kees, and Miller C.T. Mixed finite element methods and higher order temporal approximations for variably saturated groundwater flow. *Adv. Water Resour.*, 27:373–394, 2004.

[61] T. Feseker. Numerical studies on saltwater intrusion in a coastal aquifer in northwestern Germany. *Hydrogeol. J.*, 15:267–279, 2007.

[62] P. Frolkovič. Consistent velocity approximation for density driven flow and transport. In R Van Keer et al., editor, *Advanced Computational Methods in Engineering, Part 2.*, pages 603–611. Maastricht: Shaker Publishing, 1998.

[63] P. Frolkovič and H. De Schepper. Numerical modeling of convection dominated transport coupled with density driven flow in porous media. *Adv. Water Resour.*, 24:63–72, 2001.

[64] R.R. Goswami and T.P. Clement. Laboratory-scale investigation of saltwater intrusion dynamics. *Water Resour. Res.*, 43:1–11, 2007.

[65] S.M. Hassanizadeh. Modeling species transport by concentrated brine in aggregated porous media. *Transp. Porous Media*, 3:299–318, 1988.

[66] S.M. Hassanizadeh and T. Leijnse. A non-linear theory of high-concentration-gradient dispersion in porous media. *Adv. Water Resour.*, 18:203–215, 1995.

[67] H.R. Henry. Effects of dispersion on salt encroachment in coastal aquifers, sea water in coastal aquifers. *U.S. Geological Survey Water Supply Paper*, 1613-C, 1964.

[68] A.W. Herbert, C.P. Jackson, and D.A. Lever. Coupled groundwater flow and solute transport with fluid density strongly dependent upon concentration. *Water Resour. Res.*, 24(10):1781–1795, 1988.

[69] P. Houston, C. Schwab, and E. Suli. Stabilized hp-finite element methods for first-order hyperbolic problems. *SIAM J. Numer. Anal.*, pages 1618–1643, 2000.

[70] P. Houston, C. Schwab, and E. Süli. Discontinuous hp-finite element methods for advection-diffusion-reaction problems. *SIAM J. Numer. Anal.*, pages 2133–2163, 2002.

[71] T. Hughes and M. Mallet. A new finite element formulation for computational fluid dynamics: Iv. a discontinuity-capturing operator for multidimensional advective-diffusive systems. *Comput. Methods Appl. Mech. Engrg.*, 58:329–336, 1986.

[72] T. J. R. Hughes, M. Mallet, and A. Mizukami. A new finite element formulation for computational fluid dynamics: Ii. beyond supg. *Comput. Methods Appl. Mech. Engrg.*, 54:341–355, 1986.

[73] H.E. Huppert and A.W. Woods. Gravity-driven flows in porous layers. *J. Fluid Mech.*, 292(1):55–69, 1995.

[74] P.S. Huyakorn, P.F. Andersen, J.W. Mercer, and H.O. White Jr. Saltwater intrusion in aquifers: Development and testing of a three-dimensional finite element model. *Water Resour. Res.*, 23(2):293–312, 1987.

[75] K. Johannsen, W. Kinzelback, S.E. Oswald, and G. Wittum. The saltpool benchmark problem - numerical simulation of saltwater upconing in a porous medium. *Adv. Water Resour.*, 25:335–348, 2002.

[76] R. Juanes and T. Patzek. Multiscale-stabilized solutions to one-dimensional systems of conservation laws. *Comput. Methods Appl. Mech. Engrg.*, 194:2781–2805, 2005.

[77] C. Kees, M. Farthing, and C. Dawson. Locally conservative, stabilized finite element methods for variably saturated flow. *Comput. Methods Appl. Mech. Engrg.*, 197:4610–4625, 2008.

[78] C. E. Kees and M. W. Farthing. Parallel computational methods and simulation for coastal and hydraulic applications using the proteus toolkit. In *Supercomputing11: Proceedings of the PyHPC11 Workshop*, 2011.

[79] J. Kerrou and P. Renard. A numerical analysis of dimensionality and heterogeneity effects on advective dispersive seawater intrusion processes. *Hydrogeol. J.*, 18:55–72, 2010.

[80] P. Knabner and P. Frolkovič. Consistent velocity approximation for finite volume or element discretizations of density driven flow in porous media. In A.A. Aldama et al., editor, *Computational Methods in Water Resources XI, vol*

1: Computational methods in subsurface flow and transport problems., pages 340–352. Southhampton: Computational Mechanics Publication, 1996.

[81] O. Kolditz, R. Ratke, H.-J.G. Diersch, and W. Zielke. Coupled groundwater flow and transport: 1. Verification of variable density flow and transport models. *Adv. Water Resour.*, 21(1):27–46, 1987.

[82] L.F. Konikow, W.E. Sanford, and P.J. Campbell. Constant-concentration boundary condition: Lessons from the HYDROCOIN variable-density groundwater benchmark problem. *Water Resour. Res.*, 33(10):2253–2261, 1997.

[83] G. Kopsiaftis, A. Mantoglou, and P. Giannoulopoulos. Variable density coastal aquifer models with application to an aquifer on Thira Island. *Desalination*, 237:65–80, 2009.

[84] C.D. Langevin. Simulation of submarine groundwater discharge to a marine estuary: Biscayne Bay, Florida. *Ground Water*, 41(6):758–771, 2003.

[85] C.D. Langevin and W. Guo. User's guide to SEAWAT: A computer program for simulation of three-dimensional variable density ground-water flow. *US Geol. Surv. Water Resour. Invest.; (6, A7)*, 2002.

[86] M. Larson and A. Niklasson. A conservative flux for the continuous Galerkin method based on discontinuous enrichment. *CALCOLO*, 41:65–76, 2004.

[87] C.H. Lee and R.T.-S. Cheng. On seawater encroachment in coastal aquifers. *Water Resour. Res.*, 10(5):1039–1043, 1974.

[88] P. Lesaint and P.A. Raviart. On a finite element method for solving the neutron transport equation. In C. de Boor, editor, *Mathematical Aspects of Finite Elements in Partial Differential Equations*, pages 89–145. Academic Press, New York, 1974.

[89] D.A. Lever and C.P. Jackson. On the equations for the flow of concentrated salt solution through a porous medium. Technical Report DOE/RW/85.100, U.K. DOE Report, 1985.

[90] Xiaoye S. Li and James W. Demmel. SuperLU_DIST: A scalable distributed-memory sparse direct solver for unsymmetric linear systems. *ACM Trans. Mathematical Software*, 29(2):110–140, June 2003.

[91] J.-L. Lions. Problèmes aux limites non homogènes à donées irrégulieères: Une méthode d'approximation. In *Numerical Analysis of Partial Differential Equations (C.I.M.E. 2 Ciclo, Ispra, 1967)*, pages 283–292. Edizioni Cremonese, Rome, 1968.

[92] C. MacMinn, J. Neufeld, M. Hesse, and H. Huppert. Spreading and convective dissolution of carbon dioxide in vertically confined, horizontal aquifers. In preparation.

[93] A. Mazzia and M. Putti. Mixed-finite element and finite volume discretizations for heavy brine simulations in groundwater. *J. Comput. Appl. Math.*, 147:191–213, 2002.

[94] P.E. Misut and C.I. Voss. Freshwater-saltwater transition zone movement

during aquifer storage and recovery cycles in Brooklyn and Queens, New York City, USA. *J. Hydrol.*, 337:87–103, 2007.

[95] J. A. Nitsche. Über ein variationsprinzip zur lösung von Dirichlet-problemen bei verwendung von teilräumen, die keinen randbedingungen unterworfen sind. *Abhandlungen aus dem Mathematischen Seminar der Universit at Hamburg*, 36:9–15, 1971.

[96] J.T. Oden, I. Babuška, and C.E. Baumann. A discontinuous hp finite element method for diffusion problems. *J. Comput. Phys.*, 146:491–519, 1998.

[97] C.M. Oldenburg and K. Pruess. Dispersive transport dynamics in a strongly coupled groundwater-brine flow system. *Water Resour. Res.*, 31(2):289–302, 1995.

[98] C. Oltean and M.A. Buès. Coupled groundwater flow and transport in porous media. a conservative or non-conservative form? *Transp. Porous Media*, 44:219–246, 2001.

[99] S.E. Oswald and W. Kinzelbach. A three-dimensional physical model for verification of variable-density flow codes. *Calibration and Reliability in Groundwater Modelling (Proceedings of the ModelCARE 99 Conference held at Zurich, Switzerland, September 1999)*, 265:399–404, 2000.

[100] S.E. Oswald and W. Kinzelbach. Three-dimensional physical benchmark experiments to test variable-density flow models. *J. Hydrol.*, 290:22–44, 2004.

[101] E.D.P. Perera, K. Jinno, Y. Hiroshiro, and A. Tsutsumi. Evaluation of seawater intrusion to a coastal aquifer by developing a three dimensional numerical model. In Taniguchi et al., editor, *From Headwaters to the Ocean*, pages 231–236. Taylor & Francis Group, London, 2009.

[102] I. Perugia and D. Schötzau. An hp-analysis of the local discontinuous Galerkin method for diffusion problems. *J. Sci. Comp.*, 17(1):561–571, 2002.

[103] G.F. Pinder and H.H. Cooper Jr. A numerical technique for calculating the transient position of the saltwater front. *Water Resour. Res.*, 6(3):275–882, 1970.

[104] V. Post and E. Abarca. Preface: Saltwater and freshwater interactions in coastal aquifers. *Hydrogeol. J.*, 18:1–4, 2010.

[105] V. Post, H. Kooi, and C. Simmons. Using hydraulic head measurements in variable-density ground water flow analyses. *Ground Water*, 45:664–671, 2007.

[106] V.E.A. Post. Fresh and saline groundwater interaction in coastal aquifers: Is our technology ready for the problems ahead? *Hydrogeol. J.*, 13:120–123, 2005.

[107] M. Putti and C. Paniconi. Picard and Newton linearization for the coupled model of saltwater intrusion in aquifers. *Adv. Water Resour.*, 31(7):1809–1814, 1995.

[108] W.H. Reed and T.R. Hill. Triangular mesh methods for the neutron transport equation. Technical report, Los Alamos Scientific Laboratory, 1973.

[109] G.R. Richter. The discontinuous Galerkin method with diffusion. *Math. Comp.*, 58(198):631–643, 1992.

[110] B. Rivière. *Discontinuous Galerkin Methods for Solving Elliptic and Parabolic Equations: Theory and Implementation.* SIAM, Philadelphia, 2008.

[111] B. Rivière and M.F. Wheeler. Discontinuous Galerkin methods for flow and transport problems in porous media. *Commun. Numer. Meth. En.*, 18:63–68, 2002.

[112] B. Rivière, M.F. Wheeler, and V. Girault. Improved energy estimates for interior penalty, constrained and discontinuous Galerkin methods for elliptic problems. part I. *Comp. Geo.*, 3:337–360, 1999.

[113] B. Rivière, M.F. Wheeler, and V. Girault. A priori error estimates for finite element methods based on discontinuous approximation spaces for elliptic problems. *SIAM J. Numer. Anal.*, 39:902–931, 2001.

[114] R.J. Schotting, H. Moser, and S.M. Hassanizadeh. High-concentration-gradient dispersion in porous media: experiments, analysis and approximations. *Adv. Water Resour.*, 22:665–680, 1999.

[115] G. Segol, G.F. Pinder, and W.G. Gray. A Galerkin-finite element technique for calculating the transient position of the saltwater front. *Water Resour. Res.*, 11(2):343–347, 1975.

[116] C.T. Simmons. Variable density groundwater flow: From current challenges to future possibilities. *J. Hydrol.*, 13:116–119, 2005.

[117] C.T. Simmons, T.R. Fenstemaker, and J.M. Sharp Jr.. Variable-density groundwater flow and solute transport in heterogeneous porous media: approaches, resolutions and future challenges. *J. Contam. Hydrol.*, 52:245–275, 2001.

[118] M.J. Simpson and T.P. Clement. Improving the worthiness of the Henry problem as a benchmark for density-dependent groundwater flow models. *Water Resour. Res.*, 40:1–11, 2004.

[119] S. Sun and M.F. Wheeler. Discontinuous Galerkin methods for coupled flow and reactive transport problems. *Appl. Numer. Math.*, 52:273–298, 2005.

[120] S. Sun and M.F. Wheeler. Symmetric and nonsymmetric discontinuous Galerkin methods for reactive transport in porous media. *SIAM J. Numer. Anal.*, 43(1):195–219, 2005.

[121] S. Sun and M.F. Wheeler. Mesh adaptation strategies for discontinuous Galerkin methods applied to reactive transport problems. In H.-W. Chu, M. Savoie, and B. Sanchez, editors, *in Proceedings of International Conference on Computing, Communications and Control Technologies (CCCT 2004)*, volume I, pages 223–228, 2006.

[122] C.I. Voss. A finite-element simulation model for saturated-unsaturated fluid-density-dependent ground-water flow with energy transport or chemically-

reactive single-species solute transport. *US Geol. Surv. Water Resour. Invest. (Rep 84-4369)*, 1984.

[123] C.I. Voss, C.T. Simmons, and N.I. Robinson. Three-dimensional benchmark for variable-density flow and transport simulation: matching semi-analytical stability modes for steady unstable convection in an inclined porous box. *Hydrogeol. J.*, 18:5–23, 2010.

[124] C.I. Voss and W. Souza. Variable density flow and solute transport simulation of regional aquifers containing a narrow freshwater-saltwater transition zone. *Water Resour. Res.*, 23(10):1851–1866, 1987.

[125] M. Walther, J.-0. Delfs, J. Grundman, O. Kolditz, and R. Liedl. Saltwater intrusion modeling: Verification and application to an agricultural coastal arid region in oman. *J. Comp. Appl. Math.*, 2012. In press.

[126] M.F. Wheeler. An elliptic collocation-finite element method with interior penalties. *SIAM J. Numer. Anal.*, 15(1):152–161, 1978.

[127] M.F. Wheeler and B. Darlow. Interior penalty Galerkin procedures for miscible displacement problems in porous media. In J. T. Oden, editor, *Comp. Meth. Nonlinear Mechanics*, pages 485–506. North-Holland, Amsterdam, New York, 1980.

[128] R.A. Wooding. Steady state free thermal convection of liquid in a saturated permeable medium. *J. Fluid Mech.*, 2:273–285, 1957.

[129] A. Younes. On modelling the multidimensional coupled fluid flow and heat or mass transport in porous media. *Int. J. Heat Mass Tran.*, 46:367–379, 2003.

[130] A. Younes, P. Ackerer, and R. Mose. Modeling variable density flow and solute transport in porous medium: 2. Re-evaluation of the salt dome flow problem. *Transp. Porous Media*, 35:375–394, 1999.

[131] A. Younes, M. Fahs, and S. Ahmed. Solving density driven flow problems with efficient spatial discretizations and higher-order time integration methods. *Adv. Water Resour.*, 32:340–352, 2009.

[132] A. Younes, M. Konz, M. Fahs, A. Zidane, and P. Huggenberger. Modelling variable density flow problems in heterogeneous porous media using the method of lines and advanced spatial discretization. *Math. Comput. Simulat.*, 81:2346–2355, 2011.

[133] Q. Zhou, J. Bear, and J. Bensabat. Saltwater upconing and decay beneath a well pumping above an interface zone. *Transp. Porous Media*, 61:337–363, 2005.

Vita

Lieutenant Colonel Timothy James Povich attended the University of Notre Dame where he received his Bachelor of Science in Mechanical Engineering in May 1993. He was commissioned a second lieutenant in the United States Army immediately following graduation and is still serving in the Army. In June 2002, he received his Master of Arts in Mathematics at the University of Texas at Austin and upon completion, taught for three years as an instructor and assistant professor in the Department of Mathematical Sciences at the United States Military Academy (USMA) in West Point, New York. He began his research on discontinuous Galerkin methods applied to variable density flow and transport in September 2009. He is currently an assistant professor in the Department of Mathematical Sciences at USMA.

Permanent address: 42 Embree Street, Tarrytown, New York 10591

This dissertation was typeset with LaTeX[†] by the author.

[†]LaTeX is a document preparation system developed by Leslie Lamport as a special version of Donald Knuth's TeX Program.